Molecular Approach to Engineer Two-Dimensional Devices for CMOS and beyond-CMOS Applications

Yuda Zhao, Marco Gobbi, Luis E. Hueso, Paolo Samorì

Molecular Approach to Engineer Two-Dimensional Devices for CMOS and beyond CMOS Applications

Yuda Zhao[1,5], Marco Gobbi[2,3,4], Luis E. Hueso[3,4], Paolo Samorì[1]*

[1] University of Strasbourg, CNRS, ISIS UMR 7006, 8 allée Gaspard Monge, F-67000 Strasbourg, France

[2] Centro de Fisica de Materiales (CSIC-UPV/EHU), Paseo Manuel de Lardizabal 5, E-20018 Donostia-San Sebastián, Spain

[3] CIC nanoGUNE, 20018 Donostia-San Sebastian, Basque Country, Spain

[4] IKERBASQUE, Basque Foundation for Science, 48009 Bilbao, Spain

[5] School of Micro-Nano Electronics, ZJU-Hangzhou Global Scientific and Technological Innovation Centre, Zhejiang University, 38 Zheda Road, 310027 Hangzhou, People's Republic of China

Contents

ABSTRACT

Two-dimensional materials (2DMs) have attracted tremendous research interest over the last two decades. Their unique optical, electronic, thermal and mechanical properties make 2DMs key building blocks for the fabrication of novel complementary metal-oxide-semiconductor (CMOS) and beyond-CMOS devices. Major advances in device functionality and performance have been made by the covalent or non-covalent functionalization of 2DMs with molecules: while the molecular coating of metal electrodes and dielectrics allows for more efficient charge injection and transport through the 2DMs, the combination of dynamic molecular systems, capable to respond to external stimuli, with 2DMs makes it possible to generate hybrid systems possessing new properties, by realizing stimuli-responsive functional devices thereby enabling functional diversification in More−than−Moore technologies. In this review, we first introduce emerging 2DMs, various classes of (macro)molecules, and molecular switches and discuss their relevant properties. We then turn to 2DM/molecule hybrid systems and the various physical and chemical strategies used to synthesize them. Next, we discuss the use of molecules and assemblies thereof to boost the performance of 2D transistors for CMOS applications and to impart diverse functionalities in beyond CMOS devices. Finally, we present the challenges, opportunities, and long-term perspectives in this technologically promising field.

1 Introduction

Ever since the first commercial microprocessors were introduced in the early 1970s, the number of transistors fitting in an integrated circuit (IC) has doubled every two years, yielding the continual improvement in performance that characterizes modern electronics. By complying to the Moore's law,[1] the smallest achievable feature size in metal-oxide-semiconductor field-effect transistors (MOSFETs) has impressively been reduced from the initial 10 μm fifty years ago to the today's nominal 5 nm-node technology. As feature sizes approach the atomic scale, however, completely new challenges arise and must be overcome. For instance, short channel effects are observed when the channel length approaches the size of the depletion layer of the source and drain junctions. To eliminate this effect, the transistor's traditional planar structure was replaced with the three-dimensional fin field-effect transistor (FinFET) structure, which allows a better gate control (Figure 1).

In Si MOSFETs with gate lengths below 5 nm, the quantum-mechanical tunneling between the source and the drain electrodes comes to dominate the electrical transport. For this reason, IC manufacturers are encouraging the transition from today's FinFETs to next-generation gate-all-around (GAA) FETs (Figure 1), in which the channel, composed of one or several separate nanosheets, penetrates the gate and is therefore in contact with it on all four sides ("all around").[2] Although first generation GAA FETs may initially adopt Si nanosheets, subsequent versions will likely incorporate higher mobility channel materials: within the realm of traditional bulk semiconductors, options include introducing strain in the Si channel, which has been shown to

enhance Si's mobility[3], and using high-mobility III-V or Ge channels is another possibility that is being intensely researched[4,5]. A more novel approach relies on the use of 2D materials (2DM) such as transition metal dichalcogenides (TMDs), black phosphorus and graphene. These materials offer a wealth of possibilities for new device concepts and may prove to be the ideal components to develop ultrathin channels for GAA transistors. The ability to control the channel thickness at the atomic level translates into an improved gate control over the channel barrier and into reduced short channel effects. These are two key features in ultra-scaled devices, together with low fabrication costs and power consumption. Therefore, 2DMs have the potential to be incorporated into future electronic systems.[6]

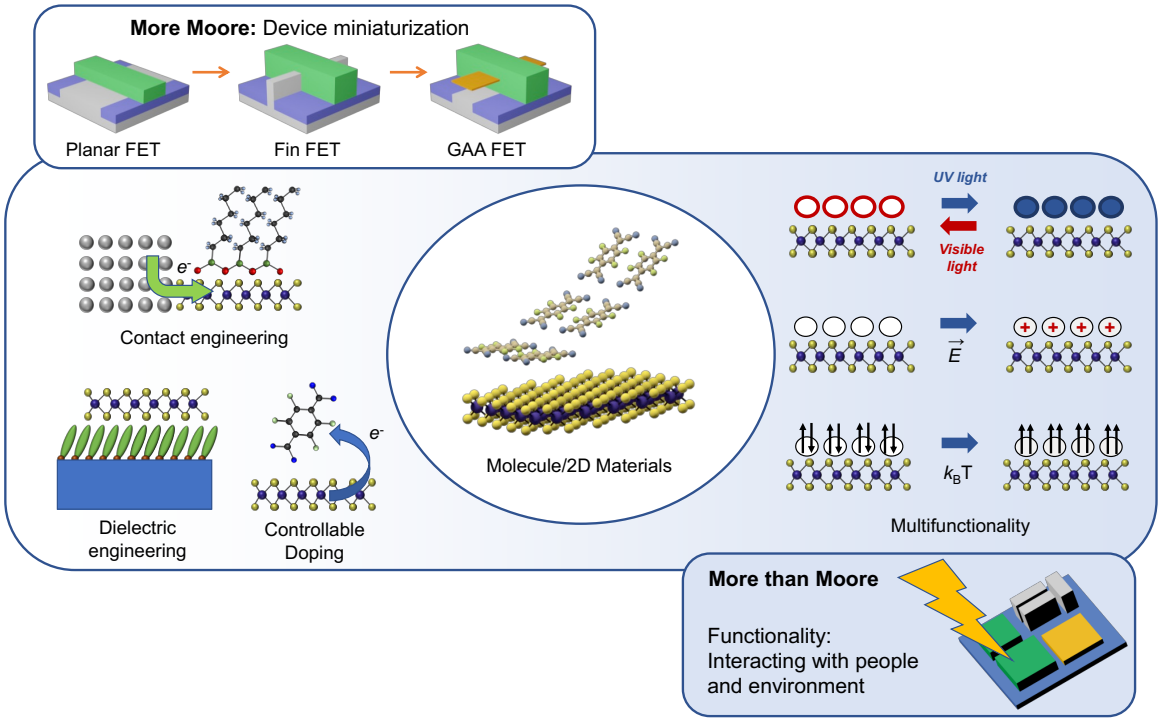

Figure 1. *Molecular functionalization of 2D Materials offers intriguing possibilities to pursue the More−Moore and More-than-Moore approaches, which aim at the device miniaturization beyond the current technology and the integration of multiple functionalities, respectively. In the More−Moore panel, the device architectures of planar FET, FinFET and GAA FET are schematically shown; the gate is displayed in green.*

In recent years, great efforts have been made to develop 2D-based electronic devices to complement or even replace Si in post-Moore electronics.[6] 2DMs have the potential to break through the scaling limits, allowing a further reduction in device size while still preserving device performance.[7,8] Although 2D FETs have shown better performance in logic circuits when compared with FETs based on atomically thin Si,[9-11] several challenges remain to be overcome, such as unintentional carrier doping, large contact resistance and strong surface scattering from the dielectric.[12] It is therefore essential to develop scalable and cost-efficient strategies to engineer 2DMs devices to meet the industrial requirements,[13] which is above all a great challenge for electronic engineers, materials scientists and chemists. Chemical approaches have yielded viable methods to functionalize 2DMs and engineer 2D devices.[14,15] Small organic molecules and self-assembled monolayers as well as polymers have been used to effectively tune the carrier density of 2DMs, reduce the Schottky barrier and minimize surface scattering. These efforts will contribute to next-generation nanosheet GAA transistors with high performance and promote further downscaling, in the so-called More−Moore approach.

By contrast, the More-than-Moore approach aims for the functional diversification in electronic systems based on the integration of multiple functional devices into complementary metal–oxide–semiconductor (CMOS) digital circuits.[16] Besides their role as basic elements in electronic circuits, 2D FETs provide a suitable platform for the fabrication of functional devices with the ability to interact with the environment. On the one hand, 2DMs with ultrahigh surface-to-volume ratio are extremely sensitive to changes in their local environment, and can directly interact with and respond to outer stimuli. On the other hand, the generation of hybrid heterostructure by combining 2DMs with tailor-made molecular switches allows conferring new properties to the 2DMs, realize stimuli-responsive functional devices and enable diversification in More−than−Moore technologies. Molecular switches, whose optical, electronic or magnetic properties are able to change in response to an external stimulus,[17-19] can interact with 2DMs, thereby affecting the electrical signals through the hybrid device. The incorporation of molecular switches into 2D devices will promote their applications beyond CMOS, especially in stimuli-responsive functional devices. These functional devices can be stacked on the integrated CMOS circuits and add value to the electronic system.

Finally, it is worth considering that the More-Moore and More-than-Moore approaches intend to improve the performance and expand the capabilities of Si-technology, new computing paradigms are being explored which do not rely (only) on semiconductors to perform logic operations. For instance, researchers at Intel have proposed the use of spintronic devices as scalable and energy-efficient solutions to replace CMOS in future CPUs.[20] Following another approach,

quantum computation aims to exploit the quantum nature of nanoscale objects to solve complex problems that are beyond the capabilities of conventional computers.[21] To be successful, these approaches demand suitable hardware materials with the required physical properties, posing a fierce challenge to engineers, materials scientists and chemists.[20,22] As we will highlight, while 2DMs are being studied in the context of spintronics[23] and quantum computing[24], engineering their intrinsic physical properties via molecular functionalization is still a relatively unexplored research direction which in our view holds tremendous potential.

This review offers a comprehensive and critical assessment of the use of chemical approaches to engineer 2DM/molecule-based devices. Because of the unique structure of 2DMs, conventional device engineering methods established for Si-based technology are not suitable for 2D devices. We will provide a review of the electronic properties of two-dimensional materials, outlining their potential as a technological option beyond scaled Si CMOS switches. We will discuss the roadmap for the design of device structures, the working mechanism of devices based on molecules/2D hybrids with a particular focus on methods which enable to boost device performance and to construct multifunctional devices.

2 Basic Electronic Properties of 2D Materials

The compelling demand for higher performance and lower power consumption in electronic systems represents one of the main driving forces in the electronics industry's quest for devices and architectures based on new materials. In this section, we will introduce the electronic

properties of graphene, TMDs and other emerging 2DMs. Then we will discuss their unique functions and roles in logic devices and functional devices.

2.1 Graphene

The groundbreaking experimental studies of graphene's electronic transport properties by Konstantin Novoselov and Andre Geim triggered enormous research interest in 2DMs, especially on their electronic properties.[25] Graphene is a monolayer of carbon atoms in a two-dimensional hexagonal lattice formed by sp^2 hybridization (Figure 2a) and its thickness amounts only to 0.335 nm (Figure 2b).[26,27] The strong in-plane σ bonds are responsible for graphene's hexagonal structure and its unique mechanical properties (superior strength and stiffness),[28,29] while electrons in the perpendicularly oriented half-filled p_z orbitals are responsible for its conductive properties, forming an occupied valence band and an empty conduction band.[30] The conduction and valence bands meet at the Dirac points, giving rise to a zero-bandgap semimetal with high electrical conductivity (Figure 2c). The electrons in graphene obey a linear dispersion relation and behave as massless Dirac particles, exhibiting high carrier mobility. Ambipolar transfer characteristics have been observed in graphene FETs with two branches separated by the Dirac point, indicating a change in both the carrier density and the carrier type in the graphene channel (Figure 2d). The charge carrier concentration can be tuned continuously up to values as high as 10^{13} cm^{-2}.[26] The position of the Dirac point characterized in graphene FETs is dependent on the charges at the graphene/dielectric interfaces and the doping of graphene. Mobility values exceeding 10^4 cm^2V^-

$^{1}s^{-1}$ at the temperature between 10 and 100 K have been observed in graphene transistors.[31] The mobility remains high even at high carrier concentration (>10^{12} cm^{-2}) in both electrically and chemically-doped devices.[32] A further indication of the system's exceptional charge transport properties is the quantum Hall effect that can be observed in graphene even at room temperature.[31,33] However, the carrier mobilities measured in experiments are lower than the theoretical predictions, being limited by defects, impurities and interface scattering.[34] Meanwhile, the zero-bandgap nature of graphene determines a low I_{on}/I_{off} ratio (in the range of 2-20) and a high static power consumption of graphene FETs, limiting their practical applications in logic devices. A viable strategy to improve the I_{on}/I_{off} ratio consists in opening a bandgap by cutting graphene into graphene nanoribbons. However, this method reduces the mobility to the range of 10^{2}-10^{3} $cm^{2}V^{-1}s^{-1}$, which is directly related to the width of the nanoribbon.[35,36] It is desirable to find a method to simultaneously preserve the high carrier mobility of graphene and increase the I_{on}/I_{off} ratio.

Alongside FETs, graphene-based functional devices have become the research focus for applications in photonics, optoelectronics, radio frequency devices and sensors (chemical sensing, mechanical sensing, etc.).[37-39] In view of its high conductivity and low optical absorption, graphene has been used to produce transparent electrodes for solar cells, light-emitting diodes (LEDs), touch screens, etc. [40-42] Graphene can also work as channel layers in radio frequency (RF) devices,[43] photodetectors, [44] sensors,[45] etc. Several outstanding review articles have discussed the promising

applications of graphene in functional devices[37-39] and we will focus on graphene-based responsive devices in section 6.

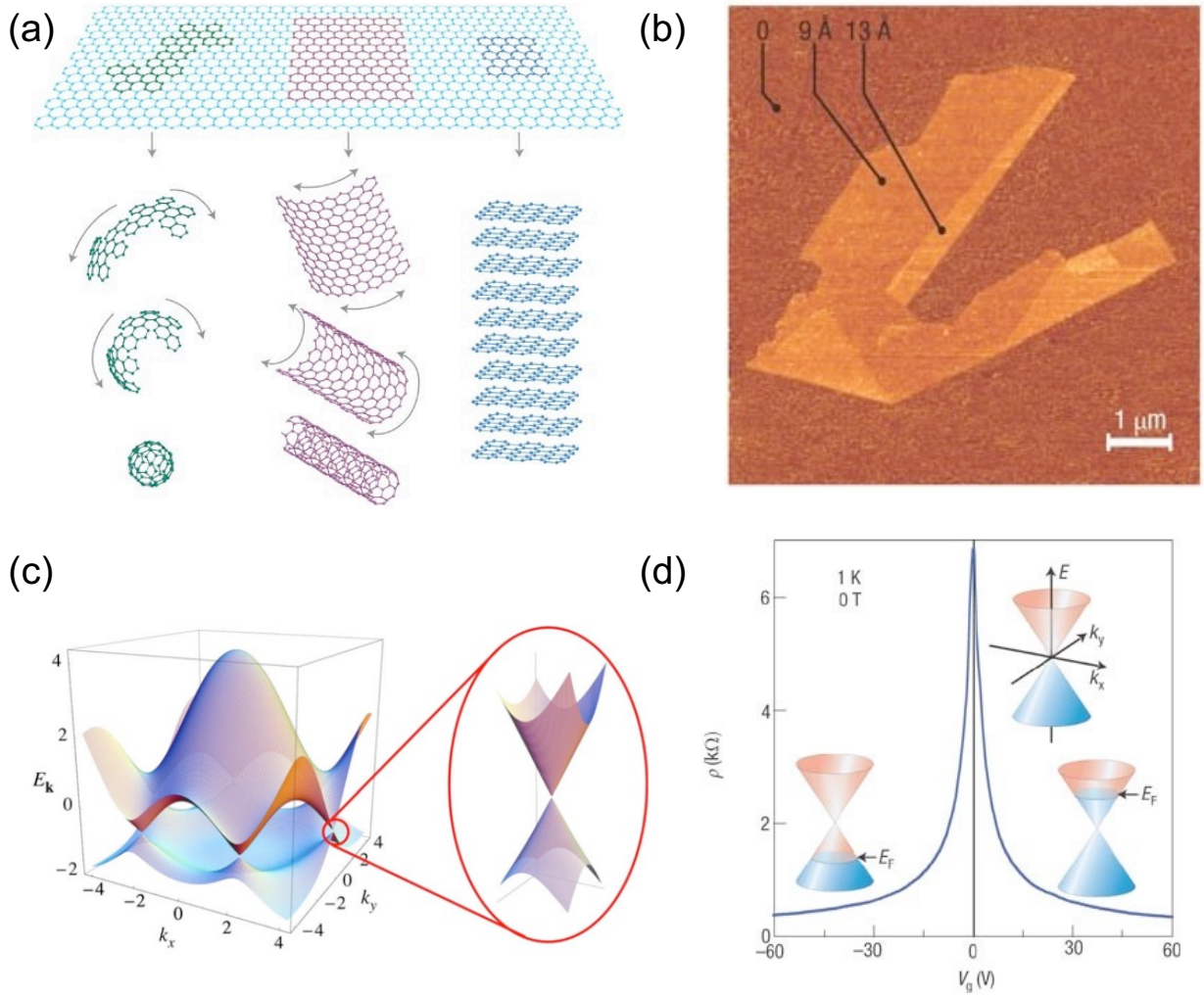

Figure 2. *(a) The crystal structure of graphene and its relationship with carbon materials of all other dimensionalities. (b) Atomic force microscopy image of one graphene flake showing the height of monolayer graphene as ~4 Å from the folded region. (c) Electronic dispersion of monolayer graphene. Right: zoom in of the energy bands close to one of the Dirac points. (d) The transfer curve of monolayer graphene transistor showing ambipolar transport characteristics. The insets show the shift of the Fermi energy E_F with changing gate voltage V_g. Figures are reproduced*

with permission from ref ([34]). Copyright 2007 Nature publishers and ref([30]). Copyright 2009 American Physical Society

2.2 Transition Metal Dichalcogenides

TMDs are a family of 2DMs with the general formula MX_2 (Figure 3a).[46,47] M is a transition metal atom, including groups 4, 5, 6, 7, and 10 transition metals; X is a chalcogen atom (S, Se or Te). Structurally, one layer of M atoms is sandwiched between two layers of X atoms and hence, the thickness of monolayer TMDs (~0.65 nm) is larger than that of monolayer graphene (~0.34 nm). TMDs exhibit diverse phase structures, including 2H (2 layers per Hexagonal unit cell), 1T (one layer per Trigonal unit cell), and 1T' phases (distorted 1T phase).[46] 2H-phase TMDs have a hexagonal lattice with D_{3h} symmetry (space group $P\bar{6}m2$), while 1T-phase crystals have a trigonal lattice with D_{3d} symmetry (space group $P\bar{3}m1$). The favored phase of TMDs is determined by the d-electron number in the transition metal (Figure 3b). Group 4 and group 10 TMDs with few or many d-electrons are prone to adopt the thermodynamically favored 1T phase with the d^2sp^3 hybridization in which fewer d orbitals are involved, while group 5 and group 6 TMDs with a moderate number of d-electrons tend to adopt the 2H phase with d^4sp hybridization in which more d orbitals are involved.[48] The number of d-electrons also determines the electronic band structure of TMDs. Figure 3b shows the qualitative location of non-bonding d bands of TMDs between the bonding and antibonding bands of the M-X bonds. With the increase of d-electrons from group 4 to group 10 TMDs, non-bonding d bands will be progressively filled, resulting in their different

electronic properties.[46] For example, group 5 and group 7 TMDs (e.g., 2H-$NbSe_2$ and 1T ReS_2) with partially filled orbitals exhibit metallic features, while group 4, group 6 and group 7 TMDs (e.g., 1T-HfS_2, 2H-MoS_2 and 1T-PtS_2) with fully occupied orbitals mostly display semiconducting properties. Although the electronic properties of TMDs are mainly determined by transition metals, the chalcogen atoms with increasing atomic number have been observed to reduce the bandgap.[49]

Reducing a TMD's thickness from bulk to monolayer causes dramatic changes in the band structure, including a shift of valence and conduction band edges, an increase in the bandgap, and an exceptional transition from indirect to direct bandgap semiconductor in Group 4 TMDs (Figure 3c).[50,51] In monolayer MoS_2, the valence band maximum and the conduction band minimum are located at the two inequivalent high-symmetry points K and K', which correspond to the corners of the hexagonal Brillouin zone (Figure 3d). This unique band structure enables the observation of valley-dependent physical phenomena and point to the potential applications of TMDs in valleytronics.[52,53] Furthermore, because of the spin-orbit interaction, the conduction and valence bands in monolayer TMDs show strong spin splitting. The spin splitting values in the valence band range from 0.15 eV in monolayer MoS_2 to 0.46 eV in monolayer WSe_2.[52-54] The lack of inversion symmetry of monolayer 2H TMDs results in the opposite spin splitting of bands at two inequivalent K and K' points, and this effect referred to as spin-valley coupling. It implies that the valley polarization of charge carriers is automatically translated into their spin polarization, which can be used to design spintronic devices.

The carrier mobility of monolayer TMDs has been predicted to be higher than that of conventional semiconductors at the ultrathin limit.[11] The room-temperature electron mobility of a monolayer MoS_2 transistor can reach over 150 $cm^2V^{-1}s^{-1}$ and the hole mobility of a monolayer WSe_2 transistor can exceed 250 $cm^2V^{-1}s^{-1}$.[55,56] These carrier mobilities can be further improved by mastering defect and interface engineering.

Besides their common semiconducting properties, some TMDs exhibit unique properties such as metallicity, superconductivity, magnetism, piezoelectricity, topologically protected states, etc.[46,57,58] These provide ample opportunities to design functional devices. Furthermore, the creation of 2D van der Waals (vdW) heterojunctions by combining distinct 2D layers is a powerful strategy to construct functional material systems with unique properties.[59] The dangling-bond-free surface of one 2D layer will interact with another 2D layer through vdW interaction. For instance, TMDs have been used as the tunneling barrier between two graphene layers to create a field-effect tunneling transistor (FETT).[60] Because the position of the Fermi level in graphene can be modified by the gating effect, a high I_{on}/I_{off} ratio in FETT has been achieved using MoS_2 (10^3-10^4) and WS_2 (10^6) tunneling barriers.[60,61] Benefiting from the large optical absorption and the controllable doping condition of TMDs, vdW heterostructures can form planar or vertical p-n junctions, acting as the basic element in optoelectronic devices, including photodetectors, photovoltaic devices and light-emitting diodes.[62] The concept of vdW heterostructure can be further extended to integrate 2DMs with non-2DMs (such as small molecules (0D), nanowires (1D), and bulk Si (3D)) through non-covalent interactions.[15] Small organic donor and acceptor molecules and photosensitive

molecules are the excellent building blocks in the field of flexible optoelectronics and electronics. The combination of organics with 2D TMDs to create 0D-2D vdW heterostructures is a viable strategy to bring together useful qualities of both systems, thereby extending the device functionality. Following a discussion of the engineering of TMD logic devices in Section 5, we will examine the construction of functional devices in Section 6.

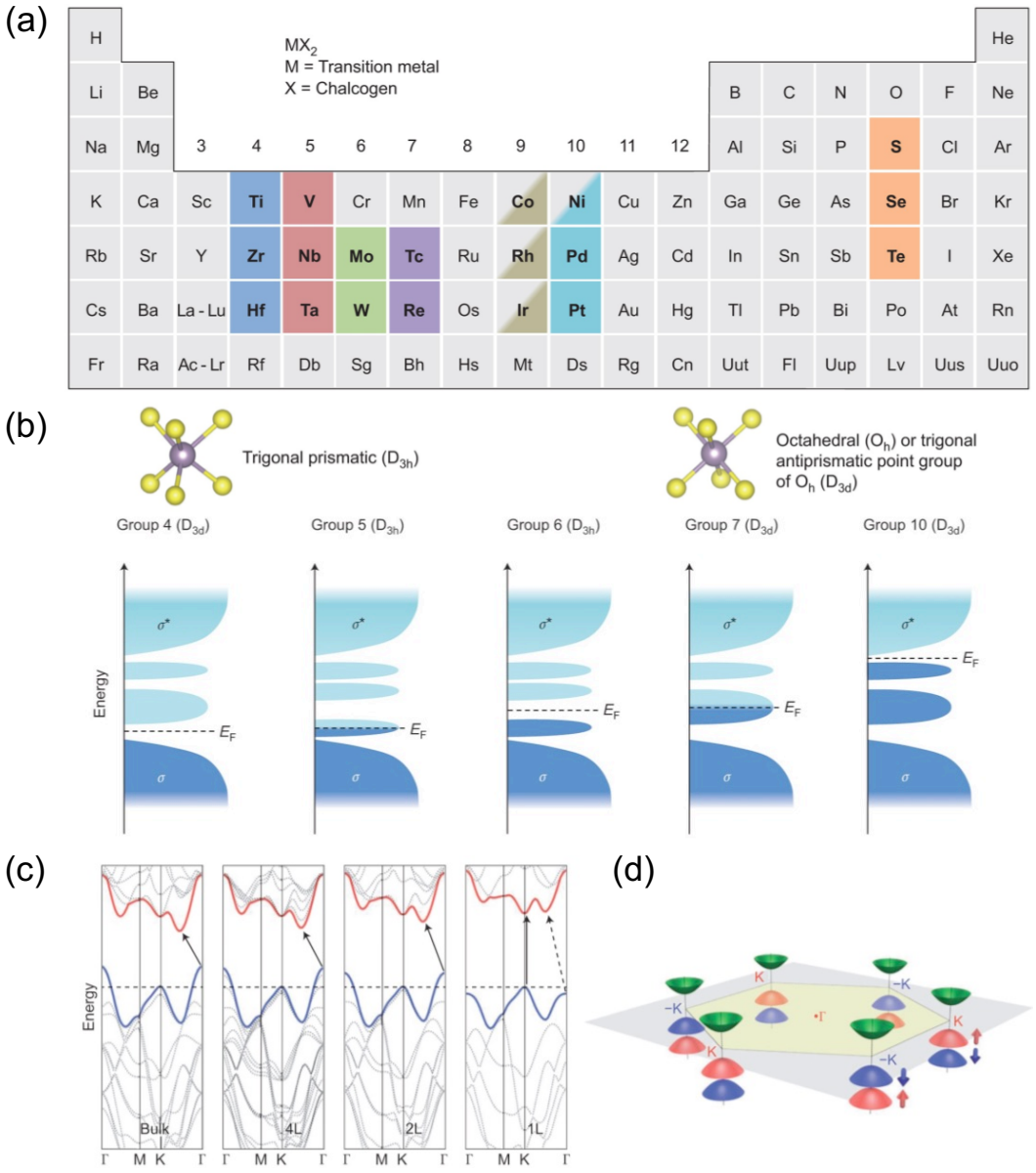

Figure 3. *(a) The material library of layered TMD compounds. (b) Qualitative illustration of band structure of group 4, 5, 6, 7 and 10 TMDs, showing the d-electron dependent crystal structure and the electronic property. (c) The layer-number dependent band structure of MoS_2, showing the transition from indirect to direct bandgap semiconductor. (d) Band structure of monolayer MoS_2 showing opposite spin–orbit splitting of the valence band in adjacent valleys at the K and −K (K')*

points. Figures are reproduced with permission from ref ([46]). Copyright 2013 Nature Publishing Group.

2.3 Black Phosphorus and Emerging Layered Materials

Black phosphorus (BP), the thermodynamically stable form of phosphorus, shows an orthorhombic pleated honeycomb structure. Each phosphorus atom forms sp^3 hybridization with the adjacent three phosphorus atoms. Because of the pleated atomic arrangement, two kinds of P-P bonding exist in the BP lattice, which are in-plane zigzag type and out-of-plane armchair type.[63] From the electronic band structure, BP shows a largely tunable direct bandgap ranging from 1.51 eV in the monolayer to 0.15 eV in bulk BP (Figure 4a).[64] Furthermore, the unique puckered crystal structure induces angle-dependent optical and electronic properties, enabling the design of novel polarization-dependent and angle-resolved optoelectronic devices. The theoretical hole mobilities of monolayer BP can reach values as high as 1.0×10^4 $cm^2V^{-1}s^{-1}$ to 2.6×10^4 $cm^2V^{-1}s^{-1}$ depending on the transport direction.[64] The experimental carrier mobilities of BP extracted from FETs are also higher than those of TMDs at room temperature (Figure 4b). The first reported BP FETs showed hole-dominated transport behavior with chromium as metal contact. The hole mobility of a 10-nm-thick BP FET is up to ~1000 $cm^2V^{-1}s^{-1}$.[63] Through channel doping, channel thickness selection and contact engineering, BP FETs have been tuned to exhibit highly-controllable unipolar or ambipolar transport behavior. Perello et al. reported that the 3-nm-thick BP FETs with aluminum metal contacts displayed unipolar n-type transport and an electron

mobility of 275 $cm^2V^{-1}s^{-1}$, while the 13-nm-thick device showed symmetric ambipolar transport with electron and hole mobilities of up to 950 $cm^2V^{-1}s^{-1}$.[65]

Apart from exhibiting the unique properties mentioned above, BP flakes have been found to seriously degrade in ambient conditions, which was attributed to their easy oxidation when exposed to O_2 gas (Figure 4c).[66,67] For this reason, flakes must be passivated for the processing and device fabrications stages. Wood et al. demonstrated that effective passivation of BP layer could be achieved by AlO_x coating and that devices with a passivation layer maintained the high I_{on}/I_{off} ratios and high carrier mobilities for over two weeks in ambient conditions.[68] Chemical functionalization has also been used to promote the ambient stability of BP nanosheets. The edges of BP flakes can be covalently functionalized with C_{60} molecules.[69] Owing to its hydrophobic character, C_{60} molecules can serve as a sacrificial shield and effectively protect BP nanosheets from oxidation under ambient condition. Although these passivation processes can suppress degradation in ambient conditions, the poor stability of BP flakes caused difficulties in device fabrication and processing, greatly inhibiting their use in logic and optoelectronic devices. Some other single element 2DMs, such as silicene, germanene, stanene, have also been observed to degrade quickly in ambient conditions.[70,71] Unlike bulk Si, whose mobility is greatly reduced in atomically thin layers, these 2DMs appear to retain their properties in the 2D limit. However, ultimately, a tradeoff between material's propensity to undergo degradation and complexity in the fabrication process becomes inevitable.

A series of emerging layered materials, such as tellurium (Te), bismuth (Bi), antimony (Sb), tin sulfide (SnS) and indium selenide (InSe), have been recently characterized at the atomically thin limit.[72] These materials exhibit several unique properties, including a tunable bandgap, high carrier mobility, and a high on/off current ratio in transistors. Most importantly, they have exhibited better environmental stability than BP, making them suitable for practical applications. Alongside the aforementioned 2DMs, some emerging 2D compounds have become extremely popular, including transition metal oxides, MXene, ternary 2DMs, metal–organic frameworks (MOFs), covalent organic frameworks (COF), etc.[73] These materials exhibit superior properties, which can boost the performance of electronic devices in various applications; however, their exploration is still in its infancy and molecular functionalization strategies have only been tested in very few works. Therefore, in sections 4-6 we will mostly focus on the molecular engineering of graphene, TMDs and BP. In section 7, we will highlight some recent works showing the potential of combining molecules and novel 2DMs to tailor the intrinsic physical properties of the latter, leading to particularly interesting results for advanced computing paradigms such as spintronics and quantum computing.

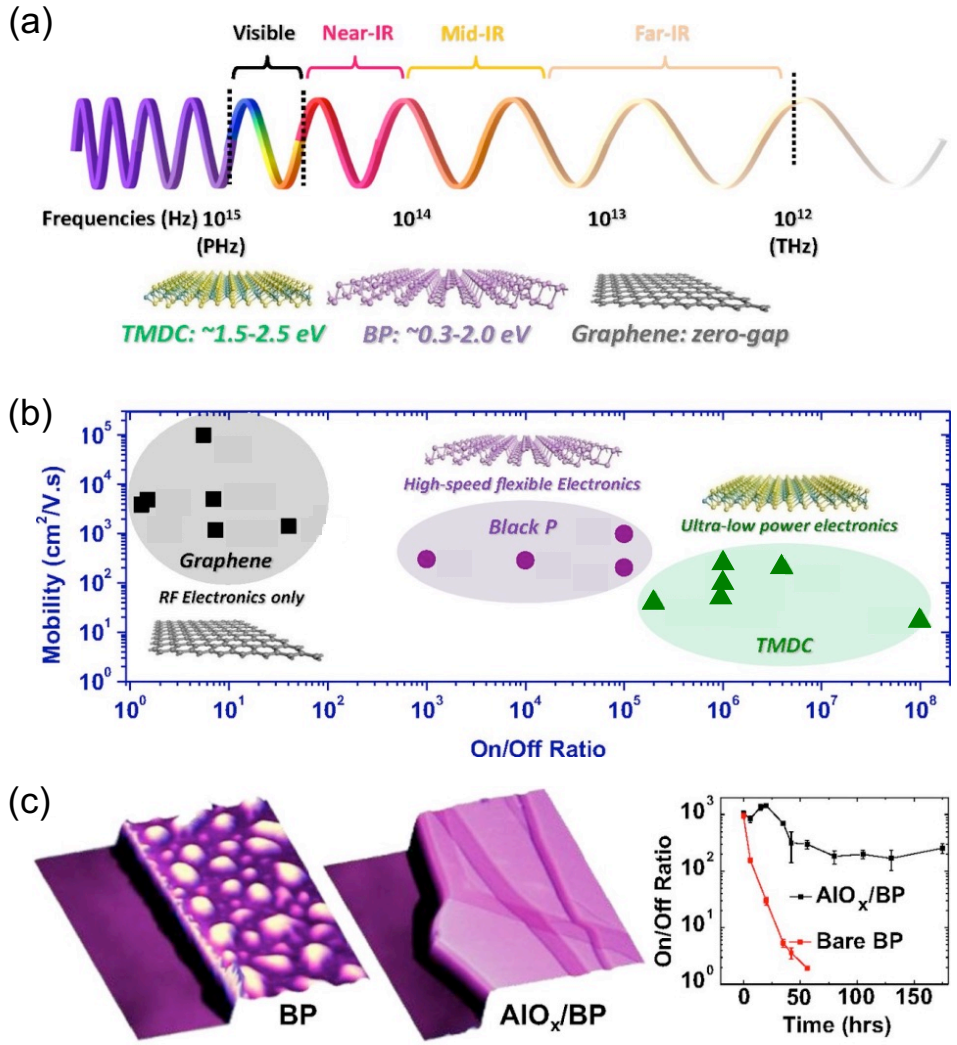

Figure 4. *(a) The bandgap of BP shows the large tunability from ~0.3 eV to ~2.0 eV, covering the spectral range from visible to mid-infrared. (b) The carrier mobility and I_{on}/I_{off} ratio of 2D transistors, including graphene (black squares), BP (purple dots), and TMD (green triangles) transistors. (c) Time-dependent characterization of BP degradation in ambient environment without and with AlO_x overlayer protection. Left: AFM images. Right: I_{on}/I_{off} ratio of BP FETs. Figures are reproduced with permission from ref ([66]). Copyright 2015 United States National Academy of Sciences.*

3 Organic Materials Commonly Used in 2D Devices

The full control of charge carrier concentration in 2DMs is mandatory to produce CMOS circuits. This is also essential for minimizing the contact resistance at metal–semiconductor interfaces and manufacturing logic devices (p-n junctions, inverters, etc.) with reproducible electrical characteristics. However, the conventional doping techniques, such as ion implantation and dopant diffusion, are too aggressive to be easily implemented on 2DMs, since the generated defects in 2DMs during the doping process will have detrimental effects on the electrical properties, resulting in degraded device performances.[74-76] This has been a real bottleneck in the realization of high-performance 2D CMOS devices. Various customized methods have been proposed to break through the limit,[77,78] such as alloying,[79] substitutional doping during growth,[80-83] plasma-assisted doping,[84] defect generation and engineering,[85,86] and molecular functionalization acting as adlayers.[87,88] Being essentially all surface, 2DMs are extremely sensitive to the variables of the surrounding environment, exhibiting distinct electrical properties.[89,90] Therefore, the use of molecular systems interfacing 2D sheets can effectively tune the carrier density via a non-destructive way, emerging as a promising versatile method. In Section 3.1, we will discuss a large variety of small molecules and polymers with tailored-made properties, which can be used to tune the characteristics of 2DMs.

As a particularly interesting case, we will focus on molecules characterized by dynamic properties, like molecular switches. Due to their unique functions, molecular switches have been

introduced into stimuli-responsive devices to confer them dynamic properties. Specific molecular groups in molecular switches possess optical, magnetic, and electronic properties that can be controllably toggled between two or more (meta-) stable states in response to external stimuli.[18,91] The combination of 2DMs with molecular switches have made possible to impart 2DMs with novel functionalities and new responsive capabilities, the latter being key for the realization of unprecedented devices displaying a stimuli-responsive nature. In Section 3.2, we will introduce the basic properties of three kinds of molecular switches.

3.1 Small Molecules and Polymers

The design and synthesis of (macro)molecules have made it possible to program their fundamental physical and chemical properties. In this way, unique properties can be transferred (partially) to 2DMs by simply interfacing these two components at the covalent or non-covalent level. Covalent bonds are more robust but are typically created by introducing structural defects on 2D monolayers, i.e. by modifying their electronic structure, thereby lowering their unique electronic characteristics. Moreover, specific chemically reactive groups should be used, sometime under stringent experimental conditions, to generate the covalent linkage, limiting the general applicability of the approach. Conversely, the use of non-covalent bonds via molecular physisorption onto the surface of 2DMs has the advantage of retaining the crystalline structure of the 2DMs unchanged, thus not affecting their outstanding electronic properties. Moreover, they feature less stringent requirements in terms of molecular design and experimental conditions for

the interaction to take place, usually via van der Waals forces and π–π stacking. The phenomena taking place at molecule/2DM interfaces will be discussed in detail in section 4.

Independent of the bonding nature, the organic molecules can intimately interact with 2DMs, inducing a doping effect on 2D layers. One major mechanism leading to the molecular doping is charge transfer. Charge transfer occurs when the energy level alignment between molecules and 2DMs complies with certain conditions. When the redox potential of the molecular dopant lies below the valence band maximum (VBM) of the 2D semiconductor, electron can transfer from the 2DM to the molecule, resulting in electron depletion (*p*-type doping);[92] *vice versa*, when the redox potential of the molecules lies above the conduction band minimum (CBM) of 2D semiconductors, electrons are transferred from the molecules to 2D layers, inducing electron accumulation (*n*-type doping).[93]

Based on numerous reports, typical functional groups can induce charge transfer between molecules and TMD layers. Molecules with the amine group (-NH_2), such as nicotinamide adenine dinucleotide (NADH)[92], mercaptoethylamine (MEA)[94], polyethyleneimine (PEI)[95], and hydrazine[96], are more electron rich, therefore being prone to donate electrons and showing strong n-doping effect on MoS_2. Molecules containing fluorine and fluorinated functional groups, such as 1H,1H,2H,2H-perfluorodecanethiol (FDT)[94], tetrafluoro-7,7,8,8-tetracyanoquinodimethane(F4-TCNQ)[92,97,98], and fluorinated fullerene ($C_{60}F_{48}$)[99], are more electron deficient, thus displaying a propensity to accept electrons and showing p-doping effect on group-6 TMDs. A class of metallophthalocyanine molecules (MPc, where M is the metal centre,

e.g. NaPc, MgPc, TiPc, FePc, NiPc, CuPc, PtPc, *etc.*) have shown advantages in doping TMDs due to their metal-center dependent redox potentials.[100] Based on the relative positions between the band edges of TMDs and the redox potential of MPcs, the direction of the charge transfer between the TMDs and the MPc molecules has been predicted .[100] For example, NiPc and MgPc were used to functionalize monolayer MoS_2, WSe_2 and $MoSe_2$ (Figure 5a). The PL spectra showed that the physisorbed NiPc molecules can quench the PL emission of $MoSe_2$ and WSe_2, but not MoS_2 (Figure 5b). This is because the reduction potential of NiPc is lower than the conduction band minimum (CBM) of monolayer $MoSe_2$ and WSe_2 but is higher than that of MoS_2. Based on the same principle, MgPc molecules only quenched the PL emission of WSe_2, not MoS_2 and $MoSe_2$ (Figure 5c). Interestingly, the work functions of the metal centers in MPcs determined their redox potentials. By *ad hoc* selecting appropriate MPcs, the carrier polarity of TMDs and the desired charge-carrier density in hybrid MPc/TMD systems can be easily achieved. For instance, NaPc induced *n*-type doping in WSe_2 and showed the ambipolar to electron-dominated unipolar transition in WSe_2 FETs, whereas FePc and CuPc resulted in *p*-type doping and hole-dominated unipolar transport.[101] A quenching in the PL of TMDs has also been reported for MoS_2 covered by thin films of the conjugated molecule diindenoperylene.[102] In most cases, this simple charge transfer model is adequate to explain the molecular doping effect, but some other factors can still affect the molecular doping on 2DMs, including hybridization and electrostatics, molecular orientation and thin-film morphology, non-frontier orbitals and defects, excitonic states, spin, and chirality.[103]

Dipolar interaction is another mechanism to tune the charge-carrier doping in ultrathin 2D layers. A molecule with permanent dipole moments exerts an electric field on the 2D-sheet surface, acting as a nanoscopic electric gate which modulates the local charge carrier density. When the dipole orientation from numerous molecules lying on the 2D surface point in the same direction, the electric field from single-molecule effects can sum up collectively leading to a macroscopic modification of the Fermi level of 2D layers. In particular, the formation of well-aligned molecular dipoles adjacent to semiconducting 2D layers played the crucial role in the realization of charge carrier modulation,[104] resulting in *p*- or *n*- type doping depending on the dipole direction.[105] Self-assembled monolayers (SAMs) of molecules via suitable structure design can be well packed on the targeted surface (SiO_2 substrate or 2D layers). The anchoring group promotes the chemisorption or physisorption on the targeted surface. Organosilanes can be covalently tethered to hydroxyl-covered surfaces (such as SiO_2) to form SAMs, stabilized by van der Waals interactions among neighboring long alkyl chains. The functional headgroup determines the direction of molecular dipoles. Experimentally (Figure 5d), Li et al. employed three kinds of SAMs with unique functional headgroups characterized by different dipole moments and polarities to cover the SiO_2 substrate.[104] The molecules used to form SAMs include octyltrichlorosilane (OTS, CH_3-SAM), 3-(trimethoxysilyl)-1-propanamine (APTES, NH_2-SAM), and trichloro-(1H,1H,2H,2H-perfluorooctyl)silane (FOTS, CF_3-SAM). Then mechanically exfoliated MoS_2 sheets were transferred onto different SAMs and the Fermi level shift was characterized by Kelvin probe force microscopy (Figure 5e). The upward (downward) shift of Fermi level on APTMS

(FOTS) substrate directly displays the n (p)-doping effect. The amine groups in APTES and the trifluoromethyl group in FOTS contributed to the out-of-plane molecular dipoles and caused a profound change of surface energy and electronic properties of 2D layers. In the work of Gobbi et al., the supramolecular lattice with a long alkyl chain was self-assembled lying flat on the basal plane of the 2DM surface.[106] The diazirine group was selected as the molecular headgroup because it can efficiently undergo photoactive reactions. The latter is accompanied by a change in the chemical nature of the headgroup, which determines a modification of the sign and of the magnitude of the molecular dipole moment, which ultimately leads to a controlled molecular induced doping effect on 2DMs via the dipole interactions. The design and construction of hybrid molecules/2D vdWs heterostructure provide a method to alter the electronic properties of 2D layers. In a recent work, Wang et al. reported a novel method to control the orientation and the magnitude of molecular dipoles via the supramolecular approach.[107] Metal phthalocyanine, such as ZnPc or CoPc molecules, were first self-assembled on the surface of MoS_2 and then pyridines were coordinated onto the surface of MPcs. The type and the position of substitution groups in pyridine rings showed pronounced effect on the control of dipole orientation and dipole magnitude, resulting in n- or p-type doping on MoS_2 layer.

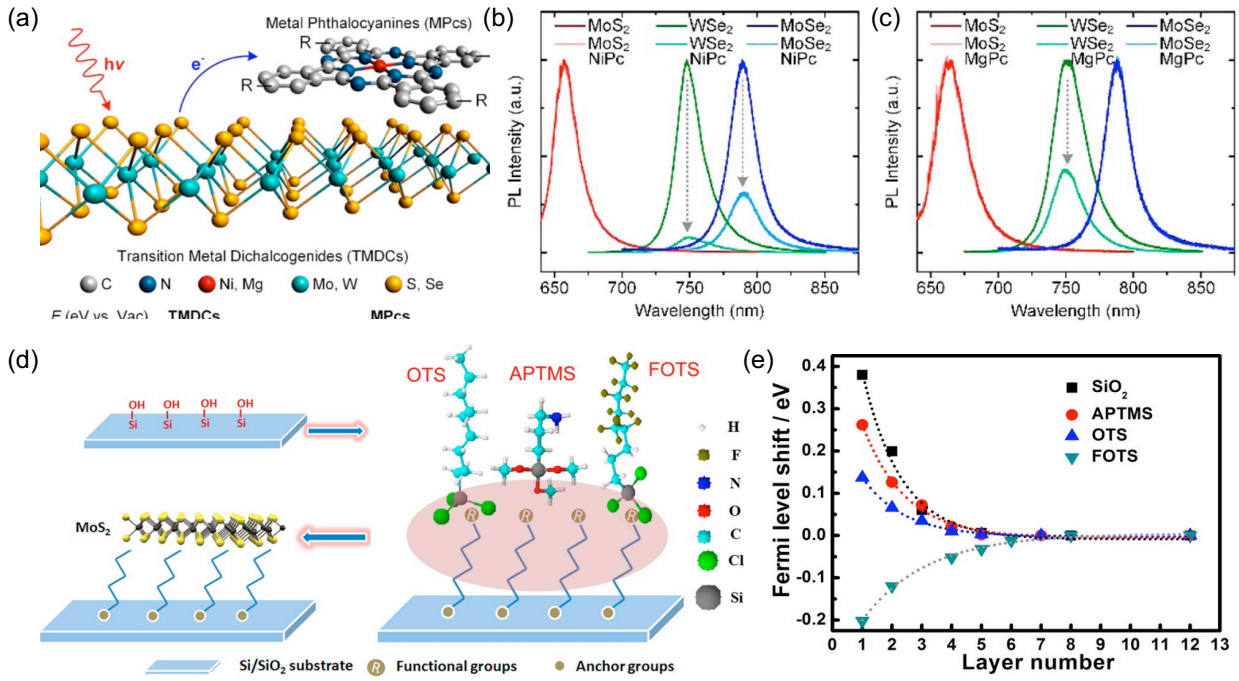

Figure 5. *(a) The relative position of band edges of MoS_2, $MoSe_2$, and WSe_2 with respect to the redox potentials of NiPc and MgPc. By selecting appropriate TMDs and MPc molecules, the optical and optoelectronic properties of TMDs can be effectively modulated. (b,c) PL spectra of MoS_2, $MoSe_2$, and WSe_2 before and after functionalization with (b) NiPc and (c) MgPc molecules. (d) Schematic illustration of surface functionalization of SiO_2 substrates with self-assembled monolayers of molecules and the transfer of MoS_2 onto the modified substrates. (e) The Fermi level shift of MoS_2 nanoflakes on various substrates as a function of the layer number. Four kinds of substrates are used including bare SiO_2/Si, SiO_2/Si functionalized with octyltrichlorosilane (OTS), 3-(trimethoxysilyl)-1-propanamine (APTMS), and trichloro(1H,1H,2H,2H-perfluorooctyl)silane (FOTS), respectively. (a-c) Reproduced with permission from ref ([100]). Copyright 2016 American Chemical Society. (d-f) Reproduced with permission from ref ([104]). Copyright 2013 American Chemical Society.*

In addition, considerable effort has been made to covalently connect 2DMs with molecules, in a scenario characterized by the sharing of electrons between the two components. Covalent functionalization on 2D layers can be performed by selective adsorption on edge and defect sites. Many studies reported that organosulfur compounds were used to adsorbed at sulfur vacancy sites of the MoS_2 surface (Figure 6a), including (3-mercaptopropyl)trimethoxysilane,[108] butanethiol,[109] bis(trifluoromethane)sulfonimide,[110] etc. The passivation of sulfur vacancies improved the electronic transport performance[108] and photoluminescence quantum yield[110]. Recently, the thiol functionalization was performed on monolayer WSe_2 with Se vacancies. [111] Scanning tunneling microscopy (STM) studies made it possible to demonstrate the successful adsorption of thiol molecules on the vacancy sites (Figure 6b). These works provided evidence that the thiol functionalization can act as a universal approach to boost the material properties. Beyond that, Vera-Hidalgo et al. presented a mild covalent functionalization method for the chemical modification of 2H-phase TMDs via a click reaction (Figure 6c).[112,113] The maleimide molecules are the prototypical electrophiles for sulfur-based nucleophiles, reacting through Michael addition, typically under mild conditions and orthogonally to most other functional groups. The robustness of this chemistry has been tested in the biochemistry and polymer chemistry realms, where it has become part of the "click" chemistry toolbox. The double bonds in maleimides readily react with the S atoms in TMDs to form a stable carbon-sulfur bond, as demonstrated through extensive characterizations. The thermal gravimetric analysis (TGA) of N-benzylmaleimide-functionalized

MoS_2 flakes (Bn-succ-MoS_2) showed a significantly higher desorption temperature of organic molecules when compared to physisorbed N-benzylmaleimide on MoS_2. The degree of functionalization was estimated to be 24 wt % by TGA.[112] In the XPS spectra, the S peak became significantly broader and an additional peak at lower energy 160.9 eV made a major contribution to the overall spectra (Figure 6d).[112] It demonstrated that the negative charge on the S atoms contribute to the electron extraction and to the formation of hypervalent S. This work introduced a novel methodology for the covalent functionalization of TMDs and improved the practical applications of chemically functionalized 2D flakes.

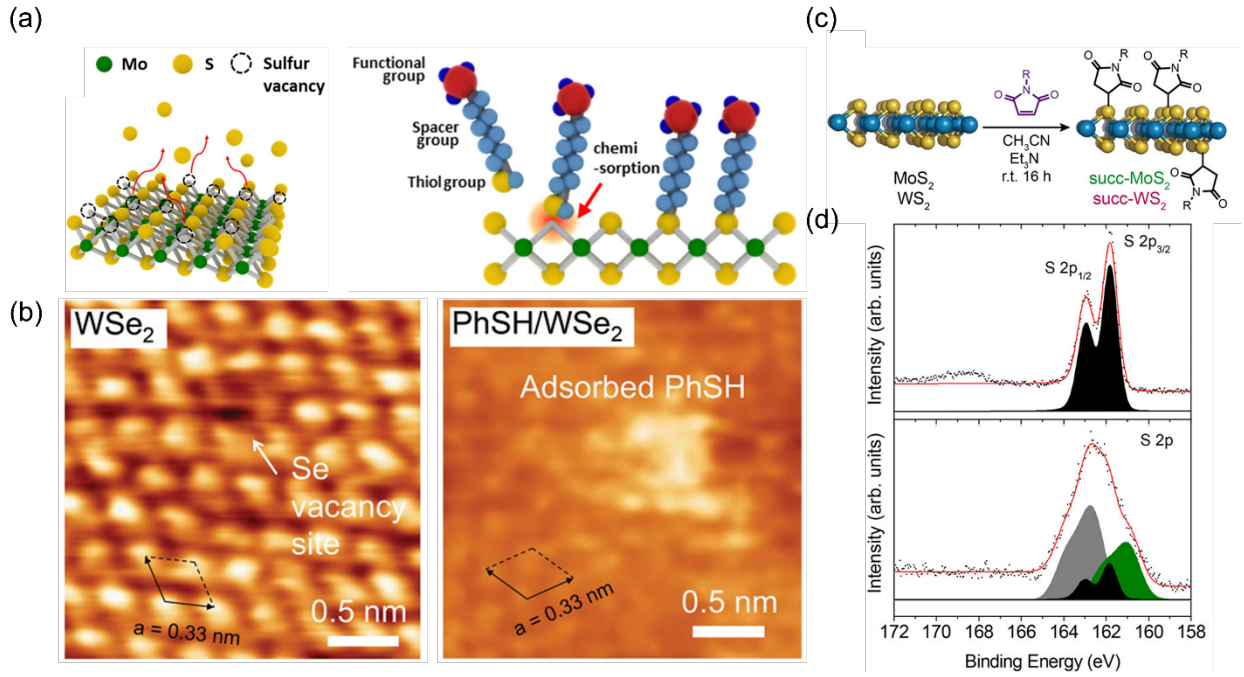

***Figure 6**. (a) Schematic of monolayer MoS_2 with sulfur vacancies (left) and chemisorption of thiol molecules onto sulfur vacancies (right). (b) Experimental scanning tunneling microscopic (STM) height image of the freshly exfoliated WSe_2 surface, showing the Se vacancy site (left), and the WSe_2 surface with the adsorption of thiophenol molecules (right). (c) Schematic illustration for*

the functionalization of TMDs with maleimides (R = Bn or Me). (d) XPS spectra of S $2p_{3/2}$ level for the bulk MoS_2 material (top) and N-benzylmaleimide-functionalized MoS_2 flakes (Bn-succ-MoS_2). (a) Reproduced with permission from ref ([94]). Copyright 2015 American Chemical Society. (b) Reproduced with permission from ref ([111]). Copyright 2020 Wiley-VCH. (c-d) Reproduced with permission from ref ([112]). Copyright 2019 American Chemical Society.

Polymer thin films have been widely utilized as encapsulation layers that have the advantage of high-yield, low-cost, and facile implementation to deposit from a processing perspective. In 2D devices, the engineering of the upper and bottom interfaces of 2DMs has been a crucial step to improve the device performance. Several kinds of polymer films have been used to perform the dielectric interface engineering and top surface encapsulation, such as CYTOP,[114] bisbenzocyclobutene (BCB),[115] poly(methyl methacrylate) (PMMA),[116] and poly(4-vinylphenol) (PVP)[117]. Compared with SiO_2, these polymer layers have less hydroxyl groups, thereby minimizing charge trapping and scattering. Recently, polymer layers with multiple functions have been demonstrated in several works. Zhang et al. reported that poly(4-styrenesulfonate) (PSS) induced the self-healing of sulfur vacancy in monolayer MoS_2 (Figure 7a-b).[118] The sulfur adatom clusters fulfilled the sulfur vacancy sites via a PSS-induced hydrogenation process. From the PL spectra, the self-healed region displayed enhanced PL emission intensity due to the decreased n-type doping from sulfur vacancies (Figure 7c-d). In this device, the electrically conductive PEDOT:PSS simultaneously acted as electrode and as carrier density modulation layer. Pagaduan

et al. synthesized sulfobetaine-based zwitterionic random copolymers with variable substituents (Figure 8a-b). The orientation of molecular dipoles relative to the graphene sheets was adjusted via suitable structure design and thus, the surface potential of polymer/graphene system was modulated via the selection of substituents.[119] Ultraviolet photoelectron spectroscopy (UPS) characterizations showed that the polymer zwitterions induced a significant work function reduction on monolayer graphene corresponding to the n-doping of graphene (Figure 8c-d). PMMA with a small molecular dipole (1.7 D) produced the smallest work function shift (0.15 eV for 1 nm film), while polymer zwitterions with piperidinyl-substituents exhibited more pronounced work function reduction (0.45 eV for 1 nm film).[119] The piperidinyl-substituted version produced the largest dipole perpendicular to the graphene basal plane, thereby inducing the maximum work function reduction. Meanwhile, the polymer zwitterions as the negative-tone resist were directly patterned via photolithography and simultaneously modulated the work function of 2D layer with high spatial resolution.

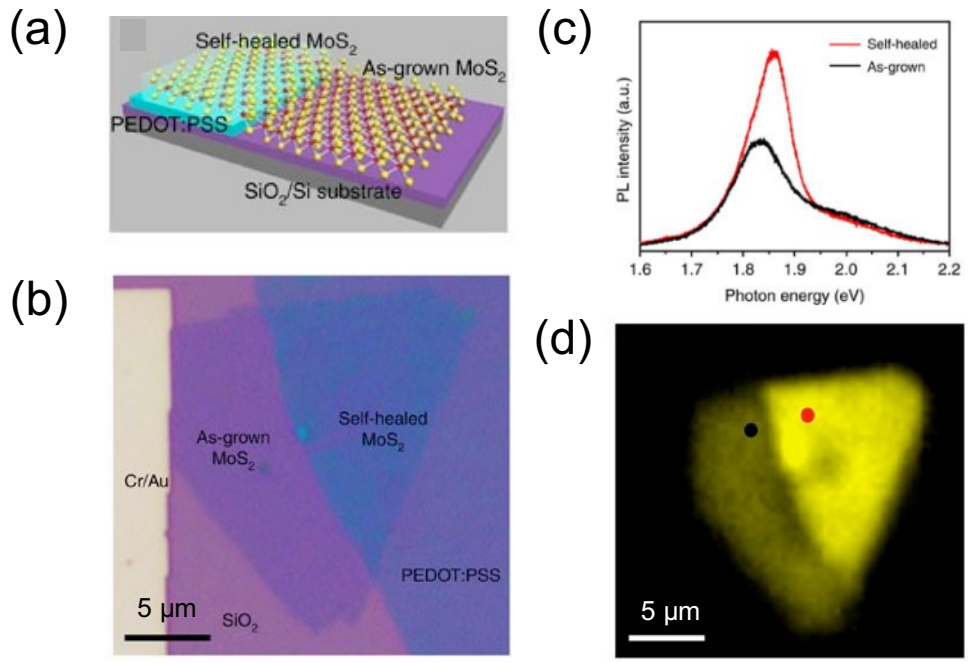

***Figure** 7. (a) Schematic and (b) optical microscopy image of the pristine and poly(4-styrenesulfonate) (PSS) functionalized MoS_2 flake. (c) Photoluminescence spectra and (d) peak intensity mapping of the pristine and self-healing MoS_2 flake. Reproduced with permission from ref ([118]). Copyright 2017 Nature publishing group.*

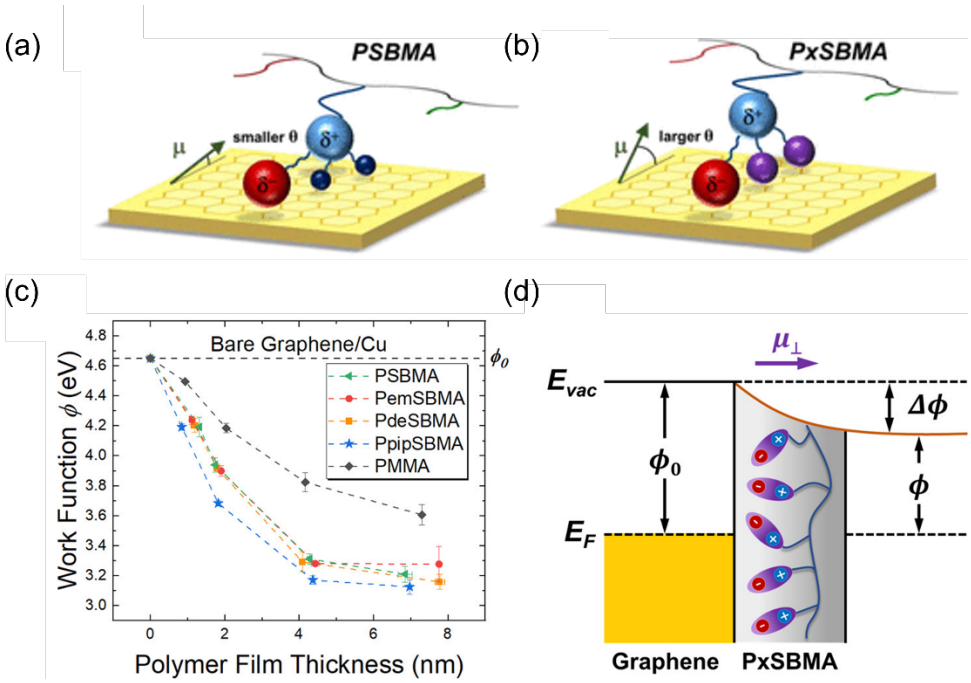

Figure 8. *(a) Illustration of poly(sulfobetaine methacrylate) (PSBMA) on monolayer graphene, showing the dipole moment μ and dipole orientation θ. (b) The dipole orientation θ can be modulated by selection of ammonium substituents. (c) Comparison of work function ϕ of PMMA- and zwitterionic polymer-coated graphene measured by UPS. (d) Illustration of interface dipole induced by contacting graphene with polymer. Reproduced with permission from ref ([119]). Copyright 2021 American Chemical Society*.

Another important category of functional polymers is ferroelectric polymers, which includes among others polyvinylidene fluoride (PVDF) and its copolymers. They exhibit spontaneous electric polarizations which can be switched by an external electric field.[120] In β-phase PVDF, the repeat unit is (CF_2-CF_2) with all-trans conformations. Thus, it is highly polar and their dipoles point to the same directions, exhibiting the strong ferroelectric properties. Under the external

electric field, the electric polarization of PVDF can be switched between different directions. The electric polarization can maintain a nonzero value when the applied electric field decreases to zero, rendering it ferroelectricity. The remnant polarizations of the ferroelectric polymers at zero field show either upward or downward dipole orientation, which can be denoted as "1" or "0" in the binary non-volatile memory system.[121] Therefore, several groups have constructed hybrid heterostructures composed of 2D semiconductors as the channel layer and the ferroelectric polymers as the gate dielectric materials.[122-125] As both 2D materials and ferroelectric polymers are flexible, the 2D ferroelectric memories show promising applications in the emerging fields of flexible and wearable electronic devices. We will discuss more details about device applications in section 5.

3.2 Molecular Switches to Impart Specific Functions to 2D Materials

Any chemical system that can be controllably interconverted, by means of external stimuli, between at least two forms possessing different spectral, electrochemical, or magnetic properties can be regarded as a molecular switch. Moreover, these forms should be relatively stable, and the transition of one into the other should not proceed spontaneously, but only upon stimulation with chemical, optical, electrical, or magnetic inputs. The physicochemical processes behind may be very different: energy level rearrangement upon protonation/deprotonation, geometrical isomerization, proton transfer, changes in electron distribution (valence isomerism), spin state changes, bond formation/cleavage (the consequence of chemical reactions), photoexcitation,

oxidation/reduction, or specific interactions with ions and molecules. In this section, we will review the basic principles of several kinds of molecular switches, including photochromic molecules, redox switchable molecules, and spin/magnetic switches. We will discuss their switching behavior, the switching mechanism, and their unique properties, etc.

3.2.1 Photochromic Molecules

Photochromic molecules undergo reversible isomerization between two states characterized by different absorption spectra with exposed to light at specific wavelengths (Figure 9a).[126] Consequently, the photoinduced isomerization is accompanied by a change in color which can be appreciated by naked eyes. Apart from the optical absorption, several other molecular properties are modified upon isomerization, including the steric hindrance, the energy levels, the polarity and the electrical conductivity.[127-130]

Photochromic molecules have been the subject of intense study in very different disciplines, from biology[131] to electronics,[132] since they offer the possibility to reversibly modulate and configure the nanoscale properties of materials using an external stimulus. The use of light as the external stimulus is particularly appealing, since it is a non-invasive tool which allows changes with fast temporal resolution and diffraction-limited spatial resolution (typically 500 nm – 1 μm). There are several organic molecules displaying photochromism, such as azobenzenes (AZO),[127,130] diarylethenes (DAE),[128] spiropyrans/merocyanine (SP/MC),[129] stilbenes,[133] fulgides,[134] hydrazones,[135] indigoids.[136] In each of them, the photo-isomerization determines specific changes in the molecular properties. As a result, each family of photochrome has its own relevance for given applications. For example, AZOs are characterized by a large conformational change,[127,130] and are therefore ideal for imposing major mechanical movements; DAEs feature important changes in the position of the energy levels,[128] so they are particularly intriguing for applications involving charge transfer and charge transport; SP/MC

exhibit a large change in the molecular electrical dipole,[129] which can be extremely useful to modify the dielectric environment of materials.

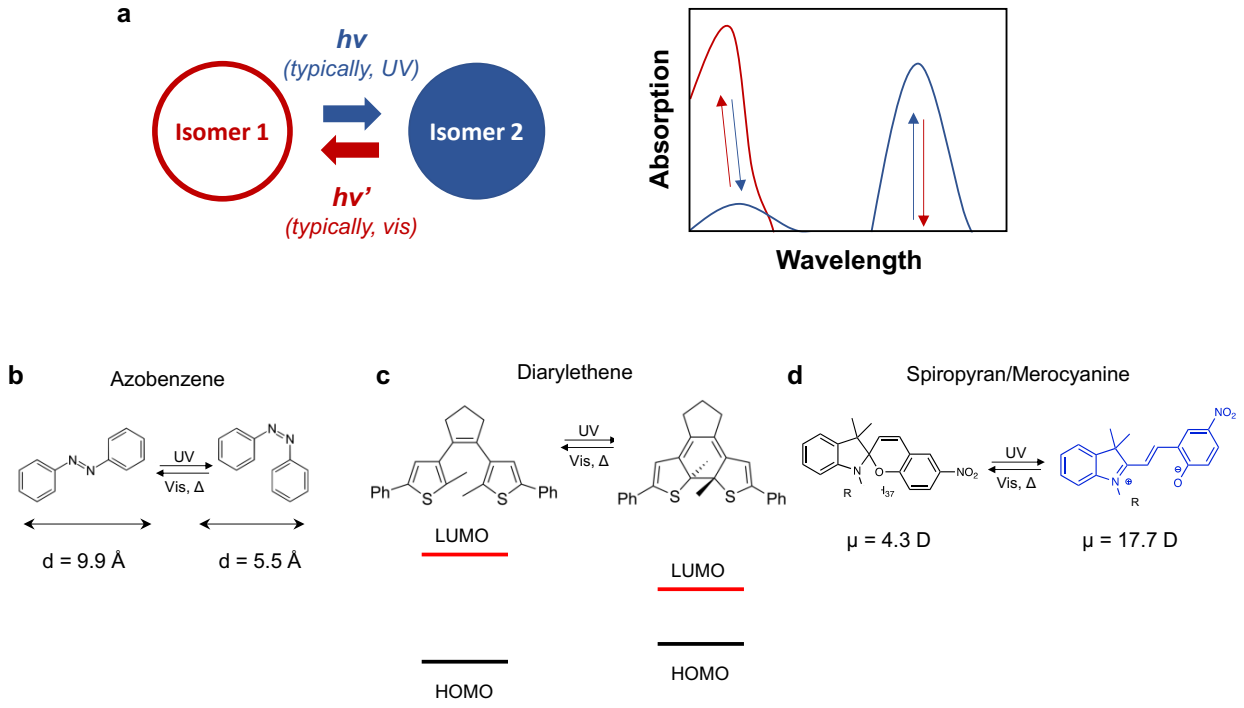

Figure 9. *Photochromic molecules. (a) Schematic of the photoisomerization process. Reversible isomerization between two (meta)stable states characterized by different absorption spectra is achieved using light irradiation at different wavelength. Chemical structure of (b) azobenzene, (c) diarylethene, and (d) spiropyran/merocyanine. Underneath each molecule, the main physical parameter modified upon the isomerization is highlighted, which is the structural conformation for azobenzene, the conjugation and the position of electronic levels for diarylethene, and the molecular dipole for spiropyran/merocyanine.*

In this section, we will first describe the photochemical properties of AZOs, DAEs and SP/MCs, which have been frequently used in combination with 2DMs. Then, we will introduce the reader to

different methods to integrate photochromic molecules in electronic devices, highlighting how their combination with 2DMs, which will be reviewed in detail in section 4 and 6, represents a highly promising approach to confer new properties to the 2DMs. Finally, we will discuss how the dynamic properties of photoswitches are modified on surfaces, which is particularly important for the hybrid interfaces between 2DMs and photoswitches.

3.2.1.1 Azobenzenes

AZO contains two phenyl rings connected by a N=N double bond. Exposure to light both in the visible range and in the UV region promotes the reversible isomerization between the more extended *trans* form and the more compacted *cis* state and vice versa, respectively (Figure 9b). In most azobenzene derivatives, the *trans* configuration is thermodynamically stable, so that in equilibrium, in dark and at room temperature, the vast majority of molecules are in their *trans* state.[127,130] A significant fraction of the *cis* isomer can be produced upon irradiation with UV light (typically, < 350 nm); the *cis* → *trans* back isomerization occurs thermally in view of the thermodynamical stability of the *trans*-AZO, and it can be accelerated through irradiation with visible light (typically, 450 nm). At the single molecule level, the *trans* → *cis* photoisomerization occurs on the picosecond timescale;[137] the average thermal lifetime of the metastable *cis* state in solution is much longer, as it ranges from microseconds to days at room temperature.[130] There are also a few cases in which the *cis* isomer is the most thermodynamically stable.[138]

Similar to other photochromic molecules, the *trans* and *cis* states are characterized by different absorption spectra. In particular, the absorption of the *trans* state is characterized by a

strong UV band which corresponds to the $\pi \rightarrow \pi^*$ transition, and a much weaker band in the visible, which corresponds to the $n \rightarrow \pi^*$ transition. For the *cis* state, the $\pi \rightarrow \pi^*$ band is weaker, and the $n \rightarrow \pi^*$ stronger. Irradiation with UV light triggers the *trans* → *cis* isomerization, but since the absorption bands partially overlap, it also induces the opposite *cis* → *trans* transition (albeit often with less efficiency). As a consequence, the *trans* → *cis* switch is not quantitative, and continuous irradiation of *trans*-AZO with UV light results in a photostationary state composed of a significant fraction of *cis*-AZO and a residual population of *trans*-AZO. Typically, the fraction of *cis*-AZO in the photostationary state varies for different AZO derivatives in a range between 70 % and 95 %,[130] depending on the isomerization quantum yield and on the lifetime of the *cis*-AZO, and it can be tuned by the light irradiation wavelength and power. Similarly, the visible-light-induced *cis* → *trans* reconversion is not quantitative; on the contrary, the thermal recovery of the *trans* state returns an essentially 100 % population of *trans*-AZO, due to its thermodynamical stability.[127]

What makes AZO compounds unique among other photochromic compounds is the large change in shape which accompanies the isomerization. While the *trans* isomer is planar,[139,140] the phenyl rings in the *cis* state are twisted at an angle of approximately 55° relative to each other. Moreover, the end-to-end distance in the *cis* isomer is 3.5 Å shorter than in the *trans* state.[140] For this reason, AZO have been commonly used whenever a mechanical movement is required, for instance in actuators,[141] nanomachines[142] and in several biological systems.[131] More importantly

for electronics, the two states possess different dipolar moments,[140] and the difference can be engineered through molecular design by inserting polar functional groups.[143-145]

The advantages of AZO include its structural simplicity, facile synthesis and low rate of photobleaching, combined with a very limited fatigue resistance after several cycles of irradiation.

3.2.1.2 Diarylethenes

The photoisomerization in DAE involves a ring opening/closing reaction which introduces a large modification in electronic configuration, and consequently, a change in the energetic position of the HOMO and LUMO levels (Figure 9c).[128,146] While the π-conjugation for the open-ring isomer is localized on the thiophene rings, it delocalizes across the molecule for the closed-ring isomer. As a consequence, the light absorption changes dramatically. While the (transparent) open-ring isomer does not absorb in the visible range, the (colored) closed-ring isomer presents an absorption band typically centered at 540 nm, which can be shifted significantly through the insertion of opportune substitutional groups in the molecular structure.[147] Apart from light irradiation, the ring opening/closing reaction can be triggered by an electrochemical stimulus,[148] providing DAE with multi-responsivity.

DAE derivatives are characterized by several properties which compare very positively with those of other photochromic molecules. Unlike AZO derivatives, both isomers in DAE are thermodynamically stable[149] and the photoisomerization in the two directions can be complete (approaching 100 % quantum yield).[128,146] At the single molecule level, the ring opening and closing events occur on the timescale of a few tens of ps, which is highly appealing for ultrafast

electronics.[150] Additionally, DAE exhibits very high fatigue resistance. Indeed, while it is known that for some derivatives a photo-inactive byproduct is irreversibly generated by prolonged irradiation with UV light,[151] this effect can be understood and minimized by molecular design.[152] As a result, some DAE derivatives were reported to undergo more than 10^4 switching cycles without degradation.[128,146,153]

Perhaps the most distinctive feature of DAE is the shift in energy of the HOMO and LUMO levels which accompanies the isomerization. This characteristic offers the opportunity to use the photonic input to switch on and off charge and energy transfer between DAE derivatives and other materials in their proximity. Indeed, charge and energy transfer depend on the energy level alignment between the chemical species involved in the process, which is modified during the irradiation process. By exploiting the optically tunable charge and energy transfer, DAE derivatives have been used to modulate the fluorescence of chromophores and the charge transport in polymers.[154-156] Importantly, the position of the HOMO and LUMO levels of both DAE isomers can be engineered at the synthesis stage[147] for tuning the energetic coupling to target systems. For this reason, DAE are also particularly attractive to act as light reversible dopant species for 2DMs, as detailed in section 6.1.

3.2.1.3 Spiropyran/Merocyanine

Spiropyrans are composed of an indoline and a chromene group oriented orthogonally to each other and connected by a single C atom in a spiro architecture.[129] UV irradiation induces a ring opening event resulting in a planar zwitterionic compounds named merocyanine (Figure 9d).

Similarly to DAEs, the photoisomerization is accompanied by a redistribution of the electronic charge density, with the merocyanine state characterized by a more extended π-conjugation delocalized between the indoline and the chromene moieties. As a consequence, the absorption spectrum is drastically modified, as the SP isomer is characterized by an absorption band in the UV, and the merocyanine by a band typically at 550-600 nm. Likewise AZOs, the MC isomer has a limited stability and switches back to SP at room temperature; such back switch can be accelerated through light irradiation in the visible. Even in this case, the photoinduced SP → MC switch is ultrafast at the single molecule level (ps),[12] while the average lifetime of the MC isomer is longer and depends on the solvent polarity. The SP → MC switch can be achieved through a variety of inputs, including electrochemical stimuli, or the addition of different solvents, metal ions, acids and bases.[129] In this regard, SP/MC are not only photochromic, but truly multiresponsive molecules. Unlike most AZO, the conversion yield of the SP→ MC isomerization can reach 100%.

Importantly, the MC and SP isomers are characterized by very different physicochemical properties and, in particular, by a very different electrical dipole. The zwitterionic character of the MC results in a significant molecular dipole on the order of 15 – 17 D, which is much larger than that of the SP (approximately 4 – 6 D). This characteristic makes spiropyran particularly suited for applications in which the generation of nanoscopic electric fields is required. In the context of electronics, SP/MC serve as molecular gates, generating electric fields which can modify the current flowing in a nearby material. In addition to molecular dipole and conjugation, the SP and

MC isomers are also characterized by a markedly different shape, with the planar MC isomer occupying more volume than the non-planar SP.[157]

It is worth noticing that the SP/MC isomers are not the only (meta)stable states which can be reached by the molecule. The basic MC isomer can undergo reversible protonation/deprotonation, offering the possibility to reach yet another stable state, again characterized by different physico-chemical properties.[129] While on the one hand the rich chemical activity of SP/MC isomers offers multiple control knobs to modify different molecular properties, on the other hand it leads to side reactions, such as irreversible oxidation, ultimately yielding to photo-inactive byproducts.[158] As a consequence, SP/MC possess limited fatigue resistance, which is perhaps their main drawback. This issue can be partially solved by working in controlled atmospheres or immobilizing MC/SP via covalent bonds on surfaces,[129] which is a strategy often followed also for applications in electronics.

3.2.1.4 Photochromic molecules for electronics

The light responsive nature of photochromic molecules is highly intriguing for electronics, as it offers a mean to modulate the electrical conductance of devices using an optical stimulus, thus employing light as an unconventional gate electrode. Per se, a photo-induced change in the conductance of a device is not uncommon, as in most conventional semiconductors light irradiation increases the conductance by generating extra charge carriers via photon absorption. However, in semiconductors the photo-generated extra current typically vanishes when the light irradiation is switched off. What makes photochromic molecules unique for electronics is their

optical memory effect, in turn directly related to the (meta)stability of their two states, which makes it possible to maintain the light-induced change in conductance even after the removal of the optical stimulus. In this regard, photochromic molecules are highly interesting as they offer the opportunity to generate multistate memory elements in which light (or other stimuli, as discussed in the previous section) is used to write/erase information.

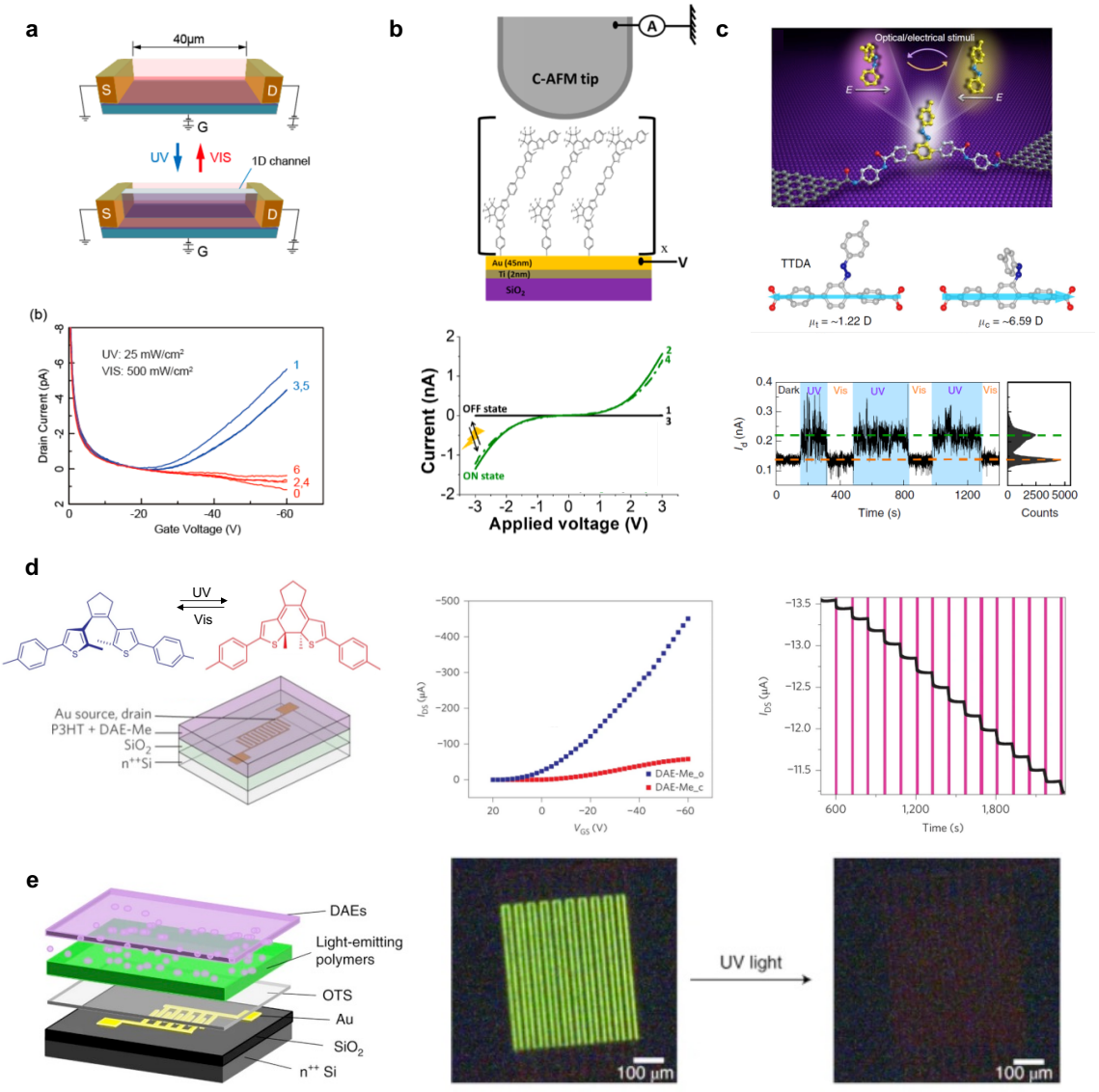

Figure 10. *Photochromic molecules for opto-electronics. (a) Transfer characteristics of a field-effect transistor employing a DAE thin film as active channel. Light irradiation triggers the reversible opening/closing events in the DAE film, introducing a modification in the current flowing in the device. In all cases, the current is very low (< 10 pA) due to the bad charge transport properties of diarylethenes. (b) Current-Voltage characteristics measured across a DAE multilayer on Au using a conductive AFM tip. Light irradiation enables the switch between two resistance states characterized by an ON/OFF ratio above 300 for 9-nm-thick films. (c) Electrical current flowing through a single molecule contacted by two graphene electrodes. An AZO side group acts as a gate electrode, modulating the current flowing in the molecular backbone. (d) Organic field-effect transistor based on a p-type semiconducting polymer blended with a DAE derivative. Light irradiation causes a change in the current flowing in the transistor; multiple resistance states were achieved by switching only a fraction of the DAE molecules in the active channel. (e) Interfacing DAE with light emitting polymers offers the possibility to modulate not only the current flowing through the device, but also the light emission. (a) Reproduced with permission from ref ([159]). Copyright 2016 American Chemical Society. (b) Reproduced with permission from ref ([160]). Copyright 2020 American Chemical Society. (c) Reproduced with permission from ref ([161]). Copyright 2019 Nature publishing group. (d) Reproduced with permission from ref ([156]). Copyright 2016 Nature publishing group. (e) Reproduced with permission from ref ([154]). Copyright 2019 Nature publishing group.*

Perhaps the most straightforward approach to exploit the photochromic switch in electronic devices involves the use of photochromic molecules as charge transporting material in an organic field-effects transistor architecture. However, this approach has been hampered by the poor electrical performances of photochromic molecules, which are not capable to transport charge carriers efficiently. As an example, Figure 10a displays the transfer characteristics of an OFET composed of a DAE film as charge transporting material.[159] This device structure permitted the authors to demonstrate the modulation of the current flowing in the active layer using both back gate and light irradiation. Interestingly, the use of a focused laser enabled the irradiation of a spatially confined region of the DAE film, resulting in a local modification of the conductance of the molecular layer. However, even in the best conditions, the measured current was below 10 pA, providing evidence for the modest capability of DAE thin films as charge conductors.

A different situation was encountered whenever charges move transversally across ultrathin molecular (mono)layers,[160,162-167] or in single molecule junctions.[161,168-174] In these cases, the charge transport does not need to be very efficient, as the conductance is dominated by quantum tunneling.[175] The first experiments studying charge transport across monolayers of photochromic molecules were performed more than ten years ago.[163-165] In several studies, a monolayer of photochromic molecules covalently bound to a conductive substrate was contacted by a soft top electrode, for instance a drop of a liquid (semi)metal,[162,167] a conductive polymer,[164] a conductive AFM tip[160,163,165] or a graphitic layer[166]. In these structures, which differ substantially in terms of area and therefore in terms of number of probed molecules, the tunneling current flowing vertically

across the photochromic layer is recorded from the bottom substrate to the top electrode, and it is modulated through light irradiation. The conductance of AZO,[163,165] DAE[160,164,166] and SP/MC[167] has all been tested using this device architecture; in all cases, a large difference in the current flowing in the device was measured for the two isomers. The different resistance measured in the different cases was ascribed to different effects, depending on the photochromic molecule. In particular, the large conformational change of AZO causes a modification of the thickness of the molecular layer, and thus of the tunneling distance, which is shorter for the *cis* than for the *trans*; the large change in DAE conjugation results in a modified single-molecule conductance, leading to a more efficient electron transport for the closed form; for SP, the change in electrical dipole and molecular length result in a higher current for the MC isomer. Recently, conductive AFM was employed to investigate the evolution of the charge transport across ultrathin layers of photochromic molecules of different thicknesses.[160] In particular, thin layers of DAE derivatives were covalently grafted on gold and glassy carbon conductive substrates by electrochemical reduction of a diazonium salt, resulting in films with variable thickness in the range 3-9 nm (Figure 10b). The charge transport across the layers was studied using the tip of a conductive AFM as a top electrode. The authors found that while in 3-nm-thin layers the ratio between the conductance of closed and open form was only 3, in 9-nm-thin layers it increased to above 300. This finding was explained as a non-complete isomerization in the first layer in contact with the conductive substrate, decreasing the light-induced change in resistance.

The conductance across single molecules was accessed either in STM studies or in lateral devices.[161,169-174] In the first case, an STM tip is used to probe the charge transport across a single molecule on a conductive substrate; in the second case, individual molecules are contacted by two electrodes separated by a narrow gap developed by means of a break-junction approach.

DAE are often used as ideal conductance switches,[169-174] as the π conjugation extending over the closed isomer provides a large extent electron delocalization, which favors charge transport in comparison to the highly insulating non-conjugated open form. While pioneering experiments were performed almost 20 years ago,[169,170] several steps forward were made recently in terms of performances and reproducibility of single-molecule devices. For instance, the use of graphene electrodes[172] enabled to demonstrate lateral single-molecule devices in which the conductance could be switched reversibly and cycled between two stable states. More recently, another interesting approach was put forward to modulate the current flowing in a single-molecule device using an AZO derivative.[161] In this case, the electrical current flowed across a molecular backbone onto which the photochromic molecule was embedded in a lateral position (Figure 10c). The photo-induced modification in the dipole of an AZO moiety resulted in an electric field effect which modulated the electrical current similarly to a gate terminal. This approach demonstrated how photochromic molecules can be used not only as charge transport media, but also to modify the conductivity of a material in their proximity, permitting to overcome the limitation of poor charge transport.

This possibility has been widely explored by interfacing photochromic molecules with other organic compounds displaying efficient charge transport characteristics. [154-156,176-178] For these studies, polymers FET with SP or DAE as photochromic moiety have been commonly used. DAE derivatives are designed and synthesized with their HOMO within the polymer energy gap when in the closed form, and outside the band gap when in the open form. Under such scenario, the closed-DAE isomers act as charge trapping sites which decrease the charges available for electrical transport, while open-DAE do not interfere significantly with the charge transport. As a result, the open $\rightarrow$ closed isomerization causes a remarkable decrease in the current through the transistor. Based on this concept, Leydecker et al.[156] demonstrated 256 conductance levels in a polymer/DAE device, obtained through an optimized light irradiation with low areal power density to trigger the isomerization of a modest fraction of molecules in each laser pulse, thereby yielding to a 8-bit memory (Figure 10d). In a more recent work, a single device acting as a 11-bit memory element was demonstrated by combining a polymer/DAE blend with a ferroelectric polymer.[179] Another interesting option was demonstrated by Hou et al.,[154] who combined light-emitting polymers with DAE. In this case, the decrease in current related to the UV-induced open $\rightarrow$ closed isomerization caused a quenching of the light emission (Figure 10e). The effect could be reversed by shining green light, and interestingly, spatially confined light irradiation was employed to pattern light-emissive regions with a few-micrometer resolution.

These examples showed that photochromic molecules can be employed to demonstrate truly multiresponsive transistors, in which both light irradiation and electric-field effect modulate

efficiently the drain-source current. However, the electronic performances of semiconducting polymers are not good enough for representing a realistic alternative to Si for CMOS technology. For this reason, the use of photochromic molecules to modulate the conductance of high-performance devices is very intriguing. As discussed in section 6.1, the combination of photochromic molecules with high-performance and ultra-sensitive 2DMs represents a natural step forward in this direction. Very simply, one could think of "dressing" the surface of a 2DM with photochromic molecules and use their light-triggered isomerization to introduce a change in the 2DM dielectric environment, and ultimately in its conductance. As discussed in section 6.1, hybrid devices can be envisioned in which photochromic molecules on the surface of 2DMs can be used to modify reversibly the number of charge carriers, and demonstrate novel reconfigurable devices, such as a p-n junctions in which the p- and n- regions can be erased and reversed, or light-emitting devices in which light emission can be spatially confined.

To be effective, this simple approach requires that the photoswitch is retained even when molecules are in contact with 2DMs, hence demanding for a comprehensive understanding of the phenomenon on surfaces. The examples discussed above in which the electrical current is measured across a SAM[160,162-167] provided an indirect indication (based on the conductance) that in those cases the switching is maintained for molecules grafted on metallic surfaces. However, this is not a general rule, as the photoswitch is often modified or quenched due to the interaction between the surface and photochromic molecules.

More insights on this topic have been obtained through surface science techniques,[169,180-195] which allow to characterize the molecular switch in direct contact with surfaces. In particular, the isomer on the surface can be identified by direct real-space imaging through scanning probe techniques [169,180-187,191-193] or by spectroscopic investigation accessing the molecular core levels.[183,188-190] In several cases the behavior of photochromic moieties interacting strongly with a substrate differs remarkably from that of the same compound in solution. This is the case for photochromic molecules lying flat on metallic surfaces, for which the electronic coupling between the molecule and the surface modifies the energetic positions of the HOMO and LUMO levels, and reduces the lifetime of molecular excited states. As a result, the photoswitch is often quenched, and the stability of the two isomers is modified and, in some cases, reverted.[183,185] Similar effects were reported for the cases of SP/MC[183], AZO[194,195] and DAE[185] derivatives.

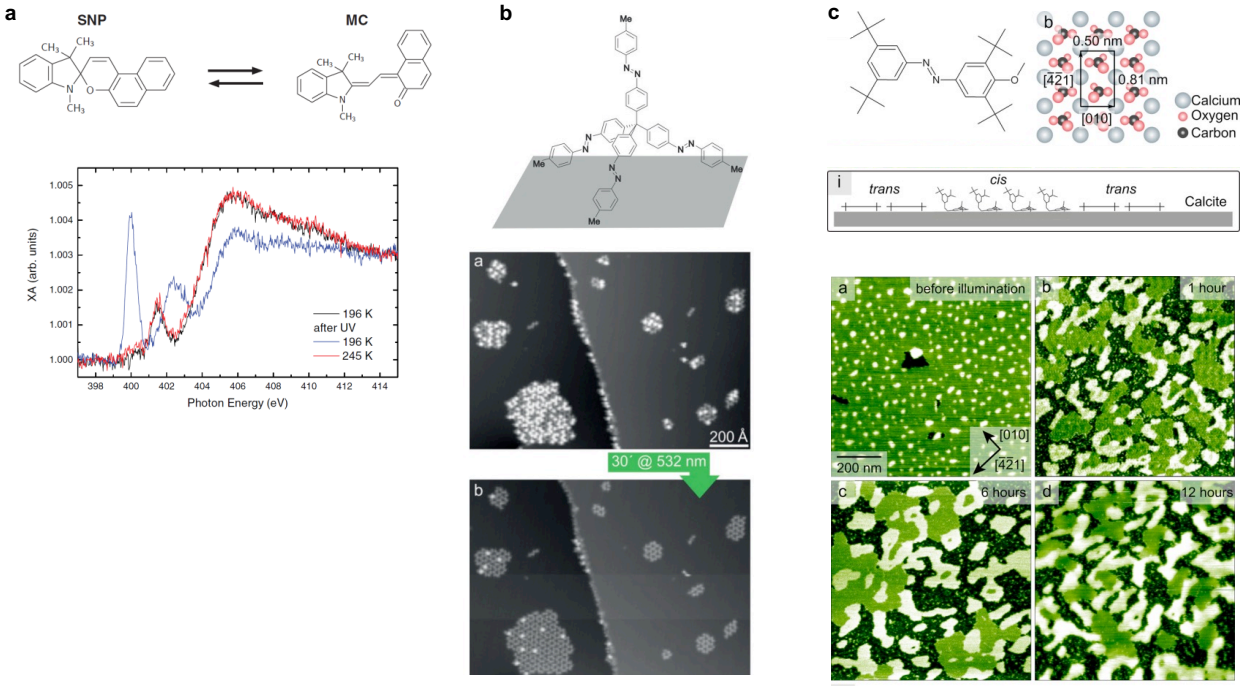

Figure 11*. Switch of photochromic molecules on surfaces. (a) A spirooxazine derivative displayed a reversible switch on the surface of Au and Bi, as monitored through X-Rays absorption. (b) STM study of a 3D compound consisting of four tetrahedrally arranged AZO units on the Ag surface. While the three AZO groups close to the surface lost their switching ability, the AZO unit further form the surface displayed a reversible photo-isomerization. (c) The photoisomerization in a monolayer of AZO molecules physisorbed on the insulating surface of calcite leads to a structural rearrangement. (a) Reproduced with permission from ref ([189]). Copyright 2016 Wiley-VCH. (b) Reproduced with permission from ref ([192]). Copyright 2018 Wiley-VCH. (c) Reproduced with permission from ref ([191]). Copyright 2018 American Chemical Society.*

Molecular design can be tailored to engineer photochromic molecules that retain their photoswitching properties on surfaces. For example, the switching of a spirooxazine derivative on the Bi and on Au surfaces was achieved through the replacement of the electron-withdrawing nitro group on the pyran moiety by an electron-donating naphtho-group[189,190] (Figure 11a). In this way, the MC isomer was artificially made less stable, so that the SP form regained its thermodynamically stable character even in direct contact with the metallic surfaces. As a result, a reversible isomerization process could be achieved either thermally or by light irradiation, as monitored through spectroscopic techniques (Figure 11a).

Another intriguing and widely explored approach to retain the photoswitching capability on surfaces entails separating the photochromic moiety from the surface using suitably designed side

groups. This approach is followed in most of the above discussed cases in which the conductance of a photoswitchable SAM is measured in a vertical device geometry, with the change in the conductance indirectly confirming the effective photoisomerization on surfaces. [160,162-167]

A recent work shows in an exemplary way how the distance between the surface and the photochromic moiety affects the photoswitching ability.[192] The behavior of a 3D compound consisting of four tetrahedrally arranged AZO units was studied by STM on the Ag surface. The molecule adsorbs on the metal with three AZO units pointing downward towards the surface and one standing in a direction orthogonal to the surface (Figure 11b). It was found that while the AZO groups in the proximity of the surface lose their switching ability, the group sticking out retained it. Moreover, the state of the switchable isomer — *trans* or *cis* — of the upright oriented azobenzene group was found to influence the diffusion of the molecule on the surface, with the molecules in the *trans* state displaying higher mobility on the surface.

We highlight that the surface of van der Waals materials is often less reactive than that of the metallic substrates typically used in surface science experiments, so that the switching capabilities are expected to resemble more closely the behavior in solution. As an example Figure 11c displays the investigation of the switching of AZO molecules physisorbed on the insulating and inert surface of calcite.[191] AFM characterizations made it possible to observe a molecular layer on the surface characterized by different thicknesses, which were ascribed to the presence of self-assembled islands of *trans* or *cis* isomers (Figure 11c). The *cis* isomers, which is less stable at room temperature, were found on the surface already directly after preparation by means of AFM

characterization. Prolonged irradiation using UV/vis light led to a photostationary state where the area covered by the *cis* and *trans* islands was approximately of the same size. Subsequent irradiation with a 450 nm laser resulted in a situation in which most of the surface was covered by the *trans* isomer, demonstrating an efficiency comparable to molecules in solution. Interestingly, this report also indicated that the switching event on surface possess a certain degree of cooperativity. In fact, no *cis* isomers were observed within *trans* islands upon illumination with 450 nm, indicating qualitatively that light irradiation produces a collective change in the self-assembly. A similar effect was also observed in early studies of AZO-SAMs.[182] From a technological point of view, the cooperativity is very intriguing, as it offers the possibility to convert and amplify a single molecule effect into a mesoscopic reorganization taking place on a length scale comparable to that of conventional micro or nanodevice. We highlight that achieving an efficient switch on a surface ensures a modulation in the physical properties on the surface. For instance, the work function of a gold surface was modified by the switching of an AZO SAM on it, due to the different molecular dipole of the two isomers.[144] This effect is particularly relevant for the 2DM, for which a work function change is associated to a change in conductance.

3.2.2 Redox Switchable Molecules

Redox switchable molecules are another class of molecular systems which can impart new properties to 2DMs and enrich the functionalities of 2D electronic devices. Redox switchable molecules, also called electrochemically driven molecular switches, can undergo reversible

electrochemical reactions. The electroactive molecular switches such as ferrocenes, viologens, quinones, and tetrathiafulvalenes, have two or three stable redox states and their electrochemical interconversion is completely reversible. Therefore, the redox molecules have been extensively used as active components in electrochemically switchable supramolecular systems. These molecules can be classified into electron donors including ferrocene, tetrathiafulvalene (TTF), etc., and electron acceptors based on viologen framework and quinone derivatives. We will briefly introduce the basic properties of representative electrochemically switchable molecules in which the changes in physical properties (absorption, fluorescence, electron occupation in molecular orbitals) can be switched by redox reactions. Then we will talk about the redox switchable supramolecular systems and the redox-controlled molecular geometry/conformation switching. In section 6.2 we will discuss the redox-switchable devices based on the redox molecules.

3.2.2.1 Ferrocene

Ferrocene has been under the spotlight since its discovery in 1951.[196] The sandwich structure of the compound with the d-π interactions between Fe(II) center and the cyclopentadienyl (Cp) moieties makes it unique in terms of its chemical properties (Figure 12a).[197] The delocalized electrons from *d* orbitals of Fe directly interact with π orbitals of Cp and make the two rings acquire a partial negative charge.[198] With one extra electron from Fe, each Cp ring has six π-electrons, making it aromatic. And the two Cp rings shared the total twelve electrons with Fe(II) center, filling the Fe orbitals up to 18 electrons. The interaction of metal and Cp orbitals imparts a strong

covalent character to the metal-ligand bond. The most exclusive property of ferrocene is its ability to undergo reversible oxidation to ferrocenium ion (Figure 12b), which is assisted by the lower oxidation potential of ferrocene to lose an electron thus creating two stable redox states Fc/Fc^+ with Fe(II) and Fe(III) centers, respectively.[199,200] When removing one electron from ferrocene, the sandwich geometry is maintained with only a slight change of the Fe–C bonding distances. The Fc/Fc^+ self-exchange reaction at the solid electrode is simple and equally fast independent of the solvent. In the cyclic voltammetry profile of Fc/Fc^+, the ratio between the reverse peak current and the forward peak current is constant, and the peak-to-peak separation at 25 °C is very close to the canonical value, i.e., 59 mV. These properties make ferrocene widely used as an internal standard in electrochemical measurements.[201]

Ferrocene shows high stability up to 400 ºC in air and it can maintain the properties in an autoclave containing carbon monoxide up to ~150 ºC at 200 bar.[197] Also, either one or both of the Cp rings in ferrocene can be easily functionalized with identical or different substituents. For example, in order to form SAMs on silicon surface, the binding group, the organic linkers and the substitutive groups can be ad hoc designed to display distinguishable surface properties (Figure 12c).[199] Hence, these unique properties, including ease of derivatization and retainment of its electrochemical reversibility, rendered ferrocene widely used during the last decades. One promising application of ferrocene as electrochemically driven molecular switches is the electrical switch in electronic devices. Ferrocene-modified surfaces could be used as charge storage components with the ferrocene center as the memory element. When a positive potential is scanned,

ferrocene is oxidized to its corresponding ferrocenium form. This redox change is equivalent to the change of one bit of storage from the "0" to "1" state. Upon the application of the negative potential scan, all the generated ferrocenium can be reduced to erase the stored charge and return the device to its initial state.

In another unique application, ferrocene can work as the redox switch of fluorescence. The redox system to switch the fluorescence typically consists of two components: a light-emitting subunit and a control subunit. The control subunit can employ a redox couple with two stable forms. One form (e.g., the oxidized one) quenches the fluorophore (state OFF) and the other form (e.g., the reduced one) contributes to the light emitting (state ON), or vice versa. Martínez et al. reported one ferrocene-based redox switch of fluorescence.[202] Pyrene acted as the fluorescent unit and was connected to ferrocene through an electron-permeable C=N–N=C conjugated molecular wire.[202] Upon irradiation at 350 nm, electrons were transferred from the electron-rich ferrocene subunit to the excited state of the pyrene moiety, resulting in the quenching of fluorescence. After the oxidation of Fc to Fc^+ by adding oxidizing agent, the system lost the electron-donating organometallic fragment, interrupting the electron transfer and reactivating the fluorescence. Upon addition of ascorbic acid, Fc^+ was reduced back to Fc and fluorescence emission was quenched again.

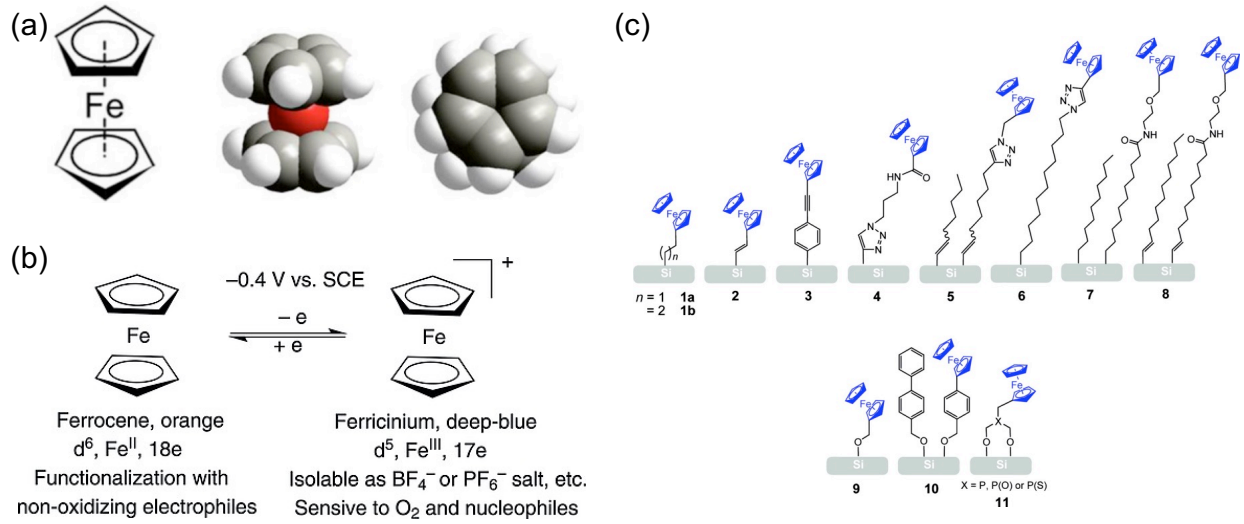

Figure 12. *(a) The chemical structural formula of ferrocene and the molecular structure with overlapping spheres. (b) Reversible oxidation of ferrocene around +0.4 V versus saturated calomel electrode (SCE). (c) Molecular design of binding group, organic linker and ferrocene functional group. (a) Reproduced with permission from ref ([197]). Copyright 2020 Springer Nature. (b) Reproduced with permission from ref ([200]). Copyright 2017 Wiley-VCH. (c) Reproduced with permission from ref ([199]). Copyright 2010 American Chemical Society.*

3.2.2.2 Tetrathiafulvalene (TTF)

Since the first-time synthesis,[203] tetrathiafulvalene (TTF) has been extensively explored as a π-electron donor in supramolecular systems. TTF is a non-aromatic 14 π-electron molecule and can be easily and reversibly oxidized to $TTF^{\bullet+}$ and TTF^{2+}. Hence, it behaves as a classical Weitz type redox system with three different stable oxidation states (Figure 13a).[204] Neutral TTF is composed of two pro-aromatic 1,3-dithiolylidene rings connected by a C=C double bond. It can

loss one electron to be oxidized into the radical cation $TTF^{\bullet+}$ and to convert one ring into an aromatic 6π-electron system. Stabilized by a mixed-valence resonance structure, $TTF^{\bullet+}$ shows long-term stability and can even be isolated, exhibiting its rareness. TTF can undergo a second oxidation step, yielding two aromatic 1,3-dithiolium cations (2 × 6π electrons) which are connected by a C–C single bond. The oxidation potentials of this two-step redox transitions are surprisingly low, which are 0.37 V and 0.74 V vs Ag/AgCl in CH_3CN, respectively.[205] This enables easily achievable electrochemical reactions and a reversible redox switching of TTF under ambient conditions. The excellent stability and the reversible switching ability are crucial for the efficient operation and characterization of TTF-based supramolecular systems and functional devices.

The gradual oxidation of TTF also induces the conformational changes of the molecular structure.[206] TTF in the neutral state has a boat-shaped structure and it transforms into a planar configuration in the radical-cation state. Taking advantages of this change, the intermolecular interaction can be tuned to cofacial stacking. When TTF is further oxidized to TTF^{2+} dication, it leads to the rotation of the ring and adopts a twisted conformation.

TTF in different redox states shows distinct optical absorption properties, which have been characterized by UV-Vis spectrophotometer.[207] As shown in Figure 13b, the spectrum of the neutral state shows very weak absorption above 350 nm without any obvious absorption peaks.[208] The absorption at the band edge corresponds to the HOMO→LUMO transition of the molecule. The spectrum of $TTF^{\bullet+}$ exhibits two strong absorption peaks at 450 nm and 800 nm. The low-energy band (800 nm) is resulted from an intrinsic SOMO-1→SOMO transition in the radical

cation.[209] And the dication shows a strong adsorption at 700 nm. The shift of these adsorption peaks results in the color change of the solution from pale-yellow to orange-brown, and finally to deep-blue. These strong color changes make it very easy to follow the electrochemical switching of TTF, even with the naked eye.

In the neutral state, TTF is a strong π-donor molecule and it widely acts as the functional group in charge-transfer molecules.[210] In supramolecular chemistry, TTF with remarkable π-donor properties are frequently used to construct donor–acceptor (D-A) complexes with π-electron deficient unit.[211] The unique design of D-A systems can facilitate the intramolecular charge transfer and photoinduced electron transfer. When TTF undergoes oxidation, the tendency to donate electrons decreases, and the TTF^{2+} dication can be considered as a molecule lack of π-electrons. By controlling the redox states of TTF moieties, it is possible to reversibly modulate the intramolecular charge transfer process within the D-A systems and change the optical properties of D–A systems accordingly. In general, by adjusting the π-donor ability of TTF derivatives and taking advantage of the three redox states, it has proved possible to develop a broadest variety of switchable molecular and supramolecular architectures with multifunctionality. For instance, interlocked compounds, such as rotaxanes and catenanes, have been prepared by using TTF to display electrochemically driven molecular motions.[212,213] These systems are of particular importance as prototypical molecular machines and molecular-level devices.

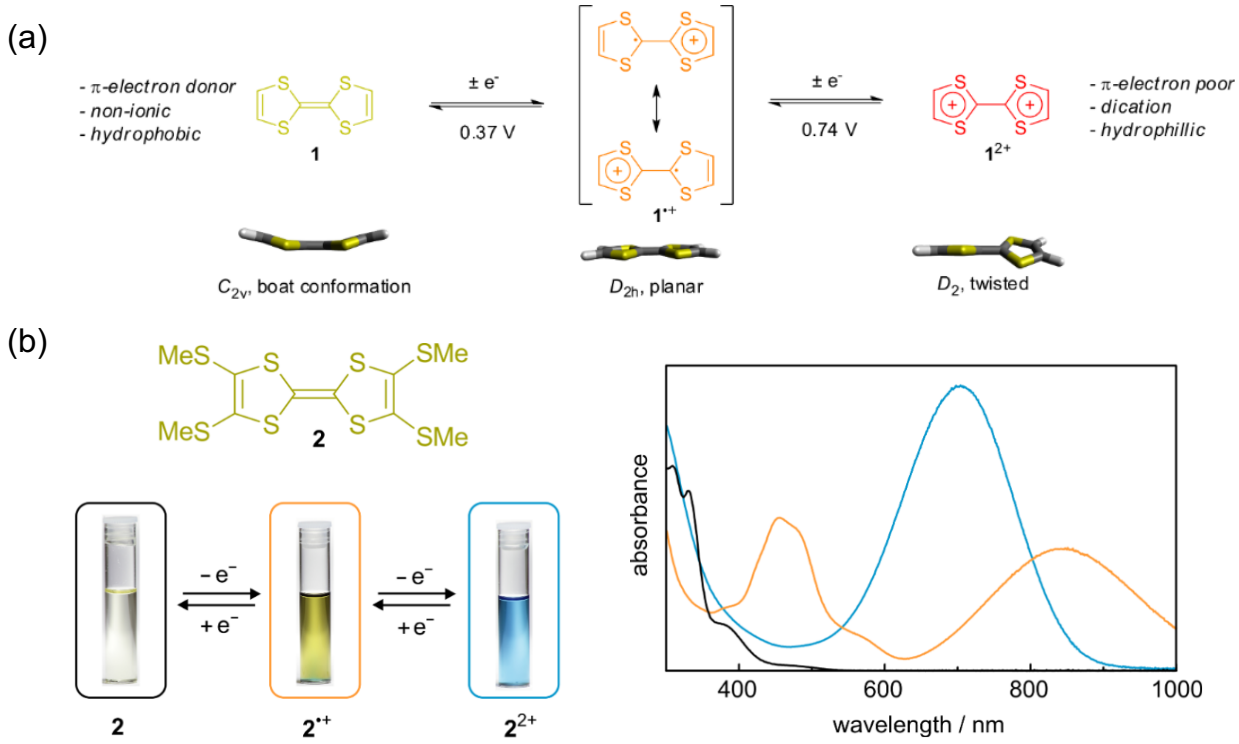

Figure 13. *(a) The two one-electron oxidation reactions of tetrathiafulvalene (TTF, 1) and the corresponding structure and property changes. (b) Photographs and UV–vis spectra of TTF 2 solution in its three stable redox states (black line = 2, orange line = $2^{\bullet+}$, blue line = 2^{2+}). Reproduced with permission from ref ([208]). Copyright 2018 Beilstein-Institut.*

3.2.2.3 Viologen

Viologens are bipyridinium derivatives, formally known as 1,1′-disubstituted 4,4′-bipyridyl ions. They have been first reported in the 1930s by Michaelis on their electrochemical behaviors and since that time viologens have been hot research topics due to their unique and interesting properties.[214] We must highlight several important properties of viologens, including three stable redox states, the desirable electron-accepting capability and the tunability of the nitrogen

substituents. Viologen salts have three ionic states, which are the dication (V^{2+}), the radical cation ($V^{\bullet+}$) and the neutral state (V). Figure 14a shows the electrochemical switching of methyl viologen (MV), one of the commonly known viologens. Its most stable state, MV^{2+}, can undergo two stable, reversible reductions, forming a radical cation ($MV^{\bullet+}$) and a neutral species (MV). Only a low driving voltage is enough to induce the switchable electrochemical reactions. It is worth noting that viologen radical cations are considered among the most stable organic radicals, and the ionic materials containing dication (V^{2+}) units are air-stable salts.[215] Viologens can function as dyes and the solution of viologen salts exhibit three primary colors in the corresponding redox states. For example, the color of MV^{2+} turns from colorless to a characteristic brilliant violet-blue (the radical cation forms, $MV^{\bullet+}$), and then changes to yellow-brown (the neutral species, MV). The colors of viologens can dramatically change in different types of derivatives which are dependent on the quaternized substituents and the counteranion.[216] The commonly utilized non-coordinating counteranions include halides, triflate and hexafluorophosphate.[217]

3.2.2.4 Redox switchable supramolecular systems

Electrochemically switchable supramolecular systems take advantages of the electrochemically controlled translocation of molecular fragments and induce geometrical/topologic changes upon oxidation/reduction. The representative molecular system encompasses various transition metal complexes containing two different sets of donor atoms within one supramolecular assembly. Upon change in oxidation state of the central metal ion, the

geometry of the supermolecule rearranges to achieve the most favorable coordination environment around the metal ion.[218] Figure 14b shows the electroswitchable systems with a large ligand incorporating two sets of tetracoordinating cavities based on hydroxoquinoline and bipyridine moieties, respectively. The first cavity preferentially binds Cu^{2+} cations, while the latter binds Cu^{+}. Sequential reduction and oxidation of the metal center results in translocation of the copper ion between the two binging sites. Related systems were developed and reviewed by Jean-Pierre Sauvage and coworkers demonstrating the first example of nanometer scale artificial molecular muscles.[219,220] Another frequently studied supramolecular system is based on supramolecular assemblies containing donor and acceptor moieties incorporated into pseudorotaxanes, rotaxanes, or catenanes. Oxidation of donor or reduction of acceptor moieties results in weakening of interaction and subsequent dissociation or rearrangement of the supermolecule (Figure 14c).[212] Conformationally switchable [2]rotaxanes[221,222] and [2]catenanes[223] have led to considerable promising results in the specific field of mechanical bonds and interlocked systems. The movement of the wheel in mechanical interlocked molecules via aromatic donor-acceptor interactions in turn dramatically changes the electrochemical and/or physical properties of the system (absorption, fluorescence, electron occupation in molecular orbitals), which can be utilized in (opto-)electronic devices.

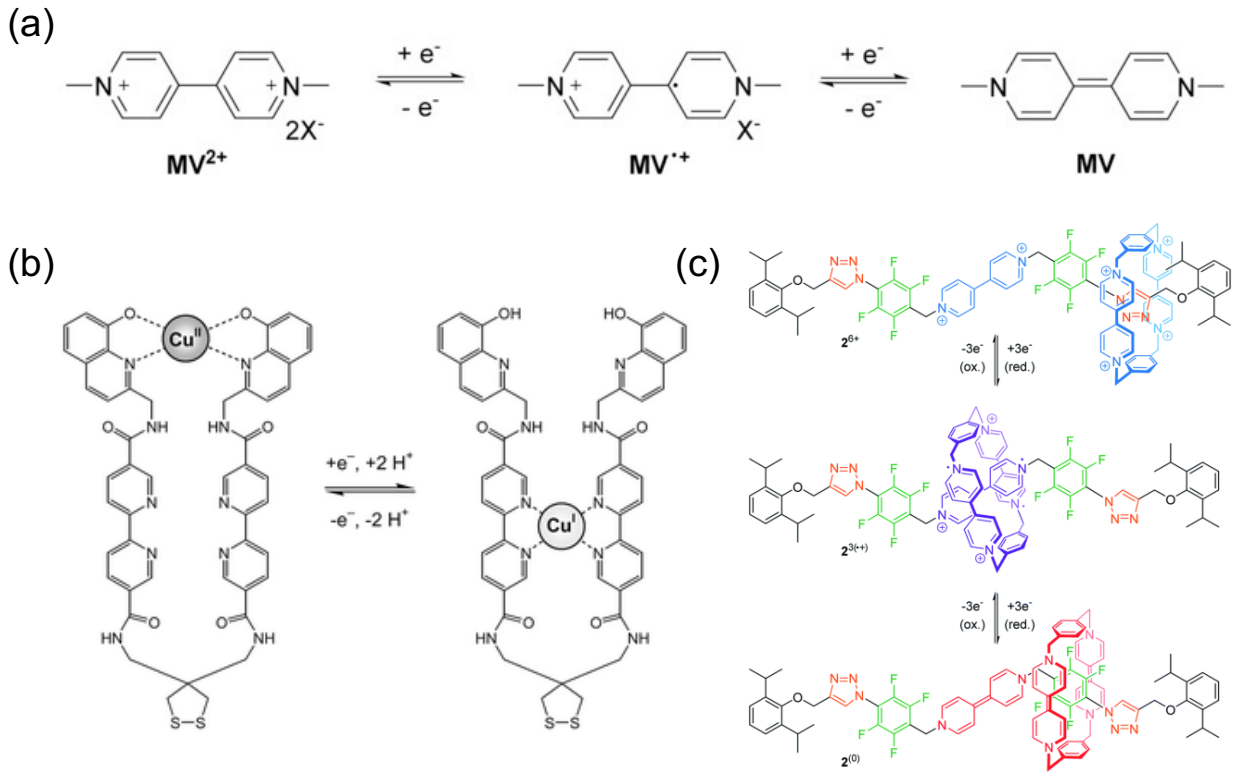

Figure 14. *(a) The three reversible redox states of methyl viologen. (b) Chemical structures of the double-stranded mononuclear cupric* $Cu^{II}\mathbf{L}_{N2O2}$ *and cuprous* $Cu^{I}\mathbf{L}_{N4}$ *species, showing a chemically triggered motion of cations in a supramolecular edifice. (c) Tristable [2]rotaxane* 2^{6+} *in its three different redox-states and resulting co-conformations. The unusual CBPQT*$^{(0)}$*/tetrafluorobenzene charge-transfer complex is stabilized by the mechanical bond. (a) Reproduced with permission from ref (*[224]*). Copyright 2017 Wiley-VCH. (b) Reproduced with permission from ref (*[218]*). Copyright 2002 Royal Society of Chemistry. (c) Reproduced with permission from ref (*[212]*). Copyright 2019 Royal Society of Chemistry.*

3.2.3 Spin/Magnetic Switches

One among the most promising technology for beyond-CMOS computing is spintronics, which uses the electron spin to store, manipulate and transport information.[225] Spintronic devices have been proposed to replace FETs in binary logics, offering the possibility to reduce power consumption.[20] Moreover, exploiting the spin degree of freedom bears a high potential for completely new computing paradigms based on neuromorphic[226] or quantum operations.[227]

2DMs are emerging as an intriguing material platform for building new spintronic devices.[228,229] Not only different members of the 2DM family are characterized by intrinsic electronic and magnetic properties which are highly favorable for transporting and manipulating spins,[230] but also their magnetic properties can be engineered by mastering proximity effects[231-235] or applying electrostatic gating.[236-238] This possibility distinguishes 2DMs from other materials conventionally used for spintronics, and it enables the design of novel devices.

In this context, the possibility to manipulate the magnetic properties of 2DMs using molecules is highly appealing. In particular, several organo-metallic molecules are characterized by a well-defined spin state,[239] which could couple to the spins in 2DMs and thus influence their magnetic properties *via* proximity effects.[240] Taking a step further, a molecular switch in which an external stimulus modifies the spin state might offer the possibility to dynamically tune the magnetic response of 2DMs, hence providing an additional tool to control the output of spintronic devices. In this section, we will review three systems in which molecular spin switches take place. We will dedicate a particular attention to spin crossover complexes, which are the prototypical spin-switches, characterized by a thermally driven diamagnetic-to-paramagnetic switch.[17,241,242]

Afterwards, we will highlight how in some simple organometallic compounds, the spin state can be reversibly modified by a chemical stimulus;[243] finally, we will mention that in single molecule magnets the spin can be manipulated using magnetic fields.[244] In each case, we will discuss whether the spin-switch is maintained on surfaces, which is a crucial ingredient for integration with 2DMs.

3.2.3.1 Spin Crossover molecules

Spin crossover (SCO) complexes are the prototypical molecular spin switches,[17,241,242] as they can be reversibly interconverted between two states characterized by a different spin configuration. While several reviews offer a detailed description of the SCO phenomenon,[17,241,242,245-247] here we will limit to summarize the basic principles at the basis of SCO, with a particular focus for the case of Fe(II) complexes in a octahedral configuration, which are by far the most studied complexes.

In an octahedral configuration, the ligand field splits the five 3d orbitals of transition metals into two different sets of sublevels, the t_{2g} and the e_g (Figure 15a).[248] How the electrons are distributed between the two sets depends on the relative strength of ligand field and spin pairing, which accounts for the exchange interaction. When ligand fields are weaker than the spin pairing, the electrons occupy the orbitals in a high spin (HS) configuration. This can be naively understood considering that weak fields do not significantly perturb the environment of the central metal ion, so that the orbital occupancy will follow the Hund rule. On the contrary, ligand fields stronger than the spin pairing increase the energy splitting between t_{2g} and e_g, eventually making a low spin (LS) state more favorable in energy. In most octahedral coordination compounds, the ground state is

either HS or LS, and it cannot be modified with an external stimulus. However, there are certain compounds in which the energy barrier between the two states is comparable to the thermal energy, so that a temperature-driven SCO process takes place. In particular, the low temperature ground state is LS, but the thermally activated transition to the HS state is entropically favored, since the HS state is 15-fold degenerate and it possess a higher density of vibrational states than the single-degenerate LS state.[245] Therefore, at high temperatures almost the totality of molecules transitions to the HS state, even if the LS ground state remains the lowest in energy. Figure 15a schematically illustrates this process for the case of Fe(II) complexes, wherein the LS state is diamagnetic, while the HS state is paramagnetic, with S=2. As an example, Figure 15b shows the chemical structure of the $[Fe(trz)_3]X_2$ family, where trz is a triazole derivative and X is the counter anion, which is one among the prototypical SCO complexes.[249] In these compounds, the metal ions are arranged in 1D polymeric structures and exhibit a cooperative transition displaying thermal hysteresis around room temperature. Apart from the magnetic properties, other physical properties change during the SCO transition, including the molecular volume,[250] the color,[249] the dielectric constant and electrical conductance.[251-253]

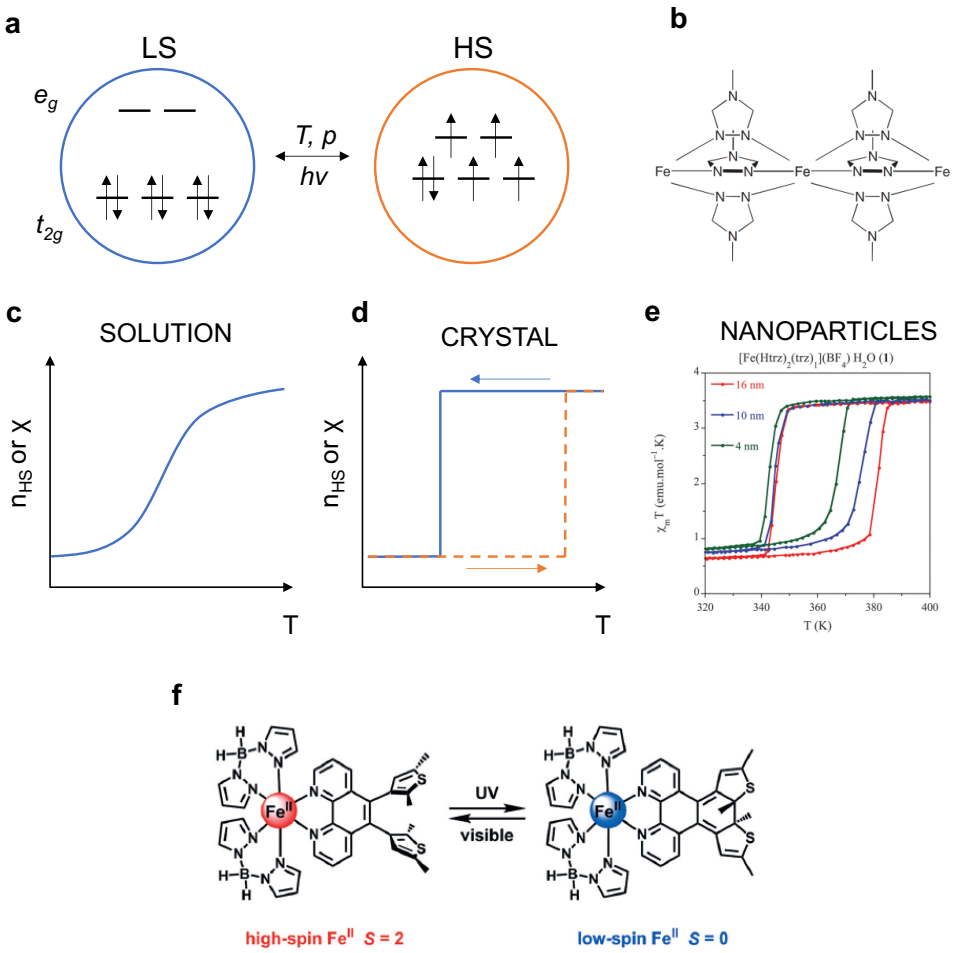

Figure 15. *Spin crossover compounds. (a) Two possible electronic configurations of Fe(II) in an octahedral complex. Due to the different orbital occupation, the low spin state is diamagnetic, the high spin state is paramagnetic. In spin crossover compounds, the two electronic configuration can be reversibly switched using different stimuli, such as temperature, pressure, light. (b) Chemical structure of the prototypical SCO complex* $[Fe(trz)_3]X_2$ *where trz is a triazole derivative and X is the counter anion, which forms polymeric structures in which the metal ions are arranged in 1D. (c-d) Schematic dependence of SCO transition on the molecular environment. While a shallow transition is observed in solution, in solid crystals the transition can be abrupt and display*

thermal hysteresis. (e) Thermal hysteresis measured in Nanoparticles of $[Fe(Htrz)_2(trz)_1](BF_4)H_2O$. *(f) Photochromic SCO compound incorporating an iron(II) complex and a photoisomerizable diarylethene-derived ligand, which permits the photo-switching of the spin state at room temperature. (b) Reproduced with permission from ref (*[254]*). Copyright 2007 Wiley-VCH; (e) Reproduced with permission from ref (*[255]*). Copyright 2015 Royal Society of Chemistry. (f) Reproduced with permission from ref (*[256]*). Copyright 2015 Wiley-VCH.*

The SCO transition is an ultrafast event at the single molecule level, as the change in the electronic configuration takes place at the sub-ps timescale.[257] On the contrary, how the LS → HS transition occurs in a large population of molecules depends critically on their environment, as schematically shown in Figure 15c,d.[17,241,242,245,246] In this case, the transition is often characterized by plotting the number of molecules in the HS state n_{HS} as a function of temperature. If the interactions among SCO molecules are weak, for instance for molecules in solution, the molecules behave as isolated molecules, and the SCO transition follows the Boltzmann statistics and it displays a shallow thermally activated LS → HS transition (Figure15c). In the opposite case, in crystalline SCO solids characterized by strong intermolecular interactions, an abrupt transition characterized by a thermal hysteresis is observed (Figure 15d). This behavior, which is hallmark of a first-order phase transition, can be understood on the basis of cooperative effects involving electron-phonon coupling and elastic interaction between neighboring molecules.[258,259]

The hysteretic behavior is very intriguing for device applications, as it provides a window of bistability, often around room temperature,[249] which could serve as memory, offering a knob to achieve the functional diversification required in the More-than-Moore approach. Therefore, the question naturally whether the thermal hysteresis is maintained in reduced dimensions, at the intermediate range between single molecules and bulk solids. Importantly, SCO nanoparticles have been synthesized which retain the thermal hysteresis,[254] as shown for the compound $[Fe(Htrz)_2(trz)_1](BF_4)H_2O$ in Figure 15e. Importantly, thermal hysteresis is maintained even for 4-nm nanoparticles indicating the presence of important cooperative effects even for nanoparticles containing as few as 40 Fe(II) ions.[255] As we will discuss in the following, the SCO nanoparticles retain the thermal hysteresis even when deposited on surfaces and integrated into devices.[251,253,260] However, the presence of the nanoparticle shell, which on the one hand is very effective in preserving the bulk SCO properties at the nanoscale, on the other hand introduces an additional distance between the SCO core and the surface, which might be detrimental for an effective magnetic coupling.

Apart from temperature, early works showed how pressure[49] and low-temperature light irradiation[261] could trigger the SCO phenomenon. The effect of pressure can be understood simply considering the change in molecular volume which accompanies the SCO transition. In particular, pressure favors the LS state, which is characterized by a shorter metal-ligand bond length, hence it presents smaller volume.[248] Light irradiation at low temperature was also found to induce the SCO transition, by a process called light-induced excited spin-state trapping (LIESST).[261] In this

process, optical excitation provides the SCO complexes with enough energy to overcome the LS → HS energy barrier via excitation of higher energy states, resulting in a metastable HS state which at low temperatures (4K) is stable over weeks. More recently, light irradiation was used to induce the spin transition in SCO crystals at higher temperature, in the bistability window within the hysteresis.[262,263] However, the physical origin of this effect is thermal, as it is related to the induced annealing by light exposure. In order to employ a purely optical input to switch the spin state of as SCO complex at room temperature, an elegant approach exploits molecular design to provide the same molecule with both a photochromic and a SCO capability. As an example, the compound shown in Figure 15f is composed of a SCO complex connected to a DAE derivative.[256,264] The opening/closing of the ring at room temperature changes the ligand field at the Fe(II) ion, which in turn causes the HS → LS switch, as demonstrated by recording the magnetic susceptibility under light irradiation. Following another approach, a switch between a diamagnetic and a paramagnetic state was achieved in a nickel porphyrin connected to an azobenzene moiety.[265] The mechanical movement introduced by the azobenzene enabled the reversible coordination of the Ni atom with a tethered pyridine ligand. In this case, the physical mechanism leading to the spin switch is markedly different from that of SCO complexes, but it leads to an analogous switch between a paramagnetic and a diamagnetic state. In addition to these classical stimuli to induce the SCO phenomenon, a few studies explored the possibility to switch the magnetic state using electric fields. Almost ten years ago, STM studies demonstrated that the HS → LS switch of a single SCO molecule could be induced at low temperature by applying a

voltage pulse in the proximity of the molecule using the STM tip as a local electrode.[266,267] A similar effect was observed in a lateral device, where individual SCO nanoparticles were sandwiched between lateral electrodes separated by a nanosized channel.[251] In this case, a sudden change in the resistance was recorded during a voltage sweep, which was interpreted as an indication of electric-field induced spin switch. In another work, the spin state of sublimable SCO compound evaporated onto a ferroelectric polymer was found to depend on the ferroelectric polarization of the substrate.[268] The possibility to modify a magnetic state using an electric field is certainly extremely intriguing, as materials characterized by unconventional magnetoelectric properties are central in the proposed spin-electronic circuitry.[20]

3.2.3.2 SCO on surfaces

A crucial aspect to address the relevance of SCO complexes for the 2DM research is whether the SCO phenomenon is maintained in thin films deposited on surfaces.[269] This issue has been investigated in different works focusing on ultraclean surface/molecule interfaces obtained by vacuum evaporation of sublimable SCO compounds onto target surfaces.[246] In particular, two distinct questions have been addressed, which are (i) whether the SCO is preserved at the single molecule level, and (ii) whether on-surface intermolecular interactions are sufficiently strong to generate a cooperative effect, leading to abrupt transitions and hysteresis. While we refer the reader to a recent review for a detailed discussion of the results,[246] here we summarize the findings as follows.

At the single molecule level, the behavior of the same SCO complex on a substrate or in a solid crystal can be very different.[270,271] On metallic surfaces with a large density of states at the Fermi level, the interaction can be so strong that SCO molecules do not preserve their structural integrity,[272,273] or they coexist in the HS and LS state,[120274] losing the switching ability.[272,275] On the contrary, weak substrate/molecule interactions preserve the switching properties of molecules.[267,275-278] Importantly, graphite is often taken as an example of weakly interacting surface, since it is dangling-bond free and possess a vanishing density of states at the Fermi level.[275-277] The same behavior can be expected for the case of other layered van der Waals materials, such as semiconducting transition metal dichalcogenides.[278]

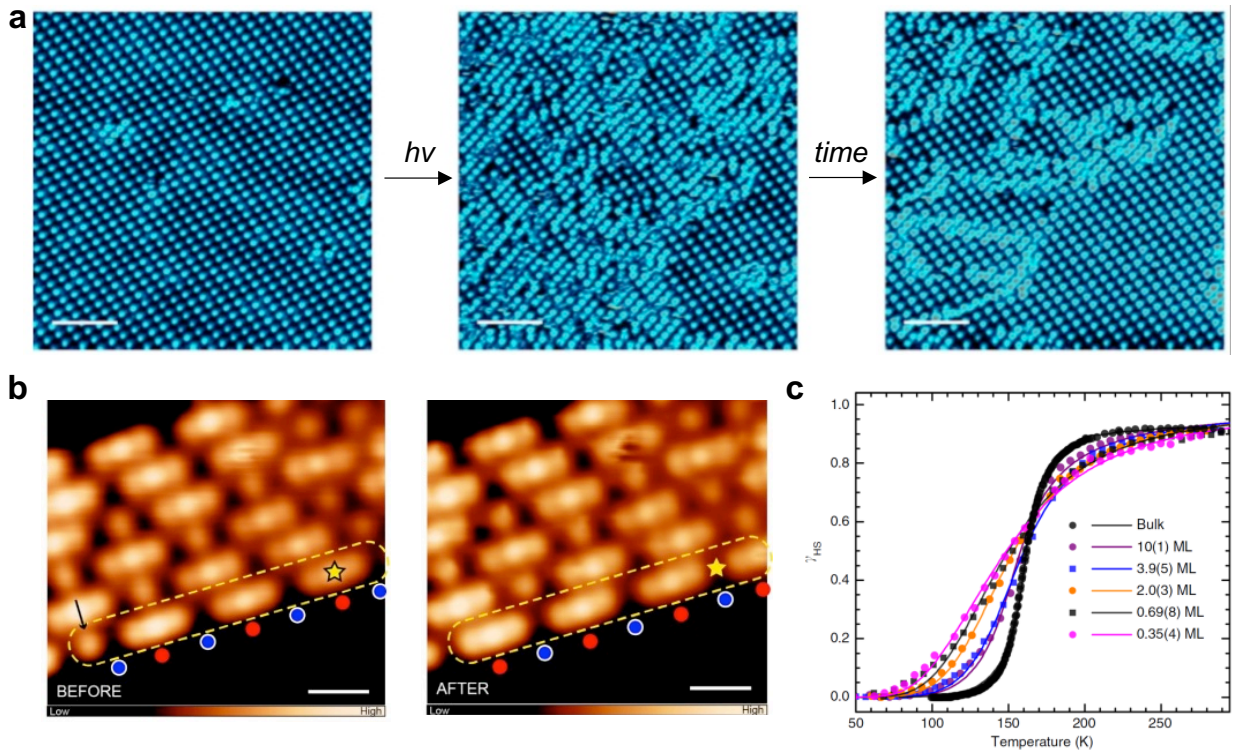

Figure 16. *Molecular cooperativity in self-assembled SCO adlayers. (a) Scanning tunneling microscope image of an assembly of the SCO complex [Fe((3,5-(CH₃)₂Pz)₃BH)₂] (Pz = pyrazolyl)*

deposited onto the Au(111) surface before and after low temperature (4 K) light irradiation. Light irradiation at low temperature induced a modification in the self-assembled adlayer by triggering the LS→HS transition; the starting self-assembled structure could be partially recovered after 10 hours in dark. Signature of cooperativity were found by imaging the transition between the two structures in real time. (b) STM images showing how Ni atoms coordinated by deprotonated tetrahydroxybenzene linkers on Au(111) form 1D metal-organic structures, characterized by the alternance of diamagnetic and paramagnetic Ni ions. A current pulse applied by an STM tip in the proximity of a Ni atom (yellow star) effectively changed the spin state of that atom and of its neighbors, demonstrating an cooperative magnetoelastic effect. Scale bars: 1 nm (c) Thermal transition in films of [Fe(H$_2$B(pz)$_2$)$_2$(bipy)] characterized by different thickness evaporated on HOPG. The fraction of molecules in the HS and LS state was measured via X-Ray absorption. The transition becomes more abrupt as the layer thickness is increased, indicating the emergence of cooperative effects. (a) Reproduced with permission from ref ([279]). Copyright 2016 Nature Publishing Group; (b) Reproduced with permission from ref ([280]). Copyright 2020 American Chemical Society. (c) Reproduced with permission from ref ([277]). Copyright 2018 Nature Publishing Group.

At the ensemble level, two STM studies indicate of the potential of on-surface self-assembly to forge a certain degree of cooperativity. An interesting insight on the presence of cooperative effects on surfaces was provided by Bairagi et al.,[279] who carried out a low temperature STM

characterization of the low-temperature light induced switch of the molecule [Fe((3,5-$(CH_3)_2Pz)_3BH)_2$] (Pz = pyrazolyl) deposited onto the Au(111) surface (Figure 16a). Before light irradiation, the authors observed a highly ordered self-assembled monolayer in which molecules in the HS and LS state co-existed and self-organized generating an ordered superstructure (Figure 16a). Irradiation with light at 405 nm induced the LS $\rightarrow$ HS transition by LIESST, which resulted in the formation of a different superstructure, characterized by a higher fraction of HS molecules. Importantly, the STM images showed that the light-induced phase propagated across the field of view following a transition front, indicating the presence of elastic interactions within the self-assembled layer similar to those found in macroscopic SCO solids.

An analogous effect was recently reported for a 1D metal–organic chains on Au(111), in which Ni atoms are coordinated by deprotonated tetrahydroxybenzene linkers.[280] This system is not strictly composed of SCO compounds, but it resembles a SCO polymer, as the Ni atom possess a well-defined and switchable spin state imposed by the ligand fields of the linkers. Using scanning tunneling spectroscopy, the authors found that Ni atoms possessing a low-spin (S = 0) or a high-spin (S = 1) state alternate along the chains. In analogy to the case of SCO compounds, a current pulse applied by an STM tip in the proximity of a Ni atom effectively changed its spin state. Importantly, the authors observed a change in the spin configuration not only in the spin configuration of the Ni atom in the proximity of the tip, but also of other Ni atoms within the same 1D chain (Figure 16b). The authors described this effect as a domino-like phenomenon induced by a magneto-elastic cooperative effects mediated by the organic ligands.

The evolution of on-surface cooperativity was investigated by Kipgen et al.,[277] who investigated the spin transition in thin films of $[Fe(H_2B(pz)_2)_2(bipy)]$ evaporated on highly oriented pyrolytic graphite for thicknesses spanning from 0.35 to 10 monolayers. X-ray absorption was employed to identify the electronic configuration of the evaporated SCO complexes. The LS $\rightarrow$ HS thermal transition was found to evolve with the thickness of the layer, becoming more abrupt at higher coverage (Figure 16c). Since the slope of the transition is related to the cooperativity, an accurate analysis of the experimental data led the authors to conclude that multilayers starting from double layer exhibit cooperative switching, while sub-monolayers do not. This study is particularly relevant for the 2DMs community in view of the use of the graphite substrate, which is the prototypical van der Waals compound. These studies highlight how molecular cooperativity in 2D can be mediated by self-assembly in thoroughly designed systems, offering a path to obtain abrupt SCO transition and hysteresis on surfaces.

3.2.3.3 Alternative approaches to spin transition on surfaces

The difficulties encountered in achieving bulk SCO properties in SCO complexes in contact with surfaces have motivated the search for alternative strategies to achieve a reliable switch of molecular spin state on a surface. Moreover, the Fe(II) ion in SCO complexes is surrounded by relatively bulky ligands, which separate it from the surface and weaken the magnetic interaction. Indeed, magnetic proximity effects, which are caused by short-range exchange interactions, have not yet been detected at SCO/surface interfaces. Here we highlight two alternatives to SCO

complexes for achieving molecular spin switching on a surface, using (i) planar organometallic compounds and (ii) single molecule magnets.

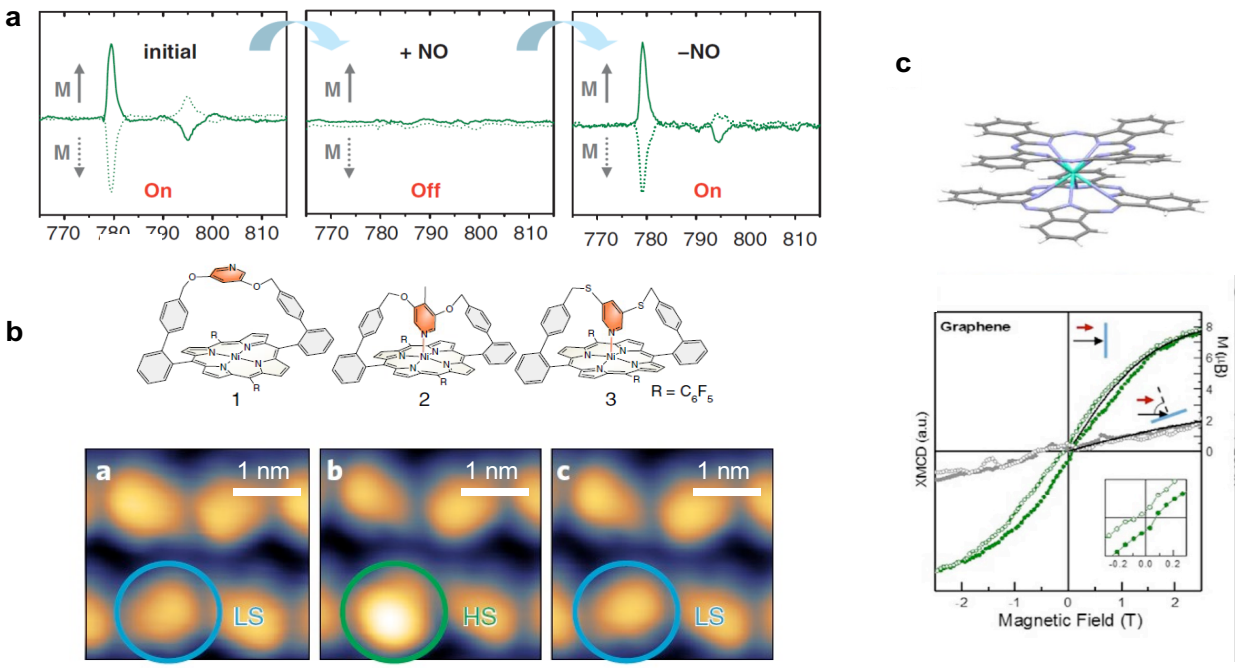

Figure 17*. Spin switches other than spin crossover molecules. (a) X-Ray Magnetic Circular Dichroism (XMCD) of the Co atom in cobalt-porphyrin molecules deposited on Ni(001). The non-zero XMCD signal demonstrates the presence of a molecular spin on the surface, indicating that the molecule is paramagnetic. Adsorption of nitric oxide as an axial ligand causes a change in the magnetic state of the molecule, which becomes diamagnetic. Desorption of nitric oxide restores the initial paramagnetic state. (b) Reversible coordination of the metal center in a Ni-containing porphyrin ring can be achieved through a covalently attached and mechanically movable ligand, causing a change in its magnetic configuration. An STM tip is used to induce the mechanical movement. A difference in the STM contrast is observed for the molecule in the HS and LS state.*

(c) prototypical single molecule magnet double decker $TbPc_2$, composed of a Tb ion sandwiched between two phtalocyanine ligands. XMCD of a $TbPc_2$ sub-monolayer deposited on graphene shows that the magnetic hysteresis is kept on the surface. (a) Reproduced with permission from ref [281]. Copyright 2010 Nature Publishing Group; (b) Reproduced with permission from ref [282]. Copyright 2020 Nature Publishing Group. (c) Reproduced with permission from ref [283]. Copyright 2018 Royal Society of Chemistry.

Planar organometallic molecules composed of a central metal ion surrounded by organic ligands, such as metal phthalocyanines and porphyrins, are particularly interesting for investigating the magnetic coupling of molecular spins on surfaces. Their electronic configuration is characterized by a well-defined spin state, which depends on the central metal atom and can be modified by choosing different elements in the transition metal row.[239] In bulk crystals and thin films, magnetic ordering develops at low temperatures, wherein the spins of different molecules generally couple antiferromagnetically.[284,285] On surfaces, several organometallic compounds maintain a paramagnetic configuration, characterized by a non-zero spin which aligns to magnetic fields.[281] Importantly, the planar geometry of the molecules promotes their self-assembly on different surfaces (including van der Waals) displaying a flat configuration,[286] so that the central ion carrying the molecular spin lies in the close proximity of the surface.[243] Since the early 2000, several studies have shown how organometallic compounds deposited on ferromagnetic substrates couple to the magnetization of the substrate.[287,288] More recently, it was shown that the molecular

magnetic coupling is strong enough not only to generate long-range ordering in the molecular spins, but also to modify the magnetism of ferromagnetic metal substrates, for instance introducing exchange bias.[285] This effect was recorded also in solid state devices, demonstrating the potential of organometallic compounds for applications in spintronics.[289,290]

In view of these favorable spin properties, organometallic compounds have become a playground to investigate interfacial magnetism and magnetic coupling. A highly promising development in this direction is the possibility of controllably switch their spin through axial coordination chemistry. In particular, the coordination of an extra ligand to the central metal ion modifies its electronic configuration, and hence its spin. This effect has been reported in a number of studies,[243,281,291-293] in which a substrate surface is first covered by a self-assembled monolayer of organometallic molecules, and then it is subsequently exposed to another coordinating molecule which binds to the central metal ion and changes its spin state. This approach represents a highly promising way to engineer the magnetic state of an interface employing a chemical stimulus. As an example, Figure 17a shows how the spin of a cobalt-porphyrin molecule could be switched between a diamagnetic and a paramagnetic state by adsorbing and desorbing nitric oxide as an axial ligand.[281] More recently, an interesting development in this line was achieved by employing a molecule with a mechanically movable ligand attached to a Ni-containing porphyrin ring.[282] In this molecule, excitation through electron injection from an STM tip induced mechanical movements in the molecule which led to reversible coordination of the metal center, causing to a change in its magnetic configuration (Figure 17b). The obvious advantage of this strategy is that

the coordination ligand embedded is in the molecule, so that the additional step of exposure to a coordinating molecule is not required. As a disadvantage, the coordination switching is only achieved at the single molecule level, and the feasibility of employing other external stimuli to change the spin state of all molecules still needs to be demonstrated.

As a last class of spin switches which can be coupled to 2DMs, single molecule magnets are organometallic compounds characterized by a large magnetic anisotropy and an extremely long magnetization relaxation time at low temperatures[244,294,295]. As in the case of SCO complexes and porphyrins, uncompensated spins in the metal ion(s) point in one of two directions parallel to each other due to the magnetic anisotropy, along the so-called easy axis. In order to flip the spin direction, a finite energy is required, which determines the magnetization relaxation time, i.e. the average time between thermally induced random spin-flip events. Below a certain (molecule dependent) blocking temperature, the thermal energy becomes too low to switch the spins, which remain pinned a direction. In this condition, a magnetic field is required to reverse the molecular spin, giving rise to a magnetic hysteresis visually similar to that of conventional ferromagnetic materials. We highlight that the hysteresis has a fundamentally different origin: while in conventional ferromagnets it is the result of long-range interactions, in single molecule magnets it arises from a single blocked (super)paramagnetic configuration with a trapped spin state. This behavior also highlights the difference between single molecule magnets and the other organometallic compounds mentioned in this section. In particular, the molecular spin in single molecule magnet and in other paramagnetic metallic compound both align to an applied magnetic

field, but their behavior differs drastically when the field is removed. While single molecule magnets retain their spin in the same direction even after removing the field,[244] the molecular spin of other organometallic compounds lose the magnetic memory, as the ultra-fast and random spin-flip events occur even at low temperatures.

The first works on single molecule magnets employed transition metal ions, which possessed a relatively low blocking temperature (around liquid helium).[296] Subsequently, lanthanides emerged as an intriguing group of elements for molecular magnets in view of the highly directional f orbitals, which render a high anisotropy energy barrier between the opposite spin orientations. Importantly, dysprosium-based single molecule magnets have been demonstrated with blocking temperature above liquid nitrogen.[297]

Single molecule magnets are very intriguing for quantum computing, as they host a plethora of exotic quantum effects which could be exploited to store and manipulate quantum information.[298,299] For instance, they show quantum tunneling in the magnetization, which displays as a butterfly shape in the magnetic hysteresis,[300,301] and quantum coherence.[302] Therefore, interfacing 2DMs with single molecules magnets offer the possibility to electrically access, and possibly manipulate, molecular quantum states.

In analogy to the case of SCO molecules, it is crucial to verify whether single molecule magnets retain their properties when deposited on surfaces. This has been investigated for several single molecule magnets, including the prototypical single molecule magnet double decker TbPc2,[301,303] composed of a Tb ion is sandwiched between two phtalocyanine ligands (Figure

17c).[283,304] Even in this case, it was found that the magnetic behavior of single molecule magnets on surfaces depends critically on the specific substrate/molecule interaction. Interestingly, $TbPc_2$ was recently shown to maintain its magnetic properties when deposited on graphite and on epitaxial graphene on SiC.[283] In particular, the hysteresis loop measured by means of XMCD shows a small remnant magnetization characterized by a finite coercive field and by the typical butterfly shaped hysteresis. This result indicates how van der Waals materials are ideal to maintain the favorable properties of single molecule magnets, and possibly access their states.

4 2D Materials/Molecules Interfaces

The 2DMs employed for fabricating devices are atomically thin and they typically extend over at least several micrometers in the lateral dimensions. As a consequence, their surface area is several orders of magnitude larger than the footprint of any small molecules used for their functionalization. Therefore, the interfacing 2DMs and (quasi-0D) molecules with molecules is characterized by a dimensionality mismatch. To overcome this problem, it is possible to distinguish between two different functionalization approaches. In one obvious strategy, the surface of 2DMs is covered by a large number of molecules organized in a (semi-) continuous thin film. While the morphological and structural properties of the molecular thin film as well as its thickness vary greatly in different experiments, the formation of the thin film ensures the dimensionality matching. Within this approach, the interplay of molecule-surface and molecule-molecule interactions acquires a central role, as it determines the degree of structural order in the

molecular film and ultimately its collective interaction with the 2DMs. In another strategy, scattered and isolated functional molecules are anchored at specific sites of the 2DM crystal, providing a local effect which can impact the electronic performances of devices.

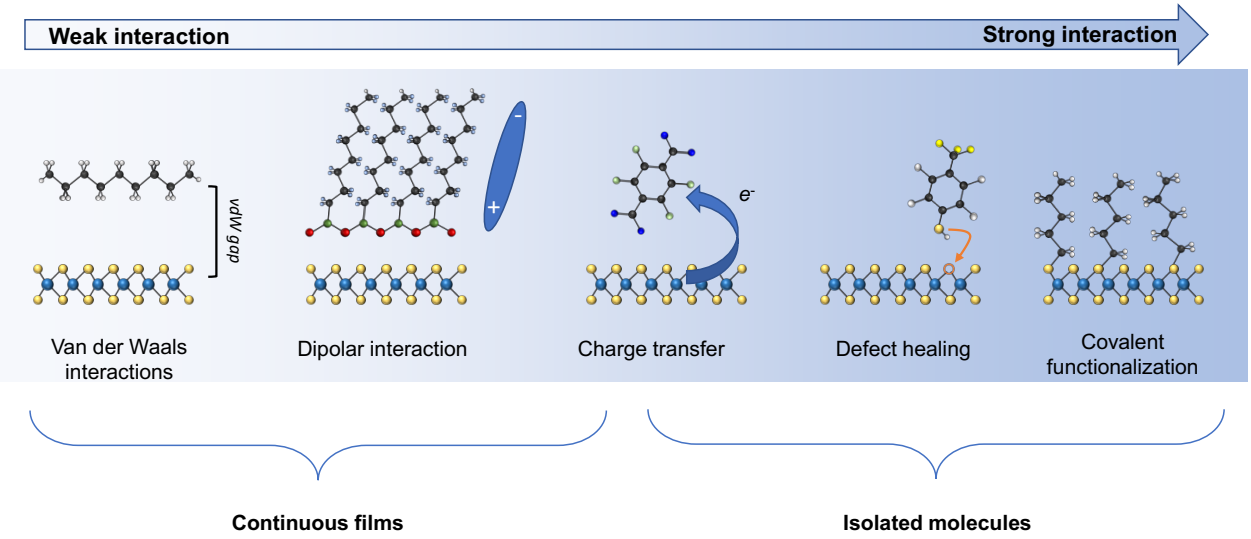

***Figure 18**. Schematic representation of different phenomena taking place at 2D materials molecule interfaces, plotted in order of increasing molecule/2D materials interaction.*

We highlight that the choice of the two strategies is dictated by the specific interaction between the functional molecule and the 2DM in use. For instance, isolated molecules need to be strongly tethered to the 2DM surface, otherwise at room temperature they would diffuse on the 2DM surface and eventually desorb from it, whereas the formation of a continuous and densely packed film reduces the diffusion and enables to interface weakly interacting molecules to 2DMs. On the other hand, generating ordered films based on strongly interacting molecules is challenging, since the molecules may have the propensity to remain anchored close to the place in which they

enter in contact with the 2DM surface, preventing further interactions with other molecules to generate ordered self-assembled structures. Therefore, it is important to briefly address which interactions can be expected at 2DM/molecule interfaces, as listed in Figure 18 in order of increasing strength. Subsequently, we will briefly mention what are the methods employed to produce different molecule/2DM interfaces. We note that the optimization in the device performance enabled by molecular functionalization does not impact only the (beyond-)CMOS technology, which is the main topic of this review. For instance, several of the interactions and functionalization strategies discussed in this section are exploited to improve the performances of sensors[45] and photodetectors[305].

4.1 Van der Waals interactions

The van der Waals interactions are unspecific forces which mediate the interaction between different sheets in layered materials and are ubiquitous at molecule/2DM interfaces.[306] Indeed, layered materials typically possess a dangling-bond-free surface prone to interact with other materials via van der Waals forces (hence often referred to as van der Waals surface), and the forces governing supramolecular interactions are often of van der Waals nature. Hence, for several molecule/2DM interfaces, the interactions are mediated primarily by van der Waals forces.[307] In these cases, the molecules are relatively free to diffuse at room temperature over relatively large distances and interact with other molecules, often generating highly ordered self-assembled structures in which the architectural motifs are determined by molecule-molecule and molecule-substrate interactions.[306-313] The self-assembly of these weakly bound (physisorbed) molecules on

the surface of bulk layered materials has been investigated for decades in the field of supramolecular chemistry at surfaces. As an example, it is well known that long alkanes possess high affinity to graphitic surfaces,[307] where the van der Waals substrate-molecule interactions result in the formation of highly crystalline monolayers in which alkanes lie flat forming a lamellar superstructure. Similarly, conjugated molecules like pyrenes often form ordered layers on layered materials[314] in which they lie flat to maximize the π-π interactions,[310,315] being a particular type of van der Waals interactions. A recent work shows how the assembly of the π-conjugated molecule pentacene is dramatically different on the vdW surface of hBN and on SiO_2, resulting in a marked difference in the morphology and optical properties.[316] Additionally, it was shown that the assembly of pentacene and perfluoropentacene on hBN depends critically on the number of defects on the hBN quality.[317]

In the last decade, several works demonstrated that alkanes and aromatic molecules self-assemble in the same way on monolayer graphene[106,309,318-322] and other exfoliated van der Waals materials, including boron nitride[323] and several transition metal dichalcogenides.[324,325] The expression "van der Waals epitaxy" is often used to describe the growth of these ultrathin molecular layers on dangling-bond free surfaces,[326] to stress the fact that the process is driven by van der Waals interactions and the alignment between the crystallographic orientation of the layered material and the molecular adlayer is atomically precise.

In this regard, the knowledge generated by fundamental studies of supramolecular arrangement on surfaces has been exploited for engineering the functionalization of 2DMs. For

instance, both alkyl chains[106,319-322] and conjugated groups (typically, pyrene[327-330]) have been used as anchoring groups to graft non-covalently other functional groups with lower affinity for layered materials.

Finally, we note that the fact that van der Waals forces are weak does not mean that the effect of a physisorbed molecular layer on the electronic properties of 2DMs is negligible. As an example, it was shown that the deposition of a thick layer of long unfunctionalized alkanes on graphene significantly increased its charge carrier mobility.[331] This rather surprising finding was explained considering that in view of the high affinity of alkanes to the graphene surface, which results in the removal of other unintentional dopant adsorbates, such as water and oxygen. Moreover, the presence of the alkane film resulted in a change in the graphene morphology, accompanied by a lowering of its interaction with the SiO_2 substrate and it silanol traps, ultimately yielding a more homogeneous and electronically performant layer.

4.2 Dipolar interactions

Polar molecules possess an intrinsic permanent electrical dipole arising from a non-symmetric charge density distribution, usually caused by the presence of different atoms with different electronegativity. Many functional groups are known to host a large dipolar moment, including -CF_3, -CN, -NH_2 among others. When a polar molecule interacts with a 2DM, the electric field generated by its dipole locally perturbs the 2DM surface. This effect is particularly important whenever the 2DM is a (semi)conductor, where the molecular electric field affects and redistributes the charge carriers in its proximity. We highlight that a stable effect is only obtained

if the molecular dipole is oriented along a fixed position, while for the opposite extreme situation of a molecular dipole randomly moving in all directions, the net electric field sensed by the charge carriers over time is zero.[319] Moreover, dipolar effects can be locally very strong, but their spatial extent is confined in the proximity of the polar molecule; therefore, in order to measure a macroscopic effect in the characteristic of mesoscopic devices, the permanent dipoles of the different molecules must point in the same directions, since otherwise the overall effect would cancel out.[332] As a consequence, mastering molecular self-assembly is particularly interesting for engineering dipolar interactions, since a closely packed molecular arrangement ensures that the electrical dipoles are oriented in one and the same (fixed) direction for all molecules, thereby offering access to vectorial properties.[106,107]

A particularly important situation occurs when molecular dipoles possess a strong component in the direction orthogonal to the 2DM surface. In this case, the electric fields at the 2DM surface are strong in the out-of-plane direction and cause a sizeable change in the 2DM work function.[333] In turn, a change in the 2DM work function can be detected at the macroscopic level as a change in the charge carrier concentration. In this regard, the electrostatic field effect generated by out-of-plane aligned molecular dipole is analogous to that generated by applying a fixed gate potential in three-terminal devices[334]. While it has been proposed that the presence of periodic in-plane electric fields might also generate a modification in the 2DM,[106] we are not aware of any work in which this effect has been characterized and exploited to modify the 2DM charge transport.

Dipolar interaction is often at the basis of the doping effect induced by polar molecules on 2DMs. For instance, in the early days of graphene it was noticed how water molecules induce p-type doping, which was explained in terms of the dipolar moment of water molecules absorbing on graphene with a preferential orientation.[332] More recently, interfaces between 2DM and alkanes functionalized with polar groups were investigated. As explained before, alkanes provide non-covalent grafting and ensure an ordered alignment via the formation of highly ordered self-assembled structures, generating a spatially homogeneous field effect which could be measured as doping in macroscopic devices.[106,319-322]

The studies in which 2DMs are interfaced to chemisorbed self-assembled monolayers (SAMs) represents a text-book example of dipole-mediated interactions.[104,107,335-338] SAMs are ultrathin molecular adlayers which have been widely studied in the past decades to functionalize metallic or dielectric surfaces (typically, Au and SiO_2).[339] The molecules in the SAM are typically composed of an anchoring group forming a covalent bond to the surface (thiols and silane for Au and SiO_2, respectively) and a tail which interacts via supramolecular forces with the other adjacent tails,[339] generating an ordered molecular arrangement in which molecular dipoles point in the same out-of-plane direction. When graphene and other 2DMs are exfoliated onto a SAM-functionalized dielectric surface,[104,107,333,335-338] the bottom surface of the 2DM is in close contact with out-of-plane aligned molecular dipoles, resulting in a field-effect-induced doping.

Additionally, organosilane molecules have been used in a few studies to functionalize the top surface of a 2DM,[105,333,340-343] and different studies have reported that organosilanes form ordered

monolayers firmly attached to van der Waals surfaces. The formation of these self-assembled structures was understood considering that silane groups formed covalent bonds to substitutional oxygen atoms and other point defects naturally present in the 2DM structure, and then cross-polymerized, forming covalent bridges between silanol groups in different molecules.[333,340,341,343] These SAMs on the top surface of 2DMs were used to provide encapsulation to 2DMs,[341] introduce predictable doping levels,[105,333,342] improve the charge injection[333] and modulate the superconductivity.[343] Moreover, they offered the possibility to functionalize in an asymmetric way the two surfaces of 2DMs, accessing the bottom surface via substrate functionalization and the top surface via direct functionalization.[333]

4.3 Charge transfer

Charge transfer between a molecular dopant and 2DM occurs in the presence of an appropriate alignment between the molecular HOMO/LUMO levels and the relevant energy level in the 2DM.[92] In particular, if the molecular LUMO lies at an energy below the conduction band in a 2D semiconductor (or the Fermi level in a 2D semi-metal), it becomes energetically favorable for an electron in the 2DM conduction band to occupy the molecular LUMO, resulting in electron transfer from the 2DM to the molecule, or hole doping in the 2DM. On the contrary, if the molecular HOMO lies above the valence band in a 2D semiconductor (or the Fermi level in a 2D semi-metal), an electron will be donated from the molecule to the 2DM, resulting in electron doping. For this reason, efficient p-type (n-type) molecular dopants are engineered to possess a LUMO[92,344] (HOMO) level particularly far from (close to) the vacuum level. In both cases, the

dopant molecules remain on the 2DM surface as charged impurities after the charge is transferred to the 2DM.

Charge transfer doping can be extremely efficient. Assuming that each dopant molecule is involved in the transfer of one entire charge carrier and approximating the footprint of each molecule at 1 nm^2, a doping level on the order of 10^{14} charge/cm^2 could be achieved in principle by covering the whole 2DM surface. However, the effective charge donated by each molecule is often a fraction of *e*,[345] but doping levels above 10^{13} charge/cm^2 have been reported[92,93] (to have a reference, the maximum charge carrier density introduced by a Si/SiO_2 back gate before dielectric is typically on the order of 10^{13} charge/cm^2). Moreover, a recent study reported that the doping efficiency of an organic reductant based on 4,4'-bipyridine was in the range of 0.63 to 1.26 electrons per molecule,[346] permitting to achieve doping levels well above 10^{13} charge/cm^2.

Among the effective p-type dopants, one of the most used is F_4TCNQ,[92,98,344,347-350] characterized by a LUMO level at approximately – 5.2 eV.[349] In this case, very large doping levels have been reported for graphene WSe_2 and MoS_2.[92,344,347-349] Additionally, bis(trifluoromethane) sulfonimide (TFSI) was also used as hole dopant, capable of boosting the PL of MoS_2 by balancing the hole/electron ratio.[110] We note that the physical origin of the PL boosting is not completely understood, and recent works show how cation donors lead to an even stronger PL increase.[351] On the other hand, a typical example of n-type dopant is reduced benzyl viologen, which has a reducing potential of approximately – 0.3 eV and was used to introduce electron accumulation in various 2DMs, including again the prototypical 2DMs graphene[352] and MoS_2.[93] In several cases,

charge transfer and dipolar interactions are simultaneously present,[353] and the effects measured at the device level are the result of the two combined phenomena.[354]

Apart from the conventional charge transfer taking place between a molecular dopant and 2DMs, a dynamic photo-induced charge (and/or energy) transfer take place when a photo-generated charge is transferred at a 2DM/molecule interface. This phenomenon does not significantly modify the charge carrier density of the 2DM in dark, but it can lead to significant changes in its optical properties, especially in its PL.[100,351,353,355,356]

In Figure 18 we have placed the charge transfer interaction at the border between the case of isolated molecules and continuous films. Indeed, in the case of charge transfer complexes the nanoscale molecular arrangement is not as crucial as it is for dipolar interaction. While obviously the effect is maximized when the whole surface is covered by dopants, charge transfer takes place also for isolated molecules, yielding a significant change in the 2DM charge carrier density even before reaching full coverage. As a consequence, in studies involving charge transfer dopants, the nanoscale molecular arrangement has been often loosely investigated, and the number of molecules on the surfaces was inferred on the basis of the effects measured at the device level.

In some of the cases, the high charge carrier densities exchanged during the charge transfer process had an impact on the 2DM which goes beyond the change in charge carrier density. As an example, when MoS_2 is treated with the strong reductant n-butyl-Li, the increased electron density triggered a structural phase transition, with MoS_2 transiting from the thermodynamically stable

semiconducting 2H phase to the metallic 1T phase.[357,358] This semiconductor-to-metal transition was exploited to improve the charge injection and optimize the performance of MoS_2 transistors.

Finally, we mention that charge transfer is closely connected to the process the intercalation of organic molecules into layered materials.[88,359-362] During intercalation, organic molecules occupy the van der Waals gap between adjacent sheets of layered materials, resulting in an increased layer spacing and a modified charge carrier concentration. Typically, the process is driven by a redox reaction in which organic ions are intercalated, and the sheets are consequently doped with electrons to compensate the charge unbalance.[359,360] Organic salts have been often used as intercalating agents,[363-365] and an electrochemical process is employed to intercalate them. In actual intercalated compounds, each intercalated molecule is mirrored by one electron injected in the sheet, leading to an ultra-high doping above 10^{14} electrons/cm^2 per layer which can introduce a semiconductor to metal transition[364,366] and important differences in other physical properties. While intercalated compounds have been investigated for decades,[367] a renewed interest in these materials has appeared recently in view of the 2DM research.

4.4 Defect healing

Even the highest-quality 2DMs possess point defects in their lattice,[86] such as atom vacancies[368] and substitutional defects.[369] A recent study showed that an Argon plasma can be used to generate highly reactive defects in graphene, which can be readily functionalized.[370] In the case of semiconducting materials, chalcogen vacancies introduced energy levels within the gap states, which act as charge scatterers and traps,[371] resulting in lower mobility,[109] larger hysteresis and

slower photo-response.[372] Importantly, while high-quality 2DMs obtained by mechanically exfoliation possess a low number of intrinsic defect sites, sheets generated by other strategies such as CVD,[373] chemical and liquid-phase exfoliation[374] are characterized by a high density of defects, which limit their optoelectronic performances. In this regard, "repairing" the defects is highly desirable to provide high electronic performances to 2DMs compatible with large-area fabrication.[375] While the dangling-bond free surface of semiconducting transition metal dichalcogenides is typically inert and difficult to functionalize covalently,[376] chalcogen vacancies are characterized by dangling bonds which are more reactive and can be used as anchoring sites for specific molecular species.[377,378] Therefore, molecular functionalization at defect sites can be explored as a defect healing strategy to improve the electronic performances of defective 2DMs and, eventually, to impart additional functions to 2DMs.

As an example of defect healing strategy, thiol-based molecules were used to functionalize sulfur vacancies in S-terminated transition metal dichalcogenides, both supported on substrates[94,108,109,379] and in solution.[380-382] According to this functionalization scheme, the sulfur atom in the thiol group forms a covalent bond at a sulfur vacancy site, achieving the goal of simultaneously repairing and functionalizing the defect. As a result, it was demonstrated in a few works that thiol functionalization improves the electronic performances of MoS_2 devices, repairing either intrinsic defects[94,108,379] or on-purpose engineered vacancies introduced by ion irradiation.[109] Moreover, it was reported that an annealing step resulted in a cleavage of the S-C bonds,[108] which released the molecule grafted by the thiol and fully recovered the MoS_2 lattice. The use of thiol-

based dopant groups provided not only defect healing but also a simultaneous doping effect.[94] More recently, a similar thiol functionalization strategy was shown to effectively improve the opto-electronic performances of WSe_2,[111] demonstrating that this approach is effective not only for S- but also for Se- terminated transition metal dichalcogenides.

Chalcogen vacancies in transition metal dichalcogenides can also be filled with isoelectronic oxygen atoms[368,383,384] and chloride.[385] In particular, it was demonstrated that the optoelectronic properties of defective WSe_2 could be significantly improved by laser irradiation in air, which promoted the binding of oxygen atoms at Se vacancies.[368] Moreover, a recent work focusing on the role of traps in InSe photodetectors shows that trap states related to Se vacancies in InSe can be passivated by simply exposing the sample to air, resulting in a profound modification of the photoresponse.[372] The fact that substitutional oxygen atoms might be more frequent than anticipated in the crystal structure of transition metal dichalcogenides was also pointed out in another work,[369] in which nanoscale characterization techniques were employed to address the origin defects in $MoSe_2$ and WS_2. In turn, the oxygen substitutional atoms can be used as anchoring sites for further functionalization, as previously discussed for SAMs on the top TMD surface.[105,333,340-343]

4.5 Covalent functionalization

Covalent functionalization of the basal plane of 2DMs has also been explored in several works.[386-392] While the defect functionalization strategies described in the previous section also results in the formation of covalent bonds, here we want to focus on those approaches for which covalent

binding does not require the presence of defects. The main difference between the two schemes is that in the defect healing strategy the number of molecules which could bind to the surface is limited by the number of defects; on the contrary, a larger number of molecules can be immobilized by directly grafting them covalently to the 2DMs basal plane. Since graphene and semiconducting transition metal dichalcogenides are very inert, aggressive chemical reactions were necessary to induce substantial covalent functionalization. In the case of graphene, diazonium chemistry[386] was employed in several works to break the sp^2 conjugation and form a covalent bond to C atoms in the graphene basal plane. In this process, an aryl diazonium cation becomes an aryl radical after releasing a N_2 molecule, as consequence of electron transfer from graphene. The so-obtained aryl radical binds covalently to a carbon atom in graphene, changing its hybridization to sp^3. The efficiency of this process could be boosted with an electrochemical approach favoring the charge transfer from graphene to the diazonium aryl, leading to a highly functionalized graphene where the average distance between two covalently attached molecules was estimated to be on the order of 1-4 nm for the highest degree of sample functionalization.[389] However, the electronic properties of functionalized graphene are often degraded by the covalent binding, as the sp^3 carbon atoms act as a scattering defect in the crystal structure.

The covalent functionalization of semiconducting transition metal dichalcogenides has been studied mostly for chemically exfoliated compounds obtained by intercalation of Li in solution. The so-obtained single and few layer thick flakes are negatively charged, due to electron transfer from the Li atoms. Chhowalla and coworkers developed a method to generate a carbon–sulfur

bond on the MoS_2 basal plane by reducing the negatively charged chemically exfoliated sheets using an organohalide reactant,[390] yielding a 20% functionalization degree, calculated as functional group / MoS_2 formula unit. Following a similar approch,[387,393,394] diazonium chemistry was also employed to functionalize negatively charged chemically exfoliated transition metal dichalcogenides in solution. More recently, a chemical approach has been followed to functionalize the surface of MoS_2 using aryl-diazonium salt.[395] It should be noted that the chemical exfoliation generates rather defective sheets,[377] so that part of the functionalizing molecules might are likely binding at defects sites.

4.6 Methods for interfacing 2D materials and molecules

After having discussed the main interactions occurring at the interface between 2DMs and molecules, we briefly mention which methods have been used to generate the interfaces between molecules and 2DMs. The methods are listed in order of increasing complexity and degree of control. The interactions are determined by the specific molecules and 2DMs employed, while to some extent they are not dependent on the methods used for depositing the molecules.

Drop-casting. Drop-casting is perhaps the simplest method to generate a 2DM/molecule interface, and it has been used in several works.[92,93,321,396-399] Typically, a drop of solution is applied onto the 2DM sheets exfoliated on a substrate, and a molecular layer is left on the substrate after the evaporation of the solvent. For this approach, volatile solvents are often employed, and a mild thermal annealing is sometimes used to ensure the solvent evaporation. The films generated by drop-casting are typically not uniform, since they are determined by the largely uncontrollable

surface dewetting and solvent evaporation dynamics, which produce material accumulation at the drop edges similarly to the "coffee ring" effect. However, the interface between a drop cast film and a 2DM is not necessarily disordered, since the nanoscale molecular arrangement depends on the molecule and 2DM in use. For instance, the drop-casting of long alkanes on graphene resulted in highly ordered epitaxial films.[331] Unfortunately, not all molecules display a sufficiently high solubility in common solvents. This is for example a problem of large and unsubstituted polyaromatic molecules. Such a modest solubility jeopardizes the use of any solution processing method.

Soaking/Dip-coating. Dip-coating is another widely used and extremely practical method to generate 2DMs/molecule interfaces.[93,94,96,100,107,342,400-403] 2DMs supported on a substrate are dipped into a solution, where molecules interact with the 2DM surface and impart the desired functionality. Normally, dip-coating refers only to situations in which the substrate is immersed in the solution and quickly removed, while soaking when the substrate remains immersed for some time. Even in this case, low boiling point solvents and mild annealing are often employed to obtain solvent-free molecular films.

In contrast with the molecular films obtained by drop-casting, dip-coated layers are generally very thin, as often only those molecules in direct contact with the sample surface get attached to it, while others remain in solution. Therefore, dip-coating generates molecular monolayers,[321] or even sub-monolayers. Interestingly, it is sometimes found that upon keeping the 2DM immersed in the solution for a longer time yields a larger effect on its electronic properties, which can be

explained considering that more molecules have time to interact with the 2DM surface and impart their functionality.

Spin-coating. Spin-coating is a widely used technique to form homogeneous films extending over large areas onto 2DMs supported on a substrate. In spin-coating, a drop of solution containing the target molecules is applied at the center of the substrate supporting the 2DMs, and then it is spread across the whole surface by rotating the substrate at high speed thereby generating centrifugal force. A low boiling point solvent is often used, in some cases followed by an annealing step to eliminate any solvent residuals. As compared to drop-casting and dip-coating, spin-coating has the advantage of producing homogeneous films, for which the thickness can be finely tuned by optimizing the molecular concentration in solution, the solvent boiling point and the rotation speed. As a result, spin-coating was used to grow molecular films from sub-monolayer to the tens-of-nm range on 2DMs. [106,115,319,348,354,404] Moreover, spin-coating of a bi-component blend composed of a dopant molecule and a polymer resulted in a phase separation which provided the desired doping level and stability in air.[348]

Vapor phase deposition. In this functionalization scheme, 2DMs on a substrate are sealed in a closed container with a small amount of functionalizing molecules. The container is annealed and the molecular vapors saturate the environment, condensing on the substrate and forming a film.[107,333,340,343] This process is typically employed to grow thin films showing an ordered molecular arrangement, and a relatively long incubation time (often a few hours) favors the intermolecular interactions and self-assembly. In fact, this approach was carried out to grow silane-

based SAMs on the surface 2DMs, as the optimization of annealing temperature and time enabled the formation of ultrathin and ordered films. Even in this case, the molecular films can be homogeneous over macroscopic distances (on the order of several cm^2), so this approach allows to functionalize not only small mechanically-exfoliated flakes, but also large-area 2DMs.[343]

Sublimation in (ultra-)high vacuum. Subliming molecules in vacuum onto substrate-supported 2DMs offers the possibility to generate ultraclean interfaces,[99,344,347,405-407] in which the thickness of the molecular layer can be monitored precisely using a quartz microbalance. Several parameters can be optimized to engineer the layer growth (e.g. substrate type and sublimation temperature), offering the possibility to control precisely the film morphology. The obvious disadvantage of this technique is the need of expensive, slow and rather cumbersome equipment for vacuum evaporation. Moreover, several organic molecules cannot be evaporated in vacuum, since they decompose before the sublimation temperature is reached. The ultraclean and highly controllable interfaces grown via sublimation are ideal for studies involving surface science technique, which are extremely sensitive to any surface contamination.

Functionalization in solution. Structurally controlled 2DM/molecule interfaces have been extensively obtained through the functionalization of 2DMs supported on a substrate, either as micromechanically exfoliated flakes or as large-area films. More recently, molecular functionalization of 2DMs has been explored in solution, by employing dispersions of layered materials exfoliated with an electrochemical approach or by sonication. Even in this case, the molecule/2DM interaction depends primarily on the chosen materials, so that mixing in solution

the same exfoliated 2DM with different molecules allows to explore the whole spectrum of interactions described above, from van der Waals interactions[408] to covalent functionalization.[387] Moreover, the method employed to exfoliate the 2DM in solution has also a strong impact on the functionalization strategy, since electrochemical exfoliation and sonication result in flakes characterized by different physico-chemical properties. Generally, electrochemical exfoliation yields many highly electron-doped ultrathin flakes (one-two layers) with large lateral size, while liquid phase exfoliation results in thicker flakes with smaller lateral size.[374] In the case of sonicated 2D flakes, molecular functionalization is often studied to improve the stability and processability of the dispersion.[380-382] In the case of chemical exfoliation, the flakes are sometimes functionalized to induce a phase transition, as in the case of MoS_2, where the exfoliation induced 2H 1T phase transition can be reverted by chemical functionalization.[390]

Ink-jet printing. While several techniques have been used to deposit solution-processed 2DM/molecule hybrids on target substrates, printing is particularly relevant from a technological perspective, as it enables the low-cost production of large-area films.[409-411] In all printing processes, which include inkjet, screen and roll-to-roll printing, the ink formulation plays a central role and ultimately determines the physical properties of the deposited films. Molecules and polymers are often introduced in 2DM dispersion to generate functional inks with the desired rheological properties, which have been used to fabricate photodetectors[409] and rudimentary memory elements[411], thus offering the possibility to add functionalities to CMOS technology in the More-than-Moore approach.

5 Molecular Approach to Boost the Performance of 2D Transistors for CMOS Applications

Transistors are the basic building blocks in digital and analog circuits with the function of signal switching and amplification. MOSFET is one main category of transistors with three terminals, namely source, drain and gate. The channel is situated between source and drain and the gate is separated from the channel by a thin insulating layer. The applied drain–source voltage V_d drives a drain current I_d through the channel and the applied gate–source voltage V_g determines the conductivity of the channel and the switching of the drain current.

2D layered semiconductors have emerged as plausible candidates for the next-generation channel materials in MOSFETs since the shrinking of transistor dimensions requires extremely thin channel layers. Figure 19a shows the device structure of planar Si MOSFET, together with the schematics of top-gate and back-gate 2D MOSFETs. The advantages of 2DMs include good carrier transport characteristics even at atomic-level thickness and the high immunity to short-channel effects. In comparison with Si, the scale length for planar 2D FETs with monolayer TMD channel and 2-nm-thick high-k dielectric ($k > 10$) is approximately 1 nm,[412] revealing the promising scalability of 2D FETs. A 10-nm top-gate MoS_2 FET has been successfully demonstrated by using a novel self-aligned gate fabrication process. The device showed record saturation current (>400 μA μm^{-1}) and good subthreshold slope (80 mV per decade).[413] Another work reported a MoS_2 FET with even shorter gate length down to 1 nm by using a carbon nanotube as the gate electrode (Figure 19b).[7] Figure 19c shows the superior transport behavior of this short-

channel MoS_2 FET with ~65 mV per decade and an I_{on}/I_{off} ratio of ~10^6. These works provided new insight into the ultimate scaling of gate lengths for a FET by surpassing the 5-nm limit.

The switching of a Si-based MOSFET depends on the depletion of majority carrier on the channel surface and the generation of minority carriers in the inversion layer. In contrast, 2D MOSFETs belong to a Schottky-barrier type and the switching is related to the tuning of metal-semiconductor Schottky barrier height. Therefore, the basic challenges to improve performance of 2DMs are inefficient source/drain doping, difficult carrier type modulation, lower mobility, and large contact resistance. Great efforts have been made to boost the performance of 2D devices based on the molecular approach. In this section, we will talk about the doping of 2D layers, contact and dielectric engineering via molecular approaches.

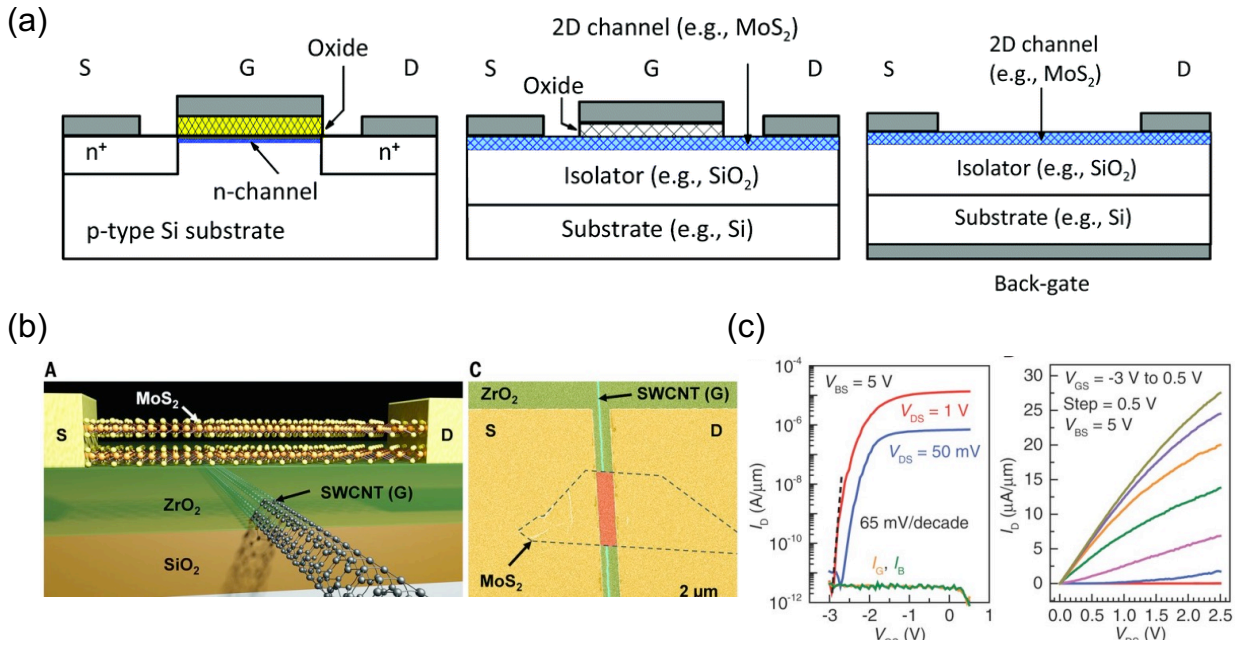

Figure 19. *(a) Basic device structure of conventional Si n-channel MOSFET, top-gate 2D MOSFET and back-gate 2D MOSFET frequently used for proof-of-concept purposes. (b)*

Schematic and false-colored SEM image of MoS_2 FET with carbon nanotube as gate. (c) Transfer curves and output curves of a bilayer MoS_2 FET with carbon nanotube as gate. (a) Reproduced with permission from ref (414). Copyright 2015 Royal Society of Chemistry. (b-c) Reproduced with permission from ref (7). Copyright 2016 American Association for the Advancement of Science.

5.1 Doping Engineering

In section 3 and 4, we have already discussed several types of electroactive molecules and molecular switches which can induce doping effect on 2DMs. Surface molecular doping can modulate the carrier density and carrier type of 2D layers and even realize defect healing or covalent functionalization on defective sites. From the point of view of device engineering, molecular doping can contribute to an improved device performance and to the construction of different logic devices, such as p-n diode, inverters, and memory devices.

Mobility is an important parameter to determine the switching speed of an FET. The carrier mobility of 2DMs is significantly limited by charge traps, impurities and short-range defect scattering. Sulfur vacancies are the most common defects in as-prepared MoS_2.[415] In Section 3.1 and 4, we have shown that thiol molecules can be covalently tethered on the vacancy sites. Yu et al. revealed that (3-mercaptopropyl) trimethoxysilane (MPS) molecules can repair the sulfur vacancies.[108] Figure 20a shows the improved transport properties of MoS_2 transistor after the healing of sulfur vacancies. Higher conductivities and electron mobilities were obtained from the MPS treated MoS_2 flake. A high electron mobility of 81 $cm^2V^{-1}s^{-1}$ at room temperature was

achieved from the double-side treated MoS_2 sample. In disordered materials, such as defective MoS_2, electrons are localized near the defects and carrier transport is dominated by variable-range hopping. In contrast, in perfect MoS_2, electron density is periodic in space and transport is band-like. The healing of defects can promote the transition from variable-range hopping to band-like transport (Figure 20b).[371]

Compared with physisorption, chemisorption on 2DMs shows higher functionalization stability and increases the doping density. In the meantime, the covalent bonding of molecules on the 2D defective sites can simultaneously heal the defects and dope 2D semiconductors, which is the preferable method to perform doping engineering. In order to increase the ratio of covalent functionalization, several groups have developed mild etching methods to induce more single-vacancy defects in TMDs. Argon-ion bombardment has been utilized to introduce sulfur vacancies in monolayer MoS_2 (Figure 20c).[109] The electron field-effect mobility μ_{FE} decreased as $\approx 1/V_s^2$ with the increasing density of vacancies up to $V_S \approx 5\%$, in which V_s is the created sulfur vacancy density. This trend is in line with predictions from a Coulomb impurity (CI) scattering model. The electrical properties of pristine and ion-irradiated FETs can be largely improved and recovered by exposing the devices to vapors of short linear thiolated molecules (Figure 20d). Another method is the laser-assisted etching of TMDs. High-power laser has been demonstrated to create sulfur vacancies in MoS_2 and selenium vacancies in WSe_2.[111,416] PH_3 molecules were adsorbed chemically on the vacancy site of MoS_2, and the FET device shows decreased drain current after the doping. These results confirm the depletion of electrons and *p*-doping effect by PH_3.[111,416] In another case,

thiophenol molecules were functionalized on a monolayer WSe_2 surface containing Se vacancies (Figure 20e). It was demonstrated that the defect healing via thiophenol adsorption improved the performance of WSe_2 transistors, including over ten-fold increase in the current density, the electron mobility, and the I_{on}/I_{off} ratio (Figure 20f).

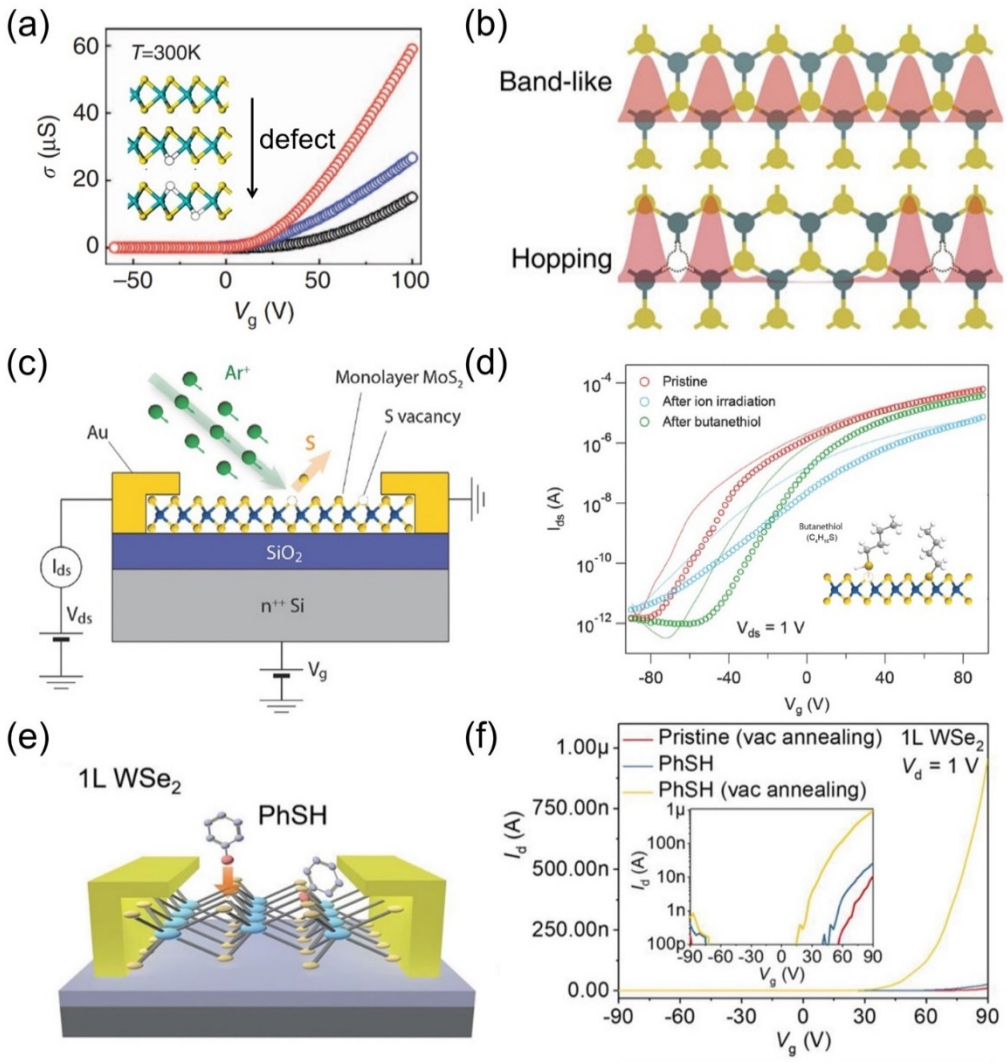

Figure 20. *(a) Typical σ-Vg characteristics of monolayer MoS_2 FET at T=300 K for as-exfoliated sample (black), single-side molecular treated sample (blue) and double-side molecular treated*

sample (red). Reproduced with permission from ref ([108]). Copyright 2014 Nature publishing group. (b) Schematics of carrier transport mechanism in perfect and defective MoS_2. Reproduced with permission from ref ([371]). Copyright 2013 Nature publishing group. (c) Schematic illustration of the Ar-ion irradiation on the monolayer MoS_2 FET. (d) Transfer characteristics of a pristine monolayer MoS_2 FET before (red circles) and after (blue circles) the ion bombardment, and after exposure to butanethiol vapors (green circles). (c-d) Reproduced with permission from ref ([109]). Copyright 2017 Wiley-VCH. (e) Schematic of back-gated monolayer WSe_2 field-effect transistor with the adsorption of thiophenol molecules. (f) Transfer characteristics of a pristine monolayer WSe_2 FET before (red line) and after (blue line) laser irradiation, after exposure to thiophenol vapors (yellow line), and after vacuum annealing (green line). (e-f) Reproduced with permission from ref ([111]). Copyright 2020 Wiley-VCH.

The effective control of carrier type is a prerequisite for 2DMs as active components in CMOS logic gates. By adjusting the contact metal electrodes, WSe_2 and BP FETs have shown n-type, p-type and ambipolar transport behaviors. An alternative method is to use organic layers as dopants to tune the carrier type in the 2DMs. Although previous sections have discussed the molecular doping, the control of carrier type in transistors requires the selection of suitable molecules to induce strong carrier injection. Ultrathin WSe_2 back-gated transistors using Au contacts mostly exhibit weak ambipolar or unipolar transport behavior, severely hindering its application in complementary circuitry and logic devices. To address the above issues, Stoeckel et

al. proposed the covalent functionalization of WSe_2 surfaces with ordered and ultrathin SAMs (Figures 21a-b).[333] Two SAMs, namely trichloro(1H,1H,2H,2H-perfluorooctyl)silane (PFS) and N-[3-(trimethoxysilyl)propyl]ethylenediamine (AHAPS) were adopted for the treatment of WSe_2 surfaces by vapor sublimation in a sealed reactor. The CF_3 groups in PFS and the NH_2 groups in AHAPS are electron acceptor and electron donor, which can result in p-type and n-type doping, respectively. After vapor-phase exposure of the two different SAMs on the top surfaces of a mechanically exfoliated WSe_2 flake with ozone treatment, the transistor showed significantly improved charge carrier mobility by >5 orders of magnitude (i.e., hole mobility of 150 $cm^2V^{-1}s^{-1}$ in Figure 21a and electron mobility of 17.9 $cm^2V^{-1}s^{-1}$ in Figure 21b, respectively). In addition, a double-sided molecular functionalization strategy to both the top and bottom surfaces of bilayer WSe_2 flakes were further exploited, acquiring almost balanced ambipolar transport with hole mobility of 20 $cm^2V^{-1}s^{-1}$ and electron mobility of 5.7 $cm^2V^{-1}s^{-1}$ (Figure 21c). The results demonstrated the robustness of the molecular doping technique to effectively engineer the charge transport in ultrathin 2D layered materials by simultaneous defect modification and energy level manipulation.

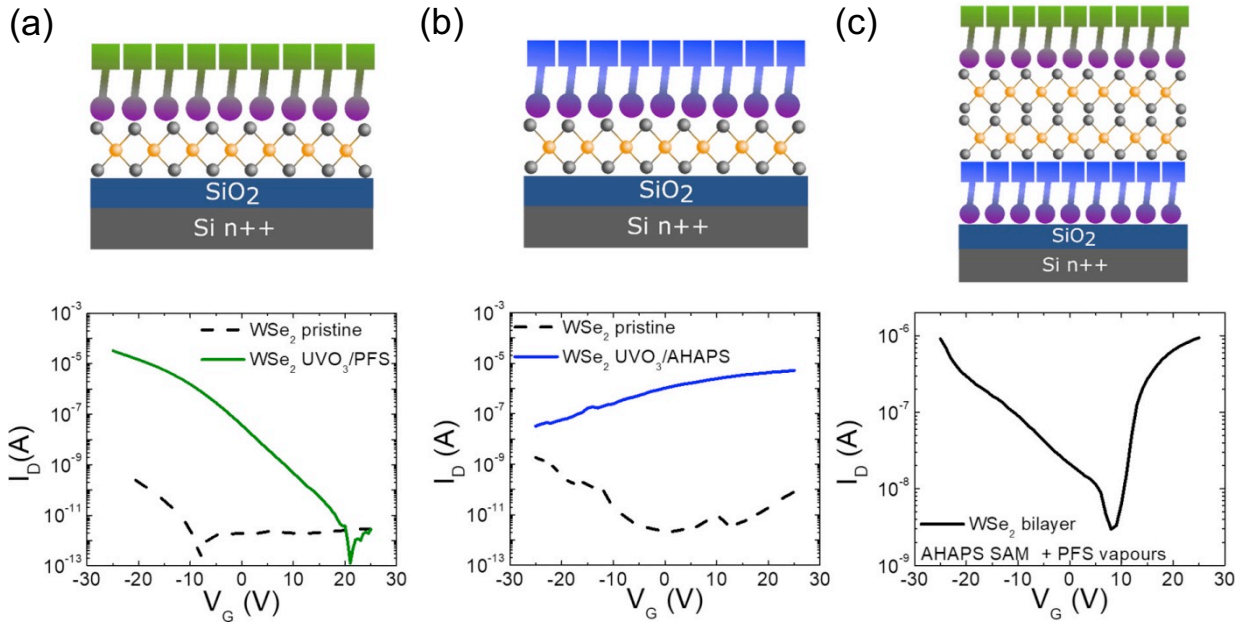

Figure 21. *Device architecture and corresponding transfer curves of ozone treated WSe_2 single layer with (a) PFS vapor and (b) AHAPS vapor. For the sake of comparison, the transfer curves of the pristine WSe_2 single layers are also shown (dashed black lines). (c) Device architecture and corresponding transfer curve of bilayer WSe_2 after asymmetric functionalization: the bottom WSe_2 layer is in contact with AHAPS-treated SiO_2 dielectric, while the top WSe_2 layer was exposed to ozone and PFS vapor. Reproduced with permission from ref ([333]). Copyright 2019 American Chemical Society*.

By taking advantages of the carrier type control, homogeneous 2DMs p–n junctions can be constructed. Li et al. reported a vertical MoS_2 p–n homogeneous junction. [417] In the as-fabricated back-gate FET, a few-layer mechanical exfoliated MoS_2 flake with thickness of 11 nm was used as the channel. The bottom surface was n-doped by benzyl viologen (BV) layer, and the top surface

was p-doped by $AuCl_3$. A Cr/Pd top electrode (drain) and a Cr/Pd/Cr bottom electrode (source) were contacted with the top and bottom surfaces of the MoS_2 flake, respectively. Ambipolar carrier transport characteristics were observed for both positive and negative sweeps with a hysteresis window of 60 V, due to the presence of electron and hole transport at the bottom n-doped MoS_2 and the top p-doped MoS_2 regions, respectively. The output curves showed a clear rectifying effect, with the current rectification ratio extracted to be ~100. In another case, the vertical MoS_2 p–n homogeneous junction was fabricated via the p-doping of top MoS_2 layer by $AuCl_3$ treatment.[418] The device works as a phototransistor and the junction facilitates the separation of photogenerated carriers. The device produced a photoconductive gain of $>10^5$ electrons per photon, external quantum efficiency greater than 10%, responsivity of 7×10^4 AW^{-1}, and a time response on the order of tens of ms. The formation of the out-of-plane p–n junction serves as a novel photoresponse unit for 2D TMDs phototransistors and paves the way towards high performance and broadband response optoelectronic devices.

Besides the vertical junction, homogeneous lateral 2DMs p–n junctions were fabricated by Ji et al.[419] The unsatisfactory ambipolar character of the pristine WSe_2 transistor was converted to unipolar electrical behavior by two different molecular dopants: 4-nitrobenzenediazonium tetrafluoroborate (4-NBD, p-type dopant) and diethylenetriamine (DETA, n-type dopant), together with a drastically enhanced hole mobility of 82 $cm^2V^{-1}s^{-1}$ and electron mobility of 25 $cm^2V^{-1}s^{-1}$ (Figure 22a). The authors fabricated the lateral p-n junction with spatially controlled p- and n-doping (Figure 22b). Output characteristics of the WSe_2 before and after the formation of the p-n

junction are shown in Figure 22c. While the pristine WSe_2 flake exhibited an almost linear I_d–V_d curve with high resistivity (black curve), after the spatially controlled p-n doping, the device showed a clear rectifying behavior (red curve). Such asymmetric transport behavior is a strong evidence for the formation of a p-n junction. Moreover, the molecular-doped monolayer WSe_2 transistors were further integrated into a more sophisticated CMOS inverter. The V_{out} was kept at a value of V_d for V_{in} lower than -28 V and dropped to 0 V for V_{in} higher than -25 V, with a sharp inversion (Figure 22d). Figure 22e shows the voltage gain, defined as $V_{gain} = -dV_{out}/dV_{in}$, which is one of the most important performance parameters of CMOS inverters. The inverter displayed a voltage gain of 10 and picowatt power consumption, demonstrating valuable contributions of the molecular doping technique for advanced integrated electronics.

The widely used p-type (i.e., $AuCl_3$) and n-type (i.e., N_2H_4) doping molecules have also been reported to fabricate lateral p-n junction devices based on MoS_2 and WSe_2, respectively.[420,421] Some other molecules with unique properties can be functionalized on 2D semiconductors to simultaneously perform device engineering and realize p-n junction. For example, cetyltrimethyl ammonium bromides (CTAB) solutions have high coordination with nonionic amphoteric surfactants. CTAB comprises two key moieties which could have combined effects to greatly improve the rectified properties of the TMDs p–n junction: Br^- could preferentially occupy sulfur vacancies of TMDs and enable electron injection into TMDs; quaternary ammonium cations could induce the formation of favorable interfacial dipoles to lower the work function of the metal electrode. The p–n junction device showed an ideal rectifying behavior with the forward/reverse

current ratio about 10^3 and the ideal factor of 1.64, due to the improved contact and the less trap states. The junction device also displayed a strong photoresponse under 450 nm light irradiation with the current ratio of 10^5, the responsivity of 30 A/W (7989% external quantum efficiency) and the detectivity of over 10^{11} Jones, demonstrating the potential applications as sensitive photodetector and low power photoelectronic devices. Therefore, CTAB is an ideal n-type doping molecule on TMDs to improve device performance and construct p-n junction devices.[422] Finally, irradiation with deep ultraviolet light in a nitrogen atmosphere was found to introduce n-type doping,[423] and it was exploited to generate p-n heterojunction in thin $MoTe_2$ flakes.[424]

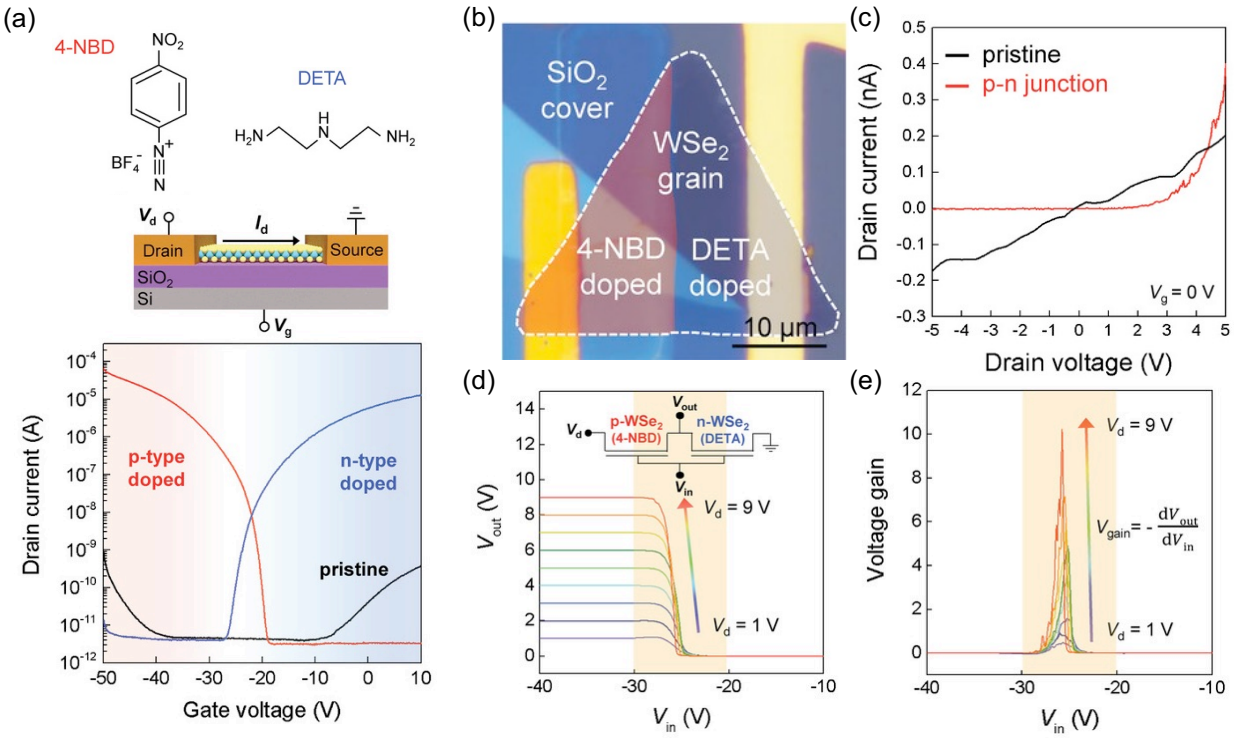

***Figure 22**. (a) The top panel displays the schematic of device structure and the 4-NBD and DETA molecules used for p- and n-type chemical doping, respectively. The bottom panel shows transfer characteristics of pristine (black) and 4-NBD doped (red) and DEA doped (blue) WSe_2 devices.*

(b) Optical micrograph of a p-n junction made by the spatially controlled p/n doping within single WSe_2 grain. (c) Output curves of the pristine and p-n junction monolayer WSe_2 device. The p-n junction device shows clear rectification behavior. (d) V_{out} plotted as a function of V_{in}. Inset shows the circuit diagram of CMOS inverter operated with p- and n-doped WSe_2. (e) Voltage gain and power consumption of the CMOS inverter. Reproduced with permission from ref ([419]). Copyright 2019 Wiley-VCH.

5.2 Contact Engineering

The control of the charge carrier injection from the metal electrode to the 2D semiconducting channel via a gating effect is the main working principle of 2D MOSFETs. In another word, the metal-semiconductor Schottky barrier height (SBH) can be tuned by the gate voltage and finally affect the charge carrier flow in the 2D semiconductors. In the Schottky-Mott theory, the SBH is equal to the difference between the work function of metal electrode and the Fermi level of semiconductor. However, the SBH extracted from the experiments often showed large deviation from the theoretical values. Das *et al*. adopted four kinds of metal materials with different work functions to fabricate few-layer MoS_2 transistors.[425] The low work function metals, e.g., Sc and Ti electrodes are predicted to facilitate the electron transport, while the hole transport will be dominant in MoS_2 FETs with high work function electrodes, such as Ni and Pt. From the experimental results, all MoS_2 FETs showed the electron-dominant unipolar transport behavior and no polarity transition has been observed. The extracted SBH for electron transport was 230

and 30 meV for Pt and Sc electrode, respectively, which is far from the theoretical value. Fermi level pinning effect has often been used to explain the weak dependence of SBH on the metal work function.[426] The surface states and the metal-induced gap states (MIGS) are two main reasons to cause the Fermi level pinning. The surface states are originated from the crystal defects in the semiconductor itself and the MIGS are caused by the tails of metal wave functions at the contact regions. The charges trapped in the gap or interfacial states can induce the band bending at the semiconductor surface and weaken the influence from the metals. One key factor to evaluate the Fermi level pinning is the dependence of SBH on the metal work function ($S=d\Phi_{SB}/d\Phi_{M}$). This number is 0.1 extracted from the few-layer MoS_2 transistors,[425] indicating the strong Fermi level pinning effect. Therefore, the quality of the electrical contact between metal and 2DMs plays a crucial role on the performance of 2D FETs.

In order to eliminate the Schottky barrier, the degenerate doping of 2DMs at the contact region is a possible solution. A transition from semiconducting to metallic property of TMDs by phase engineering can be adopted to optimize the contact. Figure 23a shows that the 2H-phase TMDs were selectively transformed into 1T phase by immersing into the *n*-BuLi solutions. The Li ions were intercalated into the interlayer of 2H phase TMDs and donate electrons into 2D layers, which induces the phase transition. The selective 1T phase region became metallic and can be the edge-contact material for the 2D semiconductor channel. Figure 23b shows the MoS_2 transistor with the metallic 1T phase MoS_2 as metallic contact and the semiconducting 2H phase MoS_2 as the channel.[357,358] The lowest contact resistance at that time was achieved as ~200 Ω·μm for MoS_2

without gate bias. Superior transistor performance was also observed from the transfer curves of the device with 1T phase contact (Figure 23c), including high electron mobility (~50 $cm^2V^{-1}s^{-1}$), large I_{on}/I_{off} ratios (>10^7), low subthreshold swing (below 100 mV/dec), high drive currents (~100 μA/μm), and excellent current saturation. The 2H to 1T phase transition of WSe_2 was also achieved by a similar immersion process in *n*-BuLi solution. Monolayer 2H-phase WSe_2 FETs with metallic 1T phase contact exhibited an I_{on}/I_{off} ratio of 10^7 and a hole mobility of 66 $cm^2V^{-1}s^{-1}$. As 1T phase is the metastable structure, the thermal annealing can drive the conversion from 1T phase to the thermodynamically favored 2H phase. Therefore, the reversible phase transition of WSe_2 between 2H and 1T has been effectively controlled.[427] Although the transition from semiconducting phase to metallic phase at the contact region is the best solution to minimize the contact resistance, it is still challenging to improve the stability of metallic-phase TMDs and promote their applications in the electronic devices.[428] Chemical approaches have been proposed to induce the degenerate doping of 2DMs at the contact region via organic molecular functionalization. As a representative example, the aforementioned surface doping methods have been employed to reduce the contact resistance of TMD-based FETs with NO_2 or BV adsorption.[56,93] Similarly, Du et al. reported that chemical doping using polyethylenimine (PEI) could reduce the contact resistance of multilayer MoS_2 FETs.[95] This is because that PEI, an amine-rich aliphatic polymer, can strongly donate electrons into MoS_2. These approaches require the spatial resolution to modulate the contact region only, otherwise they will lead to undesirable phenomena, such as a poor I_{on}/I_{off} ratio.

Fermi-level pinning effect is related to surface defects and surface contaminations. The surface defects can contribute to the gap states and induce the Fermi level pinning. It has been theoretically predicted that the insertion of thin tunneling layers between the metal contacts and the 2D channel can reduce the interaction at the contact interface, remove the interfacial states, and suppress the negative influence of MIGS.[429] Wang et al. reported that an inserted thin h-BN could improve the charge injection properties of TMD-based FETs by achieving ohmic contact behavior, even at low temperatures.[429] Ultrathin metal oxide layers (MgO, Ta_2O_5, etc.) have also been demonstrated to effectively reduce the Fermi-level pinning effect.[430,431] Previous works have shown that thiol functional groups tend to passivate the sulfur vacancies of MoS_2 via the formation of covalent bonds.[108,109] Taking advantage of this methodology, Cho et al. reported the vapor deposition of thiol molecules on the contact regions of MoS_2 FETs to act as the tunneling layer (Figure 23d).[432] Figure 23e showed the linear output curves of thiol-treated FETs even at the low V_d regime, indicating the formation of a good metal-semiconductor contact with a low contact resistance. Two dominant factors determined the carrier injection at the thiol-treated contact region, including the Schottky barrier and the tunneling process. The treatment of thiol molecules created additional tunneling paths, reduced the pinning effect, and lowered the Schottky barrier. Through the design of the molecular structure, the Schottky barrier and the tunneling process can be tuned. Decanethiol (DT)-, perfluorodecanethiol (PFDT)-, and hexadecanethiol (HDT)-treated devices all exhibited much smaller activation energy than untreated devices (Figure 23f). However, DT and PFDT exhibited opposite electric dipole moments, slightly affecting the Schottky barrier. The

longer carbon chain length of HDT induced a relatively higher activation energy among the three used molecules and resulted in a larger tunneling resistance. This work demonstrated that the interfacial molecular layer can tune the dominant carrier injection mechanism from thermionic emission to field emission.

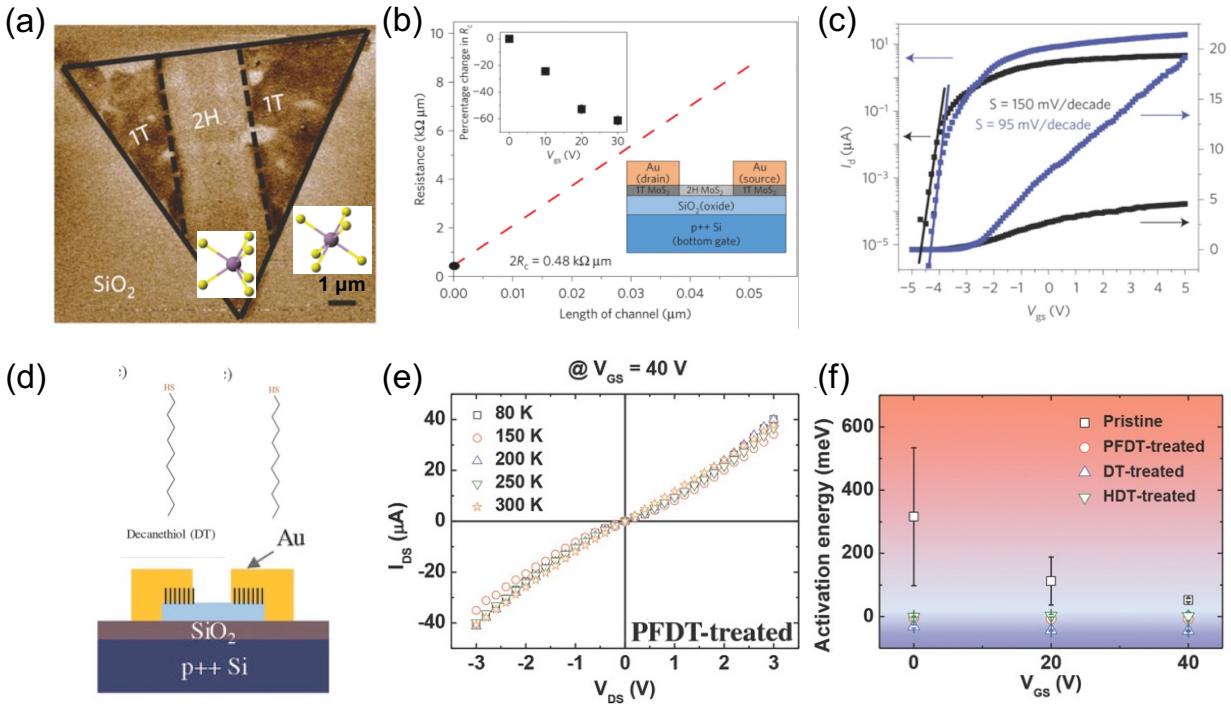

Figure 23. *(a) Electrostatic force microscopy phase image of a monolayered MoS_2 nanosheet showing the difference between locally patterned 2H (bright color) and 1T (dark color) phases. Inset shows the crystal structures of the 2H and 1T phase MoS_2. (b) Extrapolation of the red lines yields contact resistances (R_c) of 0.24 kΩ μm for 1T contacts at zero gate bias. Inset shows the decreased percentage of contact resistance with the increasing gate bias. (c) Transfer characteristics of top-gated devices, measured at V_{ds} = 1 V. Blue curves represent devices with 1T phase electrodes and the black curves are with Au on the 2H phase. (a-c) Reproduced with*

permission from ref ([357]). Copyright 2014 Nature publishing group. (d) Schematics of the decanethiol (DT) and perfluorodecanethiol (PFDT) molecule. And the schematic of MoS_2 transistor with thiol-treated contact. (e) Output curves of PFDT-treated MoS_2 FETs at fixed gate bias with varying temperature from 80 to 300 K. (f) Extracted activation energies of untreated, DT-treated, PFDT-treated, and HDT-treated MoS_2 FETs at different gate bias conditions. Red region represents "thermionic emission dominant" and blue region represents "field emission dominant". (d-f) Reproduced with permission from ref ([432]). Copyright 2018 Wiley-VCH.

The quality of the 2DMs and the fabrication process determines the surface defects/impurities and directly affects the tuning of Schottky barrier height. Liu et al. reported that the high-energy metal deposition process created considerable damages to the MoS_2 channel layer and produced a glassy layer with apparent defects, interface diffusion, chemical bonding and atomic disorder (Figure 24a). [433] In order to prevent physical damages from the high-energy deposition process, they transferred pre-deposited metal electrodes to the target MoS_2 flake via a dry transfer process (Figure 24b). Extracted from device with different transferred metal contacts, the Schottky barrier height Φ_{SB} was strongly dependent on the metal work functions, and the Schottky barrier type was tuned from electrons to holes. The fitted S parameter was 0.96, approaching the limit of the Schottky–Mott law defined by electrostatic energy alignment (Figure 24c). For control devices with deposited metals, the extracted S parameter was 0.09, confirming strong Fermi level pinning effect near the conduction band edge at the metal/MoS_2 interface. In another work, Wang et al.

emphasized the importance of an ultraclean interface between metal and 2D channel on the reduction of contact resistance. A super low contact resistance of ~800 Ω μm and a small Schotteky barrier of 110 meV was achieved in monolayer MoS_2 FETs with the deposition of indium (In) metal on contact regions (Figure 24e).[434] The authors stated that the evaporation of a thin layer of In on MoS_2 did not cause any damages including lattice distortion and defects (Figure 24d), and hence the devices exhibited excellent contact properties. They also demonstrated a low contact resistance on ultrathin NbS_2, WS_2 and WSe_2. The contact resistance between NbS_2 and In/Au electrode was ~220 Ω μm with near-ideal band offsets, indicative of defect-free interfaces. Recently, Shen et al. reported the use of semimetallic bismuth as the contact materials of TMDs transistors.[13] In addition to the excellent interface, low work function and zero density of state at the Fermi level of bismuth electrodes contributed to zero Schottky barrier height, a contact resistance of 123 Ω μm and an on-state current density of 1.1×10^3 μA μm^{-1} in a monolayer MoS_2 transistor.

By and large, compared to the methods reported by Liu et al.[433], Wang et al.[434] and Shen et al.[13], the attractive advantage of the molecular approaches is the wide versatility of modulation of the injection properties by the ad hoc design of molecular structures.[432] The Schottky barrier height, the tunneling process, and the carrier injection mechanism can be modulated by changing the bonding groups, the molecular lengths, the electric dipole moments and the conductivity of molecular backbone. In the meantime, the disadvantages of molecular approaches include the

limited operating conditions, such as low temperature and low voltage bias conditions, because molecules cannot withstand harsh environment. This should be improved in future research.

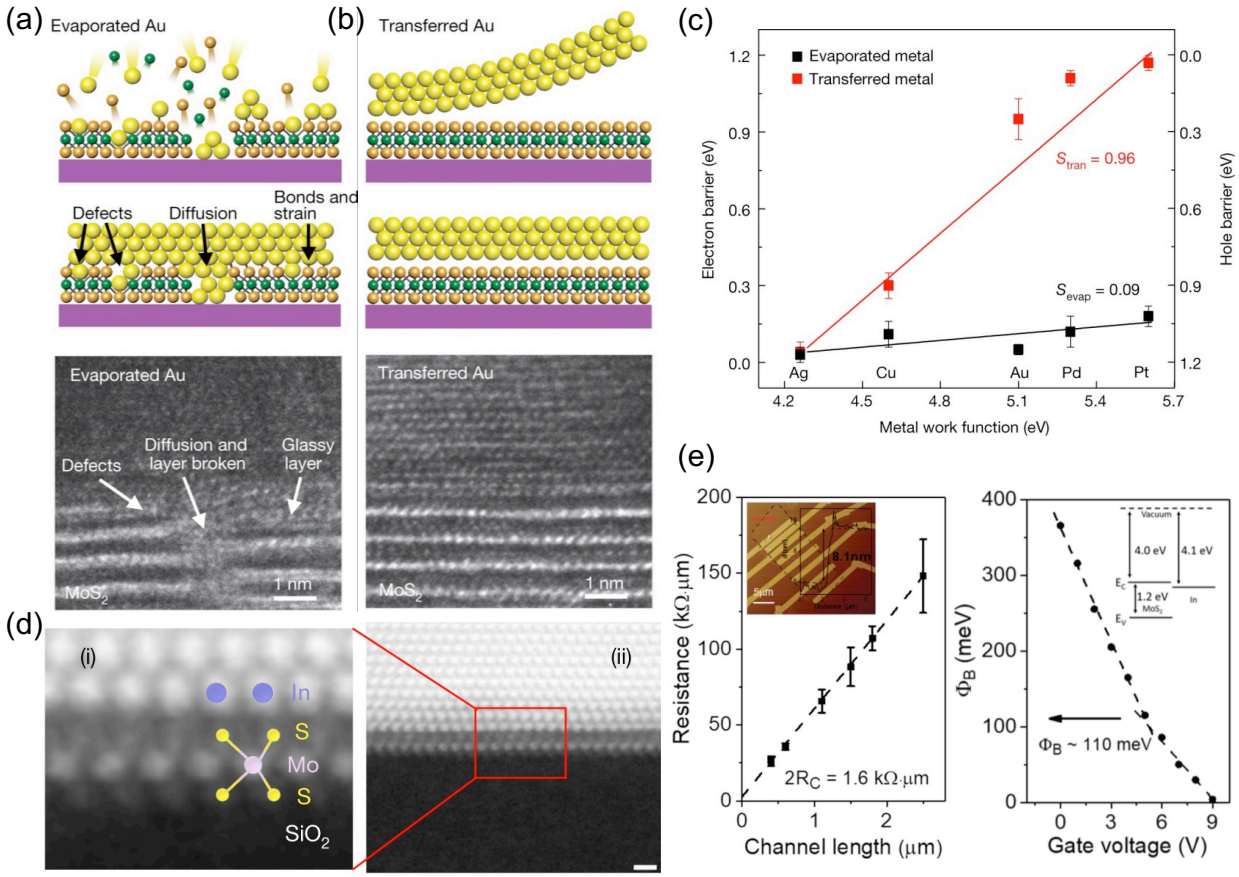

Figure 24. *(a) Cross-sectional schematics and TEM images of conventional electron-beam-deposited Au electrodes on top of MoS_2, where the bombardment of the MoS_2 surface by high-energy Au atoms and clusters creates considerable damage to the MoS_2 surface. (b) Cross-sectional schematics and TEM images of the transferred Au electrode on top of MoS_2, with atomically sharp and clean metal-semiconductor interfaces. (c) For transferred metal electrodes, the majority carrier type and corresponding Schottky barrier height is strongly dependent on the metal work function with a slope (S = 0.96) approaching unity, suggesting excellent obedience to*

the Schottky–Mott law. With the conventional evaporation-deposited metal electrodes, the devices invariably show n-type behaviour with a small electron Schottky barrier and a slope S = 0.09, indicating the strong pinning effect at the metal–semiconductor interface. (a-c) Reproduced with permission from ref ([433]). Copyright 2018 Nature publishing group. (d) Atomic-resolution images of In/Au on monolayer MoS_2 (i) and low-pass filtered ADF STEM image showing Mo, S and In/Au atoms (ii). (e) Contact resistance of In/Au contacts on few-layered MoS_2 and Schottky barrier (Φ_B) extraction indicating ideal In contacts with MoS_2. The inset shows the energy band diagram of MoS_2 and In. (d-e) Reproduced with permission from ref ([434]). Copyright 2019 Nature publishing group.

5.3 Dielectric Engineering

The theoretically predicted phonon-limited mobility of monolayer MoS_2 at room temperature is about 200~410 $cm^2V^{-1}s^{-1}$.[435,436] However, the field-effect mobility of monolayer MoS_2 quantified experimentally is much smaller, ranging from 0.1 to 20 $cm^2V^{-1}s^{-1}$ in back-gated transistors without any device engineering.[9,437-439] Apart from the influence of Schottky contact in two-probe configuration, the discrepancy between theoretical and experimental results originates from several extrinsic scattering sources, such as defects in the 2D channels, charge impurities at the interface, and charge traps. In previous sections, we have discussed the negative impact of 2DMs defects on the carrier transport. In this section, we will focus on the dielectric interface engineering, which provides promising routes to achieve the mobility close to theoretically predicted value. We

will discuss the engineering at the 2DMs/dielectric interface and its effects on the field-effect mobility.

The charge impurities can be regarded as point charges and they can interact with carrier in semiconductor by long-range Coulomb interaction. Several excellent works demonstrated that the inferior device performance of 2DM FETs partially resulted from the charge-impurity scattering of.[440-442] The source of the impurities include metal ions inside the substrates, the dangling bonds at the 2DMs/dielectric interface, and the adsorbates on 2DMs surface. SiO_2 is the most used dielectric material in 2DMs transistors due to its ultra-flat surface, stable properties, mature manufacture process. However, the 2D transistors fabricated on SiO_2/Si substrate showed inferior carrier mobility. Wang *et al*. fabricated suspended MoS_2 FET with the air/SiO_2 as the back-gated dielectric.[443] After getting rid of the scattering from the dielectric layer and the surface impurities, the mobility showed dramatic improvement from 46 to 105 cm^2/Vs. Such an increase was a clear demonstration that Coulomb scattering from charge impurities at the 2D/ SiO_2 interface strongly affected the carriers transport and was responsible for the unsatisfactory carrier mobility. Hence, the replacement of SiO_2 with other dielectric materials or the engineering of dielectric surface appear as promising strategies for the improving FET performances.

High-*k* dielectrics have been predicted to effectively suppress the scattering from the charge impurities. This is because the Coulomb potentials of impurities can be screened in the high-*k* dielectric environment and the carrier mobility in 2D transistors can be enhanced.[444,445] The mobility of multilayer MoS_2 increased to over 100 $cm^2V^{-1}s^{-1}$ at room temperature with Al_2O_3

bottom gate.[446] Yu *et al*. systematically compared the performance of MoS_2 FET with SiO_2, Al_2O_3 and HfO_2 as the gate dielectric.[55] The electron mobility of monolayer MoS_2 at room temperature increased from 80 $cm^2V^{-1}s^{-1}$ on SiO_2 substrates ($\varepsilon_e = 3.9$), to 113 $cm^2V^{-1}s^{-1}$ on Al_2O_3 substrate ($\varepsilon_e = 10$), being 31% improvement. This mobility can be further increased to 148 $cm^2V^{-1}s^{-1}$ on HfO_2 substrate ($\varepsilon_e = 16.5$). It showed that the screening of charged impurities by high-*k* dielectric is a viable method to improve the carrier mobility.

Although the screening effect can contribute to the mobility increase, remote phonon scattering originating from the lattice vibrations of metal-oxide bonds in high-*k* dielectric layer leads to the reduction of carrier mobility. In addition, the conventionally used dielectric layers, such as SiO_2, Al_2O_3 and HfO_2, are rich with hydroxyl groups and other charge traps at the surface, which also degrades the carrier mobility. Therefore, the chemical approach to engineering the surface of conventional dielectric layer represents a potentially powerful route to realize interface improvement. Najmaei *et al*. reported the use of self-assembly monolayers to modify the surface condition of conventional substrates.[447] As shown in Figure 25a-b, the molecular monolayers employed a variety of functional groups including amine ($-NH_2$), methyl ($-CH_3$), fluoro ($-CF_3$), and thiol (-SH). Then monolayer MoS_2 was transferred onto the functionalized substates to fabricate transistor devices. From the transfer curves in Figure 25c, these functional groups on the substrates shifted the threshold voltage of the transistor and changed the carrier density of MoS_2 layer. This can be explained by the different built-in dipole fields of the functional groups. Positive dipoles ($-CH_3$ and -OH) on the substrates depleted the carriers in the MoS_2 conduction bands, while negative

dipoles fields (-NH_2, -SH and –CF_3) pushed the charge carriers in the interface into the MoS_2 channel. The authors also found that devices on thiol-treated substrates showed a significant enhancement in the mobility (Figure 25d), which was attributed to the passivation of defects and trap states in MoS_2. In another case, trichloro(1H,1H,2H,2H-perfluorooctyl)silane (PFS) and N-[3-(trimethoxysilyl)propyl]ethylenediamine (AHAPS) were selected for the functionalization of SiO_2 substrate to form the self-assembled monolayer (SAM).[333] Then mechanically exfoliated WSe_2 monolayers were transferred onto SAM-functionalized SiO_2 substrates and subsequently contacted with metal electrodes. The transfer characteristics of a monolayer WSe_2 transistor on untreated SiO_2 substrate were compared with that on SAM-treated substrates. The PFS-treated device displayed improved charge transport, with higher current and balanced ambipolarity. In contrast, AHAPS SAM induced strong n-doping on WSe_2 and the device displayed an electron mobility approaching 0.4 $cm^2V^{-1}s^{-1}$.

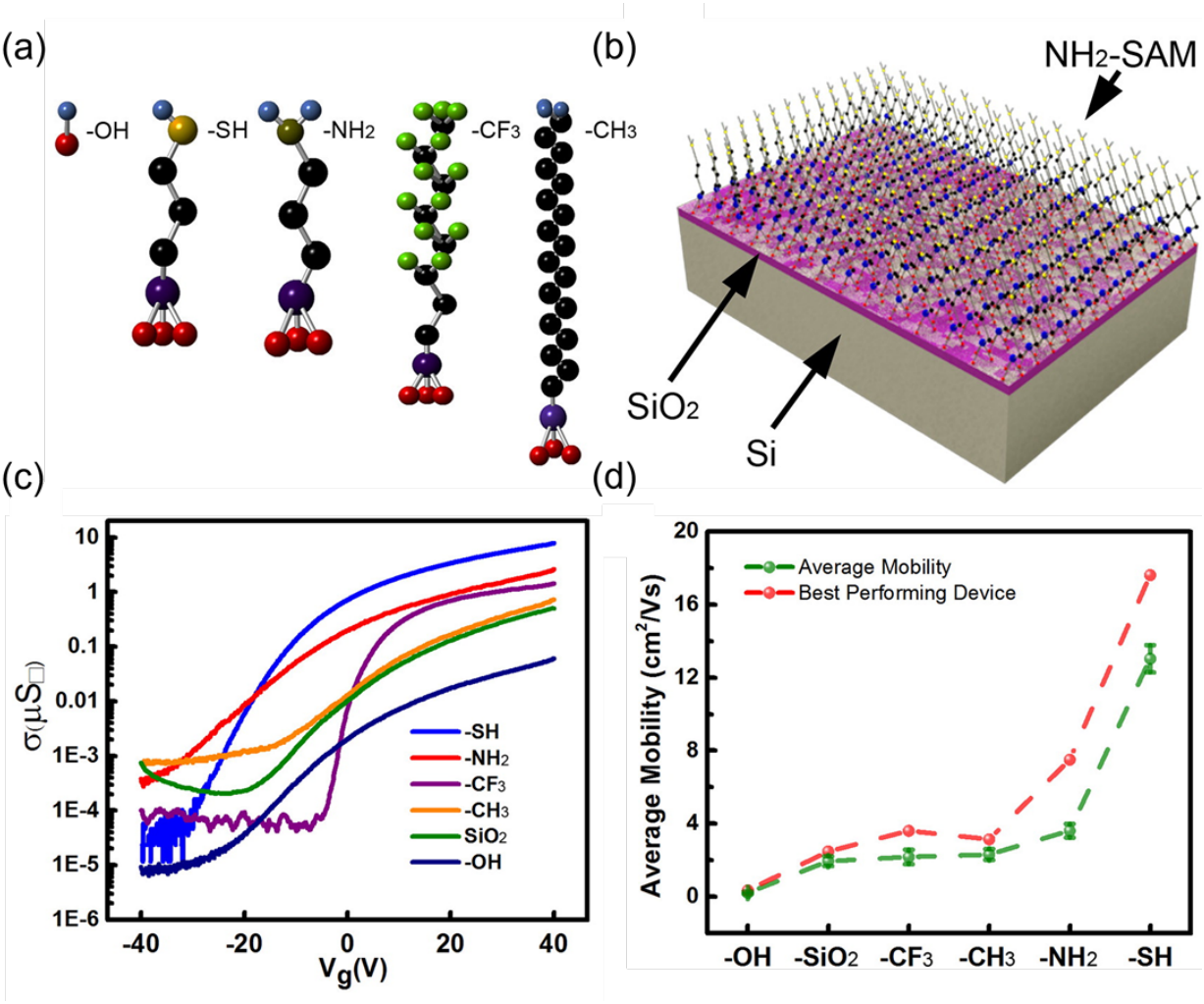

Figure 25. *(a) Molecules with different functional groups used to form self-assembled monolayer (SAM) on SiO_2/Si substrate and their orientation relative to MoS_2 monolayers. (b) The schematic of surface functionalization on SiO_2/Si substrate with the assembled configuration of NH_2-SAM molecules. (c) Transfer curves of representative MoS_2 transistor devices on a variety of modified and pristine substrates. (d) Changes in the field-effect mobility of MoS_2 samples on varied substrates and the highest mobility from the best performing device. Reproduced with permission from ref ([447]). Copyright 2014 American Chemical Society.*

Another feasible method to engineer the conventional dielectric surface consists in the construction of a double dielectric layer via coating polymer layer. Feng *et al.* fabricated a PMMA/Al_2O_3 double dielectric layer to passivate the hydroxyl groups on the Al_2O_3 surface.[448] After PMMA coating, the dielectric surface became less hydrophilic and the contact angle for water changed from 54° to 73°. The mobility of multilayer InSe on double dielectric layer showed a dramatic increasement from 64 $cm^2V^{-1}s^{-1}$ to over 1000 $cm^2V^{-1}s^{-1}$. The PMMA layer acted as the interfacial layer between 2D channel and high-k dielectric to suppress the Coulomb impurities scattering. However, the disadvantages of PMMA layer lied in the incompatibility with lithography process. Zhao et al. and Wang et al. used an appropriate hydroxyl-free polymer as the interfacial layer of gate dielectric, that is, divinyltetramethyldisiloxanebis(benzocyclobutene) (BCB), in order to optimize the 2D/dielectric interface and decrease the Coulomb and phonon scattering.[115,449] 2D FETs were fabricated on the BCB/SiO_2 substrates with patterned top metal electrodes. Figure 26a showed that the conductivity of monolayer MoS_2 at V_g = 0 V on the BCB/SiO_2 substrates was decreased to a quarter of that on untreated SiO_2 substrate, and the threshold voltage (V_{th}) shifted 20 V to a more positive value, indicating the deceased carrier density on BCB/SiO_2 substrates.[115] From the hysteresis results of the MoS_2 FET in Figure 26c-d, the value decreased from 7.3 V on the SiO_2 substrate to 4.1 V on the BCB/SiO_2 substrate. Compared to the MoS_2/SiO_2 interface, the trap density at the MoS_2/BCB interface was reduced by 40% from 4.69 × 10^{12} cm^{-2} eV^{-1} to 2.86 × 10^{12} cm^{-2} eV^{-1}. The lower trap density at the MoS_2/BCB interface leaded to the increase of MoS_2 mobility due to the suppressed scattering effect. In another case,

the field-effect mobility of InSe underwent a dramatic increase from a value of 0.01 $cm^2V^{-1}s^{-1}$ on SiO_2 to 688.2 $cm^2V^{-1}s^{-1}$ on BCB/SiO_2 substrate. [449] BCB dielectric layer can fabricated by spin coating on the arbitrary substrate, which is a simple and large-scale fabrication process. The post annealing can achieve the optimal cross-linking and render it compatible with the conventional microfabrication process. Compared with PMMA layer, BCB shows the advantages with low processing temperature, high thermal stability, and excellent compatibility, and it acts as a universal solution to engineer the dielectric surface. In addition, the low-trap-density substrate can enhance photoresponse dynamics of 2D transistors and minimize the persistent photoconductivity (PPC) effect. Figure 26b shows the time-resolved photoresponse of the MoS_2 FET under 530 nm light on both substrates without gate bias.[115] The device on the BCB substrate displayed a steep photocurrent change and a fast photocurrent saturation, whereas the photocurrent continuously increased during the 20 s light illumination on the SiO_2 substrate. It provided the evidence for the presence of more trap states at the MoS_2/SiO_2 interface. Under illumination, the photoexcited carriers were trapped at these states, thereby hindering the recombination of the electron-hole pair and continuously increasing the photocurrent. By and large, the use of the BCB dielectric represents a powerful method to improve the dielectric interface for both logic and functional devices.

The top surface of TMDs can also be encapsulated with polymer layers to modify the interfacial states. The fluoropolymer (containing $–CF_2$-CF_2- functional groups) is a good candidate to act as the buffer layer between *p*-type TMDs (such as WSe_2) and dielectric layer.[450] The dipole

fields formed by the C-F bonds in fluoropolymers can cause hole accumulation in the 2D channel. The increase of the hole carrier density further contributed to the higher on-current and the hole mobility. In the meanwhile, it is a great challenge to deposit high-quality, ultrathin high-*k* dielectric on 2D channels in the atomic layer deposition (ALD) process. Shokouh et al. reported that the use of fluoropolymer capping layer avoided the damage on the underneath TMDs during the ALD process, and improved the device performance.[450] And Li et al. further reported that the growth of a monolayer molecular crystal as a seeding layer on 2D channels before the ALD process facilitated the deposition of ultrathin high-k dielectric layer and promoted the film quality, including a reduced roughness, low interface density and small leakage current.[451] These works demonstrate that molecular chemistry approaches have the ability to optimize the fabrication process of 2D transistors.

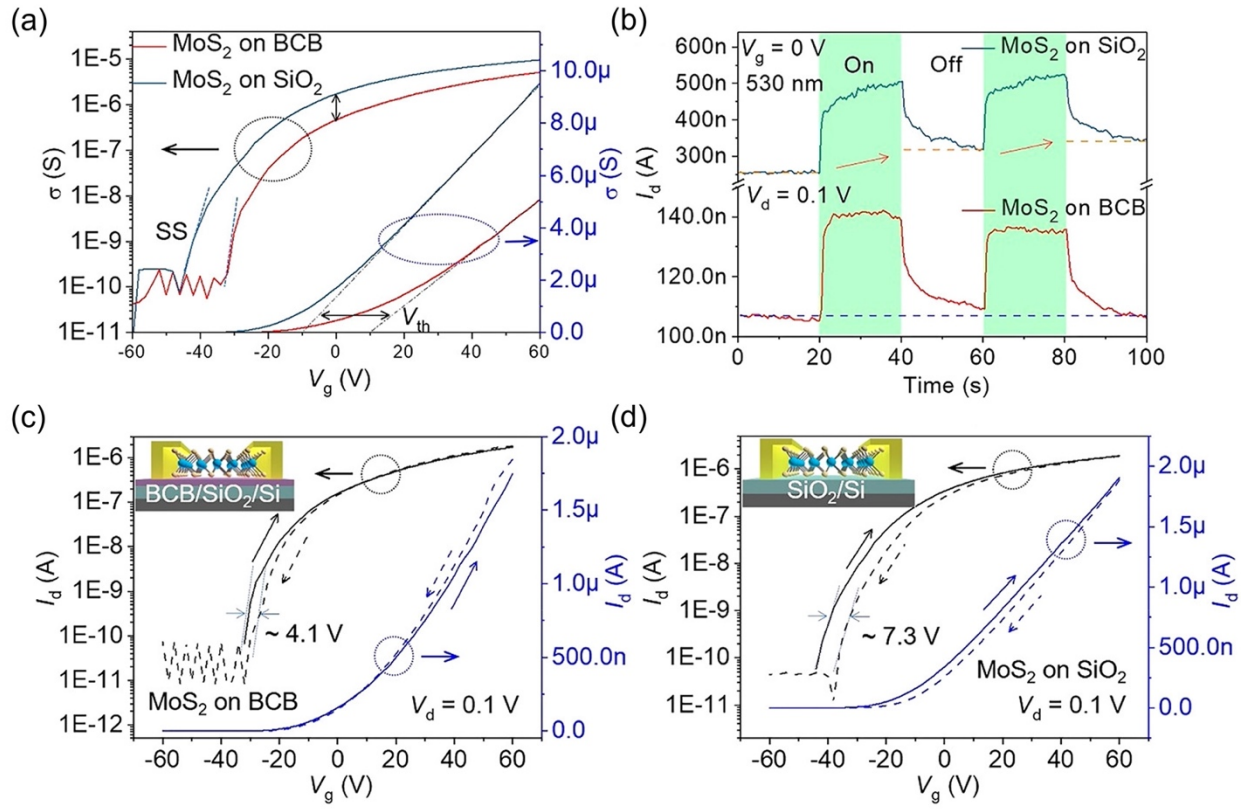

Figure 26. *(a) Transfer curves of monolayer MoS_2 FETs on BCB/SiO_2 and untreated SiO_2 substrates. (b) Time-resolved photoresponse of MoS_2 FETs on BCB/SiO_2 and untreated SiO_2 substrates under 530 nm light illumination. Hysteresis test: transfer curves of monolayer MoS_2 for one gate sweeping cycle on (c) BCB/SiO_2 and (d) untreated SiO_2 substrates. Inset shows the schematic of the device structure. The hysteresis decreases from 7.3 V on the SiO_2 substrate to 4.1 V on the BCB substrate. Reproduced with permission from ref (*[115]*). Copyright 2019 American Chemical Society*.

We have mentioned in section 3.1 that functional high-k polymers, such as ferroelectric polymers, have been used in the 2D logic devices. The replacement of the common dielectric layer

with ferroelectric polymers enables the demonstration of ferroelectric FETs (Fe-FETs) based on 2DMs, in which the strong electric fields in the ferroelectric film allow to modulate the doping in the 2DM and introduce a non-volatile memory function. Here, we review some works focusing on the prototypical ferroelectric polymer PVDF. We include this discussion here since ferroelectricity is not a unique molecular feature, and the Fe-FETs are a rather standard element in electronics. In the next sections, we will review experiments in which devices exhibit peculiar functions inherited by unique molecular capabilities.

The first 2D transistor with ferroelectric polymers as a top gate was reported by Zheng et al. by using graphene as channel materials.[123,452] The dipole configurations (upwards or downwards) of P(VDF-TrFE) could be switched by the electric field, inducing two different zero-field resistance states in graphene. Although the devices showed repeatable resistance switching and non-volatile data storage, the semimetallic nature of graphene limited the on/off ratio between the high resistance state (HRS) and the low resistance state (LRS). Taking advantage from the mechanical flexibility of PVDF, similar devices were fabricated on flexible substrates, focused on the use of graphene/PVDF stacks as transparent substrates,[453] acoustic actuators[454] and transistors[455].

The use of a polymeric ferroelectric gate was later reported for semiconducting 2DMs, including MoS_2,[456-464] $MoSe_2$,[463] $MoTe_2$,[465-468] In_2Se_3,[469] black phosphorus,[122] and WSe_2[470-472]. For instance, in 2012, Im et al. fabricated a MoS_2 FET with 200-nm-thick P(VDF-TrFE) polymer top-gate.[456] The monolayer MoS_2 device showed good retention properties in both static and dynamic

switching, maintaining a high current ratio of ~5×10^3 between HRS and LRS. Im et al. further fabricated a CMOS invertor comprising of p-type BP FET and n-type MoS_2 FET with P(VDF-TrFE) polymer as the common gate.[122] The complementary inverter circuit displayed a clear memory window of 15 V and a high memory output voltage efficiency of ~95%. In other studies, a ferroelectric polymer was employed to improve the performances of photodetectors based on different 2DMs (MoS_2,[457] $MoTe_2$[465] and In_2Se_3[469]) by reducing the dark current. The MoS_2 photodetectors displayed detectivity up to 2.2×10^{12} Jones and 2570 A W^{-1} and photoresponse in the infrared (extending up to 1.5 μm).[457] Graphene/PVDF and MoS_2/PVDF stacks were also employed as touch sensors.[461,473]

Ferroelectric polymers also offer the intriguing possibility to modulate the doping profile of a 2DM in the lateral direction by polarizing the ferroelectric polymer "up" or "down" in different regions of the same flake. To achieve a high lateral resolution, the tip of a scanning probe microscope is typically used to apply the poling voltage in a spatially confined region. This approach was initially demonstrated for a MoS_2/ P(VDF-TrFE) Fe-FET,[458] which could be switched between an ohmic state with a homogeneous polarization in the P(VDF-TrFE) layer and a rectifying state with the PVDF polarized in opposite directions at the source and drain contacts.

Lv et al. employed a similar approach to engineer the charge carrier profile in MoS_2 and demonstrate re-configurable photodetectors, which displayed responsivity of 12 A W^{-1}, a detectivity of over 10^{13} Jones with a response time of 20 μs.[459] More recently, a locally polarized P(VDF-TrFE) layer was used to define lateral heterostructures between regions with different

doping levels in $MoTe_2$.[466-468] In this way p–n, n–p, n–n and p–p heterojunctions were demonstrated, with rectification ratio as high as 10^3 and responsivity of 1.5 A W^{-1} for the case of p-n junction.[468]

Another interesting possibility enabled by 2DM/ferroelectric heterostructures is the demonstration of negative-capacitance field-effect transistors.[125] In these devices,[474] the presence of a ferroelectric thin film in contact with the semiconducting channel was predicted to provide hysteresis-free electrical characteristics with subthreshold slope below the intrinsic limit for conventional MOSFET (60 mV/dec).[474,475] This possibility has been explored in three works focusing on MoS_2 as active semiconducting channel and P(VDF-TrFE) as ferroelectric film.[462-464] In the three cases, sub 60 mV/dec SS have been reported, although the results are debated.

In recent studies by Qiu et al., P(VDF-TrFE) acted as the top-gate dielectric layer in few-layer WSe_2 transistors and the photochromic molecules were chemisorbed on the bottom dielectric surface.[471,472] The asymmetric dressing of top and bottom surface of WSe_2 layers integrated multifunctional elements into the device structure, realizing optically and electrically dual-controlled multilevel memories and quaternary-responsive transistors.

It is also important to recognize that the use of 2D channel materials is compatible with other performance-enhancing technologies, such as (but not limited to) the use of negative capacitance to boost gate-to-channel coupling[464,476-478] and the use of stacked layers of channel materials to boost current drive per area.

Overall, molecular approaches have been successfully applied in 2D logic devices. They have enabled to modulate the carrier type and density of 2DMs in a controllable manner, and to engineer the contact and the dielectric interface for an improved device performance. We summarize important figures of merit of 2D logic devices with molecular functionalization in Table 1.

Table 1. Summary of 2D logic devices with molecular functionalization.

2DM (thickness)	Molecule	Device structure	Objective	Interaction mechanism	Doping (charge/cm^2)	Parameters of functionalized devices				Ref.
						Contact material	Mobility (cm^2/Vs)	I_{on}/I_{off}	others	
MoS_2 (trilayer)	Benzyl viologen	SiO_2/MoS_2/ molecule CR	Doping, CE	CT	>10^{13} *n*	Ni/Au	20 *n*	→10^6	$S_{s\text{-}th}$~77 mV/dec	*93*
BP (few layers)	Benzyl viologen	SiO_2/BP/molecule CR	Doping	CT	*n*	Ti/Au	180 → 100 *p* → *n*		p-n junction R=180 mA/W (λ=1.47 μm)	*479*
MoS_2 (few layers)	mercaptoethylamine	SiO_2/MoS_2/ molecule	Doping	DF, CT	3.7 × 10^{12} *n*	Ti/Au		10^3→10		*94*
	1H,1H,2H,2H-perfluorodecanethiol				1.8 × 10^{11} *p*	Ti/Au				
MoS_2 (few layers)	polyethyleneimine	SiO_2/MoS_2/ molecule	Doping	CT		Ti/Au	20 → 33 *n*	10^6 → 10^2		*95*
MoS_2 (monolayers)	n-butyl lithium	SiO_2/MoS_2/ molecule CR	Doping, CE	CT	> 10^{13} *n*	Au	→ 50 *n*	→10^7	Semiconductor-metal phase transition	*357*
MoS_2 (few layers)	$AuCl_3$	SiO_2/MoS_2/ molecule	Doping, CMOS inverter	CT	*p*	Pd	38 → 72 *n* → *p*	→10^7	Inverter gain 1.1	*480*

MoS_2 (few layers)	$AuCl_3$	SiO_2/MoS_2/ molecule CR	Doping, p-n junction	CT	*p*	Pd Cr/Au			p-n junction Ideality factor ~1	*420*
WSe_2 (monolayers)	Trichloro(1H ,1H,2H,2H-perfluoroocty l) silane	SiO_2/SAM/ WSe_2/ molecule	Doping, CE	DI	*p*	Au	$10^{-6}\rightarrow 150$ *p*	$10^3\rightarrow 10^7$	Ambipola r bilayer through two-sided engineeri ng	*333*
	and N-[3-(Trimethoxys ilyl)propyl]et hylenediamin e				*n*	Au	$10^{-6} \rightarrow 18$ *n*	$10^3\rightarrow 10^3$		
$ReSe_2$ (few layers)	Triphenylpho sphine (PPh) + (APTES)	SiO_2/APTE S/$ReSe_2$/PP h	Doping, CE, photodete ction	CT, DI	1.1×10^{11} *n*	Ti/Pd	$1.1 \rightarrow 33$ *n*	$10^4\rightarrow 10^5$	R= 1.1×10^6 A/W $\tau \approx$ 50-300 ms	*481*
MoS_2 (few layers)	PPh	SiO_2/MoS_2/ PPh			1.6×10^{11} *n*	Ti/Pd	$8.8 \rightarrow 86$ *n*	$10^5\rightarrow 10^6$	R= 6.13×10^5 A/W $\tau \approx 10$ s	
WSe_2 (few layers)	cetyltrimethy l ammonium bromide	SiO_2/WSe_2/ molecule CR	Doping, p-n junctions, photodete ction	CT, DI	*n*	Cr/Au	$6 \rightarrow 36$ *n*	$10^3\rightarrow 10^5$	rectificati on 10^3 R = 30 A/W	*422*
MoS_2 (few layers)	poly(vinyl-alcohol)	SiO_2/MoS_2/ molecule CR	Doping, CE,	CT, DI	8.0×10^{12} *n*	Au	$20 \rightarrow 37$ *n*	$10^7\rightarrow 10^7$		*482*
WSe_2 (few layers)	hydrazine	SiO_2/MoS_2/ molecule	Doping, CE	CT	*n*	Ti, Co, Pt	With Pt $9 \rightarrow 0.07$ $p \rightarrow n$	$10^5\rightarrow 10^3$	enhanced hysteresis	*96*
MoS_2 (monolayer)	butanethiols	SiO_2/MoS_2/ molecule	Defect healing	DF	*n*	Au	$21 \rightarrow 33$ *n*	$10^6\rightarrow 10^7$	Reduced hysteresis	*109*

WSe_2 (monolayer)	thiophenol	SiO_2/WSe_2/ molecule	Defect healing	DF	1.0×10^{12} *n*	Au	0.01→0.8 *n*	$10^4 \rightarrow 10^6$		*111*
WSe_2 (few layers)	NO_2	SiO_2/WSe_2/ molecule	Doping, CE	CT, DF	~ 1.6×10^{12} *p*	Pd		$10^4 \rightarrow 10^1$	Decreased contact resistance 10^5	*384*
WSe_2 (few layers)	Triphenylphosphine	SiO_2/hBN/ WSe_2/molecule	Doping, CE, photodetection	CT	8×10^{11} *n*	Ti, Pt	With Ti 2.9 → 19 *n*	$10^3 \rightarrow 10^3$	R= 1.27×10^6 A/W $\tau \approx$ 2.8-20 ms	*483*
WSe_2 (few layers)	tetrafluoro-7,7,8,8-tetracyanoquinodimethane (F4-TCNQ)	SiO_2/Al_2O_3/ WSe_2/molecule CR	Doping for CMOS logic	CT	*p*	Pt, Ag	→ 42.6 *p*	→ 10^8	inverter gain = 38, pW static power	*98*
BP (few layers)	F4-TCNQ	SiO_2/BP/molecule	Doping	CT	$7.5 \times 10^{12} \rightarrow 2.2 \times 10^{13}$ *p*	Ni	181 → 229 *p*	$10^3 \rightarrow 10$	Decreased contact resistance	*484*
MoS_2 (monolayer)	titanyl phthalocyanine (TiOPc)	SiO_2/MoS_2/ molecule	Defect passivation	DI, CT	*p*	Ag/Au		$10^4 \rightarrow 10^7$	$S_{s\text{-}th}$ 1.6 → 6 V/dec	*406*
WSe_2 (few layers)	Octadecyltrichlorosilane (OTS)	SiO_2/MoS_2/ molecule	Doping, photodetection	DI, CT	2×10^{11} *p*	Pt	32 → 169 *p*	$10^6 \rightarrow 10^6$	R = 364 A/W	*342*
MoS_2 (few layers)	Aminopropyltriethoxysilane				2×10^{11} *n*	Ti	28 → 142 *n*	$10^5 \rightarrow 10^6$	R = 56 A/W	
BP (few layers)	OTS	SiO_2/BP/molecule	Protective layer			Ti/Au			High stability	*341*
MoS_2 (few layers)	oleylamine	SiO_2/MoS_2/ molecule	Doping	DI, CT	1.9×10^{13} *n*	Au	29 → 25 *n*	$10^7 \rightarrow 10^0$		*400*

MoS_2 (few layers)	Perylenediimides, Tetraphenyl porphyrins	SiO_2/MoS_2/ molecule	Photodetection, doping	CT	*n*	Au			Improved contacts, R ~ 100 A/W	*398*
WSe_2 (monolayer)	Fluorinated fullerene $C_{60}F_{48}$	SiO_2/WSe_2/ molecule	Doping, p-n junction	CT	~ 10^{12}	Pd/Au		$10^5 \rightarrow 10^6$		*99*
MoS_2 (few layers)	octyltrichlorosilane	SiO_2/SAM/ MoS_2	Doping, substrate engineering	DI	None	Al	2.0 → 1.8 *n*	$10^4 \rightarrow 10^3$		*104*
	3-(trimethoxysilyl)-1-propanamine				*n*		2.0 → 3.5 *n*	$10^4 \rightarrow 10^3$		
	trichloro-(1H,1H,2H,2H-perfluoroctyl)silane				*p*		2.0 → 0.1 *n*	$10^4 \rightarrow 10^1$		
CVD MoS_2 (monolayer)	(3-mercaptopropyl) trimethoxysilane	SiO_2/SAM/ MoS_2	Doping, substrate engineering	DI	1×10^{11} *n*	Ti/Au	→ 12 *n*	10^6		*447*
	trichloro(1H, 1H,2H,2H-perfluoroctyl) silane				8×10^{11} *p*		→ 2 *n*	10^4		
MoS_2 (trilayer)	tris(4-bromophenyl) ammoniumyl hexachloroantimonate	SiO_2/MoS_2/ molecule	Doping	CT	8×10^{12} *p*	Ti/Au		$10^3 \rightarrow 10^1$		*401*

	2-ferrocenyl N,N'-dimethylbenzimidazoline				6×10^{12} *n*	Ti/Au		$10^3 \rightarrow 10^3$		
$MoTe_2$ (few layers)	Benzyl viologen	$SiO_2/MoTe_2$/molecule CR	Doping, p-n junctions	CT	4×10^{12} *n*	Cr/Au	$5 \rightarrow 25$ *n*	$10^3 \rightarrow 10^5$	p-n junction Ideality factor 1.2	*485*
WSe_2 (few layers)	Benzyl viologen	$SiO_2/MoSe_2$ /molecule	Doping	CT	*n*	Ti/Au		$10^4 \rightarrow 10^2$	BV morphology changes the doping	*486*
WSe_2 (few layers)	Gold - meso-tetraphenylporphyrin	SiO_2/WSe_2/ molecule	Doping, photodetection	CT	*n*	Ti/Au	$10^{-3} \rightarrow 10^{-2}$ *n*	$10^4 \rightarrow 10^3$	R ~ 930 A/W	*487*
MoS_2 (mono- to few layers)	α-lipoic acid	SiO_2/MoS_2/ molecule	Doping	CT, DI	*n*	Cr/Au	$6 \rightarrow 7$ *n*	10^7		*488*
MoS_2 (few layers)	Organic Solvents N - methyl-pyrrolidone (NMP)	SiO_2/MoS_2/ molecule CR	Doping, CE	CT, DI	1.6×10^{13} *n*	Au	$19 \rightarrow 22$ *n*	$10^2 \rightarrow 10^5$		*489*
$MoS_{2-x}O_x$ (monolayer)	Oxygen	SiO_2/O-substituted	Doping, CMOS inverter		*n*	Few layer graphene	100 *n*	10^9	$S_{s\text{-}th}$~80 mV/dec Inverter gain 90	*490*
MoS_2 (monolayer)	KOH/benzo-18-crown-6	SiO_2/MoS_2/ molecule CR	Doping, CE	CT, DI	3.4×10^{13} *n*	Au/In	$52 \rightarrow 117$ *n*	$10^5 \rightarrow 10^1$	24 days air stability	*491*

MoS_2 (few layer)	Cl	SiO_2/MoS_2/ molecule	Doping	CT, DI	*p*	Cr/Au	8 → 3			[492]
$MoTe_2$ (few layers)	Benzyl viologen	$SiO_2/MoTe_2$/molecule/ metal	Doping, CE	CT	*n*		$\sim 10^{-3} \rightarrow 1$ *n*, Contact Engineer.		Improved contact resistance	[493]
BP (few layers)		SiO_2/BP/ molecule/ metal					$\sim 1 \rightarrow 20$ *n*, Contact Engineer.			
$MoSe_2$ (few layers)	poly-(diketopyrrolopyrrole-terthiophene)	$SiO_2/MoSe_2$ /Molecule	Contact engineering, photodetection	CT, DI	*n*	Ti/Au	~ 0.1→10 *n*	$10^3 \rightarrow 10^6$	R= 91 A/W	[494]
WSe_2 (few layers)	ammonium sulfide	SiO_2/WSe_2/ Molecule	Band engineering	In gap states	*p*	Ni/Au	3.5 → 22 *p*	$10^7 \rightarrow 10^9$	Ambipolarity	[495]
SnS_2 (few layers)	ethylenediaminetetraacetic acid	SiO_2/SnS_2/ Molecule CR	Defect healing, doping, CE	DI, CT	4×10^{13} *n*	Ag/Au	2 → 8 *n*	10^7 Contact engineer.		[496]
WSe_2 (bilayer)	mesitylene pentamethyl cyclopentadienyl ruthenium dimer	SiO_2/SnS_2/ Molecule	Doping, CE	CT	2.5×10^{12} *n*		$10^{-3} \rightarrow 9.6$ *n*	$10^3 \rightarrow 10^2$	Degenerate doping	[497]
MoS_2 (few layers)	Hexaazatriphenylenehexacarbonitrile (HAT-CN)	SiO_2/TMD/ Molecule	Doping, inverters	CT	*n*	Au	10 → 4 *n*	$10^4 \rightarrow 10^4$	Inverted gain: 8 → 18	[498]
$MoTe_2$ (few layers)	N_2 with the help of DUV	SiO_2/TMD/ Molecule	Doping, p-n diode	CT	3.7×10^{12} $p \rightarrow n$	Pt/Au	20 *n*	$>10^4$	diode rectifying	[424]

	O_2 with the help of DUV	CR		CT	*p*	Pt/Au			ratio up to ~3.8 × 10^4	
MoS_2 (few layers)	Benzyl viologen/Au Cl_3	SiO_2/MoS_2/ BV+$AuCl_3$ CR	Doping, heterojunctions, p-n junction, tunnel diode	CT	10^{13} *p* + *n*	Cr/Au, Pd/Au	→ 33 *p* or → 30 *n*	10^7→10	p-n junction, rectification 10^4; unstable	*499*
WSe_2 (few layers)	area-selective UV/ozone	SiO_2/WSe_2/ WO_x CR	Contact engineering	CT		Pt $3×10^4$→10^2 kΩ•μm	72.9 p	10^3→10^6		*500*
WSe_2 (few layers)	O_2 plasma	SiO_2/WSe_2/ WO_x CR	Doping, Contact engineering	CT	*p*	Ni			Channel: p-i-p Improved SS	*501*
MoS_2 (few layers)		SiO_2/MoS_2/ MoO_x		CT	*p*	Ni				
$MoTe_2$ (8L)	MgO	$SiO_2/MoTe_2$/oxide	Doping, inverter	CT	V_{th}: 17 V→-22 V on 300 nm SiO_2	Ag/Au	0.1→20 n	10^7→10^8	Inverter: DC gain of >25	*502*
MoS_2 (monolayer)	4,4'-bipyridine (DMAP-OED)	SiO_2/TMD/ Molecule	Doping	CT	>10^{13} *n*	Ti/Au		10^3→1		*346*
BP (few layer)	Cross-Linked PMMA	SiO_2/BP/ PMMA CR	Doping	CT	*n*	Ni/Au	*p*: 90.7 → 175.4 *n*: 1.4 → 3.0	10^3 →10^3-10^4	Diode, bidirectional rectifier, and inverter	*503*
BP (few layer)	cetyl-trimethylammonium	SiO_2/ monolayer BP	Increase interlayer distance	Intercalation of BP with organic		Cr/Au	721 → 328 p	<10 → >10^7	Method suitable for other	*504*

	bromide (CTAB)	molecular superlattices (MPMS)	Isolate BP monolayers	molecules, decouple the interlayer					2DMs, i.e., MoS_2, WSe_2, In_2Se_3	
BP (few layer)	3-amino-propyltrieth oxysilane (APTES)	SiO_2/BP/ self-assembled monolayer	Doping	CT	2.1 ~ 4.82×10^{11} *n*	Ti/Au				[505]
	octadecyltri chlorosilane (OTS)				1.06 ~ 1.96×10^{11} *p*				R=1.4 × 10^4 A/W at λ=520 nm	
MoS_2 (monolayer)	ZnPc/3,5-difluoropyridine	SiO_2/TMD/ Molecule	Doping	DI	*p*	Au			molecular self-assembly of metal phthalocyanine and the orientation-controlled coordination chemistry of axial ligands	[107]
	ZnPc/3-fluoropyridine		Doping	DI	*p*	Au				
	ZnPc/2-fluoropyridine		Doping	DI	*n*	Au				
	ZnPc/4-aminopyridine		Doping	DI	*n*	Au				
	CoPc/3,5-difluoropyridine		Doping	DI	*p*	Au				
	CoPc/3-fluoropyridine		Doping	DI	*p*	Au				
	CoPc/2-fluoropyridine		Doping	DI	*n*	Au				

	CoPc/4-aminopyridine		Doping	DI	*n*	Au				

Note: CR - Confined Region, referring to a situation in which molecular functionalization is carried out not only on the whole surface of the 2D materials (2DMs) channel, but also in a spatially confined region, leading to lateral heterojunctions with varying doping. CE – Contact engineering; CT – charge transfer, DF – defect functionalization; DI – dipolar interaction. We note that high level of doping often reduced the $\mathbf{I_{on}/I_{off}}$ ratio, as they effectively drive the 2DMs into a degenerate (metallic-like) state. On the contrary, degenerate doping in confined-regions allows to improve the contact resistance while retaining high $\mathbf{I_{on}/I_{off}}$.

6 Hybrid Molecular Switches/2D Materials Device System for Beyond CMOS Applications

2DMs are not only highly attractive to overcome the intrinsic scalability of Si electronics (More-Moore), but also to enable the functional diversification which is central in the More-than-Moore approach. Photodetectors, image sensors, magnetic devices, and all sorts of gas, chemical and biological sensors have all been demonstrated using 2DMs, which can be readily integrated into Si technology.[506] These diverse applications can be categorized as non-computational systems and ideally realized on an integrated CMOS chip where Si devices provide the driver, read-out and peripheral circuitry necessary to form a complete system. In section 3.2, we have introduced the properties of three kinds of molecular switches. By the use of an external remote control, it is possible to dial the state of the molecular switches, in analogy to the assignment of logic values. The switch can be toggled between different states when it is adsorbed on the surface of 2DMs, thereby acting as gates to modify the electrical characteristics of 2D material. This kind of hybrid molecular switches/2DMs system can be considered as responsive functional devices. For example, in the 2D optical memory device, the photochromic molecules can respond to the optical stimuli and the electrical signal will be read from the 2DMs. Therefore, the impressive electrical characteristics of pristine 2DMs can be retained and coupled to the unique functions of molecular switches to demonstrate high-performance multiresponsive functional devices. In this section, we will introduce three kinds of responsive devices, which are light-responsive devices, redox-switchable devices and spin/magnetic responsive devices.

6.1 Light-Responsive Devices

The hybrid systems comprising of photochromic molecules and 2D layers are the core component to construct light-responsive functional devices. After the functionalization with

photochromic molecules, the work function of graphene and the carrier density of 2D semiconductors can be effectively tuned by the remote optical control. Taking advantages of these unique features, optically controlled transistor, diode, and memory devices have been successful demonstrated to show novel functionality, which will be detailly introduced in the following subsections. First and foremost, the correlation between molecular switching and the electrical transport of 2D devices should be demonstrated experimentally. Gobbi *et al.* designed and synthesized the spiropyran derivative terminated with an 18-carbon long alkyl chain.[319] The long alkyl chain promotes the formation of a self-assembled monolayers of photochromic molecules on the surface of 2DMs. The highly ordered molecular packing and the light-induced morphology evolution of molecular switches on the surface of 2DMs can be directly characterized by scanning tunneling microscopy (STM). In the meanwhile, the electrical transport properties of functionalized 2DMs can be extracted from the transistor devices on the macroscopic scale and can be correlated with the nanoscale molecular arrangement. Upon UV irradiation, STM images exhibited apparent structural changes, indicating the photoisomerization from spiropyran to merocyanine form. The electrical transport characterizations from both graphene and MoS_2 FETs showed *n*-type doping effect on 2D channels due to the molecular photoisomerization. The increased electron density was as large as 4.4 and 4.6 × 10^{12} cm^{-2} for monolayer graphene and MoS_2, respectively.[319] The two isomers displayed the distinct molecular electrical dipoles perpendicular to the 2D surface (μ_z), which is 0.23 and 1.7 D per spiropyran and merocyanine molecule, respectively. This additional electric field leaded to a shift of the Fermi level and induced a doping effect. This work provided strong evidence that the light-induced structural reorganization of the photochromic molecules on the 2D surface is responsible for the change of the carrier density in 2D layers.

6.1.1 Light-Controlled Transistor

Compared with the presence of an ordered supramolecular arrays, the physisorption of a smaller number of photochromic molecules on 2DMs leads to the formation of loosely packed and less ordered adlayers. Representative examples are those obtained by depositing pyrene-modified azobenzenes and spiropyrans physisorbed on graphene surface *via* π-π interaction.[327,328,507] Although the pyrene-terminated photochromic molecules formed the less ordered distribution on the graphene surface, they actually displayed a preferred adsorption orientation via the π-π interaction between pyrene and graphene. Therefore, the collective dipole moment changes perpendicular to the 2D surface triggered by light stimuli were still strong enough to affect the local electronic properties of the 2D material underneath. Upon the exposure to cycles of UV and visible light, graphene transistors showed the reversible shift of Dirac point in transfer curves and the light-switchable current change in time-dependent conductance measurement.[328] The extracted hole doping density from *cis*-azobenzene was 0.8×10^{12} cm^{-2}, and electron doping density from the merocyanine amounted to 0.5×10^{12} cm^{-2}. These experimental results demonstrated that despite the reduced magnitude, the switchable doping characteristics of 2DMs resulting from the photo-isomerization of photochromic molecules were retained.

Alongside graphene, photochromic molecules have also been adsorbed on the surface of 2D semiconductors, including MoS_2, WSe_2 and BP. 2D semiconductors with a sizeable bandgap are the active components in transistors and the crucial elements to realize the logic functions with large I_{on}/I_{off} ratios. The integration of logic functions with light responsivity contributes to the novel optically controlled technology. Azobenzene and spiropyran molecules have been physisorbed on the surface of monolayer MoS_2 FET.[115,508] The switchable dipole moments of the AZO and spiropyran in two stable states make such molecules a suitable model system to explore

the reversible light-modulated doping/undoping of 2DMs when interfaced. The electric field generated by molecular dipoles, analogous to that of an external gate, can modulate the carrier concentration of 2D semiconductors. In a switching cycle, the monolayer MoS_2 FET with AZO functionalization displayed a decrease of drain current (~34% at V_g = 60 V) in the transfer curves after UV irradiation (Figure 27a-b).[115] Compared with *trans*-AZO/MoS_2 FET, the threshold voltage shifted toward the positive direction by 18.48 V. Therefore, *cis*-AZO molecules depleted the electrons in MoS_2 and the carrier concentration of MoS_2 was decreased by ~1.11×10^{12} cm^{-2}. A large current ratio I_{trans}/I_{cis} of 450 was achieved at $V_g = -38$ V, which could be further improved via the better control of molecular orientation. Triggered by visible light irradiation, the drain current and the threshold voltage got restored to the original values. Figure 27c displayed the time-dependent drain current response for one cycle of UV and visible light irradiation. The sudden current change during the switching on/off of light is generally attributed to the photoexcited carriers. The gradual current increase and decrease during the UV and visible light irradiation is related to the reversible isomerization of AZO. This work demonstrated that the hybrid channel materials combining 2D semiconductors and photochromic molecules provided a promising approach to construct optically controlled transistor. In a recent study, the asymmetric dressing of top and bottom WSe_2 surfaces with ferroelectric P(VDF-TrFE) layer and light-responsive spiropyran molecules enabled the quaternary-stimuli-responsive FETs, which can respond to heat, light, and electric field.[472] The light stimuli can modulate the current of WSe_2 channel by 82% and the electric stimuli can induce the current change by 99%. The carriers in semiconducting WSe_2 layer can be switched from n-type to p-type by synergistically controlling the light and electric stimuli. The stimuli-responsive control of the carrier density and the carrier type can effectively enrich the device functionality.

The efficient and reversible photochemical isomerization of the DAEs between the open and the closed isomer, featuring different energy levels, made possible to generate photoswitchable charge trapping levels, representing an alternative way for tuning of charge transport through the 2D semiconductor channel by the alternating illumination with UV and visible light. This requires the careful design of the DAE structure and the selection of the appropriate 2D semiconductor, in order to locate the CBM (VBM) level of the 2D semiconductor between the LUMO (HOMO) level of the open isomer DAE_o and the closed isomer DAE_c. As shown in Figure 27d, Qiu et al. used the intrinsically n - doped WSe_2 and the CBM level of WSe_2 was located between the LUMO levels of DAE_1o and DAE_1c.[509] This band alignment impeded (facilitated) the electron transfer from WSe_2 to DAE_1o (DAE_1c). In experiment, DAE_1 molecules were spin-coated on the surface of few-layer WSe_2 FETs and the light-switchable electrical transport behavior was consistent with our theoretical analysis.[509] Upon UV irradiation, the gradual conversion from DAE_1o to DAE_1c isomers induced the electron depletion in WSe_2 channels, which was observed from the upshift of threshold voltage in the transfer curves (Figure 27e). After visible light irradiation, the reverses conversion to DAE_1o released the trapped electrons and fully recover the initial electrical characteristics of WSe_2 FETs. The DAE-induced current modulation (I_{ds} at V_g = 30 V) was calculated to be ≈61.7% for over ten cycles, showing an efficient electron trapping by DAE_1c (Figure 27f).

Compared with AZO and spiropyran, the DAE coating devices showed much higher current modulation, albeit if DAE needs to be properly designed to possess energy levels well aligned to those of the chosen 2D semiconductors. In contrast, the dipolar interaction from AZO and spiropyran appears to be a more universal physical process compared to charge transfer (which requires the band alignment) in diarylethene containing hybrids and devices thereof.

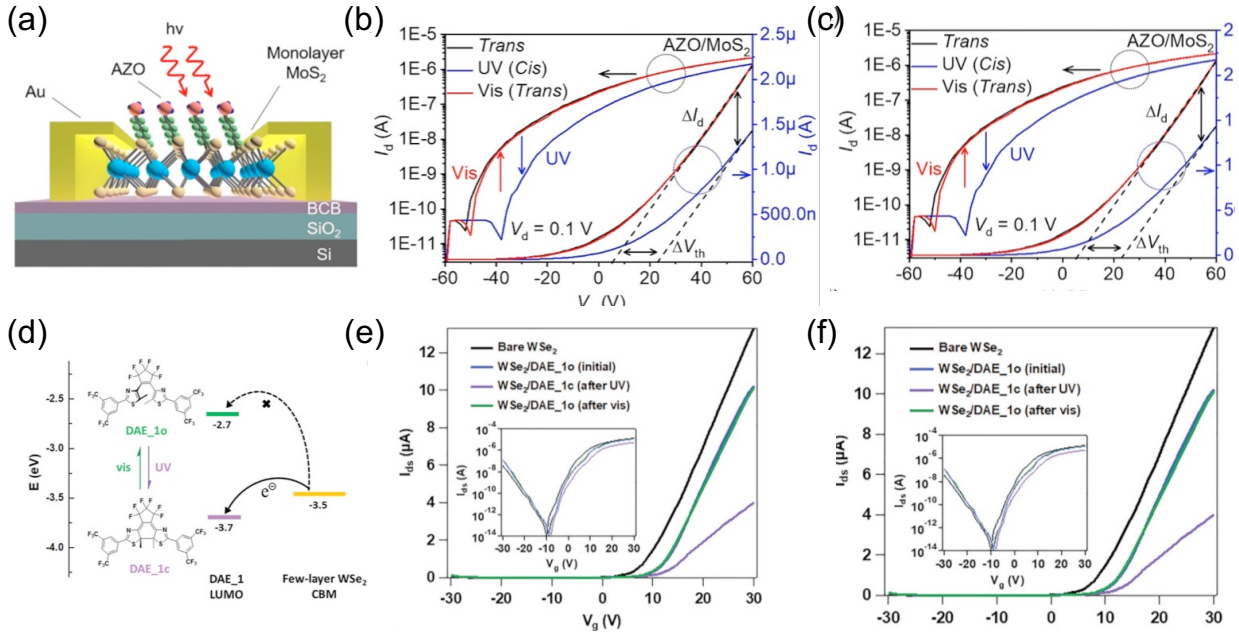

Figure 27*. (a) Schematic of the hybrid FET structure with the physisorption of AZO molecules on the MoS_2 surface. (b) Transfer curves of the hybrid AZO/MoS_2 FET for one switching cycle (trans–cis–trans transition). (c) Time-resolved photoresponse of the hybrid AZO/MoS_2 FET under UV and visible light irradiation for one cycle. Reproduced with permission from ref ([115]). Copyright 2019 American Chemical Society. (d) Energy-level diagram of WSe_2 and DAE_1, indicating the possible electron transfer direction. (e) Transfer curves of bare WSe_2, WSe_2/DAE_1 as prepared, and after UV–vis irradiation. (f) I_{ds} modulation over ten illumination cycles with alternative UV (violet shaded areas) and vis (gray shaded areas) light. All current values are normalized to the initial value obtained from the as prepared WSe_2/DAE_1o. Reproduced with permission from ref ([509]). Copyright 2019 Wiley-VCH.*

6.1.2 Light-switchable diode

Diodes are basic electronic elements and essential building blocks to construct complex (opto-)electronic circuitries. It is a two-terminal device that allows current to flow preferentially in one direction yielding asymmetric conductance. They have been widely used in over-voltage protection, photodetector, power rectifications, solar cells, etc.[62,510-513] The most widely adopted diodes are Schottky diodes and *p*-*n* diodes. The Schottky diode consists of a semiconductor-metal junction, while *p*-*n* diode is based on the formation of a *p*-*n* junction. The use of 2DMs offers more freedom to construct diodes (lateral junction and vertical junction) and gives rise to novel properties. Meanwhile, the photochromic molecules have the ability to reversibly tune the carrier concentration and carrier type in 2D semiconductors. Therefore, the incorporation of photochromic molecules in 2D diodes can further enrich their light-responsive functionality. In this subsection, light-controlled 2D diodes will be introduced detailly.

2D Schottky diodes can be fabricated by using asymmetric metals with different work functions. Beyond that, the insertion of photochromic molecules between the metal and 2D semiconductors provides a viable method to tune the Schottky barrier height by light stimuli. Therefore, it is possible to construct an optically switchable Schottky diode with tunable rectifying characteristics. Margapoti *et al.* reported a photoswitchable diode by inserting AZO molecules between the MoS_2 layer and the gold electrode.[514] In experiment, a SAM of thiolated AZO molecules in an alkanethiol matrix were first chemisorbed onto a gold electrode. Then the MoS_2 layer was transferred onto the AZO-functionalized gold substrate. Another electrode was the Pt-Ir tip used in the conductive atomic force microscopy. The current passing through the vertical metal-semiconductor-metal junction showed rectification characteristics with a turn-on voltage close to 0.5 V. After UV light irradiation, the forward current increased by 150% and the rectification behavior was completely suppressed. Finally, the current rectification got restored after white light

irradiation. Kelvin probe force microscopy was used to measure the contact potential between monolayer MoS_2 and Pt-Ir electrode, which was 1.03 V and 0.67 V on *trans*-SAM/Au and *cis*-SAM/Au substrates, respectively. Therefore, the photo-isomerization of AZO directly determined the Fermi level of MoS_2 and was responsible for the tunable Schottky barrier between MoS_2 and Pt-Ir electrode. This study showed a typical case combining the techniques of molecular electronics and 2D electronics with the ultimate goal of realizing photoswitchable electronic circuits and logic gates.

2D *p-n* diodes can be composed of 2D homojunctions or 2D heterojunctions. The latter can be mostly formed by the stacking of two different 2DMs, named van der Waals vertical heterostructures.[59] Conversely, 2D homojunctions adopt the same 2D crystal with spatially controlled carrier type by the electrostatic or chemical doping (such as molecular adsorption discussed in section 5.1).[417,420,503,511,515,516] When replacing common molecular dopants with photochromic molecules, it is possible to build photoresponsive 2D homojunctions. In this context, Gobbi *et al.* fabricated the graphene transistors with the adsorption of spiropyran on the top of the whole channel region.[319] Initially all the spiropyran molecules were converted to the merocyanine form by UV light irradiation and then the green light was irradiated to get restored to the initial state (spiropyran form) only on a spatially confined region of the channel (Figure 28a). Due to the different doping behavior of spiropyrans and merocyanines on the graphene channel, the carrier density and carrier type could be spatially different in the lateral direction, which results in a 2D homojunction. The electrical transport behavior of the homojunction showed a current plateau when the back-gate voltage was between -15 V to -5 V (Figure 28b, solid line), indicating the formation of a graphene *p-n* homojunction. In this back-gate voltage range, the carrier type of spiropyran and merocyanine doped graphene was hole and electron, respectively, which was

demonstrated by the transfer curves with the coating of only one type of isomers (Figure 28b, dashed lines). Hence, the control of light irradiation can modulate the local charge carrier density of 2D channel with high spatial resolution. By following this methodology, 2D semiconductors featuring ambipolar transport behavior have been adopted to fabricate the light-tunable *p-n* junction with micrometric resolution. Different from the spatial control of light irradiation area in the work of Gobbi et al.,[319] Zhao et al. reported the fabrication of BP-based lateral heterojunctions *via* the selective adsorption of AZO on a patterned channel area (Figure 28c).[115] The junction consisted of a side-by-side BP and AZO/BP region. A p-doping effect of *cis*-AZO had been demonstrated on BP FETs. Under a certain gate voltage, the pristine BP side was switched to n-type transport, whereas the AZO/BP side remained as the p-type transport. This contributed to the formation of a p–n junction in the lateral heterojunction structure. The gate-dependent output curves in Figure 28d displayed the obvious rectifying behavior under V_g from 10 to 30 V. At V_g = 10 V, a rectification ratio of ~600 was obtained at V_d = ±0.3 V with the ideal factor of 1.82. By controlling the molecular states and the gate voltage, the BP-based lateral heterojunction exhibited distinct electrical transport behavior (Figure 28e). With *cis*-AZO doping, the heterojunction showed a gate-dependent transition from p–p, to p–n, and finally to n–n junctions and the dramatic change of current rectification ratios. Therefore, the functional devices based on the patterned hybrid AZO/BP FET can work as the light-controllable p-n diodes. Compared with the photoswitchable diode based on a Schottky junction, [514] the patterned AZO/BP p–n diode adopted the commonly used FET architecture and showed the ability of spatially tunable doping, which is ideal for the practical applications of functional devices.

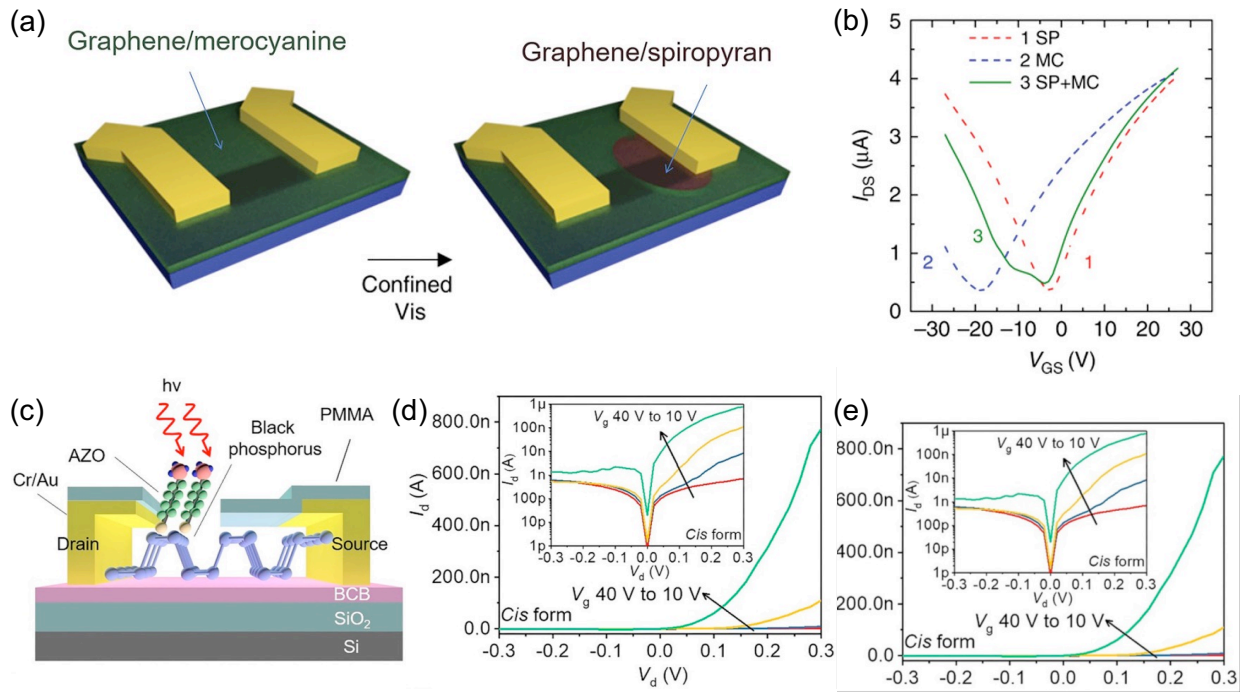

Figure 28. *(a) Schematics of the photoswitchable homojunction via spatially confined doping based on graphene/spiropyran superlattice. The green light irradiation in a well-defined area of the channel can trigger the merocyanine to spiropyran isomerization. (b) The transfer characteristics (I_{DS}–V_{GS}) of devices based on graphene/spiropyran superlattice. Trace 1 (red): graphene covered by the spiropyran layer, trace 2 (blue): graphene/merocyanine as the channel, trace 3 (green): graphene homojunction with merocyanine and spiropyran on different channel section. Reproduced with permission from ref ([319]). Copyright 2018, Nature Publishing Group. (c) Schematic illustraton of the BP-based lateral heterojunction with selective adsorption of AZO on the patterned channel area. (d) Output curves of the patterned AZO/BP FET with cis-AZO adsorption. Inset shows the logarithmic plot of the output curves. (e) Rectification ratio of the BP heterojunction under different molecular states and gate voltages. Reproduced with permission from ref ([115]). Copyright 2019, American Chemical Society.*

6.1.3 Optical Memory

The ubiquity of information technology, characterized by its relentless expansion of the amount of data which are generated daily, calls for an urgent need of miniaturing memory cells.[517] Molecular electronics use single molecules as memory elements to achieve the ultimate device miniaturization.[172,518,519] Molecular switches has gathered a great attention as the future memory elements. They had two independently stable states which can be switched by an external stimulus, enabling to encode information as "0" and "1" in the same device. Photochromic molecules can exhibit markedly different electrical properties in their switchable stable states, including the electronic energy levels, electrical conductivity, or other photophysical properties. Thus, it is promising to achieve the optically controlled memory device with electrically bistable resistance states via the photoswitching of photochromic molecules.

Diarylethenes combine key characteristics which are essential to realize memory devices such as large conductance changes, fast photo-isomerization, very high fatigue resistance, and thermodynamic stability of both open and closed isomers.[128,156,520] Kim *et al.* demonstrated that the diarylethene molecular device with rGO electrode underwent efficient switching and showed excellent memory performance.[166] The DAE molecules were sandwiched between rGO and Au electrodes and the current density of both the closed- and open-state device were measured, exhibiting two electrical states. During the whole test for up to 10^4 s, the device showed no obvious degradation and after 30-days storage under ambient conditions, the device still preserved the defined electrical states without noticeable current change. The authors further performed alternating light irradiation by UV and visible light on the memory device for 10 cycles, showing the high switching stability. It provided evidence for a high fatigue resistance of the diarylethenes with a high reproducibility of the two electrical states and the reversible photoswitching behavior.

In another representative work, graphene and diarylethene were covalently bonded to form a single-molecule junction and they functioned as electrodes and channels, respectively.[172] The device showed light-controlled current switching with I_{on}/I_{off} ratio ~100, over 1-year stability and over 100-cycle reproducibility.

Qiu et al. reported an optically switchable multilevel memory based on few-layer WSe_2 and a suitably designed bicomponent diarylethene (DAE) blend.[521] Bicomponent DAE blend consisting of two DAE molecules with specific energy levels were engineered in order to be capable of reversible trapping and de-trapping both the electrons and the holes of WSe_2. Upon ultraviolet (UV) irradiation at 312 nm, both DAE molecules were converted to their closed photoisomeric states, accompanied with a simultaneous transfer of electrons and holes from WSe_2 channel to DAEs, inducing a decrease of charge carrier density as well as the drain current in the FET device (Figure 29a). Conversely, upon visible light irradiation at 530 nm the DAE molecules were converted back to their open isomer states, resulting in the full recovery of the charge carrier density within WSe_2 and the drain current in the FET device (Figure 29a). The current modulation efficiency was as high as 97% for holes and 52% for electrons (Figure 29b). Moreover, such current modulation ratio was readily tuned by controlling the light dose, which means the FET device can reach multiple current states by adjusting the irradiation duration. The device attained 64 distinct current levels for both holes and electrons (Figure 29c-f), as evidenced through a precise control and fine-tuning over the output current thereby highlighting its potential to be further developed into multilevel memories with data storage capacity of 7 bit. The device is also implemented on a flexible and transparent poly(ethylene terephthalate) substrate, demonstrating 2D/DAE hybrid structures as promising candidates for flexible multilevel nonvolatile memories. Qiu et al. made a step further to construct an electrically and optically dual-

controlled multilevel memory device by decorating the top and bottom surface of few-layer WSe_2 flakes with light-responsive DAE layer and electrically responsive P(VDF-TrFE) layer (ferroelectric polymer).[471] The current through WSe_2 layers can be synergically controlled by the optical and electrical stimuli without mutual interferences. The device yields 9 electric-induced resistance levels and 84 light-induced resistance level, and hence a total number of 756 distinct resistance states. This work provided a new approach to realize multilevel non-volatile memory devices.

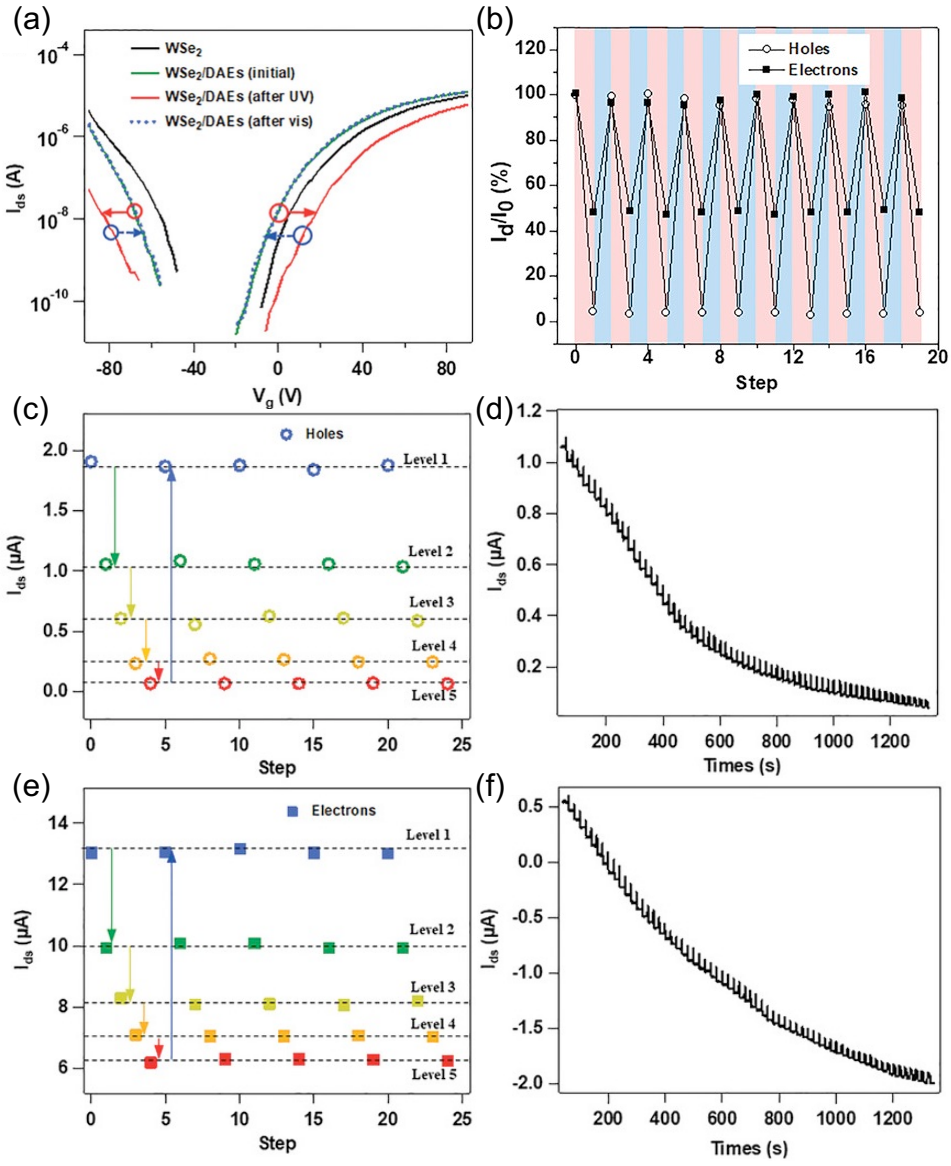

***Figure 29**. (a) Transfer curves of pristine WSe_2 and WSe_2/DAE blend as prepared and after UV–vis irradiation. (b) Drain current I_{ds} modulation as both open and closed isomers over ten illumination cycles with alternative UV (red shaded areas) and vis (blue shaded areas) light. All current values are normalized to the initial value obtained from the as prepared WSe_2/DAE blend. Five distinct current levels over five illumination cycles for (c) holes recorded at $V_g = -90$ V and (e) electrons recorded at $V_g = 90$ V. The levels are obtained by illuminating the device for different fixed times. Dynamic (d) hole and (f) electron current I_{ds}-time curves (corrected for bias stress) under periodic UV irradiation per 20 s, achieving a total of 64 levels. Reproduced with permission from ref ([521]). Copyright 2020, Wiley-VCH.*

AZO as the widely used photochromic molecules were also exploited as channel materials to construct optical memory devices. Different from diarylethene, the conductance, the molecular energy levels, and the bandgaps of the azobenzene isomers do not show significant changes. Interestingly, azobenzenes show a large conformational change during photoisomerization, which enables to achieve bistable resistance states with large I_{on}/I_{off} ratio. In this device, azobenzene molecules were sandwiched between two electrodes to work as a tunneling device. Upon light irradiation, the reversibly switching of the molecular length modulated the tunneling distance, resulting in the current switching. Following this idea, Seo *et al.* developed photoswitchable memory devices consisted of graphene electrodes and diazonium grafted AZO molecules.[522] The diazonium moiety of AZO molecules was covalently bonded onto the bottom graphene electrode and the AZO unit, the other extremity of the molecules was a photochromic azobenzene unit, was physically connected with the top graphene electrode. The custom design of the azobenzene molecules aimed at the optimization of the interaction between azobenzene and graphene

electrodes to improve the memory performance. After UV light irradiation, the molecules were converted from *trans* to *cis* form and the current increased by one order of magnitude due to the decreased molecular length and the lower tunneling barrier. Upon exposure to visible light, the *cis* to *trans* back conversion of AZO molecules induced the decreased current back to the previous value. The current density plot at 0.3 V voltage bias displayed almost identical and reproducible results at both molecular states during over 50 cycles of alternating UV and visible light irradiation , indicating the high switching stability of photoswitchable devices. The successful photoswitching between the two resistance states in photochromic molecules/2D devices with high stability demonstrated the possibility to construct 2D optical memories.

By and large, the photochromic molecules can be functionalized on the surface of 2DMs to construct light-responsive devices. The light-controlled carrier doping of 2DMs by photochromic molecules determines the responsive performance of 2D transistors, 2D diodes and optical memory. The most representative photochromic molecules/2DMs works are summarized in Table 2.

Table 2. Optical-switchable doping effect on 2D materials by photochromic molecules.

Molecule	2D material	2D Thickness	Interaction group	Bond type	Interaction mechanism	Δn (cm^{-2})	Note	Ref.
AZO	Graphene	Monolayer	Diazonium	Covalent	DI	3×10^{11}		*523*
AZO	Graphene	Bilayer	Diazonium	Covalent	DI	3.6×10^{11}		*523*
AZO	Graphene	Trilayer	Amide	Covalent	DI	4.4×10^{13}	GO	*524*
AZO	Graphene	Monolayer	Pyrene	Non-covalent	DI	8×10^{11}		*328*
AZO	MoS_2	Monolayer	Alkyl chain	Non-covalent	DI	1.11×10^{12}		*115*
SP	Graphene	Monolayer	Alkyl chain	Non-covalent	DI	4.4×10^{12}		*319*
SP	MoS_2	Monolayer	Alkyl chain	Non-covalent	DI	4.6×10^{12}		*319*
SP	MoS_2+GNR	1L+1L	Alkyl chain	Non-covalent	DI	1×10^{12}		*508*
SP	Graphene	2-bilayer	Pyrene	Non-covalent	DI	8.13×10^{11}	GO	*507*
SP	Graphene	5-bilayer	Pyrene	Non-covalent	DI	2.95×10^{11}	GO	*507*
SP	Graphene	Monolayer	Pyrene	Non-covalent	DI	4.68×10^{11}		*327*
SP	WSe_2	Few-layer	Organosilane	Covalent	DI		P(VDF-TrFE) as top gate	*472*
DAE	WSe_2	Few-layer	DAE	Non-covalent	CT	6.25×10^{11}		*509*
DAE blend	WSe_2	Few-layer	DAE	Non-covalent	CT		Simultaneous electron and hole tuning	*521*
DAE	WSe_2	Few-layer	DAE	Non-covalent	CT		P(VDF-TrFE) as top gate	*471*

Note: AZO, azobenzene; SP, spiropyran; DAE, diarylethene; DI, dipole interaction; CT, charge transfer; GO, graphene oxide.

6.2 Redox-Switchable Devices

As discussed in 3.2.2, redox-switchable molecules have multiple stable redox states and they have been widely used in molecular electronics due to the distinct electronic properties in different molecular states. One representative structure of the redox switching device is a metal/molecule/metal sandwich junction, wherein the molecules are located at the cross-section of two nanoscale metallic wires. Charge transport through single or SAM of redox molecules is of crucial importance for exploring the potential applications of molecular tunnel junctions beyond current scaling limits as diodes, memories, and switches. Traditionally, the asymmetric molecular structure or the different interactions between the top/bottom electrode and the corresponding molecular terminations will induce the current rectification behavior, operating as a diode. By the control of molecular switches with external stimuli, the molecular tunneling device can be set to high resistance state (OFF) or low resistance state (ON), providing evidence for the potential applications in memory and switch. In redox switching devices, the functional SAMs have been normally sandwiched between two bulk electrodes and isolated from the external environment. Jia et al. developed a new vertical molecular tunnel junction based on Au/ferrocene-SAM/graphene heterostructures, where monolayer graphene acted as the top electrode and electricity flowed in a cross-plane direction, perpendicular to the SAM.[525] Due to the partial electrical transparency and selective permeability, graphene allowed the *in-situ* control of the redox states and the molecule/electrode coupling via chemical and electrochemical reactions. As shown in Figure 30a, an ultra-flat Au film on conducting silicon was used as the source electrode. A monolayer of 6-ferrocenylhexanethiol (FcC6S, Fc-SAM) was then self-assembled on the surface of Au film and CVD-grown monolayer graphene was transferred on the top of Fc-SAM.[525] A small amount of reactive solution or electrolyte solution was dropped on the top of tunneling channel. Since the

graphene layer with its high impermeability can prevent direct contact between the Fc-SAM and the solution, the chemical redox reactions between the oxidant/reductant and Fc groups across graphene layer could be investigated. Furthermore, by adding both a reference and a Pt counter electrode to the electrolyte solution, the electrochemical redox reactions of the Fc groups under graphene layer could be controlled (Figure 30b). The experimental current density (J_D) versus source-drain voltage (V_D) for the junction is shown in Figure 30c. After adding oxidizing agent, the current density in J_D-V_D curve of the Fc^+-SAM junction decreased markedly and dropped by over two orders of magnitude at the negative bias.[525] After the reduction treatment, the J_D-V_D characteristics of the device almost recovered to its initial state. In response to alternate chemical oxidation and reduction treatments, the $|J_D|$ at $V_D = -0.5$ V changed between low and high conductance states with an I_{on}/I_{off} ratio of ~120. The redox reactions of the Fc-SAM in the junction were also investigated by electrochemical control. The cyclic voltammograms (CVs) of the Au/Fc-SAM/graphene sample displayed a pair of redox peaks corresponding to the electrochemical redox reactions of Fc groups (Figure 30d). When the device was sequentially treated by the electrochemical oxidation and reduction, the device reversibly switched between low-conductance state in electrochemical-oxidized state and high-conductance state for electrochemical-reduced state with high I_{on}/I_{off} ratio of two orders of magnitude ($|J_D|$ at V_D = -0.5 V) as shown in Figure 30e.[525] The authors further explained that when the molecule is oxidized, the separation between the top graphene contact and the Fc-SAM is increased due to the mutual electrostatic repulsion, resulting in the reduction of current through the device. In this device, the redox states of the Fc-SAMs could be effectively tuned by external stimuli, moving a significant step closer to realizing new functionalities for molecular electronic devices, such as chemical/biological sensors, electrochemical detectors, and logical devices.

In tunnel junction devices, conjugated polymers can replace molecules as the tunneling layer. Wang et al. studied the self-assembly of a new kind of π-conjugated polymers (CPs) on the Au bottom electrode.[526] Then the reduced graphene oxide films were transferred onto the polymer layer working as the top electrode. The unique design of the used CPs lies on the incorporation of redox-active tetrathiafulvalene (TTF) units into the polymeric backbones. By tuning the redox reaction of TTF units via chemical or electrochemical methods, the resistance was modulated between a high resistance and a low resistance state.

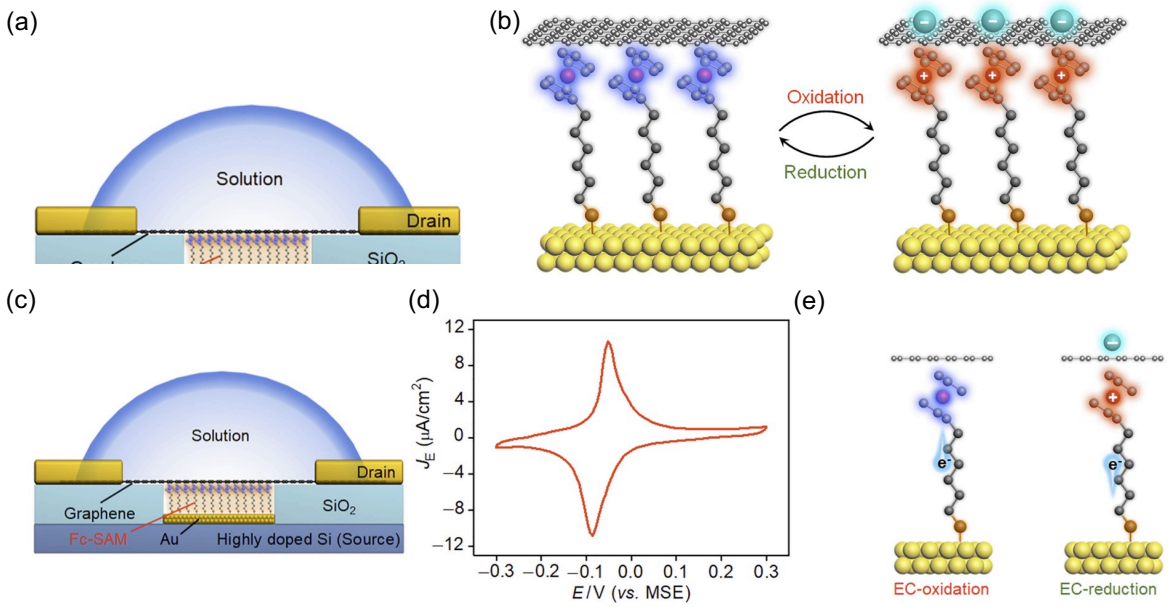

Figure 30. *(a) Schematic illustration of the whole device containing Au/Fc-SAM/graphene junction with a liquid drop on top of the chip. (b) Schematic illustration of the Au/Fc-SAM/graphene junction with oxidation and reduction treatments. (c) Current density (J_D) versus source-drain voltage (V_D) curves in one chemical oxidation and reduction cycle. (d) CVs for Au/Fc-SAM/graphene sample in electrolyte. (e) J_D-V_D curves for the junction in one electrochemical oxidation and reduction cycle. Reproduced with permission from ref ([525]). Copyright 2020, Cell Press.*

2D transistor devices functionalized with redox molecules have also been studied recently. The electrochemical applications of 2DMs are of particular interest owing to their ultrathin body. Wang et al. fabricated double-gate MoS_2 transistor with SiO_2 as a back dielectric layer and the ionic liquid as a top dielectric layer (Figure 31a).[527] Ferrocene molecules were physisorbed onto the MoS_2 surface and the electrochemical reactions took place on the MoS_2 surface. The charge transfer kinetics at monolayer MoS_2 electrodes was continuously and reversibly tuned from irreversible to near-reversible with the applied back-gate bias (V_{BG}). In Figure 31b, at V_{BG} = +90 V, MoS_2 operates as a nearly reversible electrode with respect to electrochemical reaction of ferrocene. Alternatively, at V_{BG} = -90 V, a modest oxidation is observed in the anodic scan and the reduction onset occurs at a much more negative voltage. The behavior at V_{BG} = -90 V is completely irreversible, essentially displaying a diode-like behavior. The standard heterogeneous charge transfer rate constant between MoS_2 and the ferrocene (Fc)/ferrocenium (Fc^+) redox couple was tuned by over 2 orders of magnitude, from 4×10^{-6} to 1×10^{-3} cm/s, by varying V_{BG}, which was explained by the conduction band edge shift and electron occupation with applied V_{BG}. Taking one step further, Zhao et al. demonstrated that MoS_2 FET with the adsorption of ferrocene-substituted hexanethiol molecules could be electrochemically switched reversibly.[528] 6-(ferrocenyl)hexanethiol (Fc-SH) comprises an electrochemically switchable ferrocene unit grafted at the end of an alkyl thiol, the latter being capable of chemisorption on TMDs with sulfur vacancies. Figure 31c shows the structure of electrochemically switchable transistor device. The transfer characteristics of top-gate monolayer MoS_2 FET exhibits unipolar n-type transport behavior, with the I_{on}/I_{off} ratio exceeding 10^5 (Figure 31d). The electrochemical state of ferrocene functional group could be programmed by tuning the top gate voltage (Figure 31e). Since Fc and

Fc^+ are uncharged and monocationic species, respectively, they were expected to yield different doping effect on the adjacent MoS_2 layers. Figure 31f displays a representative reversible doping cycle on monolayer MoS_2 FET with Fc-SH adsorption. After switching the molecules from the neutral Fc-SH to the charged Fc^+-SH state, an increase of drain current in the transfer curves from the back-gate configuration was observed accompanied by a shift of the threshold voltage toward the negative direction. The charged molecules were toggled back to the neutral Fc-SH state and the drain current and threshold voltage from the back-gate FET got restored almost to the original values. These results demonstrated that the doping effect from the electrochemically switchable Fc-SH molecules on monolayer MoS_2 was controllable and reversible. This device architecture represents an unprecedented and powerful strategy to fabricate switchable 2D FET with the electrochemical signal as a remote control, paving the road toward novel functional devices.

Because of the strong dependence of MoS_2 photoluminescence on doping, the changes in the local chemical potential from the redox molecules substantially modulated the photoluminescence of MoS_2. To monitor the molecular redox states in space and time, "pixel" arrays of monolayer MoS_2 were fabricated to image spatial and temporal changes in redox molecule concentration.[529] By mapping the photoluminescence of MoS_2 arrays, the redox concentrations changes with micrometer-scale spatial resolution and at 10 ms temporal resolution were acquired. The sensitivity reached 0.9 mV/$\sqrt{Hz}$ on a 5 μm × 5 μm pixel, corresponding to better than parts-per-hundred changes in redox molecule concentration down to nanomolar concentrations at 100 ms frame rates. This provides a new strategy for visualizing chemical reactions and molecules with a two-dimensional material screen.

The most representative redox-switchable 2D devices are summarized in Table 3.

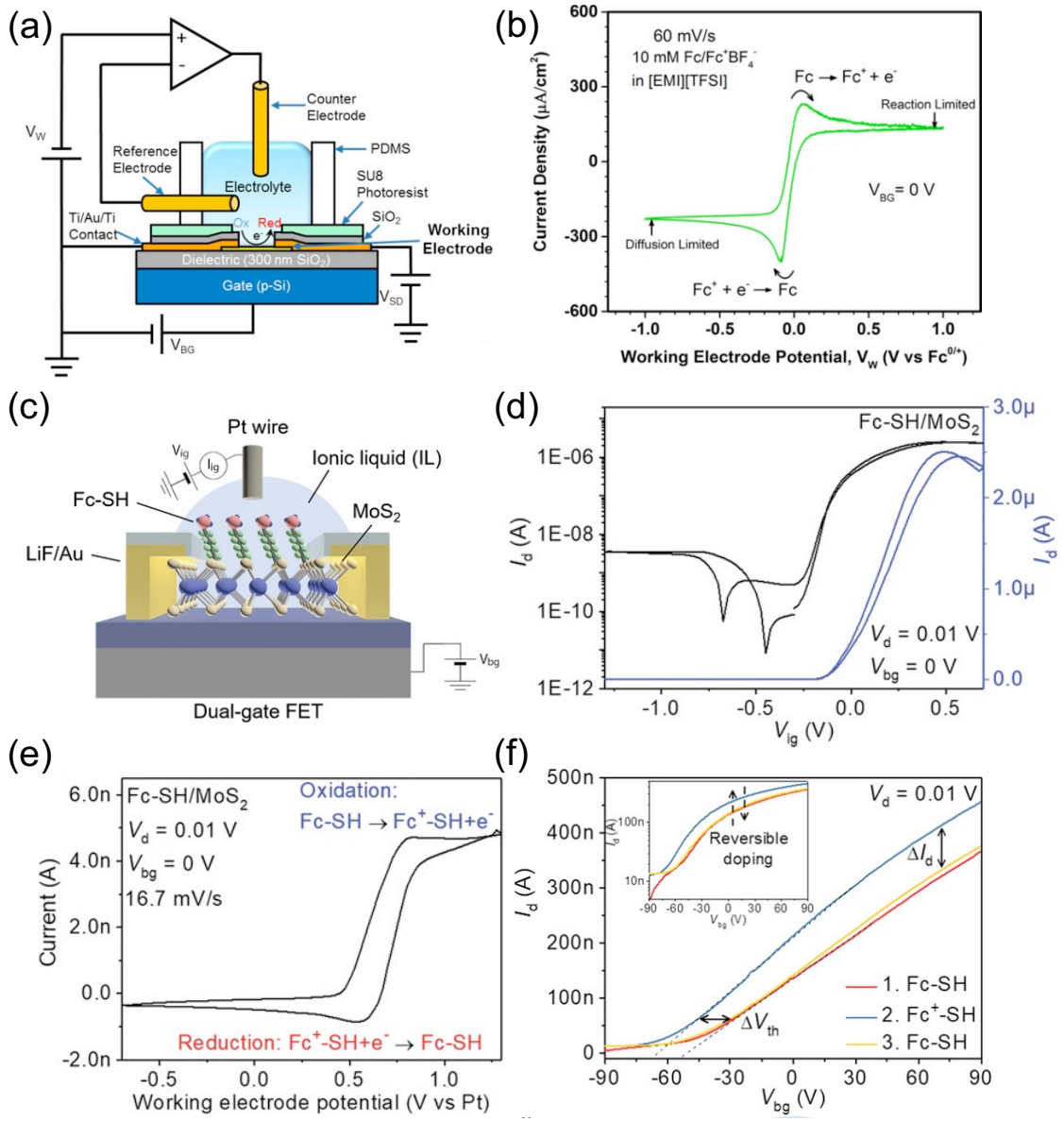

Figure 31. *(a) Schematic illustration of the back-gated electrochemical cell structure. (b) Cyclic voltammograms of 10 mM $Fe(C_5H_5)_2$/$[Fe(C_5H_5)_2]BF_4$ in [EMI][TFSI] measured at a typical back-gated MoS_2 electrode at V_{BG} = 90, and −90 V. Reproduced with permission from ref ([527]). Copyright 2017, American Chemical Society. (c) Schematic diagram of ionic liquid (IL) gated monolayer MoS_2 field-effect transistor (FET) with adsorbed 6-(ferrocenyl)hexanethiol (Fc-SH) molecules. (d) Transfer characteristics of IL-gated monolayer MoS_2 FET with adsorbed Fc-SH*

molecules. (d) The cyclic voltammogram of Fc-SH at the MoS_2−IL interface. Reproduced with permission from ref ([528]). Copyright 2020, Wiley-VCH.

Table 3. Redox-switchable 2D devices.

2D material (thickness)	Molecules	Device structure	Device mechanism	I_{on}/I_{off} ratio	Δn (cm^{-2})	Note	Ref.
Graphene (1L)	6-(ferrocenyl)hexanethiol	VTJ : 2D/Molecule/Au	Tunneling junction	>100		Switched by chemical/electrochemical redox reactions	525
Reduce graphene oxide	tetrathiafulvalene	VTJ : 2D/polymer/Au	Tunneling junction	10		Switched by chemical redox reactions	526
MoS_2 (1L)	ferrocene/ferrocenium redox couple	Dual-gate MoS_2 transistor	Physisorption			Gate dependent charge transfer rate constant	527
MoS_2 (1L)	6-(ferrocenyl)hexanethiol	Dual-gate MoS_2 transistor	Chemisorption		1.10×10^{12}		528
MoS_2 (1L)	ferrocene	Ionic liquid gate transistor	Physisorption			Redox dependent Photoluminescence	529

Notes: VTJ – vertical tunneling junction

6.3 Spin/Magnetic Responsive Devices

In this section, we will introduce the reader to some relevant examples in which 2DMs were coupled to spin switches. As discussed in section 3.2.3, we refer as spin switches to those compounds in which an external stimulus can modify the magnetic configuration, such as SCO complexes, which respond to a thermal stimulus, and single molecule magnets, where the spin is flipped by a magnetic field (see section 3.2.3).

We highlight that while the presence of two metastable and deterministically addressable molecular states for spin switches is reminiscent of the case of photochromic molecules, spin switches are characterized by a modification in the molecular magnetic properties which is not encountered in the case of photochromic molecules. For this reason, spin switches are particularly attractive for applications in which the information is encoded in the electron spin, such as spintronics[225] and quantum computing.[227] In this context, it would be very intriguing to employ molecular switches to reversibly modify the magnetism of 2DM through proximity effects,[530] generating magneto-responsive hybrid material.

As we will show, significant progress has been made to interface 2DMs and both spin crossover molecules and single molecule magnets,[531] resulting in devices characterized by multiple stable resistance states, which can be addressed through opportune external inputs. However, we will highlight how the potential offered by magnetic switches for spintronics and quantum computing has not yet been fully explored, as the switching mechanism is seldom caused by a magnetic interaction.

6.3.1 Graphene Nanoelectrodes for Spin Switches

The conductance of individual molecules has been addressed in lateral devices using graphene to provide electrical contacts.[173,329,397,532-543] In these devices, a nanogap was opened within a graphene flake, and it is subsequently filled with one molecule equipped with two functional groups designed to bind to the two graphene nanoelectrodes. Signatures of transport across single molecules were found in several studies employing this approach.[173,329,397,532-543] Here, we have chosen not to review in detail these works, for which a recent review is available, and which move towards the single-molecule electronics, eluding the topic of this work. Nevertheless, we think that it is still useful to compare the results obtained in devices based on graphene-nanogaps and in mesoscopic 2DM/spin switches, which will be the topic of next section.

Figure 32 illustrates the results obtained by contacting a single Fe(II) spin crossover compound through graphene nanoelectrodes.[329] In this case, pyrene groups were chosen to provide a non-covalent binding to the graphene electrodes, which were separated by approximately 1.7 nm to fit the molecule. Such a small gap was obtained by breaking a graphene flake through the so-called electroburning technique, in which a voltage applied across a graphene constriction causes self-heating and removal of the atoms in graphene, eventually leading to the formation of nanogaps. Such process, which is often employed for the formation of nanogaps, is not completely controllable, and provides a relatively low yield of working devices.

The conductance across the single SCO complex displayed 2 different states characterized by different resistance[329] (Figure 32b), which the authors associated to the different spin configurations in the SCO. However, the transition between the two states was not found to be triggered by temperature. Rather, the molecular conductance jumped between the two states over time (Figure 32b), and it could not be stabilized even at the lowest temperatures, where the LS state is the stable state for bulk compounds. Qualitatively, the same effect was found in different

devices, indicating that the behavior of the SCO complex in the single-molecule device is substantially different from bulk crystals. To explain this finding, the authors proposed that small and uncontrollable perturbations to the ligand distance could induce the transition between the two states. In a related work,[533] the conductance of a single Co-based SCO molecule covalently bound to two graphene electrodes was measured. While in that case the authors did not explore a possible conductance change as a consequence of the change in the spin configuration, a relatively stable resistance was found, indicating the absence of bistability. These results indicate that stabilizing and reading the spin of single SCO molecules is not trivial.

As an alternative approach, graphene electrodes were also used to contact single or few SCO nanoparticles with a length of approximately 100 nm and a width of 50 nm.[544] The use of nanoparticles instead of single molecules made it possible to use larger gaps, which were defined through conventional lithography, simplifying the sample fabrication (Figure 32c). Moreover, cooperative effects exist in nanoparticles, leading to the presence of thermal hysteresis in the spin-configuration switching and to a window of bistability close to room temperature (see section 3.2.3).

In these nanoparticle-based devices, the conductance displayed a thermal hysteresis (Figure 32d) consistent with the switching recorded by magnetometry for the powder.[544] This finding indicated that the HS and LS states possess different conductance, and in particular the conductance of the HS state was found to be higher than that of the LS state within the bistability region. The system could be cycled multiple times retaining the thermal hysteresis in the conductance; additionally, it was found that the bistability region and the relative change in conductance increased when the graphene electrodes were separated by larger distances, and the charge transport involved not a single, but a few nanoparticles. It is worth highlighting that the

conductance of the devices was always very low (below 10^{-11} S in the shortest channel device, lower for larger gaps), which is a consequence of the poor charge transport properties of SCO complexes. This motivates the search for alternative device architectures for the use of switchable SCO compounds in electronics.

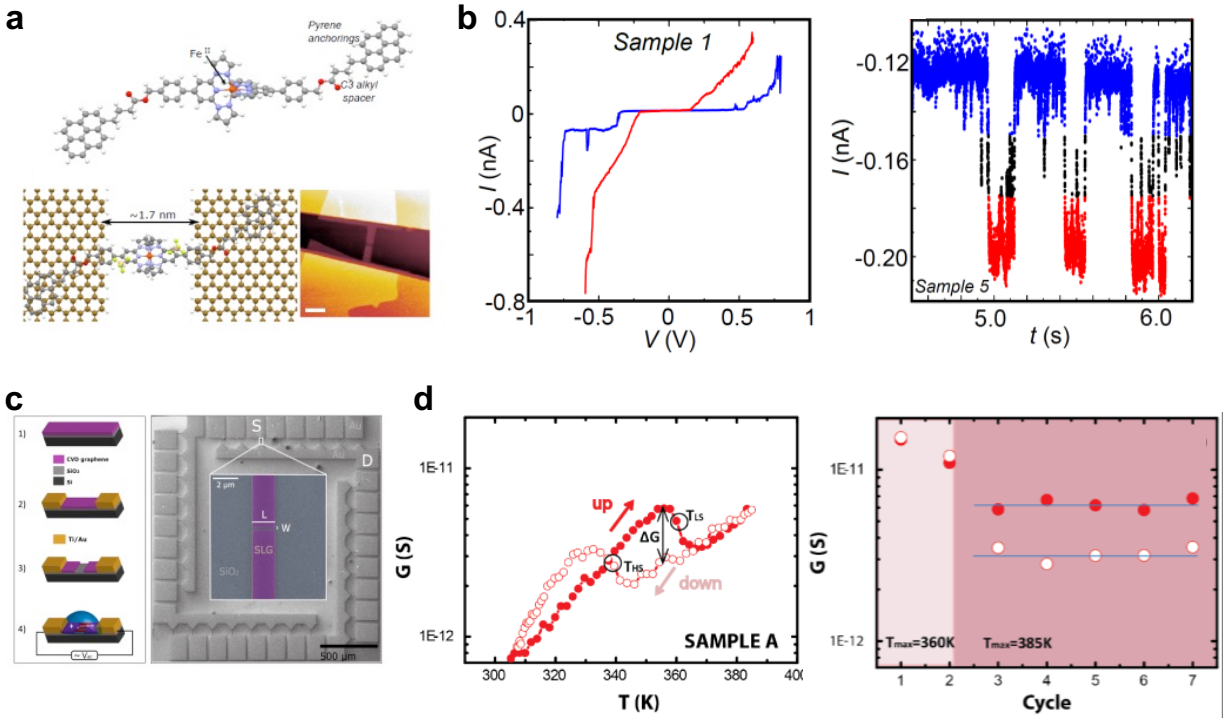

Figure 32. *Nanogapped graphene as electrodes for molecular switches. (a) Graphene nanoelectrodes are used to contact a single SCO compound, which is non-covalently attached to the two graphene contacts through pyridine side groups. (b) At any temperature, the single molecule devices show two different resistance states, which are associated to the HS and LS state of the SCO. The two states are not stable, and the molecular conductance randomly switches between the two states over time. (c) Lithographically patterned graphene electrodes with larger separation (150 nm) were used to contact a few SCO nanoparticles. (d) The conductance of the SCO nanoparticles displayed a clear temperature hysteresis, which could be recorded during*

several cycles. We note that the nanoparticle conductance is very low, in the range of 10^{-12} S. (a, b) Reproduced with permission from ref [329]. Copyright 2018 Royal Society of Chemistry; (c,d) Reproduced with permission from ref [544]. Copyright 2016 Wiley-VCH.

Finally, we highlight how graphene electrodes were also used to contact a Tb-based single molecule magnet.[536] In that case, signatures of molecular magnetism in the electrical transport properties were found in one device out of 40 tested, indicating both the intriguing possibility of using graphene-based single molecule devices to read out the molecular spin but also the intrinsically low success yield of the break junction fabrication strategy.

6.3.2 Devices based on 2D Materials/SCO Interfaces

2DMs appear as an obvious solution to overcome the problems of reproducibility and poor device performances encountered when SCO complexes are used as charge transport materials in ultrashort gap devices. Graphene has been used in a few studies as the prototypical ultra-sensitive 2D charge transport material to sense the SCO transition.[260,545] In a first study, large-area CVD graphene was employed to sense the spin transition occurring in a thin layer of SCO nanoparticles.[260] In this case, the resistance of the graphene sheet was measured as a function of temperature and gate voltage in a four-probe van der Pauw configuration (Figure 33a) before and after covering the device with a thin layers of SCO nanoparticles. Transfer curves were acquired at different temperatures, permitting to extract different representative parameters. A thermal hysteresis was observed in the resistance at the Dirac point and in the hole mobility, consistent with magnetometry data for the SCO nanoparticles in powder. We stress that within the hysteresis, found between 327 K and 374 K, graphene displayed two deterministically addressable resistance

states at the Dirac point – with the high resistance state corresponding to the LS configuration in the SCO nanoparticles. The difference in resistance could be fully accounted for considering the different dielectric constants of the SCO nanoparticles in the HS and LS configuration, which caused different phonon scattering.[260]

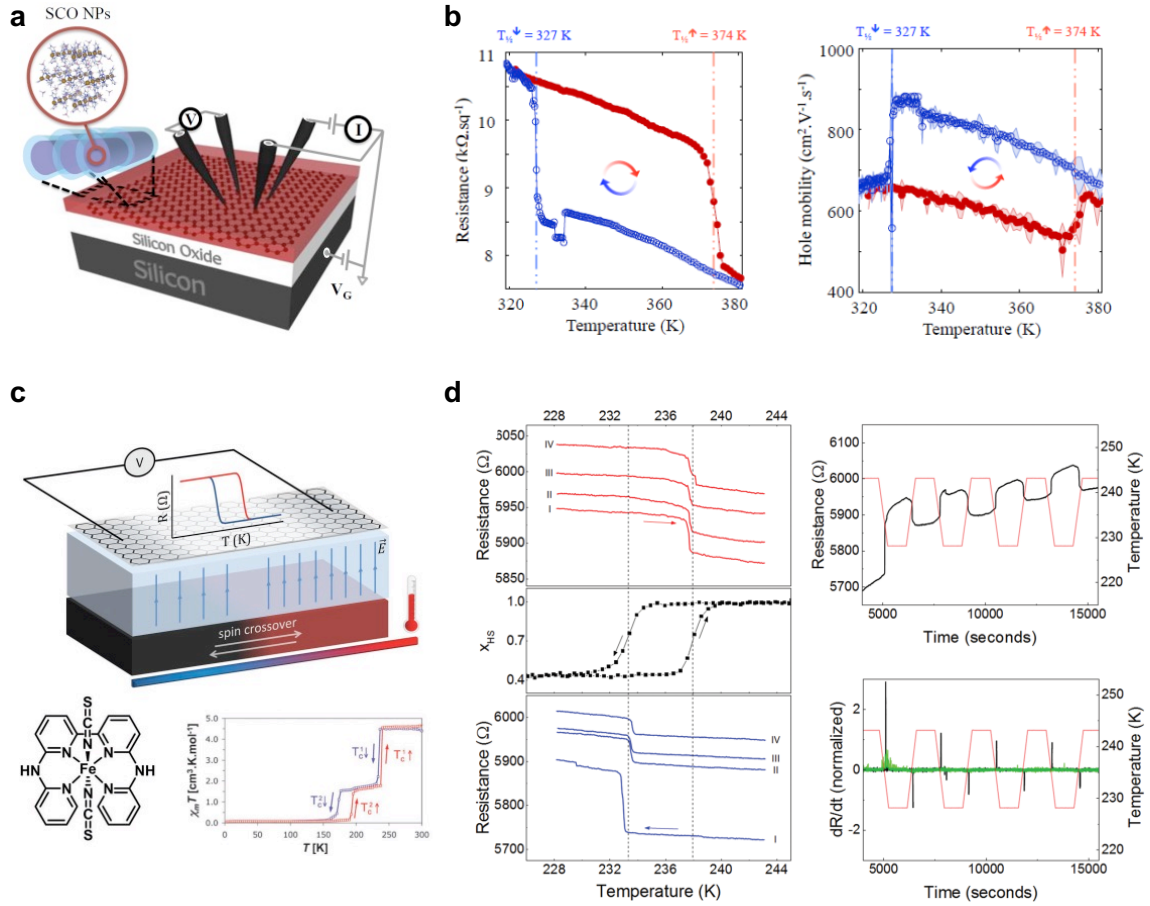

Figure 33. *Large area graphene for sensing the SCO transition. (a) A four-point probe geometry was employed to characterize back-gated CVD graphene covered with SCO nanoparticles. (b) The resistance measured at the Dirac point and the hole mobility displayed a thermal hysteresis compatible with the spin transition in the SCO nanoparticles. (c) CVD Graphene was placed above a SCO crystal, separated by a dielectric polymer. The molecular structure and the temperature dependence of the crystal susceptibility are also shown. (d) The change in the graphene resistance over temperature shows sharp transitions in correspondence of the SCO transition in the crystal.*

Even in this case, the transitions were recorded during multiple temperature cycles were performed. (a, b) Reproduced with permission from ref (260). Copyright 2018 American Chemical Society; (c,d) Reproduced with permission from ref (545). Copyright 2020 Wiley-VCH.

In a recent study[545], CVD graphene was employed to sense the spin state of a SCO crystal displaying a hysteretic switch around 235 K with sharp transitions. Interestingly, in this case the graphene monolayer was not placed in direct contact with the SCO crystal, as a dielectric polymer spacer was inserted between the two materials (Figure 33c). The resistance of graphene as a function of temperature was measured in a simple two probe configuration. A sharp change in the graphene resistance was recorded when annealing and cooling the device at temperatures which precisely matched the transition in the SCO crystal (Figure 33d). Moreover, the effect was reproducible and could be observed during four temperature cycles (Figure 33d). The authors mentioned two possible mechanisms which could cause the measured change in resistance. The SCO transition was accompanied by a change in the crystal volume, which introduces strain in graphene, in turn leading to a decrease in its electrical conductivity. However, the authors minimized this contribution employing thick polymeric spacers, which limited the mechanical stress. They ascribed the main contribution to the measured resistance change to a different electrostatic potential generated by the crystal in the HS and LS state.[545] This conclusion is based on the observation of a shift in the charge neutrality point of graphene when the crystal following the SCO transition, which indicates that the two spin configurations introduce different doping in graphene.

The two works displayed in Figure 33 prove the possibility to determine the spin state of SCO complexes with graphene using a practical device geometry, and, changing the perspective, they

show that SCO complexes can be used to introduce a thermally addressable bistability in graphene. While at a first sight the thermal hysteresis measured with graphene closely resembles that of the SCO complexes in nanogaps (compare Figure 32d with Figure 33b), it should be noted that the use of graphene as a sensor has two obvious advantages: first, it facilitates the device fabrication, thus increasing the success yield and reproducibility; second, it permits to observe the modulation of an electrical current which is several order of magnitude higher, in gateable devices characterized by high electronic performances (electron/hole mobility). To make a comparison, while for the experiment shown in Figure 32d,[544] a very high bias voltage (V = 20 V) was required to measure a current well below the nA range, the graphene resistance was in the order of 10 kΩ,[260,545] so that a 1 V bias generated a 100 μA current. In this regard, graphene amplifies the electrical response of SCO nanogaps, making it compatible with the technologically relevant currents of microelectronic industry. A recent work explored the possibility to detect the not only the temperature-induced spin crossover, but also the low temperature light-induced spin crossover (or LIESST effect, see section 3.2.3). It was found that at 10 K a two-hours irradiation with light at 647 nm introduced a change in the resistance of a CVD graphene covered with a vacuum-sublimated film of SCO complexes, which could be reversed by a subsequent irradiation with light at 850 nm.[546] Although the recorded change in resistance was modest, its temperature dependence confirmed that it stemmed from the light-induced LS $\rightarrow$ HS transition.

Graphene is not the only 2D material which has been tested in combination with SCO complexes. In a recent work, ultrathin chemically exfoliated MoS_2 flakes were covalently functionalized with SCO nanoparticles[547] (Figure 34a), and subsequently pressed to prepare electrically addressable discs. The authors found that the as-prepared MoS_2 flakes were in the metallic 1T phase, as is often the case for chemically exfoliated MoS_2. Interestingly, spectroscopic

evidence showed that the semiconducting 1H phase was restored after functionalization with the SCO nanoparticles.

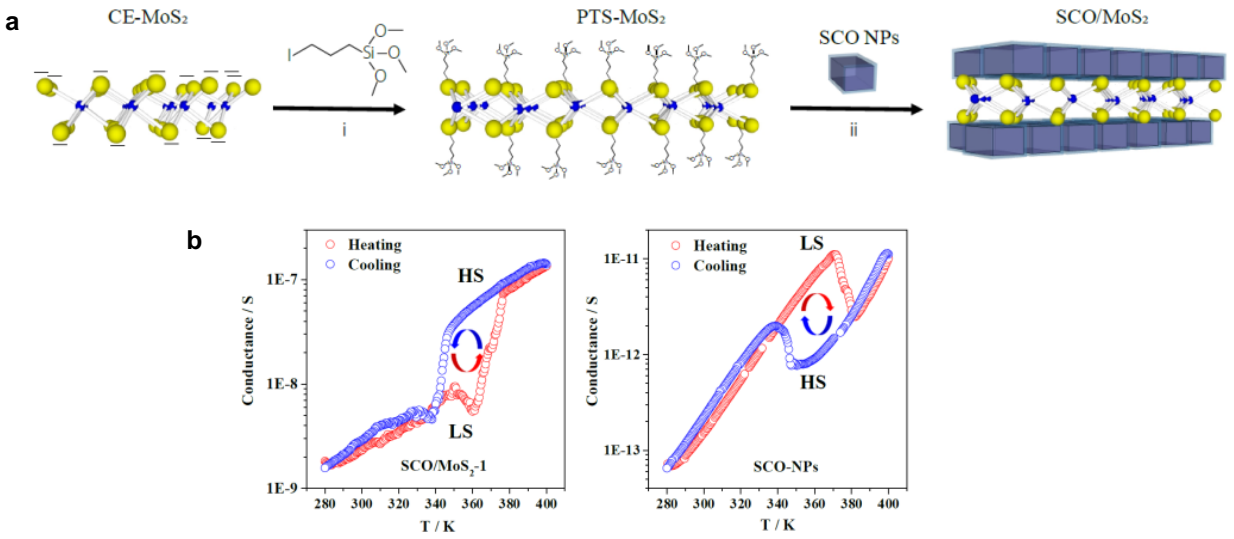

Figure 34. *SCO nanoparticles for the modification of MoS_2 hybrids. Chemically exfoliated MoS_2 was functionalized by reaction with 3-iodopropyl(trimethoxysilane), which left silane groups exposed to covalently attach silica-covered SCO nanoparticles. (b) The temperature dependence of the conductance of MoS_2/SCO hybrid was measured and compared to that of bare nanoparticles. (a, b) Reproduced with permission from ref (*[547]*).*

The conductance of the MoS_2/SCO hybrids was characterized as a function of temperature and compared to that of bare SCO nanoparticles[547] (Figure 34b). A thermal hysteresis was recorded in the conductance of hybrids, with the HS state displaying almost one-order-of-magnitude higher current. Interestingly, the opposite behavior was found for the bare nanoparticles, which displayed higher conductance in the LS state. This finding demonstrates that in the case of the MoS_2 hybrids the electrical current is flowing primarily through the MoS_2 channels, while the SCO nanoparticles modulate the current flow but do not contribute significantly to the overall conductance. The

conductance of the MoS_2/SCO hybrids was 4-5 orders of magnitude higher than that of the bare nanoparticles,[547] making it possible to measure the hysteresis with much lower (technologically interesting) voltages. The authors ascribed the measured change in the conductance of the hybrids to the strain introduced in MoS_2 by the volume change associated with the transition in the SCO nanoparticles, underpinning a different mechanism as compared to the case of graphene (Figure 33).

We highlight that in the studies presented in this section, the conductance of 2DMs is modified in response to a change in a physical property of the SCO compound related respectively to its dielectric constant,[260] electrical dipole[545] or volume.[547] On the contrary, by itself the change of the molecular spin does not introduce a significant modification in the 2DM properties, and it is only indirectly sensed through the change in other physical properties. In this respect, we mention that achieving a change in the magnetism or in the spin transport of 2DMs via the proximity of SCO complexes is extremely challenging, since (i) in SCO complexes, the metal atom where the spin transition takes place is surrounded by organic ligands, so it cannot be in the close proximity of the surface, and exchange interactions are relevant at very short distances; (ii) while there are reports of 2DM becoming ferromagnetic due to the proximity of a ferromagnetic material, the change in the SCO complexes between a diamagnetic and a paramagnetic configuration is unlikely to generate any significant change in the magnetism of the 2DMs. Therefore, while these experiments show the full potential of SCO complexes to provide multiple resistance states to 2DM-based devices, they miss the demonstration of a path for the integration of SCO complexes in spintronics. In section 7, we will further comment on this issue and we will propose possible device architectures to benefit from the SCO in spintronic devices.

The effect of a thermally-induced spin switch on the magnetotransport properties of MoS_2 and graphene was explored for a polycyclic aromatic hydrocarbon which exhibit a transition from a diradical spin-singlet state at low temperature to a thermally excited spin-triplet state above 370 K.[548] A change in both the charge carrier density and magnetoresistance of MoS_2 and graphene was recorded at temperatures below and above the spin-switch temperature, which was interpreted as the result of the exchange interaction between the molecular triplet and the conducting charges in the transporting channel. The use of the hydrocarbon spin switch overcomes some of the problems associated to the SCO complexes, e.g. the spin switching center being in direct contact with the 2DM surface, thereby making it a promising platform for the investigation of switchable molecular spins on 2DMs.

6.3.3 2D Materials/SMM Interfaces

Single molecule magnets (SMM) are particularly intriguing for quantum computing,[549,550] as their spin represent the ideal two-levels systems for storing and manipulating quantum information. Most works focusing on SMM for quantum computing aim at characterizing the quantum nature of spin in SMM, e.g. measuring coherence times and Rabi oscillations.[551] This is often achieved by performing electrons spin resonance experiments which employ optical pulses to manipulate and read out the spin dynamics.[302,550-552] Experiments in single-molecule junctions show that the (nuclear) spin of SMM can be also addressed and manipulated electrically.[553,554] As for the case of SCO complexes, employing 2DMs to read out and manipulate the spin in SMM would facilitate the device fabrication, providing a practical experimental platform to perform quantum computation. In this direction, it is crucial to understand the spin dynamics in SMM in contact with 2DMs. Indeed, in the examples discussed in section 3.2.3, the static magnetic

properties were probed under an applied magnetic field, but the spin dynamics, which are related to coherence effects and are crucial for quantum computing, were not investigated.

The spin dynamics of a SMM in contact with graphene were studied in 2015.[330] SMM/graphene hybrids were prepared by solution assembly of SMM on micromechanically or chemically-exfoliated graphene flakes (Figure 35a). The SMM were equipped with two pyrene groups for efficient anchoring to graphene. The static and dynamic magnetic properties of the so-obtained hybrids were measured and compared to those of bare SMM. The static magnetic susceptibility of the hybrids, characterized by applying an external dc field H and measuring the magnetization M, was unaltered with respect to that of the bare SMM. On the contrary, profound differences were encountered in the spin dynamics, measured applying a small oscillating field. In particular, faster spin relaxation times were found for the SMM in contact with graphene[330] (Figure 35a). This result was understood considering and theoretically modelled on the basis of the interaction between the spin in the SMM and the electrons in graphene. While typically long spin lifetimes are preferred for quantum computing, the authors noted that based on their theoretical understanding the coupling between the electrons and the spin is coherent and leads to a spin level mixing comparable to that used for qubit manipulation. The same group in 2018 addressed the magnetism of atomically precise graphenoids.[551,552] In these systems, spin coherence times in the range of microseconds were found at room temperature. It should be noted that these graphenoids resemble more closely molecular materials rather than two-dimensional graphene.

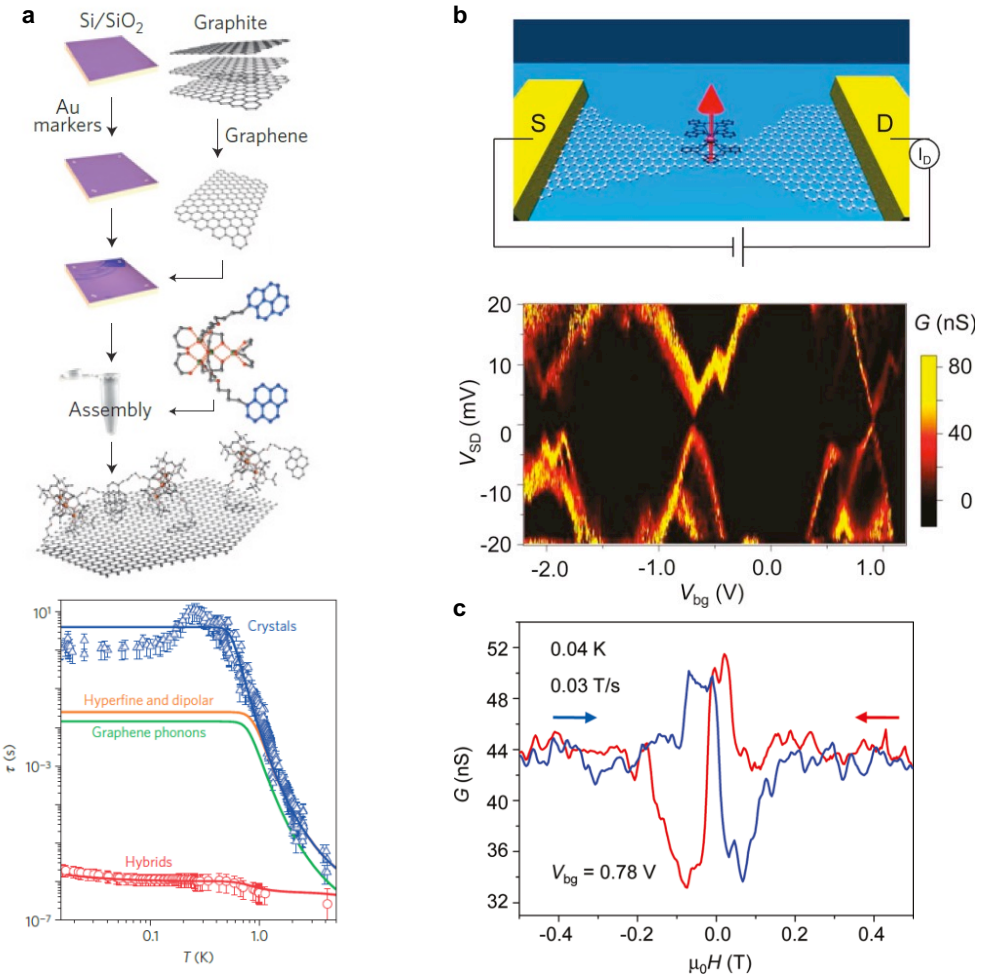

Figure 35. *Graphene/SMM interfaces. (a) scotch-tape exfoliated and chemically exfoliated graphene were non-covalently functionalized with Fe-based SMM, and the spin dynamics of the so-obtained hybrids were measured and compared to those of pure SMM crystals. The spin relaxation time for the hybrids was found to be significantly lower than for the crystals. (b) A few-nm wide graphene nanocostriction was covered with a few Tb-based SMMs. The electrical characteristics of the nanocostriction displayed clear Coulomb diamonds, indicating the presence of a set of discrete energy levels due to quantum confinement. (c) After functionalization with SMMs, the application of a magnetic field was found to change the nanocostriction conductance, resulting in a hysteretic magnetoconductance. (a) Reproduced with permission from ref* [330].

Copyright 2016 Nature Publishing Group; (b,c) Reproduced with permission from ref ([555]). Copyright 2011 American Chemical Society.

The possibility to electrically detect the spin switch in a SMM in contact with graphene was explored in 2011.[555] In this experiment, a graphene flake was patterned to define a few-nm-wide nanoconstriction. Due to quantum confinement, the band structure of graphene is profoundly modified at the nanoconstriction, which is characterized by a set of discrete levels instead of the conventional zero-bandgap Dirac point. Therefore, the graphene constriction behaves as a quantum dot, across which electrons can flow only if one of the discrete levels is aligned to the Fermi level of the large graphene electrode. By applying a back gate, the set of discrete levels was shifted in energy, giving rise to the so-called Coulomb diamond, which was observed in the experiment (see Figure 35b). Tb-SMMs were deposited from the liquid phase onto the nanocostriction device, with, also in this case, pyrene groups to ensure to non-covalent grafting to the graphene. In some devices, a hysteretic behavior of the conductance was recorded after molecular functionalization by sweeping the magnetic field at very low temperatures (Figure 35). The magnetic-field-induced change in conductance (also called magnetoconductance), which was as high as 20%, was understood as a signature of the presence of SMMs in the proximity of the constriction and explained on the basis of local stray fields generated by the SMM dipolar moment.

We should stress that the nanocostriction device is a 0D quantum dot, hence significantly different from large area 2DMs, and, in some regards, it resembles more a carbon nanotube, where similar effects were also reported.[556] However, by demonstrating that the spin-switch of SMM indeed can affect the magnetoconductivity of nano-graphene, this work how a homogeneous and macroscopic self-assembled layer of SMMs on graphene would affect its electronic and magnetic

properties. It should be noted that the possibility to make graphene and other 2DMs ferromagnetic by interfacing them with ferromagnetic materials has been explored in several cases for inorganic compounds;[54,233,557-559] the presence of SMMs might generate similar effects.

The most representative spin/magnetic-switchable devices are summarized in Table 4.

Table 4. Spin/Magnetic Responsive 2D devices.

2D material	Thickness	Spin switch	Bond type	Interaction mechanism	Effect of LS→HS transition	Stimulus	Ref.
Graphene	Monolayer	$[Fe(Htrz_2)(trz)](BF_4)$ nanoparticles	Non-covalent	DI, Change in dielectric constant	Change in resistance, mobility	T	*260*
Graphene	Monolayer	$[Fe(bapbpy)(NCS)_2]$ single crystal	Non-covalent	DI	Change in resistance, doping	T	*545*
Graphene	Monolayer	$(Fe[HB(3,5\text{-}(Me)_2Pz)_3]_2$ Thin films	Non-covalent		Change in resistance, hole doping $3.6 \times 10^{11}\ cm^{-2}$	T, hν	*546*
Graphene	Monolayer	quinoidal dithienyl perylenequinodimethane	Non-covalent	Charged impurities	Change in magnetoresistance	T	*548*
MoS_2	Monolayer	quinoidal dithienyl perylenequinodimethane	Non-covalent	Exchange interaction	Change in magnetoresistance	T	*548*
Chemically exfoliated MoS_2	(mostly) monolayer	$[Fe(Htrz_2)(trz)](BF_4)$ nanoparticles	Covalent	Strain	Change in conductance, photoluminescence	T	*547*

Notes: DI, dipole interaction; LS, low spin; HS, high spin; T, temperature.

7 Molecular Engineering of Functional 2D Materials for Alternative Computing Paradigms

2DMs are not only explored as promising candidates in the context of More-Moore or More-than-Moore approaches, but they also represent a central material platform for other computing paradigms, being spintronics[23,229] and quantum computing.[24] From the perspective of materials science, superconducting and ferromagnetic materials are particularly intriguing for building up quantum computing and spintronic devices. Indeed, whereas the most reliable implementation of electronic qubits is based on the so-called Josephson junctions, in which two superconductors are separated by a thin non-superconducting layer,[21] the prototypical spintronic device is the spin valve, composed of two ferromagnetic electrodes separated by a non-magnetic spacer.[560] While these devices are typically fabricated employing conventional non-layered materials,[21,560] Josephson junctions[561-563] and spin valves[564-567] based on 2DMs have been demonstrated in recent years. The use of 2DMs offers a few key advantages, such as the possibility to generate atomically perfect van der Waals interfaces between the different materials. Moreover, in analogy to the optoelectronic properties, both the superconducting[568-570] and the magnetic state[236,237,571,572] of 2DMs can be tuned using appropriate external stimuli (such as an electric field), offering the possibility to tailor the materials properties for specific applications. Not only this possibility makes them particularly attractive for applications, but also and it makes them the ideal playground for molecular functionalization. While a complete account on the use of 2DMs in spintronics and quantum computing is beyond the scope of this work and is the topic of excellent recent reviews, [23,24,229] here we highlight some recent results showing how molecular engineering of superconducting and ferromagnetic 2DMs could be highly beneficial for the two fields.

Figure 36 depicts different approaches to tailor the superconducting state of $NbSe_2$ via molecular functionalization. $NbSe_2$ is the prototypical 2D superconductor, and it is subject of intense study in view of its electronic correlated phases, which give rise to intriguing physical phenomena, including anomalous critical temperatures,[573,574] a quantum metallic state,[575] Ising superconductivity,[576,577] unusual superconducting transition,[578] and multifractal superconductivity,[579,580] among others. In a first study, the effect of individual Co-phthalocyanine on the superconductive state of bulk $NbSe_2$ was characterized through low temperature STM.[581] As discussed in section 3.2.3, organometallic compounds possess a non-zero paramagnetic spin, which lies in the proximity of the van der Waals surface due to the planar absorption of the phthalocyanine molecules. In general, the presence of magnetic impurities in contact with a superconductor has a dramatic effect on the superconductivity, since low energy bound states appear within the superconducting gap as a result of the interaction between Cooper pairs and unpaired spins (called Yu−Shiba−Rusinov states[582]). Interestingly, multiple Yu−Shiba−Rusinov states generated by adjacent impurities can couple and hybridize giving rise to extended electronic states which could host topologically protected phases[583-585] that are highly intriguing for quantum computation. The presence of Yu−Shiba−Rusinov states on single cobalt phthalocyanine molecules on $NbSe_2$ was confirmed by scanning tunneling spectroscopy (Figure 36a). While on the $NbSe_2$ surface the authors observed the typical superconducting features, characterized by two coherence peaks in the density of states, on single Co-phthalocyanine molecules they recorded pronounced peaks of asymmetric heights within the superconducting gap, which were ascribed to the formation of Yu−Shiba−Rusinov states.[581] In the same work, the authors demonstrated that molecular dimers hosted coupled in-gap states, which were inferred on the basis of split peaks observed in the differential conductance (Figure 36b). In another study, the same group

investigated the impact of different metal phthalocyanine on the superconductivity of $NbSe_2$.[586] Yu−Shiba−Rusinov states were found for molecules in which the unpaired electrons in the central metal ion occupied in d orbitals extending in the out-of-plane direction, and thus interacted more strongly with the superconducting substrate (Co and Mn). On the contrary, molecules with unpaired electrons occupying in-plane orbitals (Cu, Fe) displayed different spectral features, characteristic of spin-flip transitions (Figure 36c). The authors demonstrated the ability of tuning the molecule-substrate coupling by applying pressure with the STM tip, which, in the case of the Mn-phthalocyanine, resulted in the evolution of the spectral features from in-gap bound states to spin-flip transition.[586]

The presence of in-gap bound states was also investigated for the interface between $NbSe_2$ and chiral molecules.[587] Several works indicate that, despite not containing any unpaired electron spin, chiral molecules can act as magnetic impurities due to a not fully understood interplay between structural and magnetic chirality.[588-590] For this experiment, the authors combined STM/STS characterization with the fabrication of mesoscopic $NbSe_2$ devices. STS results showed how the conventional superconducting gap of the bare $NbSe_2$ surface was modified after functionalization with chiral molecules, displaying an additional conductance peak centered at zero bias. The electrical characterization of devices also displayed a similar trend. The authors placed thin $NbSe_2$ flakes onto gold contacts, and, in some cases, they observed naturally high contact resistance, which allowed them to perform spectroscopy experiments in a metal/tunnel barrier/superconductor geometry similar to the situation encountered at the tip/vacuum/superconductor junction in the STM. The devices were characterized before and after functionalization of the top $NbSe_2$ surface. Figure 36d shows that while a hard featureless superconductive gap was recorded for untreated $NbSe_2$, in-gap states were observed for some of

the functionalized flakes, which were interpreted as coupled Yu−Shiba−Rusinov.[587] These works demonstrate that paramagnetic and chiral molecules can be used to tailor the superconductivity of $NbSe_2$, introducing localized electronic states which might be harnessed for quantum computing. Although the authors employed bulk $NbSe_2$, they noted that it behaves essentially as a 2D system, because of the weak van der Waals interaction between adjacent layers.

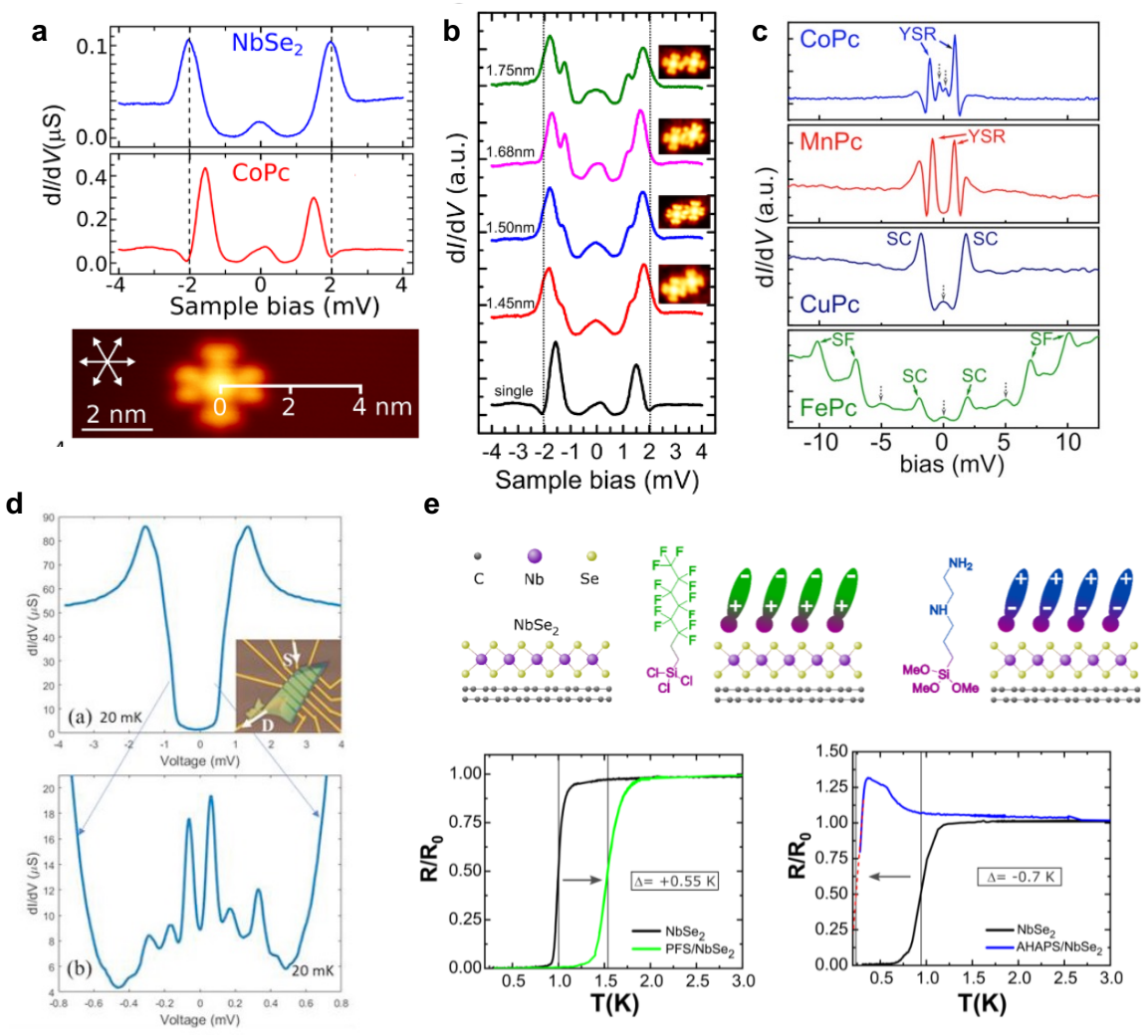

Figure 36. *Molecular tailoring of 2D superconductivity. (a) Differential conductance measured via STS on bulk superconductor $NbSe_2$ and on an isolated Co-phthalocyanine on $NbSe_2$. The STM visualization of the molecule is displayed. The different spectral features in the two cases are*

indicative of the formation Yu-Shiba-Rusinov states centered at the molecule. (b) Additional peaks in the differential conductance appear when CoPc molecules are approached, indicating coupling between the in-gap states. (c) Different metal phthalocyanines display different features on $NbSe_2$, giving rise to either Yu-Shiba-Rusinov states or spin flip events, depending on the strength of the surface interaction. (d) differential conductance of a $NbSe_2$ flake characterized by high contact resistance before (top) and after (bottom) functionalization with chiral molecules. After functionalization, in-gap states appear. (e) Self-assembled molecular adlayers were employed as a fixed molecular gate to modify the charge carrier concentration in $NbSe_2$ and hence its superconducting transition. (a, b) Reproduced with permission from ref (581). Copyright 2018 American Chemical Society; (c) Reproduced with permission from ref (586). Copyright 2019 American Chemical Society. (d) Reproduced with permission from ref (587). Copyright 2019 American Chemical Society. (e) Reproduced with permission from ref (343). Copyright 2021 American Chemical Society.

In a recent work, another approach was explored to tailor the superconductive state of $NbSe_2$ by molecular engineering. The authors showed that the critical temperature of large-area $NbSe_2$ monolayers could be modified (i.e., increased or decreased) by functionalization with ultrathin and ordered self-assembled adlayers.[343] Two different molecules containing the same silane anchoring group and functional groups characterized by opposite permanent dipoles were selected. By combining morphological and spectroscopic characterization, the authors found that the two molecules formed ultra-thin self-assembled adlayers in which the orderly aligned permanent molecular dipoles introduced opposite electric fields in $NbSe_2$ (Figure 36e). Thereby, the two molecular adlayers collectively acted as a fixed gate terminal with molecule controllable polarity.

This approach permitted to manipulate in a programmable way the superconducting transition of $NbSe_2$, which is modified by electric fields[568-570]. In particular, the molecule-induced electric fields caused a 55% increase and a 70% decrease in the $NbSe_2$ critical temperature in the case of hole and electron doping, respectively,[343] in agreement with previous experiments on electrostatically gated $NbSe_2$[568-570] (Figure 36e). The reported modification in the critical temperature is very large when compared to previous experiments reporting the same effect in $NbSe_2$-based field-effect devices,[568-570] demonstrating the efficiency of molecular functionalization. Additionally, the authors found that this molecular functionalization, which is perfectly suited to engineer 2DMs extending over large areas, increased the otherwise limited ambient stability of $NbSe_2$, acting as an encapsulation layer as previously reported for similar self-assembled adlayers on black phosphorous.[341] The possibility to exploit an ordered layer of polar molecules to modify an intrinsic quantum state of matter was also explored for 1T-TaS_2.[591] In this case, it was found that an ordered layer of water molecules could induce a profound modification in the TaS_2 charge density wave, changing its periodicity.

While these studies demonstrate the huge potential of hybrid 2D/molecule systems as a material platform for tunable superconductivity, they do not fully exploit the many possibilities offered by functional organic compounds. For instance, photoswitchable molecules introducing on-demand changes in the charge carrier density could be used to switch ON and OFF the superconductive state through light irradiation, providing an unconventional light control to 2D superconductors.

In a related topic, very few studies so far have addressed the possibility to tune via molecular functionalization the intrinsic magnetic properties of ferromagnetic 2DMs. Partly, this is because the rise in the research in ferromagnetic 2DMs is relatively new, as ferromagnetism in van der

Waals materials at the mono- and few- layer limit was reported only in 2017.[592,593] Additionally, the magnetism of 2DMs is technically difficult to be characterized, since most magnetic 2DMs are unstable in air, possess a Curie temperature well below room temperature, and are often insulating. On the contrary, the use of molecules to modify the magnetic properties of surfaces is well established for conventional ferromagnetic materials,[240] where orbital hybridization and magnetic proximity effects were reported to change the ferromagnetic anisotropy[594] and introduce exchange bias.[285] Functionalization of ferromagnetic 2DMs holds high potential since it might improve their environmental stability, as demonstrated for other 2DMs,[343] and possibly increase the Curie temperature, ultimately favoring their actual use for technological applications.

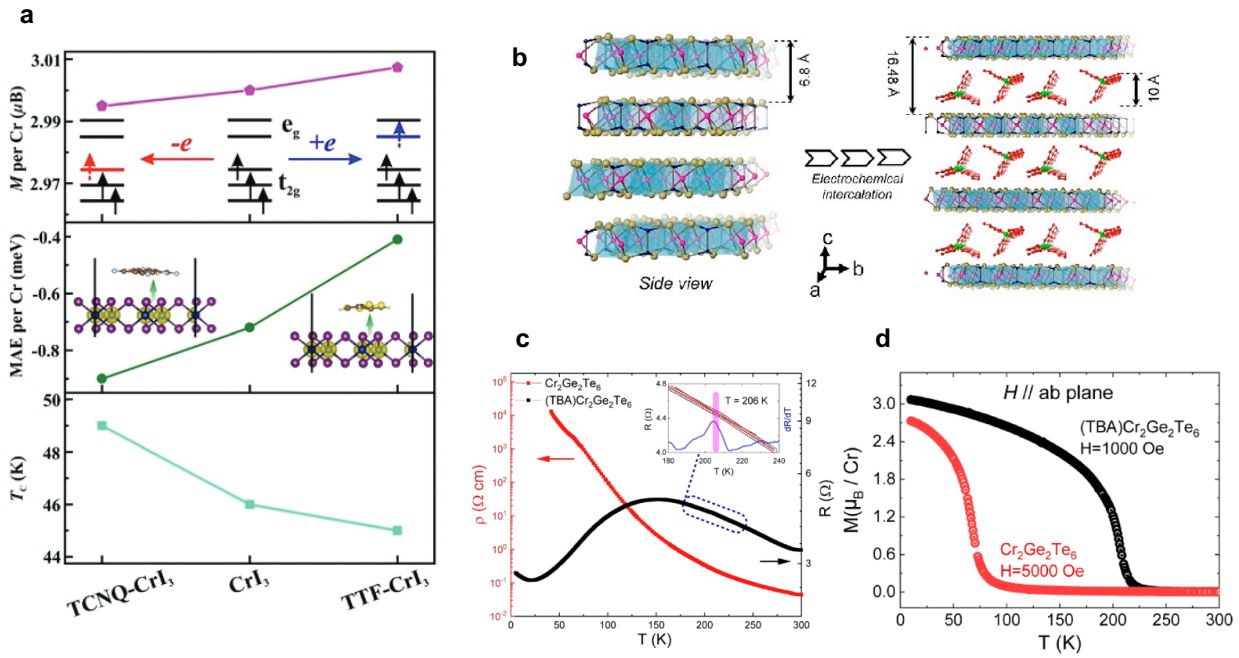

Figure 37*. Molecular tailoring of 2D ferromagnetism. (a) Theoretical investigation of the effect of molecular doping on monolayer CrI_3. Hole and electron doping, achieved by interfacing CrI_3 with TCNQ and TTF, respectively, are predicted to modify in opposite direction the magnetic moment/Cr atom, the magnetic anisotropy and the Curie temperature. (b) Intercalation of tetrabutyl ammonium into a bulk crystal of $Cr_3Ge_3Te_6$ modifies the interlayer distance and*

generates a remarkable electron doping. (c) The temperature dependence of the resistivity displays a semiconducting behavior for the pristine crystal and a metallic behavior for the intercalated compound. (d) Magnetic characterization of the pristine compound shows ferromagnetic behavior below a Curie temperature T_C = 67 K, which increases to T_C = 208 K after intecalation. (a) Reproduced with permission from ref (595). Copyright 2020 Royal Society of Chemistry; (b, c, d) Reproduced with permission from ref (364). Copyright 2019 American Chemical Society.

Here, we highlight two works which provide evidence for the potential of using organic molecules to modulate the magnetic properties of 2DMs.[364,595] Figure 37a shows the results of a theoretical work investigating the change in the ferromagnetic properties of ferromagnetic CrI_3 monolayer as a consequence of molecule adsorption.[595] The authors initially calculated the modification in magnetic anisotropy for hole and electron doping, finding results in agreement with experimental results obtained with electrostatic gating.[572] Then, they addressed the effects of two different dopant molecules, one (TCNQ) introducing hole doping, and the other one (TTF) electron doping. They predicted that the functionalization with the two molecules would affect in opposite direction the Curie temperature, the magnetic moment per Cr atom and the magnetic anisotropy[595] (Figure 37a). Therefore, this study shows a path to tailor the magnetism of 2DMs through molecular gating, considering realistic doping levels for molecular doping (below 2 10^{13} charge/cm^2).

The impact of molecular engineering was experimentally explored for the layered ferromagnetic compound $Cr_3Ge_3Te_6$.[364] In this case, the organic ion tetrabutyl ammonium was intercalated into bulk $Cr_3Ge_3Te_6$ crystals following an electrochemical approach (see Figure 37b). The intercalation is accompanied by a large electron doping, which drives a transition in $Cr_3Ge_3Te_6$

from the pristine semiconducting to a metallic state (Figure 37c). On the same time, dramatic changes were recorded for the $Cr_3Ge_3Te_6$ magnetic properties. Impressively, the Curie temperature was found to increase from 67 K of untreated $Cr_3Ge_3Te_6$ crystal to 208 K of the intercalated compound (Figure 37d). [364] Additionally, the magnetic anisotropy was modified from the out-of-plane to in-plane direction. This result demonstrates that molecular treatments can indeed change dramatically the magnetic properties of ferromagnetic 2DMs; while the reported change in Curie temperature was obtained by treating a bulk layered crystal, we anticipate that similar result could be obtained by functionalizing ultrathin layers.

Even for the case of ferromagnetic 2DM/molecule hybrids, we think that the field is still in its infancy, and further molecular capabilities could be coupled to ferromagnetic 2DMs to demonstrate multi-responsive materials. For instance, one can foresee the use of photochromic molecules to provide photo-switch to magnetic properties of 2DMs. Moreover, exchange interactions between ferromagnetic 2DMs and the molecular spin of organometallic compounds might result in exchange bias effects similar to those observed at the interface between ferromagnetic 3D metals and organometallic molecules.[285] Taking a step further, molecular spin switches such as those in which the molecular spin is modified by light irradiation[265] could be used to dynamically tune the exchange interaction, generating a photo-tunable magnetic coupling with no counterpart in any other material system.

Finally, we note that molecules can be used not only to modify the intrinsic superconductivity or magnetism of superconductive 2DMs, but also to introduce a superconductive or ferromagnetic state in an otherwise non-superconductive or non-ferromagnetic layered material. For the case of superconductivity, an experimental realization of this possibility has been demonstrated by using $SnSe_2$, which is a non-superconducting material that can be driven into a superconducting state by

a large charge carrier doping.[596] In different works, molecular intercalation of bulk $SnSe_2$ crystals was employed to achieve extremely high doping levels (Figure 38a,b), making $SnSe_2$ superconductor. [365,597-599] Two different approaches were employed to intercalate $SnSe_2$: a solvothermal process was employed to intercalate cobaltocene,[597,599] whereas different organic ions were intercalated following an electrochemical approach.[365,598] In every case, a completely intercalated compound was obtained, as demonstrated by X-ray diffraction (Figure 38c,d). For all compounds, superconductivity was recorded after intercalation, with a highest critical temperature of 7.1 K obtained in the case of CTA intercalation (Figure 38e,f).[365] The superconductivity of these intercalated compounds was found to be quasi-2D and dependent on the interlayer separation, which could be finely tuned by intercalating different compounds (Figure 38b).

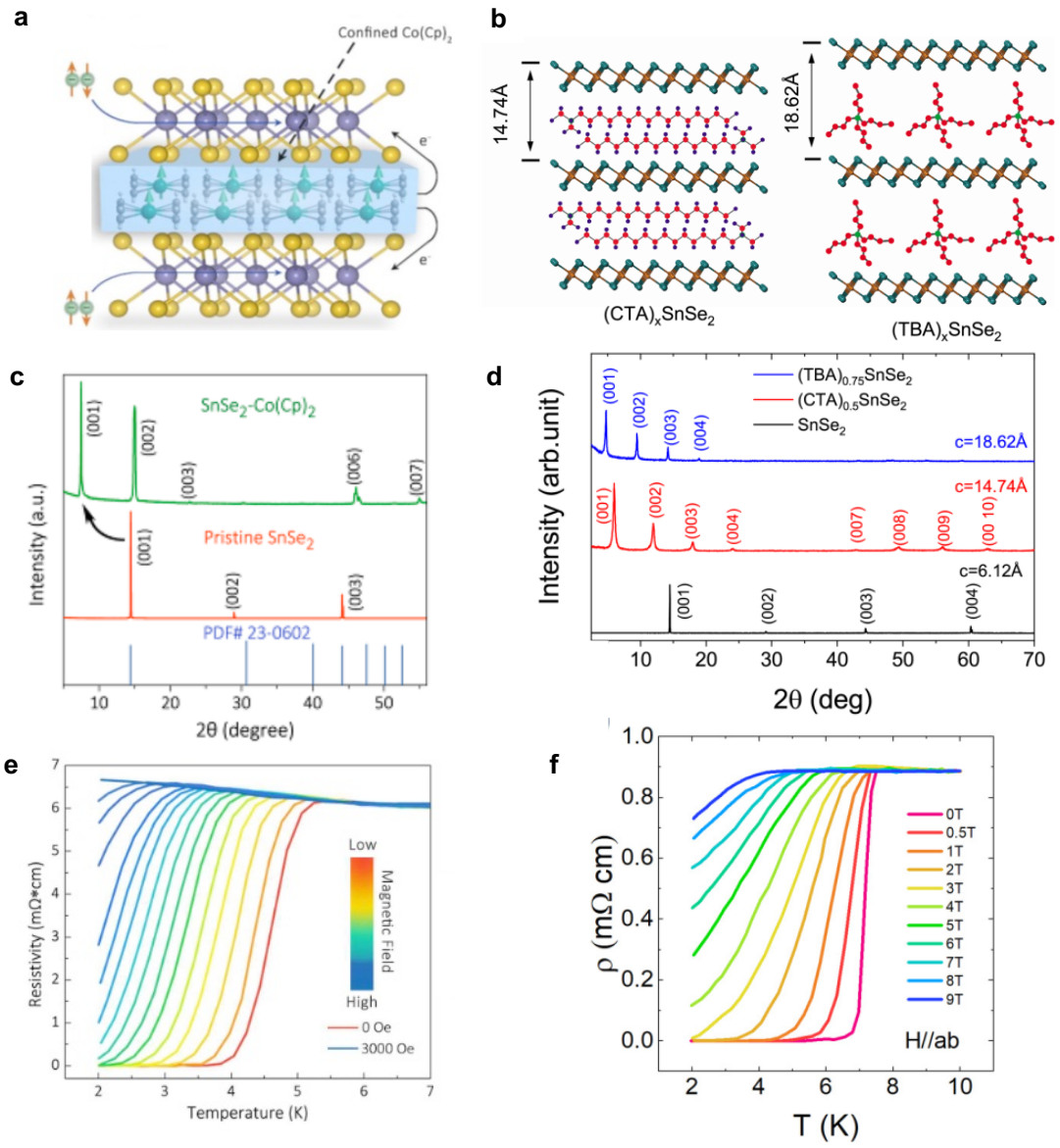

Figure 38. *Molecule induced superconductivity in an otherwise non-superconducting material. (a,b) non-superconductor $SnSe_2$ becomes superconductor after intercalation with different organic compounds, including cobaltocene (a), tetrabutyl ammonium and hexadecyl trimethyl ammonium (b). (c,d) X-ray Diffraction shows a new set of peaks for the intercalated compounds, demonstrating a complete intercalation. (e,f) The temperature dependence of the resistivity for cobaltocene and CTA intercalation shows a superconducting transition displaying different sensitivity to the magnetic field. (a, c, e) Reproduced with permission from ref (*[597]*). Copyright 2017*

American Chemical Society; (b, d, f) Reproduced with permission from ref ([365]). Copyright 2020 American Physical Society.

In the case of cobaltocene, the authors reported the presence of a ferromagnetic signal in the intercalated crystal, as measured through bulk magnetometry.[597] This result would be rather surprising, since ferromagnetism is usually detrimental to the formation of the Cooper pairs carrying the superconductivity, and only few materials show the coexistence of intrinsic superconductivity and ferromagnetism.[600,601] However, the magnetic signal recorded in this study is rather small, and its origin could not be unequivocally identified, since the presence of (weak) ferromagnetic signals measured in bulk crystals are often not related to intrinsic ferromagnetism.[602-604] Therefore, while the result is certainly intriguing, a direct, elemental resolved investigation of the magnetic properties will be required to draw a definitive conclusion. Similarly, the coexistence of ferromagnetism and superconductivity was previously reported for liquid phase exfoliated $NbSe_2$ treated with hydrazine molecules;[605] even in this case the ferromagnetic phase was inferred on the basis of bulk magnetometry measurements, so the previous caveat remains valid. In the same way, Z. Li *et al*. have recently explored the possibility to introduce ferromagnetism in superconducting 2H-TaS_2 through the intercalation of cobalt ions and organic ammonium molecules.[606] These works are among the few studies on the possibility to induce ferromagnetic ordering in otherwise non ferromagnetic 2DMs via molecular functionalization is investigated experimentally. Curiously, both studies focus on materials which are superconductors at the same time, and we are aware of no works reporting the emergence of long-range ferromagnetism in a non-superconducting 2DM by molecular engineering. However, we think that this route has high potential, as some results obtained with non-layered materials

show that interfacial effects at organic/inorganic interfaces introduce interfacial ferromagnetism in normally diamagnetic metals, such as Cu.[607,608] Additionally, several non-ferromagnetic 2DMs lie at the verge of intrinsic ferromagnetism,[602,609] so that extrinsic perturbations in their crystal structure, including defects,[610] introduce magnetic moments and might drive them into a ferromagnetic state. For these reasons, we believe that molecular functionalization might be an ideal tool to manipulate the magnetism of 2DMs, eventually offering the possibility to add a few compounds to the family of ferromagnetic layered materials, ultimately enlarging the material platform for all-2D spintronics.

8 Conclusion Remarks and Outlook

During the last few years, the downscaling of Si CMOS has encountered significant obstacles, and as a result the development of the semiconductor industry reached a crossroad. One promising approach that can be pursued aims at breaking through the physical limitation in transistor dimensions by integrating new channel materials. Compared with bulk Si, 2D semiconductors without surface dangling bonds show the advantages to confine the electrons in atomically thin channels, reduce the leakage current and hence overcome the short-channel effect. The ultra-scaled CMOS devices are very likely to adopt 2D semiconductors as channel layers with the new gate-all-around transistor structure. It is very important to explore new strategies to realize 2D CMOS electronics.

Another promising approach consists in the integration of multifunctional devices with CMOS circuits. This requires the controlled combination of different components interacting physically, with each of them contributing with specific functions which are synergically merged in a hybrid architecture. Such hybrid approach is particularly powerful when applied to 2DMs

because their large surface-to-volume ratio make them extremely sensitive to changes in the surrounding environment. Hence, 2DMs represents a versatile platform to construct multifunctional devices, via the development of new device concepts and functionalities. Nevertheless, the choice of 2DMs is limited, which defines also the limited spectra of achievable properties and functions in van der Waals heterostructures. Differently, the number of molecules which can be designed and synthesized with programmable properties is nearly infinite, thereby offering access to a largest portfolio of functionalities.

In this review, we have provided an in-depth summary on the honeymoon of the molecular science and 2DMs with the ultimate goal of engineering 2D devices for CMOS and beyond CMOS applications. The basic electronic properties of 2DMs and organic materials, with a special focus on molecular switches, have been systematically assessed. The controlled interfacing of these two classes of materials, via chemisorption or physisorption, have been discussed with a particular attention paid to how the relevant interactions enable to mutually influence the properties of the components yielding the hybrid. In CMOS applications, such as transistors, diodes, and memory devices, the optimization of all physical processes occurring at the interface between the 2DMs and the electrodes as well as the dielectric surface still represents a major challenge. On the same time, the modulation of the electronic properties of 2DMs via doping cannot be done by means of conventional doping methods (ion implantation and diffusion) which are unsuitable for the 2D ultrathin body. Yet, electroactive molecules and highly polar ones can successfully be used to dope 2DMs via charge transfer and dipolar interactions, respectively. The molecular approach can also be used to engineer the interfaces at the contact region and between 2DMs and the dielectric layer. On the one hand, molecules can induce the degenerate doping effect on the contact region to reduce the Schottky barrier. On the other hand, molecules can work as the tunneling layer to weaken the

Fermi level pinning effect. To optimize the 2D/dielectric interface, self-assembled monolayers and trap-free polymers can be used to functionalize the surface of conventional dielectric layer. The organic interfacial layer can reduce the surface and phonon scattering, which improves the performance of 2D CMOS devices.

Beyond CMOS applications, the goal is to foster the interaction of devices with people and outer environment, promoting the functional diversification. Towards this end, hybrid systems combining molecular switches with 2DMs can offer a multitude of dynamic solutions. The molecular switches can respond to the external stimuli and send the information to the surrounding 2DMs. Then output can be read from 2D electronic devices by converting light, chemical, electrochemical, spin, magnetic stimuli to electrical signals. One promising, yet unexplored field consists in the incorporation of supramolecular ferroelectrics with 2D materials to realize ferroelectric memory devices.[611,612] In addition, the incorporation of ferroelectric polymers in 2D functional devices provides another terminal to mimic the memory functions, which provides a promising approach to fabricate memristive synapse devices with multiple responsivity.[613]

Besides the aforementioned methodology, the organic molecules can directly manipulate the physical properties (e.g., magnetism) of 2DMs, offering the possibility to add the functionality of 2DMs and enlarge the material platform for 2D functional devices.

8.1 Industry applications of 2D CMOS devices

Silicon CMOS circuits represent the dominant technology used in nowadays electronic devices. The prospect of the semiconductor industry comprises the introduction of new materials and structures to break through the scaling limit of Si CMOS devices. The development of 2D electronic devices has the potential to complement Si MOSFET by adopting gate-all-around structure and vertically stacked nanosheet channels. In addition, the low-temperature process in

the fabrication of 2D FETs is compatible with the next-generation technology evolution, such as the monolithic 3D integration of logic and memory. Although extensive research efforts have been made to improve the performance of 2D transistors, the implementation of 2D semiconductors in MOSFET devices remain in its infancy, which needs further engineering efforts. In this review, we discuss that molecular approaches provide promising solutions to solve several basic issues of 2D transistors, including the reliable doping technique (control of carrier density and carrier type), the low contact resistance between 2DMs and bulk metal, and the high-quality 2D/dielectric interface. However, most of the reported strategies make use of planar 2D transistors to provide a preliminary demonstration. It is important to note that molecular approaches with their unique advantages should be extensively explored in vertically stacked multi-bridge 2D channel FETs in the future studies. In the meanwhile, there has been a very active debate about the industrial applications of molecular functionalization approaches in electronic devices due to their relatively weak thermal stability and poor CMOS compatibility. Therefore, it is important to seek potential solutions to overcome these challenges. Compared with noncovalent functionalization, the covalent functionalization of suitably designed molecules on the 2D surface offers much greater stability, which is desirable for controlled doping technology and create the molecular tunneling barrier on the contact region. But it is worth noting that the invasive covalent functionalization will unavoidably degrade the electrical performance of 2DM devices. Therefore, future studies can explore the mild covalent functionalization methods to balance the stability and device performance. The high temperature stability is a prerequisite for the trap-free polymer which needs to be used as the interfacial dielectric layer in order to be compatible with the CMOS fabrication process. The commercial polymers BCB and CYTOP have high thermal stability up to 350 ^{o}C and 400 ^{o}C, respectively, and hence they are promising candidates as the dielectric layer. In addition,

2D CMOS devices are mostly used to complement Si MOSFET in specific applications and the integration of 2D CMOS devices during or after the back end of line (BEOL) processes can lower the requirement for the 2D device fabrication. In the future studies, great efforts should be made to promote the 2D device performance via covalent molecular functionalization and develop trap-free polymers stable at high temperatures.

8.2 Multiresponsive transistors and memories

The Internet of Everything will lead us to a scenario in which interactions between humans and devices will be critical to allow people to use, monitor or configure Internet of Things devices. Interactions in such applications are based on responsive devices, leading to the generation and transfer, i.e. communication, of a huge amount of data. The efficient processing of these data relies on transistors and memories as the basic electronic elements whose integration can lead to responsive devices. Since responsiveness can be exploited for precise sensing, near-sensor and in-sensor computing can be developed in which computation tasks are moved partly to the sensory terminals.[614] One representative example is the optical memory, which exploits one device to simultaneously respond to the light signal and store the input optical signal. [613]While recent reports primarily focus on the device level,[615,616] it will be important in the future to expand such an approach to device arrays, to enable further system operation. In addition, the design and realization of novel responsive devices which can respond to more complex input signals is of paramount importance. This can include, for example, devices capable of distinguishing different optical wavelength or different chemical components. In addition, further research should be focused on the construction of a single device responding multiple types of input signals, towards multifunctional integration.

8.3 Integration on the Si device platform

The gradual evolution from device dimension scaling to functional diversification guarantees the continuous development of electronic systems. Integration is achieved via 3D monolithic construction of multifunctional chips, enabling enhanced performance by exploiting the vertical direction and the functional diversification of the silicon platform for applications in opto-electronics and sensing. 2DMs are perfect candidates for 3D monolithic integration to construct vdWs heterojunctions for advanced functionality on Si integrated circuits platform. In the early stage, the functional devices composed of 2DMs and responsive molecules will be stacked at the last layer of the back end of line (BEOL) to enhance the functionality. Further optimization and technology evolution with 2DM/molecules responsive systems will advance emerging computing paradigms, having the potential to realize near-sensor and in-sensor computing. At the moment, the integration of 2DM/molecules system on Si wafer substrates is limited by the growth techniques, the transfer processes and the lacking of suitable production tools.

The production method of 2DMs has evolved from the low-yield mechanical exfoliation (using scotch tape) to the scalable CVD growth and liquid-phase exfoliation. Continuous 2D films and heterostructure have been grown by CVD methods with high crystallinity and large-scale production capability.[373,617] Several promising applications of CVD-grown TMD films have been demonstrated in (opto)electronic devices and they have achieved a sufficiently high level of maturity to be employed in complex systems.[618] However, the CVD growth of 2DMs still meets great challenges. For instance, it's urgent to develop wafer-scale growth method to produce single-crystalline and continuous 2DM films and the reproducibility needs to be improved. The growth methods and technologies (process, parameters, substrates, etc.) should be optimized to overcome these challenges. The ultimate goal is the practical use of CVD-grown 2DM films in logic and functional devices with comparable device performance based on single-crystalline flakes (i.e.,

flakes exfoliated by scotch tape) and the integration of 2DM devices with silicon readout/control electronics. The liquid-phase exfoliation methods have been explored to produce high-concentration and high-volume TMD dispersions. In the exfoliation process, the bulk crystals are dispersed and exfoliated in a specific solvent via mechanical energy transfer that overcomes the vdWs interactions. The high-yield dispersions can be deposited in the form of thin-films by diverse techniques, including inkjet printing,[619] spray coating,[620] drop casting[621] and so on. These solution-processed 2DMs have been used for applications in in (opto)electronics, (photo)catalysis, and (bio)sensing. In recent years, the solution-processed 2DMs showed some promising results in large-area electronics.[622] Although the solution-processed exfoliation provides a good tradeoff between cost, purity and yield, the small grain size of the crystal domains and the large number of uncontrollable defects still limit their applications in high-performance logic devices. Future works should be focused on the improvement of exfoliation reproducibility and uniformity. It is also desirable to seek the unique applications of solution-processed 2DMs taking advantages of their physicochemical properties, for example in responsive functional devices. In the previous studies, mechanical-exfoliated 2DMs by scotch-tape method are mostly used in the exploration of responsive devices. The functionalization of molecular switches during the liquid exfoliation process may provide a route to realize large-scale responsive devices.

During the fabrication of 2DM devices, 2D layers need to be transferred from the grown substrate to the device substrates or to be stacked vertically as heterostructures. It is still a great challenge to develop a reliable method enabling the large-scale and uniform transfer of 2DMs. The state-of-the-art approaches include dry transfer techniques (i.e., vdW pick-up, PDMS exfoliation, thermoplastic sacrificial layer) and wet transfer techniques (i.e., substrate etching, electrochemical bubbling).[623] Keeping a clean interface on both sides of the flake is the primary aim in the transfer

process. The sacrificial layer used in the dry and wet transfer techniques can act as the carrying layer, but the complete removal of these polymer layer is a great difficulty. The vdW pick-up method by using hBN layers show the advantages of cleanness due to no sacrificial layer in the process. Another important requirement of the transfer process is suitable for industrial applications. In vdW pick-up process, the hBN supporting layer complicates the device fabrication and limit its large-scale applications in industry. From this aspect, wet transfer is favorable for transferring large-scale CVD samples. Therefore, it is important to develop a transfer method to simultaneously fulfill the requirement of the clean surface and large-scale process. And the production tool for the optimized growth and transfer process should be designed and manufactured. In summary, the technology evolution of the 2DM growth/transfer strategy and the development of 2D device performance and functionality will pave the way to deeper integration levels of 2D electronics in Si platforms.

Overall, molecular approaches to engineer 2D electronics by harnessing complexity and multifunctionality offer unprecedented opportunities for CMOS and beyond CMOS applications in the advanced next-generation circuits. The continuous developments of the molecular systems and their functionalization on 2DMs will show their potential in further disruptive electronic technologies.

AUTHOR INFORMATION

Corresponding Author

Paolo Samorì - University of Strasbourg, CNRS, ISIS UMR 7006, 8 allée Gaspard Monge, F-67000 Strasbourg, France; Email: samori@unistra.fr

Authors

Yuda Zhao - University of Strasbourg, CNRS, ISIS UMR 7006, 8 allée Gaspard Monge, F-67000 Strasbourg, France, and School of Micro-Nano Electronics, ZJU-Hangzhou Global Scientific and Technological Innovation Centre, Zhejiang University, 38 Zheda Road, 310027 Hangzhou, People's Republic of China.

Marco Gobbi - Centro de Fisica de Materiales (CSIC-UPV/EHU), Paseo Manuel de Lardizabal, 20018 Donostia-San Sebastian, CIC nanoGUNE, 20018 Donostia-San Sebastian, Spain, and IKERBASQUE, Basque Foundation for Science, 48009 Bilbao, Spain

Luis E. Hueso - CIC nanoGUNE, 20018 Donostia-San Sebastian, Basque Country, Spain and IKERBASQUE, Basque Foundation for Science, 48009 Bilbao, Spain

Notes

The authors declare no competing interests.

Biographies

Yuda Zhao

Dr. Yuda Zhao got his PhD degree from the Hong Kong Polytechnic University in 2016 under the supervision of Prof. Yang Chai. In 2017, he moved to the University of Strasbourg as a postdoctoral fellow in Prof. Paolo Samorì's group. Now he is an assistant professor in Zhejiang University. His research interest focuses on the physical properties of 2D materials, the functionalization of 2D materials by molecular approaches, and electronic devices in the post-Moore era.

Marco Gobbi

Dr. Marco is Research Fellow in the Nanodevices Group in CIC nanoGUNE. Since September 2019, he is La Caixa Junior Leader in CIC nanoGUNE and Ikerbasque Fellow at the Materials Physics Center in San Sebastian. Before taking up his current tenure track position, Dr. Marco Gobbi was a Marie Curie Fellow at the Materials Physics Center, which he joined in 2017 after a 4-year postdoctoral contract at the Institute of Supramolecular Science and Engineering in Strasbourg. His research interests focus on the engineering of physical properties of 2D Materials using molecular functionalization.

Luis E. Hueso

Luis E. Hueso is an Ikerbasque Research Professor, leader of the Nanodevices Group and scientific director of the Unit of Excellence "Maria de Maeztu" at CIC nanoGUNE. He currently acts as an Associate Editor for Journal of Materials Chemistry C, published by the Royal Society of Chemistry. Since his PhD in 2002 he has worked at the University of Cambridge (UK), the Italian National Research Council and the University of Leeds (UK).

His current research interests include organic electronics and spintronic devices, as well as advanced nanofabrication.

He is a Fellow of the Royal Society of Chemistry (FRSC). Other previous recognitions to his research include a Junior Research Fellow at Wolfson College (Cambridge) and a Molecular Science Frontier Professorship by the Institute of Chemistry of the Chinese Academy of Sciences.

Paolo Samorì

Prof. Paolo Samorì is Distinguished Professor at the Université de Strasbourg, Director of the Institut de Science et d'Ingénierie Supramoléculaires (ISIS) and Director of the Nanochemistry Laboratory. He is Fellow of the Royal Society of Chemistry (FRSC), Fellow of the European Academy of Sciences (EURASC), Member of the Academia Europaea, Foreign Member of the

Royal Flemish Academy of Belgium for Science and the Arts (KVAB), Fellow of the University of Strasbourg Institute for Advanced Study (USIAS) and Senior Member of the Institut Universitaire de France (IUF). His research interests include nanochemistry, supramolecular sciences, materials chemistry, and scanning probe microscopies with a specific focus on graphene and other 2D materials as well as functional organic/polymeric and hybrid nanomaterials for application in optoelectronics, energy and sensing. He has been awarded numerous prestigious prizes, including the E-MRS Graduate Student Award (1998), the MRS Graduate Student Award (2000), the IUPAC Prize for Young Chemists (2001), the Vincenzo Caglioti Award (2006), the Nicolò Copernico Award (2009), the Guy Ourisson Prize (2010), the ERC Starting Grant (2010), the CNRS Silver Medal (2012), the Catalán-Sabatier Prize (2017), the Grignard-Wittig Lectureship (2017), the ERC Proof of Concept Grant (2017), the RSC Surfaces and Interfaces Award (2018), the Blaise Pascal Medal in Materials Science (2018), the Pierre Süe Prize (2018), the ERC Advanced Grant (2019), the "Étoiles de l'Europe" Prize (2019), the ERC Proof of Concept Grant (2020), the RSC/SCF Joint Lectureship in Chemical Sciences (2020) and Fellow of the Materials Research Society (2021).

ACKNOWLEDGMENT

The activity in Strasbourg was supported by the EC through the ERC project SUPRA2DMAT (GA-833707) and the Graphene Flagship Core 3 project (GA-881603) as well as the Labex projects CSC (ANR-10LABX-0026 CSC) and NIE (ANR-11-LABX-0058 NIE) within the Investissement d'Avenir program ANR-10-IDEX-0002-02 the International Center for Frontier Research in Chemistry and the Institut Universitaire de France (IUF). The activity in San Sebastian was supported by the Spanish MICINN under the Maria de Maeztu Units of Excellence

Programme (MDM-2016-0618) and under the project No. RTI2018-094861-B-100 and No. PID2019-108153GA-I00. M.G. acknowledges support from la Caixa Foundation (ID 100010434) for a Junior Leader fellowship (Grant No. LCF/BQ/PI19/11690017). Y. Z. acknowledged the support from the National Natural Science Foundation of China (62090034, 62104214).

REFERENCES

(1) Moore, G. E. Cramming more components onto integrated circuits, Reprinted from Electronics, volume 38, number 8, April 19, 1965, pp.114 ff. *IEEE Solid-State Circuits Society Newsletter* **2006,** *11* (3), 33-35.

(2) Barraud, S.; Lapras, V.; Previtali, B.; Samson, M. P.; Lacord, J.; Martinie, S.; Jaud, M. A.; Athanasiou, S.; Triozon, F.; Rozeau, O.et al. 2017 IEEE International Electron Devices Meeting (IEDM), 2017; p 29.22.21-29.22.24.

(3) Rim, K.; Anderson, R.; Boyd, D.; Cardone, F.; Chan, K.; Chen, H.; Christansen, S.; Chu, J.; Jenkins, K.; Kanarsky, T.et al. Strained Si CMOS (SS CMOS) technology: opportunities and challenges. *Solid-State Electron*. **2003,** *47* (7), 1133-1139.

(4) Lee, M. L.; Fitzgerald, E. A.; Bulsara, M. T.; Currie, M. T.; Lochtefeld, A. Strained Si, SiGe, and Ge channels for high-mobility metal-oxide-semiconductor field-effect transistors. *J. Appl. Phys*. **2005,** *97* (1), 011101.

(5) Passlack, M.; Zurcher, P.; Rajagopalan, K.; Droopad, R.; Abrokwah, J.; Tutt, M.; Park, Y.; Johnson, E.; Hartin, O.; Zlotnicka, A.et al. 2007 IEEE International Electron Devices Meeting, 2007; p 621-624.

(6) Akinwande, D.; Huyghebaert, C.; Wang, C.-H.; Serna, M. I.; Goossens, S.; Li, L.-J.; Wong, H. S. P.; Koppens, F. H. L. Graphene and two-dimensional materials for silicon technology. *Nature* **2019,** *573* (7775), 507-518.

(7) Desai, S. B.; Madhvapathy, S. R.; Sachid, A. B.; Llinas, J. P.; Wang, Q.; Ahn, G. H.; Pitner, G.; Kim, M. J.; Bokor, J.; Hu, C.et al. MoS_2 transistors with 1-nanometer gate lengths. *Science* **2016,** *354* (6308), 99-102.

(8) Fiori, G.; Bonaccorso, F.; Iannaccone, G.; Palacios, T.; Neumaier, D.; Seabaugh, A.; Banerjee, S. K.; Colombo, L. Electronics based on two-dimensional materials. *Nat. Nanotechnol*. **2014,** *9*, 768–779.

(9) Radisavljevic, B.; Radenovic, A.; Brivio, J.; Giacometti, V.; Kis, A. Single-layer MoS_2 transistors. *Nat. Nanotechnol*. **2011,** *6* (3), 147-150.

(10) Esseni, D.; Mastrapasqua, M.; Celler, G. K.; Fiegna, C.; Selmi, L.; Sangiorgi, E. Low field electron and hole mobility of SOI transistors fabricated on ultrathin silicon films for deep submicrometer technology application. *IEEE Trans. Electron Devices* **2001,** *48* (12), 2842-2850.

(11) Cao, W.; Kang, J.; Sarkar, D.; Liu, W.; Banerjee, K. 2D Semiconductor FETs—Projections and Design for Sub-10 nm VLSI. *IEEE Trans. Electron Devices* **2015,** *62* (11), 3459-3469.

(12) Zhao, Y.; Xu, K.; Pan, F.; Zhou, C.; Zhou, F.; Chai, Y. Doping, Contact and Interface Engineering of Two-Dimensional Layered Transition Metal Dichalcogenides Transistors.

Adv. Funct. Mater. **2017,** *27* (19), 1603484.
(13) Shen, P.-C.; Su, C.; Lin, Y.; Chou, A.-S.; Cheng, C.-C.; Park, J.-H.; Chiu, M.-H.; Lu, A.-Y.; Tang, H.-L.; Tavakoli, M. M.et al. Ultralow contact resistance between semimetal and monolayer semiconductors. *Nature* **2021,** *593* (7858), 211-217.
(14) Gobbi, M.; Orgiu, E.; Samorì, P. When 2D Materials Meet Molecules: Opportunities and Challenges of Hybrid Organic/Inorganic van der Waals Heterostructures. *Adv. Mater.* **2018,** *30* (18), 1706103.
(15) Jariwala, D.; Marks, T. J.; Hersam, M. C. Mixed-Dimensional van der Waals Heterostructures. *Nat. Mater.* **2016,** *16*, 170-181.
(16) Waldrop, M. M. The chips are down for Moore's law. *Nature* **2016,** *530* (7589), 144-147.
(17) Bousseksou, A.; Molnár, G.; Salmon, L.; Nicolazzi, W. Molecular spin crossover phenomenon: recent achievements and prospects. *Chem. Soc. Rev.* **2011,** *40* (6), 3313-3335.
(18) Szaciłowski, K. Digital Information Processing in Molecular Systems. *Chem. Rev.* **2008,** *108* (9), 3481-3548.
(19) Zhao, Y.; Ippolito, S.; Samorì, P. Functionalization of 2D Materials with Photosensitive Molecules: From Light-Responsive Hybrid Systems to Multifunctional Devices. *Adv. Opt. Mater.* **2019,** *7* (16), 1900286.
(20) Manipatruni, S.; Nikonov, D. E.; Lin, C.-C.; Gosavi, T. A.; Liu, H.; Prasad, B.; Huang, Y.-L.; Bonturim, E.; Ramesh, R.; Young, I. A. Scalable energy-efficient magnetoelectric spin–orbit logic. *Nature* **2019,** *565* (7737), 35-42.
(21) Arute, F.; Arya, K.; Babbush, R.; Bacon, D.; Bardin, J. C.; Barends, R.; Biswas, R.; Boixo, S.; Brandao, F. G. S. L.; Buell, D. A.et al. Quantum supremacy using a programmable superconducting processor. *Nature* **2019,** *574* (7779), 505-510.
(22) de Leon, N. P.; Itoh, K. M.; Kim, D.; Mehta, K. K.; Northup, T. E.; Paik, H.; Palmer, B. S.; Samarth, N.; Sangtawesin, S.; Steuerman, D. W. Materials challenges and opportunities for quantum computing hardware. *Science* **2021,** *372* (6539), eabb2823.
(23) Ahn, E. C. 2D materials for spintronic devices. *npj 2D Mater. Appl.* **2020,** *4* (1), 17-17.
(24) Liu, X.; Hersam, M. C. 2D materials for quantum information science. *Nat. Rev. Mater.* **2019,** *4* (10), 669-684.
(25) Novoselov, K. S.; Geim, A. K.; Morozov, S. V.; Jiang, D.; Zhang, Y.; Dubonos, S. V.; Grigorieva, I. V.; Firsov, A. A. Electric Field Effect in Atomically Thin Carbon Films. *Science* **2004,** *306* (5696), 666-669.
(26) Novoselov, K. S.; Jiang, D.; Schedin, F.; Booth, T. J.; Khotkevich, V. V.; Morozov, S. V.; Geim, A. K. Two-dimensional atomic crystals. *PNAS* **2005,** *102* (30), 10451-10453.
(27) Ferrari, A. C.; Meyer, J. C.; Scardaci, V.; Casiraghi, C.; Lazzeri, M.; Mauri, F.; Piscanec, S.; Jiang, D.; Novoselov, K. S.; Roth, S.et al. Raman Spectrum of Graphene and Graphene Layers. *Phys. Rev. Lett.* **2006,** *97* (18), 187401.
(28) Lee, C.; Wei, X.; Kysar, J. W.; Hone, J. Measurement of the Elastic Properties and Intrinsic Strength of Monolayer Graphene. *Science* **2008,** *321* (5887), 385-388.
(29) Wei, Y.; Yang, R. Nanomechanics of graphene. *Natl. Sci. Rev.* **2018,** *6* (2), 324-348.
(30) Castro Neto, A. H.; Guinea, F.; Peres, N. M. R.; Novoselov, K. S.; Geim, A. K. The electronic properties of graphene. *Rev. Mod. Phys.* **2009,** *81* (1), 109-162.
(31) Novoselov, K. S.; Geim, A. K.; Morozov, S. V.; Jiang, D.; Katsnelson, M. I.; Grigorieva, I. V.; Dubonos, S. V.; Firsov, A. A. Two-dimensional gas of massless Dirac fermions in graphene. *Nature* **2005,** *438* (7065), 197-200.
(32) Schedin, F.; Geim, A. K.; Morozov, S. V.; Hill, E. W.; Blake, P.; Katsnelson, M. I.;

Novoselov, K. S. Detection of individual gas molecules adsorbed on graphene. *Nat. Mater.* **2007,** *6*, 652–655.
(33) Zhang, Y.; Tan, Y.-W.; Stormer, H. L.; Kim, P. Experimental observation of the quantum Hall effect and Berry's phase in graphene. *Nature* **2005,** *438* (7065), 201-204.
(34) Geim, A. K.; Novoselov, K. S. The rise of graphene. *Nat. Mater.* **2007,** *6* (3), 183-191.
(35) Wang, X.; Ouyang, Y.; Li, X.; Wang, H.; Guo, J.; Dai, H. Room-Temperature All-Semiconducting Sub-10-nm Graphene Nanoribbon Field-Effect Transistors. *Phys. Rev. Lett.* **2008,** *100* (20), 206803.
(36) Wang, X.; Dai, H. Etching and narrowing of graphene from the edges. *Nat. Chem.* **2010,** *2* (8), 661-665.
(37) Bonaccorso, F.; Sun, Z.; Hasan, T.; Ferrari, A. C. Graphene photonics and optoelectronics. *Nat. Photonics* **2010,** *4* (9), 611-622.
(38) Liao, L.; Duan, X. Graphene for radio frequency electronics. *Mater. Today* **2012,** *15* (7), 328-338.
(39) Nag, A.; Mitra, A.; Mukhopadhyay, S. C. Graphene and its sensor-based applications: A review. *Sens. Actuator A Phys.* **2018,** *270*, 177-194.
(40) Li, X.; Zhu, H.; Wang, K.; Cao, A.; Wei, J.; Li, C.; Jia, Y.; Li, Z.; Li, X.; Wu, D. Graphene-On-Silicon Schottky Junction Solar Cells. *Adv. Mater.* **2010,** *22* (25), 2743-2748.
(41) Jiang, G.; Tian, H.; Wang, X.-F.; Hirtz, T.; Wu, F.; Qiao, Y.-C.; Gou, G.-Y.; Wei, Y.-H.; Yang, J.-M.; Yang, S.et al. An efficient flexible graphene-based light-emitting device. *Nanoscale Adv.* **2019,** *1* (12), 4745-4754.
(42) Polat, E. O.; Uzlu, H. B.; Balci, O.; Kakenov, N.; Kovalska, E.; Kocabas, C. Graphene-Enabled Optoelectronics on Paper. *ACS Photonics* **2016,** *3* (6), 964-971.
(43) Han, S.-J.; Garcia, A. V.; Oida, S.; Jenkins, K. A.; Haensch, W. Graphene radio frequency receiver integrated circuit. *Nat. Commun.* **2014,** *5* (1), 3086.
(44) Liu, C.-H.; Chang, Y.-C.; Norris, T. B.; Zhong, Z. Graphene photodetectors with ultra-broadband and high responsivity at room temperature. *Nat. Nanotechnol.* **2014,** *9* (4), 273-278.
(45) Anichini, C.; Czepa, W.; Pakulski, D.; Aliprandi, A.; Ciesielski, A.; Samorì, P. Chemical sensing with 2D materials. *Chem. Soc. Rev.* **2018,** *47* (13), 4860-4908.
(46) Chhowalla, M.; Shin, H. S.; Eda, G.; Li, L.-J.; Loh, K. P.; Zhang, H. The chemistry of two-dimensional layered transition metal dichalcogenide nanosheets. *Nat. Chem.* **2013,** *5* (4), 263-275.
(47) Manzeli, S.; Ovchinnikov, D.; Pasquier, D.; Yazyev, O. V.; Kis, A. 2D transition metal dichalcogenides. *Nat. Rev. Mater.* **2017,** *2*, 17033.
(48) Zhao, Y.; Qiao, J.; Yu, P.; Hu, Z.; Lin, Z.; Lau, S. P.; Liu, Z.; Ji, W.; Chai, Y. Extraordinarily Strong Interlayer Interaction in 2D Layered PtS_2. *Adv. Mater.* **2016,** *28* (12), 2399-2407.
(49) Köhler, C. P.; Jakobi, R.; Meissner, E.; Wiehl, L.; Spiering, H.; Gütlich, P. Nature of the phase transition in spin crossover compounds. *J. Phys. Chem. Solids* **1990,** *51* (3), 239-247.
(50) Splendiani, A.; Sun, L.; Zhang, Y.; Li, T.; Kim, J.; Chim, C.-Y.; Galli, G.; Wang, F. Emerging Photoluminescence in Monolayer MoS_2. *Nano Lett.* **2010,** *10* (4), 1271-1275.
(51) Mak, K. F.; Lee, C.; Hone, J.; Shan, J.; Heinz, T. F. Atomically Thin MoS_2: A New Direct-Gap Semiconductor. *Phys. Rev. Lett.* **2010,** *105* (13), 136805.
(52) Mak, K. F.; He, K. L.; Shan, J.; Heinz, T. F. Control of valley polarization in monolayer MoS_2 by optical helicity. *Nat. Nanotechnol.* **2012,** *7* (8), 494-498.
(53) Xiao, D.; Liu, G.-B.; Feng, W.; Xu, X.; Yao, W. Coupled Spin and Valley Physics in

Monolayers of MoS_2 and Other Group-VI Dichalcogenides. *Phys. Rev. Lett.* **2012,** *108* (19), 196802.
(54) Zhao, C.; Norden, T.; Zhang, P.; Zhao, P.; Cheng, Y.; Sun, F.; Parry, J. P.; Taheri, P.; Wang, J.; Yang, Y.et al. Enhanced valley splitting in monolayer WSe_2 due to magnetic exchange field. *Nat. Nanotechnol.* **2017,** *12* (8), 757-762.
(55) Yu, Z.; Ong, Z.-Y.; Pan, Y.; Cui, Y.; Xin, R.; Shi, Y.; Wang, B.; Wu, Y.; Chen, T.; Zhang, Y.-W.et al. Realization of Room-Temperature Phonon-Limited Carrier Transport in Monolayer MoS_2 by Dielectric and Carrier Screening. *Adv. Mater.* **2016,** *28* (3), 547-552.
(56) Fang, H.; Chuang, S.; Chang, T. C.; Takei, K.; Takahashi, T.; Javey, A. High-Performance Single Layered WSe_2 p-FETs with Chemically Doped Contacts. *Nano Lett.* **2012,** *12* (7), 3788-3792.
(57) Avsar, A.; Cheon, C.-Y.; Pizzochero, M.; Tripathi, M.; Ciarrocchi, A.; Yazyev, O. V.; Kis, A. Probing magnetism in atomically thin semiconducting $PtSe_2$. *Nat. Commun.* **2020,** *11* (1), 4806.
(58) Kumar, N.; Guin, S. N.; Manna, K.; Shekhar, C.; Felser, C. Topological Quantum Materials from the Viewpoint of Chemistry. *Chem. Rev.* **2021,** *121* (5), 2780-2815.
(59) Novoselov, K. S.; Mishchenko, A.; Carvalho, A.; Castro Neto, A. H. 2D Materials and van der Waals Heterostructures. *Science* **2016,** *353* (6298), aac9439.
(60) Britnell, L.; Gorbachev, R. V.; Jalil, R.; Belle, B. D.; Schedin, F.; Mishchenko, A.; Georgiou, T.; Katsnelson, M. I.; Eaves, L.; Morozov, S. V.et al. Field-Effect Tunneling Transistor Based on Vertical Graphene Heterostructures. *Science* **2012,** *335* (6071), 947-950.
(61) Georgiou, T.; Jalil, R.; Belle, B. D.; Britnell, L.; Gorbachev, R. V.; Morozov, S. V.; Kim, Y.-J.; Gholinia, A.; Haigh, S. J.; Makarovsky, O.et al. Vertical field-effect transistor based on graphene–WS_2 heterostructures for flexible and transparent electronics. *Nat. Nanotechnol.* **2013,** *8* (2), 100-103.
(62) Frisenda, R.; Molina-Mendoza, A. J.; Mueller, T.; Castellanos-Gomez, A.; van der Zant, H. S. J. Atomically thin p–n junctions based on two-dimensional materials. *Chem. Soc. Rev.* **2018,** *47* (9), 3339-3358.
(63) Li, L. K.; Yu, Y. J.; Ye, G. J.; Ge, Q. Q.; Ou, X. D.; Wu, H.; Feng, D. L.; Chen, X. H.; Zhang, Y. B. Black Phosphorus Field-Effect Transistors. *Nat. Nanotechnol.* **2014,** *9* (5), 372-377.
(64) Qiao, J.; Kong, X.; Hu, Z.-X.; Yang, F.; Ji, W. High-mobility transport anisotropy and linear dichroism in few-layer black phosphorus. *Nat. Commun.* **2014,** *5*, 4475.
(65) Perello, D. J.; Chae, S. H.; Song, S.; Lee, Y. H. High-Performance n-Type Black Phosphorus Transistors with Type Control *via* Thickness and Contact-Metal Engineering. *Nat. Commun.* **2015,** *6*, 7809.
(66) Ling, X.; Wang, H.; Huang, S.; Xia, F.; Dresselhaus, M. S. The renaissance of black phosphorus. *PNAS* **2015,** *112* (15), 4523-4530.
(67) Huang, Y.; Qiao, J.; He, K.; Bliznakov, S.; Sutter, E.; Chen, X.; Luo, D.; Meng, F.; Su, D.; Decker, J.et al. Interaction of Black Phosphorus with Oxygen and Water. *Chem. Mater.* **2016,** *28* (22), 8330-8339.
(68) Wood, J. D.; Wells, S. A.; Jariwala, D.; Chen, K.-S.; Cho, E.; Sangwan, V. K.; Liu, X.; Lauhon, L. J.; Marks, T. J.; Hersam, M. C. Effective Passivation of Exfoliated Black Phosphorus Transistors against Ambient Degradation. *Nano Lett.* **2014,** *14* (12), 6964-6970.
(69) Zhu, X.; Zhang, T.; Jiang, D.; Duan, H.; Sun, Z.; Zhang, M.; Jin, H.; Guan, R.; Liu, Y.; Chen, M.et al. Stabilizing black phosphorus nanosheets via edge-selective bonding of

sacrificial C_{60} molecules. *Nat. Commun.* **2018,** *9* (1), 4177.
(70) Tao, L.; Cinquanta, E.; Chiappe, D.; Grazianetti, C.; Fanciulli, M.; Dubey, M.; Molle, A.; Akinwande, D. Silicene field-effect transistors operating at room temperature. *Nat. Nanotechnol.* **2015,** *10* (3), 227-231.
(71) Molle, A.; Grazianetti, C.; Tao, L.; Taneja, D.; Alam, M. H.; Akinwande, D. Silicene, silicene derivatives, and their device applications. *Chem. Soc. Rev.* **2018,** *47* (16), 6370-6387.
(72) Xu, Y.; Shi, Z.; Shi, X.; Zhang, K.; Zhang, H. Recent progress in black phosphorus and black-phosphorus-analogue materials: properties, synthesis and applications. *Nanoscale* **2019,** *11* (31), 14491-14527.
(73) Khan, K.; Tareen, A. K.; Aslam, M.; Wang, R.; Zhang, Y.; Mahmood, A.; Ouyang, Z.; Zhang, H.; Guo, Z. Recent developments in emerging two-dimensional materials and their applications. *J. Mater. Chem. C* **2020,** *8* (2), 387-440.
(74) Haynes, K.; Murray, R.; Weinrich, Z.; Zhao, X.; Chiappe, D.; Sutar, S.; Radu, I.; Hatem, C.; Perry, S. S.; Jones, K. S. Modulating the resistivity of MoS2 through low energy phosphorus plasma implantation. *Appl. Phys. Lett.* **2017,** *110* (26), 262102.
(75) Murray, R.; Haynes, K.; Zhao, X. Y.; Perry, S.; Hatem, C.; Jones, K. The Effect of Low Energy Ion Implantation on MoS_2. *ECS J. Solid State Sci. Technol.* **2016,** *5* (11), Q3050-Q3053.
(76) Nipane, A.; Karmakar, D.; Kaushik, N.; Karande, S.; Lodha, S. Few-Layer MoS2 p-Type Devices Enabled by Selective Doping Using Low Energy Phosphorus Implantation. *ACS Nano* **2016,** *10* (2), 2128-2137.
(77) Pham, V. P.; Yeom, G. Y. Recent Advances in Doping of Molybdenum Disulfide: Industrial Applications and Future Prospects. *Adv. Mater.* **2016,** *28* (41), 9024-9059.
(78) Zhao, Y. D.; Xu, K.; Pan, F.; Zhou, C. J.; Zhou, F. C.; Chai, Y. Doping, Contact and Interface Engineering of Two-Dimensional Layered Transition Metal Dichalcogenides Transistors. *Adv. Funct. Mater.* **2017,** *27* (19), 1603484.
(79) Zhang, M.; Wu, J. X.; Zhu, Y. M.; Dumcenco, D. O.; Hong, J. H.; Mao, N. N.; Deng, S. B.; Chen, Y. F.; Yang, Y. L.; Jin, C. H.et al. Two-Dimensional Molybdenum Tungsten Diselenide Alloys: Photoluminescence, Raman Scattering, and Electrical Transport. *ACS Nano* **2014,** *8* (7), 7130-7137.
(80) Tedstone, A. A.; Lewis, D. J.; O'Brien, P. Synthesis, Properties, and Applications of Transition Metal-Doped Layered Transition Metal Dichalcogenides. *Chem. Mater.* **2016,** *28* (7), 1965-1974.
(81) Gao, J.; Kim, Y. D.; Liang, L.; Idrobo, J. C.; Chow, P.; Tan, J.; Li, B.; Li, L.; Sumpter, B. G.; Lu, T.-M.et al. Transition-Metal Substitution Doping in Synthetic Atomically Thin Semiconductors. *Adv. Mater.* **2016,** *28* (44), 9735-9743.
(82) Suh, J.; Park, T.-E.; Lin, D.-Y.; Fu, D.; Park, J.; Jung, H. J.; Chen, Y.; Ko, C.; Jang, C.; Sun, Y.et al. Doping against the Native Propensity of MoS_2: Degenerate Hole Doping by Cation Substitution. *Nano Lett.* **2014,** *14* (12), 6976-6982.
(83) Tsai, Y. C.; Li, Y. Impact of Doping Concentration on Electronic Properties of Transition Metal-Doped Monolayer Molybdenum Disulfide. *IEEE Trans. Electron Devices* **2018,** *65* (2), 733-738.
(84) Liang, X.; Nam, H.; Wi, S.; Chen, M. 25th Annual SEMI Advanced Semiconductor Manufacturing Conference (ASMC 2014), 2014; p 365-369.
(85) Komsa, H.-P.; Kotakoski, J.; Kurasch, S.; Lehtinen, O.; Kaiser, U.; Krasheninnikov, A. V.

Two-Dimensional Transition Metal Dichalcogenides under Electron Irradiation: Defect Production and Doping. *Phys. Rev. Lett.* **2012,** *109* (3), 035503.
(86) Lin, Z.; Carvalho, B. R.; Kahn, E.; Lv, R.; Rao, R.; Terrones, H.; Pimenta, M. A.; Terrones, M. Defect engineering of two-dimensional transition metal dichalcogenides. *2D Mater.* **2016,** *3* (2), 022002.
(87) Schmidt, H.; Giustiniano, F.; Eda, G. Electronic transport properties of transition metal dichalcogenide field-effect devices: Surface and interface effects. *Chem. Soc. Rev.* **2015,** *44* (21), 7715-7736.
(88) Zhou, J.; Lin, Z.; Ren, H.; Duan, X.; Shakir, I.; Huang, Y.; Duan, X. Layered Intercalation Materials. *Adv. Mater.* **2021,** *33* (25), 2004557.
(89) Wang, H. T.; Yuan, H. T.; Hong, S. S.; Li, Y. B.; Cui, Y. Physical and chemical tuning of two-dimensional transition metal dichalcogenides. *Chem. Soc. Rev.* **2015,** *44* (9), 2664-2680.
(90) Duong, D. L.; Yun, S. J.; Lee, Y. H. van der Waals Layered Materials: Opportunities and Challenges. *ACS Nano* **2017,** *11* (12), 11803-11830.
(91) Raymo, F. M. Digital Processing and Communication with Molecular Switches. *Adv. Mater.* **2002,** *14* (6), 401-414.
(92) Mouri, S.; Miyauchi, Y.; Matsuda, K. Tunable Photoluminescence of Monolayer MoS_2 via Chemical Doping. *Nano Lett.* **2013,** *13* (12), 5944-5948.
(93) Kiriya, D.; Tosun, M.; Zhao, P.; Kang, J. S.; Javey, A. Air-Stable Surface Charge Transfer Doping of MoS_2 by Benzyl Viologen. *J. Am. Chem. Soc.* **2014,** *136* (22), 7853-7856.
(94) Sim, D. M.; Kim, M.; Yim, S.; Choi, M.-J.; Choi, J.; Yoo, S.; Jung, Y. S. Controlled Doping of Vacancy-Containing Few-Layer MoS_2 via Highly Stable Thiol-Based Molecular Chemisorption. *ACS Nano* **2015,** *9* (12), 12115-12123.
(95) Du, Y. C.; Liu, H.; Neal, A. T.; Si, M. W.; Ye, P. D. Molecular Doping of Multilayer MoS_2 Field-Effect Transistors: Reduction in Sheet and Contact Resistances. *IEEE Electron Device Lett.* **2013,** *34* (10), 1328-1330.
(96) Lee, I.; Rathi, S.; Li, L.; Lim, D.; Khan, M. A.; Kannan, E. S.; Kim, G.-H. Non-degenerate n-type doping by hydrazine treatment in metal work function engineered WSe_2 field-effect transistor. *Nanotechnology* **2015,** *26* (45), 455203.
(97) Peimyoo, N.; Yang, W. H.; Shang, J. Z.; Shen, X. N.; Wang, Y. L.; Yu, T. Chemically Driven Tunable Light Emission of Charged and Neutral Excitons in Mono layer WS_2. *ACS Nano* **2014,** *8* (11), 11320-11329.
(98) Yu, L.; Zubair, A.; Santos, E. J. G.; Zhang, X.; Lin, Y.; Zhang, Y.; Palacios, T. High-Performance WSe_2 Complementary Metal Oxide Semiconductor Technology and Integrated Circuits. *Nano Lett.* **2015,** *15* (8), 4928-4934.
(99) Song, Z.; Schultz, T.; Ding, Z.; Lei, B.; Han, C.; Amsalem, P.; Lin, T.; Chi, D.; Wong, S. L.; Zheng, Y. J.et al. Electronic Properties of a 1D Intrinsic/p-Doped Heterojunction in a 2D Transition Metal Dichalcogenide Semiconductor. *ACS Nano* **2017,** *11* (9), 9128-9135.
(100) Choi, J.; Zhang, H.; Choi, J. H. Modulating Optoelectronic Properties of Two-Dimensional Transition Metal Dichalcogenide Semiconductors by Photoinduced Charge Transfer. *ACS Nano* **2016,** *10* (1), 1671-1680.
(101) Zhang, S. N.; Benjamin, C. J.; Chen, Z. 2017 75th Annual Device Research Conference (DRC), South Bend, IN, USA, 2017; p 1-2.
(102) Khan, Y.; Obaidulla, S. M.; Rezwan Habib, M.; Kong, Y.; Xu, M. Anomalous photoluminescence quenching in DIP/MoS_2 van der Waals heterostructure: Strong charge

transfer and a modified interface. *Appl. Surf. Sci.* **2020,** *530*, 147213.
(103) Amsterdam, S. H.; Marks, T. J.; Hersam, M. C. Leveraging Molecular Properties to Tailor Mixed-Dimensional Heterostructures beyond Energy Level Alignment. *J. Phys. Chem. Lett.* **2021,** *12* (19), 4543-4557.
(104) Li, Y.; Xu, C.-Y.; Hu, P.; Zhen, L. Carrier Control of MoS_2 Nanoflakes by Functional Self-Assembled Monolayers. *ACS Nano* **2013,** *7* (9), 7795-7804.
(105) Kang, D.-H.; Shim, J.; Jang, S. K.; Jeon, J.; Jeon, M. H.; Yeom, G. Y.; Jung, W.-S.; Jang, Y. H.; Lee, S.; Park, J.-H. Controllable Nondegenerate p-Type Doping of Tungsten Diselenide by Octadecyltrichlorosilane. *ACS Nano* **2015,** *9* (2), 1099-1107.
(106) Gobbi, M.; Bonacchi, S.; Lian, J. X.; Liu, Y.; Wang, X.-Y.; Stoeckel, M.-A.; Squillaci, M. A.; D'Avino, G.; Narita, A.; Müllen, K.et al. Periodic potentials in hybrid van der Waals heterostructures formed by supramolecular lattices on graphene. *Nat. Commun.* **2017,** *8*, 14767.
(107) Wang, Y.; Gali, S. M.; Slassi, A.; Beljonne, D.; Samorì, P. Collective Dipole-Dominated Doping of Monolayer MoS_2: Orientation and Magnitude Control via the Supramolecular Approach. *Adv. Funct. Mater.* **2020,** *30* (36), 2002846.
(108) Yu, Z.; Pan, Y.; Shen, Y.; Wang, Z.; Ong, Z.-Y.; Xu, T.; Xin, R.; Pan, L.; Wang, B.; Sun, L.et al. Towards intrinsic charge transport in monolayer molybdenum disulfide by defect and interface engineering. *Nat. Commun.* **2014,** *5*, 5290.
(109) Bertolazzi, S.; Bonacchi, S.; Nan, G.; Pershin, A.; Beljonne, D.; Samorì, P. Engineering Chemically Active Defects in Monolayer MoS_2 Transistors via Ion-Beam Irradiation and Their Healing via Vapor Deposition of Alkanethiols. *Adv. Mater.* **2017,** *29* (18), 1606760.
(110) Amani, M.; Lien, D.-H.; Kiriya, D.; Xiao, J.; Azcatl, A.; Noh, J.; Madhvapathy, S. R.; Addou, R.; KC, S.; Dubey, M.et al. Near-unity photoluminescence quantum yield in MoS_2. *Science* **2015,** *350* (6264), 1065-1068.
(111) Zhao, Y.; Gali, S. M.; Wang, C.; Pershin, A.; Slassi, A.; Beljonne, D.; Samorì, P. Molecular Functionalization of Chemically Active Defects in WSe_2 for Enhanced Opto-Electronics. *Adv. Funct. Mater.* **2020,** *30* (45), 2005045.
(112) Vera-Hidalgo, M.; Giovanelli, E.; Navío, C.; Pérez, E. M. Mild Covalent Functionalization of Transition Metal Dichalcogenides with Maleimides: A "Click" Reaction for 2H-MoS_2 and WS_2. *J. Am. Chem. Soc.* **2019,** *141* (9), 3767-3771.
(113) Quirós-Ovies, R.; Vázquez Sulleiro, M.; Vera-Hidalgo, M.; Prieto, J.; Gómez, I. J.; Sebastián, V.; Santamaría, J.; Pérez, E. M. Controlled Covalent Functionalization of 2 H-MoS_2 with Molecular or Polymeric Adlayers. *Chem. Eur. J.* **2020,** *26* (29), 6629-6634.
(114) Roh, J.; Cho, I.-T.; Shin, H.; Woo Baek, G.; Hee Hong, B.; Lee, J.-H.; Hun Jin, S.; Lee, C. Fluorinated CYTOP passivation effects on the electrical reliability of multilayer MoS_2 field-effect transistors. *Nanotechnology* **2015,** *26* (45), 455201.
(115) Zhao, Y.; Bertolazzi, S.; Samorì, P. A Universal Approach toward Light-Responsive Two-Dimensional Electronics: Chemically Tailored Hybrid van der Waals Heterostructures. *ACS Nano* **2019,** *13* (4), 4814-4825.
(116) Bao, W.; Cai, X.; Kim, D.; Sridhara, K.; Fuhrer, M. S. High mobility ambipolar MoS_2 field-effect transistors: Substrate and dielectric effects. *Appl. Phys. Lett.* **2013,** *102* (4), 042104.
(117) Ma, J.; Choi, K.-Y.; Kim, S. H.; Lee, H.; Yoo, G. All polymer encapsulated, highly-sensitive MoS_2 phototransistors on flexible PAR substrate. *Appl. Phys. Lett.* **2018,** *113* (1), 013102.
(118) Zhang, X.; Liao, Q.; Liu, S.; Kang, Z.; Zhang, Z.; Du, J.; Li, F.; Zhang, S.; Xiao, J.; Liu,

B.et al. Poly(4-styrenesulfonate)-induced sulfur vacancy self-healing strategy for monolayer MoS_2 homojunction photodiode. *Nat. Commun.* **2017,** *8* (1), 15881.
(119) Pagaduan, J. N.; Hight-Huf, N.; Datar, A.; Nagar, Y.; Barnes, M.; Naveh, D.; Ramasubramaniam, A.; Katsumata, R.; Emrick, T. Electronic Tuning of Monolayer Graphene with Polymeric "Zwitterists". *ACS Nano* **2021,** *15* (2), 2762-2770.
(120) Lovinger, A. J. Ferroelectric Polymers. *Science* **1983,** *220* (4602), 1115-1121.
(121) Chen, X.; Han, X.; Shen, Q.-D. PVDF-Based Ferroelectric Polymers in Modern Flexible Electronics. *Adv. Electron. Mater.* **2017,** *3* (5), 1600460.
(122) Lee, Y. T.; Kwon, H.; Kim, J. S.; Kim, H.-H.; Lee, Y. J.; Lim, J. A.; Song, Y.-W.; Yi, Y.; Choi, W.-K.; Hwang, D. K.et al. Nonvolatile Ferroelectric Memory Circuit Using Black Phosphorus Nanosheet-Based Field-Effect Transistors with P(VDF-TrFE) Polymer. *ACS Nano* **2015,** *9* (10), 10394-10401.
(123) Zheng, Y.; Ni, G.-X.; Toh, C.-T.; Tan, C.-Y.; Yao, K.; Özyilmaz, B. Graphene Field-Effect Transistors with Ferroelectric Gating. *Phys. Rev. Lett.* **2010,** *105* (16), 166602.
(124) Kobayashi, T.; Hori, N.; Nakajima, T.; Kawae, T. Electrical characteristics of MoS_2 field-effect transistor with ferroelectric vinylidene fluoride-trifluoroethylene copolymer gate structure. *Appl. Phys. Lett.* **2016,** *108* (13), 132903.
(125) Ryu, H.; Xu, K.; Li, D.; Hong, X.; Zhu, W. Empowering 2D nanoelectronics via ferroelectricity. *Appl. Phys. Lett.* **2020,** *117* (8), 080503.
(126) Bouas-Laurent, H.; Dürr, H. Organic photochromism (IUPAC Technical Report). *Pure Appl. Chem.* **2001,** *73* (4), 639-665.
(127) Bandara, H. M. D.; Burdette, S. C. Photoisomerization in Different Classes of Azobenzene. *Chem. Soc. Rev.* **2012,** *41* (5), 1809-1825.
(128) Irie, M.; Fukaminato, T.; Matsuda, K.; Kobatake, S. Photochromism of Diarylethene Molecules and Crystals: Memories, Switches, and Actuators. *Chem. Rev.* **2014,** *114* (24), 12174-12277.
(129) Klajn, R. Spiropyran-Based Dynamic Materials. *Chem. Soc. Rev.* **2014,** *43* (1), 148-184.
(130) Crespi, S.; Simeth, N. A.; König, B. Heteroaryl azo dyes as molecular photoswitches. *Nat. Rev. Chem.* **2019,** *3* (3), 133-146.
(131) Beharry, A. A.; Woolley, G. A. Azobenzene photoswitches for biomolecules. *Chem. Soc. Rev.* **2011,** *40* (8), 4422-4437.
(132) Huang, X.; Li, T. Recent progress in the development of molecular-scale electronics based on photoswitchable molecules. *J. Mater. Chem. C* **2020,** *8* (3), 821-848.
(133) Fuß, W.; Kosmidis, C.; Schmid, W. E.; Trushin, S. A. The Photochemical cis–trans Isomerization of Free Stilbene Molecules Follows a Hula-Twist Pathway. *Angew. Chem., Int. Ed.* **2004,** *43* (32), 4178-4182.
(134) Chen, Y.; Wang, C.; Fan, M.; Yao, B.; Menke, N. Photochromic fulgide for holographic recording. *Opt. Mater* **2004,** *26* (1), 75-77.
(135) Cvrtila, I.; Fanlo-Virgós, H.; Schaeffer, G.; Monreal Santiago, G.; Otto, S. Redox Control over Acyl Hydrazone Photoswitches. *J. Am. Chem. Soc.* **2017,** *139* (36), 12459-12465.
(136) Głowacki, E. D.; Voss, G.; Sariciftci, N. S. 25th Anniversary Article: Progress in Chemistry and Applications of Functional Indigos for Organic Electronics. *Adv. Mater.* **2013,** *25* (47), 6783-6800.
(137) Tamai, N.; Miyasaka, H. Ultrafast Dynamics of Photochromic Systems. *Chem. Rev.* **2000,** *100* (5), 1875-1890.
(138) Siewertsen, R.; Neumann, H.; Buchheim-Stehn, B.; Herges, R.; Näther, C.; Renth, F.;

Temps, F. Highly Efficient Reversible Z–E Photoisomerization of a Bridged Azobenzene with Visible Light through Resolved S1(nπ*) Absorption Bands. *J. Am. Chem. Soc.* **2009,** *131* (43), 15594-15595.

(139) Tsuji, T.; Takashima, H.; Takeuchi, H.; Egawa, T.; Konaka, S. Molecular Structure and Torsional Potential of trans-Azobenzene. A Gas Electron Diffraction Study. *J. Phys. Chem. A* **2001,** *105* (41), 9347-9353.

(140) Fliegl, H.; Köhn, A.; Hättig, C.; Ahlrichs, R. Ab Initio Calculation of the Vibrational and Electronic Spectra of trans- and cis-Azobenzene. *J. Am. Chem. Soc.* **2003,** *125* (32), 9821-9827.

(141) Kobatake, S.; Takami, S.; Muto, H.; Ishikawa, T.; Irie, M. Rapid and reversible shape changes of molecular crystals on photoirradiation. *Nature* **2007,** *446* (7137), 778-781.

(142) Wang, L.; Li, Q. Photochromism into nanosystems: towards lighting up the future nanoworld. *Chem. Soc. Rev.* **2018,** *47* (3), 1044-1097.

(143) Ah Qune, L. F. N.; Akiyama, H.; Nagahiro, T.; Tamada, K.; Wee, A. T. S. Reversible work function changes induced by photoisomerization of asymmetric azobenzene dithiol self-assembled monolayers on gold. *Appl. Phys. Lett.* **2008,** *93* (8), 83109-83109.

(144) Crivillers, N.; Liscio, A.; Di Stasio, F.; Van Dyck, C.; Osella, S.; Cornil, D.; Mian, S.; Lazzerini, G. M.; Fenwick, O.; Orgiu, E.et al. Photoinduced work function changes by isomerization of a densely packed azobenzene-based SAM on Au: a joint experimental and theoretical study. *Phys. Chem. Chem. Phys.* **2011,** *13* (32), 14302-14310.

(145) Masillamani, A. M.; Osella, S.; Liscio, A.; Fenwick, O.; Reinders, F.; Mayor, M.; Palermo, V.; Cornil, J.; Samorì, P. Light-induced reversible modification of the work function of a new perfluorinated biphenyl azobenzene chemisorbed on Au (111). *Nanoscale* **2014,** *6* (15), 8969-8977.

(146) Irie, M. Diarylethenes for memories and switches. *Chem. Rev.* **2000,** *100* (5), 1685-1716.

(147) Herder, M.; Eisenreich, F.; Bonasera, A.; Grafl, A.; Grubert, L.; Pätzel, M.; Schwarz, J.; Hecht, S. Light-Controlled Reversible Modulation of Frontier Molecular Orbital Energy Levels in Trifluoromethylated Diarylethenes. *Chemistry* **2017,** *23* (15), 3743-3754.

(148) Moriyama, Y.; Matsuda, K.; Tanifuji, N.; Irie, S.; Irie, M. Electrochemical Cyclization/Cycloreversion Reactions of Diarylethenes. *Org. Lett.* **2005,** *7* (15), 3315-3318.

(149) Takami, S.; Kobatake, S.; Kawai, T.; Irie, M. Extraordinarily High Thermal Stability of the Closed-ring Isomer of 1,2-Bis(5-methyl-2-phenylthiazol-4-yl)perfluorocyclopentene. *Chem. Lett.* **2003,** *32* (10), 892-893.

(150) Ward, C. L.; Elles, C. G. Controlling the Excited-State Reaction Dynamics of a Photochromic Molecular Switch with Sequential Two-Photon Excitation. *J. Phys. Chem. Lett.* **2012,** *3* (20), 2995-3000.

(151) Irie, M.; Lifka, T.; Uchida, K.; Kobatake, S.; Shindo, Y. Fatigue resistant properties of photochromic dithienylethenes: by-product formation. *Chem. Commun.* **1999,** (8), 747-750.

(152) Herder, M.; Schmidt, B. M.; Grubert, L.; Pätzel, M.; Schwarz, J.; Hecht, S. Improving the Fatigue Resistance of Diarylethene Switches. *J. Am. Chem. Soc.* **2015,** *137* (7), 2738-2747.

(153) Miller, R. J. D. Femtosecond Crystallography with Ultrabright Electrons and X-rays: Capturing Chemistry in Action. *Science* **2014,** *343* (6175), 1108-1116.

(154) Hou, L.; Zhang, X.; Cotella, G. F.; Carnicella, G.; Herder, M.; Schmidt, B. M.; Pätzel, M.; Hecht, S.; Cacialli, F.; Samorì, P. Optically switchable organic light-emitting transistors. *Nat. Nanotechnol.* **2019,** *14* (4), 347-353.

(155) Orgiu, E.; Crivillers, N.; Herder, M.; Grubert, L.; Pätzel, M.; Frisch, J.; Pavlica, E.; Duong,

D. T.; Bratina, G.; Salleo, A.et al. Optically switchable transistor via energy-level phototuning in a bicomponent organic semiconductor. *Nat. Chem.* **2012,** *4*, 675-679.
(156) Leydecker, T.; Herder, M.; Pavlica, E.; Bratina, G.; Hecht, S.; Orgiu, E.; Samorì, P. Flexible non-volatile optical memory thin-film transistor device with over 256 distinct levels based on an organic bicomponent blend. *Nat. Nanotechnol.* **2016,** *11* (9), 769-775.
(157) Gruler, H.; Vilanove, R.; Rondelez, F. Reversible Photochemical Strain in Langmuir Monolayers. *Phys. Rev. Lett.* **1980,** *44* (9), 590-592.
(158) Baillet, G.; Giusti, G.; Guglielmetti, R. Comparative photodegradation study between spiro[indoline—oxazine] and spiro[indoline—pyran] derivatives in solution. *J. Photochem. Photobiol. A Chem.* **1993,** *70* (2), 157-161.
(159) Tsuruoka, T.; Hayakawa, R.; Kobashi, K.; Higashiguchi, K.; Matsuda, K.; Wakayama, Y. Laser Patterning of Optically Reconfigurable Transistor Channels in a Photochromic Diarylethene Layer. *Nano Lett.* **2016,** *16* (12), 7474-7480.
(160) Hnid, I.; Frath, D.; Lafolet, F.; Sun, X.; Lacroix, J.-C. Highly Efficient Photoswitch in Diarylethene-Based Molecular Junctions. *J. Am. Chem. Soc.* **2020,** *142* (17), 7732-7736.
(161) Meng, L.; Xin, N.; Hu, C.; Wang, J.; Gui, B.; Shi, J.; Wang, C.; Shen, C.; Zhang, G.; Guo, H.et al. Side-group chemical gating via reversible optical and electric control in a single molecule transistor. *Nat. Commun.* **2019,** *10* (1), 1450-1450.
(162) Ferri, V.; Elbing, M.; Pace, G.; Dickey, M. D.; Zharnikov, M.; Samorì, P.; Mayor, M.; Rampi, M. A. Light-Powered Electrical Switch Based on Cargo-Lifting Azobenzene Monolayers. *Angew. Chem., Int. Ed.* **2008,** *47* (18), 3407-3409.
(163) Mativetsky, J. M.; Pace, G.; Elbing, M.; Rampi, M. A.; Mayor, M.; Samorì, P. Azobenzenes as light-controlled molecular electronic switches in nanoscale metal-molecule-metal junctions. *J. Am. Chem. Soc.* **2008,** *130* (29), 9192-9193.
(164) Kronemeijer, A. J.; Akkerman, H. B.; Kudernac, T.; van Wees, B. J.; Feringa, B. L.; Blom, P. W. M.; de Boer, B. Reversible Conductance Switching in Molecular Devices. *Adv. Mater.* **2008,** *20* (8), 1467-1473.
(165) Smaali, K.; Lenfant, S.; Karpe, S.; Oçafrain, M.; Blanchard, P.; Deresmes, D.; Godey, S.; Rochefort, A.; Roncali, J.; Vuillaume, D. High On–Off Conductance Switching Ratio in Optically-Driven Self-Assembled Conjugated Molecular Systems. *ACS Nano* **2010,** *4* (4), 2411-2421.
(166) Kim, D.; Jeong, H.; Hwang, W.-T.; Jang, Y.; Sysoiev, D.; Scheer, E.; Huhn, T.; Min, M.; Lee, H.; Lee, T. Reversible Switching Phenomenon in Diarylethene Molecular Devices with Reduced Graphene Oxide Electrodes on Flexible Substrates. *Adv. Funct. Mater.* **2015,** *25* (37), 5918-5923.
(167) Kumar, S.; van Herpt, J. T.; Gengler, R. Y. N.; Feringa, B. L.; Rudolf, P.; Chiechi, R. C. Mixed Monolayers of Spiropyrans Maximize Tunneling Conductance Switching by Photoisomerization at the Molecule–Electrode Interface in EGaIn Junctions. *J. Am. Chem. Soc.* **2016,** *138* (38), 12519-12526.
(168) Yasuda, S.; Nakamura, T.; Matsumoto, M.; Shigekawa, H. Phase Switching of a Single Isomeric Molecule and Associated Characteristic Rectification. *J. Am. Chem. Soc.* **2003,** *125* (52), 16430-16433.
(169) Katsonis, N.; Kudernac, T.; Walko, M.; van der Molen, S. J.; van Wees, B. J.; Feringa, B. L. Reversible Conductance Switching of Single Diarylethenes on a Gold Surface. *Adv. Mater.* **2006,** *18* (11), 1397-1400.
(170) Dulić, D.; van der Molen, S. J.; Kudernac, T.; Jonkman, H. T.; de Jong, J. J. D.; Bowden,

T. N.; van Esch, J.; Feringa, B. L.; van Wees, B. J. One-Way Optoelectronic Switching of Photochromic Molecules on Gold. *Phys. Rev. Lett.* **2003,** *91* (20), 207402.
(171) Kim, Y.; Hellmuth, T. J.; Sysoiev, D.; Pauly, F.; Pietsch, T.; Wolf, J.; Erbe, A.; Huhn, T.; Groth, U.; Steiner, U. E.et al. Charge Transport Characteristics of Diarylethene Photoswitching Single-Molecule Junctions. *Nano Lett.* **2012,** *12* (7), 3736-3742.
(172) Jia, C.; Migliore, A.; Xin, N.; Huang, S.; Wang, J.; Yang, Q.; Wang, S.; Chen, H.; Wang, D.; Feng, B.et al. Covalently bonded single-molecule junctions with stable and reversible photoswitched conductivity. *Science* **2016,** *352* (6292), 1443-1445.
(173) Jia, C.; Wang, J.; Yao, C.; Cao, Y.; Zhong, Y.; Liu, Z.; Liu, Z.; Guo, X. Conductance Switching and Mechanisms in Single-Molecule Junctions. *Angew. Chem., Int. Ed.* **2013,** *52* (33), 8666-8670.
(174) Whalley, A. C.; Steigerwald, M. L.; Guo, X.; Nuckolls, C. Reversible Switching in Molecular Electronic Devices. *J. Am. Chem. Soc.* **2007,** *129* (42), 12590-12591.
(175) Kim, Y. Photoswitching Molecular Junctions: Platforms and Electrical Properties. *ChemPhysChem* **2020,** *21* (21), 2368-2383.
(176) Zhang, H.; Guo, X.; Hui, J.; Hu, S.; Xu, W.; Zhu, D. Interface Engineering of Semiconductor/Dielectric Heterojunctions toward Functional Organic Thin-Film Transistors. *Nano Lett.* **2011,** *11* (11), 4939-4946.
(177) Orgiu, E.; Samorì, P. 25th Anniversary Article: Organic Electronics Marries Photochromism: Generation of Multifunctional Interfaces, Materials, and Devices. *Adv. Mater.* **2014,** *26* (12), 1827-1845.
(178) Gemayel, M. E.; Börjesson, K.; Herder, M.; Duong, D. T.; Hutchison, J. A.; Ruzié, C.; Schweicher, G.; Salleo, A.; Geerts, Y.; Hecht, S.et al. Optically switchable transistors by simple incorporation of photochromic systems into small-molecule semiconducting matrices. *Nat. Commun.* **2015,** *6* (1), 6330-6330.
(179) Carroli, M.; Dixon, A. G.; Herder, M.; Pavlica, E.; Hecht, S.; Bratina, G.; Orgiu, E.; Samorì, P. Multiresponsive Nonvolatile Memories Based on Optically Switchable Ferroelectric Organic Field-Effect Transistors. *Adv. Mater.* **2021,** *33* (14), 2007965.
(180) Alemani, M.; Peters, M. V.; Hecht, S.; Rieder, K.-H.; Moresco, F.; Grill, L. Electric Field-Induced Isomerization of Azobenzene by STM. *J. Am. Chem. Soc.* **2006,** *128* (45), 14446-14447.
(181) Comstock, M. J.; Levy, N.; Kirakosian, A.; Cho, J.; Lauterwasser, F.; Harvey, J. H.; Strubbe, D. A.; Fréchet, J. M. J.; Trauner, D.; Louie, S. G.et al. Reversible Photomechanical Switching of Individual Engineered Molecules at a Metallic Surface. *Phys. Rev. Lett.* **2007,** *99* (3), 38301-38301.
(182) Pace, G.; Ferri, V.; Grave, C.; Elbing, M.; von Hänisch, C.; Zharnikov, M.; Mayor, M.; Rampi, M. A.; Samorì, P. Cooperative light-induced molecular movements of highly ordered azobenzene self-assembled monolayers. *PNAS* **2007,** *104* (24), 9937-9942.
(183) Piantek, M.; Schulze, G.; Koch, M.; Franke, K. J.; Leyssner, F.; Krüger, A.; Navío, C.; Miguel, J.; Bernien, M.; Wolf, M.et al. Reversing the thermal stability of a molecular switch on a gold surface: ring-opening reaction of nitrospiropyran. *J. Am. Chem. Soc.* **2009,** *131* (35), 12729-12735.
(184) Schulze, G.; Franke, K. J.; Pascual, J. I. Induction of a photostationary ring-opening-ring-closing state of spiropyran monolayers on the semimetallic Bi(110) surface. *Phys. Rev. Lett.* **2012,** *109* (2), 026102.
(185) Shimizu, T. K.; Jung, J.; Imada, H.; Kim, Y. Adsorption-induced stability reversal of

photochromic diarylethene on metal surfaces. *Chem. Commun.* **2013,** *49* (77), 8710-8712.
(186) Kumar, A. S.; Ye, T.; Takami, T.; Yu, B.-C.; Flatt, A. K.; Tour, J. M.; Weiss, P. S. Reversible Photo-Switching of Single Azobenzene Molecules in Controlled Nanoscale Environments. *Nano Lett.* **2008,** *8* (6), 1644-1648.
(187) Reecht, G.; Lotze, C.; Sysoiev, D.; Huhn, T.; Franke, K. J. Disentangling electron- and electric-field-induced ring-closing reactions in a diarylethene derivative on Ag(1 1 1). *J. Phys.: Condens. Matter* **2017,** *29* (29), 294001.
(188) Nickel, F.; Bernien, M.; Herder, M.; Wrzalek, S.; Chittas, P.; Kraffert, K.; Arruda, L. M.; Kipgen, L.; Krüger, D.; Hecht, S.et al. Light-induced photoisomerization of a diarylethene molecular switch on solid surfaces. *J. Phys.: Condens. Matter* **2017,** *29* (37), 374001.
(189) Nickel, F.; Bernien, M.; Kraffert, K.; Krüger, D.; Arruda, L. M.; Kipgen, L.; Kuch, W. Reversible Switching of Spiropyran Molecules in Direct Contact With a Bi(111) Single Crystal Surface. *Adv. Funct. Mater.* **2017,** *27* (48), 1702280.
(190) Nickel, F.; Bernien, M.; Krüger, D.; Miguel, J.; Britton, A. J.; Arruda, L. M.; Kipgen, L.; Kuch, W. Highly Efficient and Bidirectional Photochromism of Spirooxazine on Au(111). *J. Phys. Chem. C* **2018,** *122* (14), 8031-8036.
(191) Jaekel, S.; Richter, A.; Lindner, R.; Bechstein, R.; Nacci, C.; Hecht, S.; Kühnle, A.; Grill, L. Reversible and Efficient Light-Induced Molecular Switching on an Insulator Surface. *ACS Nano* **2018,** *12* (2), 1821-1828.
(192) Nacci, C.; Baroncini, M.; Credi, A.; Grill, L. Reversible Photoswitching and Isomer-Dependent Diffusion of Single Azobenzene Tetramers on a Metal Surface. *Angew. Chem., Int. Ed.* **2018,** *57* (46), 15034-15039.
(193) Rusch, T. R.; Schlimm, A.; Krekiehn, N. R.; Tellkamp, T.; Budzák, Š.; Jacquemin, D.; Tuczek, F.; Herges, R.; Magnussen, O. M. Observation of Collective Photoswitching in Free-Standing TATA-Based Azobenzenes on Au(111). *Angew. Chem., Int. Ed.* **2020,** *59* (39), 17192-17196.
(194) Cho, J.; Berbil-Bautista, L.; Levy, N.; Poulsen, D.; Fréchet, J. M. J.; Crommie, M. F. Functionalization, self-assembly, and photoswitching quenching for azobenzene derivatives adsorbed on Au(111). *J. Chem. Phys* **2010,** *133* (23), 234707.
(195) Alemani, M.; Selvanathan, S.; Ample, F.; Peters, M. V.; Rieder, K.-H.; Moresco, F.; Joachim, C.; Hecht, S.; Grill, L. Adsorption and Switching Properties of Azobenzene Derivatives on Different Noble Metal Surfaces: Au(111), Cu(111), and Au(100). *J. Phys. Chem. C* **2008,** *112* (28), 10509-10514.
(196) Kealy, T. J.; Pauson, P. L. A New Type of Organo-Iron Compound. *Nature* **1951,** *168* (4285), 1039-1040.
(197) Fabbrizzi, L. The ferrocenium/ferrocene couple: a versatile redox switch. *ChemTexts* **2020,** *6* (4), 22.
(198) Dunitz, J. D.; Orgel, L. E. Bis-cyclopentadienyl Iron: a Molecular Sandwich. *Nature* **1953,** *171* (4342), 121-122.
(199) Fabre, B. Ferrocene-Terminated Monolayers Covalently Bound to Hydrogen-Terminated Silicon Surfaces. Toward the Development of Charge Storage and Communication Devices. *Acc. Chem. Res.* **2010,** *43* (12), 1509-1518.
(200) Astruc, D. Why is Ferrocene so Exceptional? *Eur. J. Inorg. Chem.* **2017,** *2017* (1), 6-29.
(201) Gagne, R. R.; Koval, C. A.; Lisensky, G. C. Ferrocene as an internal standard for electrochemical measurements. *Inorg. Chem.* **1980,** *19* (9), 2854-2855.
(202) Martínez, R.; Ratera, I.; Tárraga, A.; Molina, P.; Veciana, J. A simple and robust reversible

redox–fluorescence molecular switch based on a 1,4-disubstituted azine with ferrocene and pyrene units. *Chem. Commun.* **2006,** (36), 3809-3811.
(203) Wudl, F.; Smith, G. M.; Hufnagel, E. J. Bis-1,3-dithiolium chloride: an unusually stable organic radical cation. *J. Chem. Soc. D* **1970,** (21), 1453-1454.
(204) Deuchert, K.; Hünig, S. Multistage Organic Redox Systems—A General Structural Principle. *Angew. Chem., Int. Ed.* **1978,** *17* (12), 875-886.
(205) Devonport, W.; Blower, M. A.; Bryce, M. R.; Goldenberg, L. M. A Redox-Active Tetrathiafulvalene [2]Pseudorotaxane: Spectroelectrochemical and Cyclic Voltammetric Studies of the Highly-Reversible Complexation/Decomplexation Process. *J. Org. Chem.* **1997,** *62* (4), 885-887.
(206) Ashton, P. R.; Balzani, V.; Becher, J.; Credi, A.; Fyfe, M. C. T.; Mattersteig, G.; Menzer, S.; Nielsen, M. B.; Raymo, F. M.; Stoddart, J. F.et al. A Three-Pole Supramolecular Switch. *J. Am. Chem. Soc.* **1999,** *121* (16), 3951-3957.
(207) Fang, C.-J.; Zhu, Z.; Sun, W.; Xu, C.-H.; Yan, C.-H. New TTF derivatives: several molecular logic gates based on their switchable fluorescent emissions. *New J. Chem.* **2007,** *31* (4), 580-586.
(208) Schröder, H. V.; Schalley, C. A. Tetrathiafulvalene – a redox-switchable building block to control motion in mechanically interlocked molecules. *Beilstein J. Org. Chem.* **2018,** *14*, 2163-2185.
(209) Khodorkovsky, V.; Shapiro, L.; Krief, P.; Shames, A.; Mabon, G.; Gorgues, A.; Giffard, M. Do π-dimers of tetrathiafulvalene cation radicals really exist at room temperature? *Chem. Commun.* **2001,** (24), 2736-2737.
(210) Bryce, M. R. Tetrathiafulvalenes as π-Electron Donors for Intramolecular Charge-Transfer Materials. *Adv. Mater.* **1999,** *11* (1), 11-23.
(211) Das, A.; Ghosh, S. Supramolecular Assemblies by Charge-Transfer Interactions between Donor and Acceptor Chromophores. *Angew. Chem., Int. Ed.* **2014,** *53* (8), 2038-2054.
(212) Schröder, Hendrik V.; Schalley, C. A. Electrochemically switchable rotaxanes: recent strides in new directions. *Chem. Sci.* **2019,** *10* (42), 9626-9639.
(213) Spruell, J. M.; Coskun, A.; Friedman, D. C.; Forgan, R. S.; Sarjeant, A. A.; Trabolsi, A.; Fahrenbach, A. C.; Barin, G.; Paxton, W. F.; Dey, S. K.et al. Highly stable tetrathiafulvalene radical dimers in [3]catenanes. *Nat. Chem.* **2010,** *2* (10), 870-879.
(214) Michaelis , L.; Hill , E. S. THE VIOLOGEN INDICATORS. *J. Gen. Physiol.* **1933,** *16* (6), 859-873.
(215) Monk, P. M. S.; Rosseinsky, D. R.; Mortimer, R. J. In *Electrochromic Materials and Devices*; Mortimer, R. J.;Rosseinsky, D. R.;Monk, P. M. S., Eds., 2013.
(216) Jordão, N.; Cabrita, L.; Pina, F.; Branco, L. C. Novel Bipyridinium Ionic Liquids as Liquid Electrochromic Devices. *Chem. Eur. J.* **2014,** *20* (14), 3982-3988.
(217) Krossing, I.; Raabe, I. Noncoordinating Anions—Fact or Fiction? A Survey of Likely Candidates. *Angew. Chem., Int. Ed.* **2004,** *43* (16), 2066-2090.
(218) Kalny, D.; Elhabiri, M.; Moav, T.; Vaskevich, A.; Rubinstein, I.; Shanzer, A.; Albrecht-Gary, A.-M. A new molecular switch: redox-driven translocation mechanism of the copper cation. *Chem. Commun.* **2002,** (13), 1426-1427.
(219) Jimenez-Molero, M. C.; Dietrich-Buchecker, C.; Sauvage, J.-P. Towards artificial muscles at the nanometric level. *Chem. Commun.* **2003,** (14), 1613-1616.
(220) Niess, F.; Duplan, V.; Sauvage, J.-P. Molecular Muscles: From Species in Solution to Materials and Devices. *Chem. Lett.* **2014,** *43* (7), 964-974.

(221) Tseng, H.-R.; Vignon, S. A.; Stoddart, J. F. Toward Chemically Controlled Nanoscale Molecular Machinery. *Angew. Chem., Int. Ed.* **2003,** *42* (13), 1491-1495.
(222) Nygaard, S.; Leung, K. C. F.; Aprahamian, I.; Ikeda, T.; Saha, S.; Laursen, B. W.; Kim, S.-Y.; Hansen, S. W.; Stein, P. C.; Flood, A. H.et al. Functionally Rigid Bistable [2]Rotaxanes. *J. Am. Chem. Soc.* **2007,** *129* (4), 960-970.
(223) Liu, Y.; Bonvallet, P. A.; Vignon, S. A.; Khan, S. I.; Stoddart, J. F. Donor–Acceptor Pretzelanes and a Cyclic Bis[2]catenane Homologue. *Angew. Chem., Int. Ed.* **2005,** *44* (20), 3050-3055.
(224) Striepe, L.; Baumgartner, T. Viologens and Their Application as Functional Materials. *Chem. Eur. J.* **2017,** *23* (67), 16924-16940.
(225) Dieny, B.; Prejbeanu, I. L.; Garello, K.; Gambardella, P.; Freitas, P.; Lehndorff, R.; Raberg, W.; Ebels, U.; Demokritov, S. O.; Akerman, J.et al. Opportunities and challenges for spintronics in the microelectronics industry. *Nat. Electron.* **2020,** *3* (8), 446-459.
(226) Roy, K.; Jaiswal, A.; Panda, P. Towards spike-based machine intelligence with neuromorphic computing. *Nature* **2019,** *575* (7784), 607-617.
(227) Awschalom, D. D.; Bassett, L. C.; Dzurak, A. S.; Hu, E. L.; Petta, J. R. Quantum Spintronics: Engineering and Manipulating Atom-Like Spins in Semiconductors. *Science* **2013,** *339* (6124), 1174-1179.
(228) Fei, Z.; Huang, B.; Malinowski, P.; Wang, W.; Song, T.; Sanchez, J.; Yao, W.; Xiao, D.; Zhu, X.; May, A. F.et al. Two-dimensional itinerant ferromagnetism in atomically thin Fe. *Nat. Mater.* **2018,** *17* (9), 778-782.
(229) Lin, X.; Yang, W.; Wang, K. L.; Zhao, W. Two-dimensional spintronics for low-power electronics. *Nat. Electron.* **2019,** *2* (7), 274-283.
(230) Han, W.; Kawakami, R. K.; Gmitra, M.; Fabian, J. Graphene spintronics. *Nat. Nanotechnol.* **2014,** *9* (10), 794-807.
(231) Wang, Z.; Ki, D. K.; Chen, H.; Berger, H.; MacDonald, A. H.; Morpurgo, A. F. Strong interface-induced spin-orbit interaction in graphene on WS_2. *Nat. Commun.* **2015,** *6*, 8339.
(232) Safeer, C. K.; Ingla-Aynés, J.; Herling, F.; Garcia, J. H.; Vila, M.; Ontoso, N.; Calvo, M. R.; Roche, S.; Hueso, L. E.; Casanova, F. Room-Temperature Spin Hall Effect in Graphene/MoS_2 van der Waals Heterostructures. *Nano Lett.* **2019,** *19* (2), 1074-1082.
(233) Seyler, K. L.; Zhong, D.; Huang, B.; Linpeng, X.; Wilson, N. P.; Taniguchi, T.; Watanabe, K.; Yao, W.; Xiao, D.; McGuire, M. A.et al. Valley Manipulation by Optically Tuning the Magnetic Proximity Effect in WSe_2/CrI_3 Heterostructures. *Nano Lett.* **2018,** *18* (6), 3823-3828.
(234) Khokhriakov, D.; Hoque, A. M.; Karpiak, B.; Dash, S. P. Gate-tunable spin-galvanic effect in graphene-topological insulator van der Waals heterostructures at room temperature. *Nat. Commun.* **2020,** *11* (1), 3657.
(235) Benítez, L. A.; Savero Torres, W.; Sierra, J. F.; Timmermans, M.; Garcia, J. H.; Roche, S.; Costache, M. V.; Valenzuela, S. O. Tunable room-temperature spin galvanic and spin Hall effects in van der Waals heterostructures. *Nat. Mater.* **2020,** *19* (2), 170-175.
(236) Deng, Y.; Yu, Y.; Song, Y.; Zhang, J.; Wang, N. Z.; Sun, Z.; Yi, Y.; Wu, Y. Z.; Wu, S.; Zhu, J.et al. Gate-tunable room-temperature ferromagnetism in two-dimensional Fe. *Nature* **2018,** *563* (7729), 94-99.
(237) Huang, B.; Clark, G.; Klein, D. R.; MacNeill, D.; Navarro-Moratalla, E.; Seyler, K. L.; Wilson, N.; McGuire, M. A.; Cobden, D. H.; Xiao, D.et al. Electrical control of 2D magnetism in bilayer CrI_3. *Nat. Nanotechnol.* **2018,** *13* (7), 544-548.

(238) Jiang, S.; Shan, J.; Mak, K. F. Electric-field switching of two-dimensional van der Waals magnets. *Nat. Mater.* **2018,** *17* (5), 406-410.
(239) Liao, M.-S.; Scheiner, S. Electronic structure and bonding in metal phthalocyanines, Metal=Fe, Co, Ni, Cu, Zn, Mg. *J. Chem. Phys* **2001,** *114* (22), 9780-9791.
(240) Cinchetti, M.; Dediu, V. A.; Hueso, L. E. Activating the molecular spinterface. *Nat. Mater.* **2017,** *16* (5), 507-515.
(241) Senthil Kumar, K.; Ruben, M. Emerging trends in spin crossover (SCO) based functional materials and devices. *Coord. Chem. Rev.* **2017,** *346*, 176-205.
(242) Molnár, G.; Rat, S.; Salmon, L.; Nicolazzi, W.; Bousseksou, A. Spin Crossover Nanomaterials: From Fundamental Concepts to Devices. *Adv. Mater.* **2018,** *30* (5), 1703862.
(243) Gambardella, P.; Stepanow, S.; Dmitriev, A.; Honolka, J.; de Groot, F. M.; Lingenfelder, M.; Sen Gupta, S.; Sarma, D. D.; Bencok, P.; Stanescu, S.et al. Supramolecular control of the magnetic anisotropy in two-dimensional high-spin Fe arrays at a metal interface. *Nat. Mater.* **2009,** *8* (3), 189-193.
(244) Woodruff, D. N.; Winpenny, R. E. P.; Layfield, R. A. Lanthanide Single-Molecule Magnets. *Chem. Rev.* **2013,** *113* (7), 5110-5148.
(245) Gütlich, P.; Hauser, A.; Spiering, H. Thermal and Optical Switching of Iron(II) Complexes. *Angew. Chem., Int. Ed.* **1994,** *33* (20), 2024-2054.
(246) Ruben, M.; Kumar, K. S. Sublimable Spin Crossover Complexes: From Spin-State Switching to Molecular Devices. *Angew. Chem., Int. Ed.* **2019,** *60* (14), 7502-7521.
(247) Gütlich, P.; Garcia, Y. In *Reference Module in Chemistry, Molecular Sciences and Chemical Engineering*; Elsevier, 2015.
(248) Hauser, A. In *Spin Crossover in Transition Metal Compounds I*; Gütlich, P.;Goodwin, H. A., Eds.; Springer: Berlin, Heidelberg, 2004.
(249) Krober, J.; Codjovi, E.; Kahn, O.; Groliere, F.; Jay, C. A spin transition system with a thermal hysteresis at room temperature. *J. Am. Chem. Soc.* **1993,** *115* (21), 9810-9811.
(250) Gütlich, P.; Ksenofontov, V.; Gaspar, A. B. Pressure effect studies on spin crossover systems. *Coord. Chem. Rev.* **2005,** *249* (17), 1811-1829.
(251) Prins, F.; Monrabal-Capilla, M.; Osorio, E. A.; Coronado, E.; van der Zant, H. S. J. Room-Temperature Electrical Addressing of a Bistable Spin-Crossover Molecular System. *Adv. Mater.* **2011,** *23* (13), 1545-1549.
(252) Rotaru, A.; Dugay, J.; Tan, R. P.; Guralskiy, I. A.; Salmon, L.; Demont, P.; Carrey, J.; Molnár, G.; Respaud, M.; Bousseksou, A. Nano-electromanipulation of Spin Crossover Nanorods: Towards Switchable Nanoelectronic Devices. *Adv. Mater.* **2013,** *25* (12), 1745-1749.
(253) Dugay, J.; Giménez-Marqués, M.; Kozlova, T.; Zandbergen, H. W.; Coronado, E.; van der Zant, H. S. J. Spin Switching in Electronic Devices Based on 2D Assemblies of Spin-Crossover Nanoparticles. *Adv. Mater.* **2015,** *27* (7), 1288-1293.
(254) Coronado, E.; Galán-Mascarós, J. R.; Monrabal-Capilla, M.; García-Martínez, J.; Pardo-Ibáñez, P. Bistable Spin-Crossover Nanoparticles Showing Magnetic Thermal Hysteresis near Room Temperature. *Adv. Mater.* **2007,** *19* (10), 1359-1361.
(255) Giménez-Marqués, M.; de Larrea, M. L.; Coronado, E. Unravelling the chemical design of spin-crossover nanoparticles based on iron(ii)–triazole coordination polymers: towards a control of the spin transition. *J. Mater. Chem. C* **2015,** *3* (30), 7946-7953.
(256) Rösner, B.; Milek, M.; Witt, A.; Gobaut, B.; Torelli, P.; Fink, R. H.; Khusniyarov, M. M.

Reversible Photoswitching of a Spin-Crossover Molecular Complex in the Solid State at Room Temperature. *Angew. Chem., Int. Ed.* **2015,** *54* (44), 12976-12980.
(257) McCusker, J. K.; Walda, K. N.; Dunn, R. C.; Simon, J. D.; Magde, D.; Hendrickson, D. N. Sub-picosecond DS = 2 intersystem crossing in low-spin ferrous complexes. *J. Am. Chem. Soc.* **1992,** *114* (17), 6919-6920.
(258) Spiering, H.; Willenbacher, N. Elastic interaction of high-spin and low-spin complex molecules in spin-crossover compounds. II. *J. Phys.: Condens. Matter* **1989,** *1* (50), 10089-10105.
(259) Spiering, H.; Boukheddaden, K.; Linares, J.; Varret, F. Total free energy of a spin-crossover molecular system. *Phys. Rev. B* **2004,** *70* (18), 184106.
(260) Dugay, J.; Aarts, M.; Giménez-Marqués, M.; Kozlova, T.; Zandbergen, H. W.; Coronado, E.; van der Zant, H. S. Phase Transitions in Spin-Crossover Thin Films Probed by Graphene Transport Measurements. *Nano Lett.* **2017,** *17* (1), 186-193.
(261) Decurtins, S.; Gütlich, P.; Köhler, C. P.; Spiering, H.; Hauser, A. Light-induced excited spin state trapping in a transition-metal complex: The hexa-1-propyltetrazole-iron (II) tetrafluoroborate spin-crossover system. *Chem. Phys. Lett.* **1984,** *105* (1), 1-4.
(262) Cobo, S.; Ostrovskii, D.; Bonhommeau, S.; Vendier, L.; Molnár, G.; Salmon, L.; Tanaka, K.; Bousseksou, A. Single-Laser-Shot-Induced Complete Bidirectional Spin Transition at Room Temperature in Single Crystals of (Fe^{II}(pyrazine)($Pt(CN)_4$)). *J. Am. Chem. Soc.* **2008,** *130* (28), 9019-9024.
(263) Sy, M.; Garrot, D.; Slimani, A.; Páez-Espejo, M.; Varret, F.; Boukheddaden, K. Reversible Control by Light of the High-Spin Low-Spin Elastic Interface inside the Bistable Region of a Robust Spin-Transition Single Crystal. *Angew. Chem. Int. Ed.* **2016,** *55* (5), 1755-1759.
(264) Milek, M.; Heinemann, F. W.; Khusniyarov, M. M. Spin Crossover Meets Diarylethenes: Efficient Photoswitching of Magnetic Properties in Solution at Room Temperature. *Inorg. Chem.* **2013,** *52* (19), 11585-11592.
(265) Venkataramani, S.; Jana, U.; Dommaschk, M.; Sönnichsen, F. D.; Tuczek, F.; Herges, R. Magnetic Bistability of Molecules in Homogeneous Solution at Room Temperature. *Science* **2011,** *331* (6016), 445.
(266) Gopakumar, T. G.; Matino, F.; Naggert, H.; Bannwarth, A.; Tuczek, F.; Berndt, R. Electron-Induced Spin Crossover of Single Molecules in a Bilayer on Gold. *Angew. Chem., Int. Ed.* **2012,** *51* (25), 6262-6266.
(267) Miyamachi, T.; Gruber, M.; Davesne, V.; Bowen, M.; Boukari, S.; Joly, L.; Scheurer, F.; Rogez, G.; Yamada, T. K.; Ohresser, P.et al. Robust spin crossover and memristance across a single molecule. *Nat. Commun.* **2012,** *3* (1), 938.
(268) Zhang, X.; Palamarciuc, T.; Létard, J.-F.; Rosa, P.; Lozada, E. V.; Torres, F.; Rosa, L. G.; Doudin, B.; Dowben, P. A. The spin state of a molecular adsorbate driven by the ferroelectric substrate polarization. *Chem. Commun.* **2014,** *50* (18), 2255-2257.
(269) Kipgen, L.; Bernien, M.; Tuczek, F.; Kuch, W. Spin-Crossover Molecules on Surfaces: From Isolated Molecules to Ultrathin Films. *Adv. Mater.* **2021,** *33* (24), 2008141.
(270) Rohlf, S.; Gruber, M.; Flöser, B. M.; Grunwald, J.; Jarausch, S.; Diekmann, F.; Kalläne, M.; Jasper-Toennies, T.; Buchholz, A.; Plass, W.et al. Light-Induced Spin Crossover in an Fe(II) Low-Spin Complex Enabled by Surface Adsorption. *J. Phys. Chem. Lett.* **2018,** *9* (7), 1491-1496.
(271) Zhang, L.; Tong, Y.; Kelai, M.; Bellec, A.; Lagoute, J.; Chacon, C.; Girard, Y.; Rousset, S.; Boillot, M.-L.; Rivière, E.et al. Anomalous Light-Induced Spin-State Switching for Iron(II)

Spin-Crossover Molecules in Direct Contact with Metal Surfaces. *Angew. Chem., Int. Ed.* **2020,** *59* (32), 13341-13346.
(272) Ossinger, S.; Naggert, H.; Kipgen, L.; Jasper-Toennies, T.; Rai, A.; Rudnik, J.; Nickel, F.; Arruda, L. M.; Bernien, M.; Kuch, W.et al. Vacuum-Evaporable Spin-Crossover Complexes in Direct Contact with a Solid Surface: Bismuth versus Gold. *J. Phys. Chem. C* **2017,** *121* (2), 1210-1219.
(273) Knaak, T.; González, C.; Dappe, Y. J.; Harzmann, G. D.; Brandl, T.; Mayor, M.; Berndt, R.; Gruber, M. Fragmentation and Distortion of Terpyridine-Based Spin-Crossover Complexes on Au(111). *J. Phys. Chem. C* **2019,** *123* (7), 4178-4185.
(274) Bairagi, K.; Bellec, A.; Fourmental, C.; Iasco, O.; Lagoute, J.; Chacon, C.; Girard, Y.; Rousset, S.; Choueikani, F.; Otero, E.et al. Temperature-, Light-, and Soft X-ray-Induced Spin Crossover in a Single Layer of Fe^{II}-Pyrazolylborate Molecules in Direct Contact with Gold. *J. Phys. Chem. C* **2018,** *122* (1), 727-731.
(275) Gruber, M.; Miyamachi, T.; Davesne, V.; Bowen, M.; Boukari, S.; Wulfhekel, W.; Alouani, M.; Beaurepaire, E. Spin crossover in $Fe(phen)_2(NCS)_2$ complexes on metallic surfaces. *J. Chem. Phys* **2017,** *146* (9), 92312.
(276) Bernien, M.; Naggert, H.; Arruda, L. M.; Kipgen, L.; Nickel, F.; Miguel, J.; Hermanns, C. F.; Krüger, A.; Krüger, D.; Schierle, E.et al. Highly Efficient Thermal and Light-Induced Spin-State Switching of an Fe(II) Complex in Direct Contact with a Solid Surface. *ACS Nano* **2015,** *9* (9), 8960-8966.
(277) Kipgen, L.; Bernien, M.; Ossinger, S.; Nickel, F.; Britton, A. J.; Arruda, L. M.; Naggert, H.; Luo, C.; Lotze, C.; Ryll, H.et al. Evolution of cooperativity in the spin transition of an iron(II) complex on a graphite surface. *Nat. Commun.* **2018,** *9* (1), 2984.
(278) Rohlf, S.; Grunwald, J.; Jasper-Toennies, T.; Johannsen, S.; Diekmann, F.; Studniarek, M.; Berndt, R.; Tuczek, F.; Rossnagel, K.; Gruber, M. Influence of Substrate Electronic Properties on the Integrity and Functionality of an Adsorbed Fe(II) Spin-Crossover Compound. *J. Phys. Chem. C* **2019,** *123* (29), 17774-17780.
(279) Bairagi, K.; Iasco, O.; Bellec, A.; Kartsev, A.; Li, D.; Lagoute, J.; Chacon, C.; Girard, Y.; Rousset, S.; Miserque, F.et al. Molecular-scale dynamics of light-induced spin cross-over in a two-dimensional layer. *Nat. Commun.* **2016,** *7* (1), 12212.
(280) Liu, J.; Gao, Y.; Wang, T.; Xue, Q.; Hua, M.; Wang, Y.; Huang, L.; Lin, N. Collective Spin Manipulation in Antiferroelastic Spin-Crossover Metallo-Supramolecular Chains. *ACS Nano* **2020,** *14* (9), 11283-11293.
(281) Wäckerlin, C.; Chylarecka, D.; Kleibert, A.; Müller, K.; Iacovita, C.; Nolting, F.; Jung, T. A.; Ballav, N. Controlling spins in adsorbed molecules by a chemical switch. *Nat. Commun.* **2010,** *1* (1), 61.
(282) Köbke, A.; Gutzeit, F.; Röhricht, F.; Schlimm, A.; Grunwald, J.; Tuczek, F.; Studniarek, M.; Longo, D.; Choueikani, F.; Otero, E.et al. Reversible coordination-induced spin-state switching in complexes on metal surfaces. *Nat. Nanotechnol.* **2020,** *15* (1), 18-21.
(283) Serrano, G.; Velez-Fort, E.; Cimatti, I.; Cortigiani, B.; Malavolti, L.; Betto, D.; Ouerghi, A.; Brookes, N. B.; Mannini, M.; Sessoli, R. Magnetic bistability of a $TbPc_2$ submonolayer on a graphene/SiC(0001) conductive electrode. *Nanoscale* **2018,** *10* (6), 2715-2720.
(284) Serri, M.; Wu, W.; Fleet, L. R.; Harrison, N. M.; Hirjibehedin, C. F.; Kay, C. W.; Fisher, A. J.; Aeppli, G.; Heutz, S. High-temperature antiferromagnetism in molecular semiconductor thin films and nanostructures. *Nat. Commun.* **2014,** *5*, 3079.
(285) Gruber, M.; Ibrahim, F.; Boukari, S.; Isshiki, H.; Joly, L.; Peter, M.; Studniarek, M.; Da

Costa, V.; Jabbar, H.; Davesne, V.et al. Exchange bias and room-temperature magnetic order in molecular layers. *Nat. Mater.* **2015,** *14* (10), 981-984.
(286) Otsuki, J. STM studies on porphyrins. *Coord. Chem. Rev.* **2010,** *254* (19), 2311-2341.
(287) Scheybal, A.; Ramsvik, T.; Bertschinger, R.; Putero, M.; Nolting, F.; Jung, T. A. Induced magnetic ordering in a molecular monolayer. *Chem. Phys. Lett.* **2005,** *411* (1), 214-220.
(288) Wende, H.; Bernien, M.; Luo, J.; Sorg, C.; Ponpandian, N.; Kurde, J.; Miguel, J.; Piantek, M.; Xu, X.; Eckhold, P.et al. Substrate-induced magnetic ordering and switching of iron porphyrin molecules. *Nat. Mater.* **2007,** *6* (7), 516-520.
(289) Jo, J.; Byun, J.; Oh, I.; Park, J.; Jin, M. J.; Min, B. C.; Lee, J.; Yoo, J. W. Molecular Tunability of Magnetic Exchange Bias and Asymmetrical Magnetotransport in Metalloporphyrin/Co Hybrid Bilayers. *ACS Nano* **2019,** *13* (1), 894-903.
(290) Jo, J.; Byun, J.; Lee, J.; Choe, D.; Oh, I.; Park, J.; Jin, M.-J.; Lee, J.; Yoo, J.-W. Emergence of Multispinterface and Antiferromagnetic Molecular Exchange Bias via Molecular Stacking on a Ferromagnetic Film. *Adv. Funct. Mater.* **2020,** *30* (11), 1908499.
(291) Wäckerlin, C.; Tarafder, K.; Girovsky, J.; Nowakowski, J.; Hählen, T.; Shchyrba, A.; Siewert, D.; Kleibert, A.; Nolting, F.; Oppeneer, P. M.et al. Ammonia Coordination Introducing a Magnetic Moment in an On-Surface Low-Spin Porphyrin. *Angew. Chem., Int. Ed.* **2013,** *52* (17), 4568-4571.
(292) Hermanns, C. F.; Bernien, M.; Krüger, A.; Walter, W.; Chang, Y.-M.; Weschke, E.; Kuch, W. Huge magnetically coupled orbital moments of Co porphyrin molecules and their control by CO adsorption. *Phys. Rev. B* **2013,** *88* (10), 104420.
(293) Gopakumar, T. G.; Tang, H.; Morillo, J.; Berndt, R. Transfer of Cl Ligands between Adsorbed Iron Tetraphenylporphyrin Molecules. *J. Am. Chem. Soc.* **2012,** *134* (29), 11844-11847.
(294) Christou, G.; Gatteschi, D.; Hendrickson, D. N.; Sessoli, R. Single-Molecule Magnets. *MRS Bull.* **2000,** *25* (11), 66-71.
(295) Liu, J.-L.; Chen, Y.-C.; Tong, M.-L. Symmetry strategies for high performance lanthanide-based single-molecule magnets. *Chem. Soc. Rev.* **2018,** *47* (7), 2431-2453.
(296) Sessoli, R.; Gatteschi, D.; Caneschi, A.; Novak, M. A. Magnetic bistability in a metal-ion cluster. *Nature* **1993,** *365* (6442), 141-143.
(297) Guo, F.-S.; Day, B. M.; Chen, Y.-C.; Tong, M.-L.; Mansikkamäki, A.; Layfield, R. A. Magnetic hysteresis up to 80 kelvin in a dysprosium metallocene single-molecule magnet. *Science* **2018,** *362* (6421), 1400-1403.
(298) Bogani, L.; Wernsdorfer, W. Molecular spintronics using single-molecule magnets. *Nat. Mater.* **2008,** *7* (3), 179-186.
(299) Gobbi, M.; Novak, M. A.; Del Barco, E. Molecular spintronics. *J. Appl. Phys.* **2019,** *125* (24), 240401.
(300) Wernsdorfer, W.; Murugesu, M.; Christou, G. Resonant Tunneling in Truly Axial Symmetry Mn_{12} Single-Molecule Magnets: Sharp Crossover between Thermally Assisted and Pure Quantum Tunneling. *Phys. Rev. Lett.* **2006,** *96* (5), 57208.
(301) Ishikawa, N.; Sugita, M.; Wernsdorfer, W. Quantum Tunneling of Magnetization in Lanthanide Single-Molecule Magnets: Bis(phthalocyaninato)terbium and Bis(phthalocyaninato)dysprosium Anions. *Angew. Chem., Int. Ed.* **2005,** *44* (19), 2931-2935.
(302) Ardavan, A.; Rival, O.; Morton, J. J. L.; Blundell, S. J.; Tyryshkin, A. M.; Timco, G. A.; Winpenny, R. E. P. Will Spin-Relaxation Times in Molecular Magnets Permit Quantum

Information Processing? *Phys. Rev. Lett.* **2007,** *98* (5), 057201.
(303) Ishikawa, N.; Sugita, M.; Ishikawa, T.; Koshihara, S.-y.; Kaizu, Y. Lanthanide Double-Decker Complexes Functioning as Magnets at the Single-Molecular Level. *J. Am. Chem. Soc.* **2003,** *125* (29), 8694-8695.
(304) Margheriti, L.; Chiappe, D.; Mannini, M.; Car, P. E.; Sainctavit, P.; Arrio, M.-A.; de Mongeot, F. B.; Cezar, J. C.; Piras, F. M.; Magnani, A.et al. X-Ray Detected Magnetic Hysteresis of Thermally Evaporated Terbium Double-Decker Oriented Films. *Adv. Mater.* **2010,** *22* (48), 5488-5493.
(305) Liu, J.; Liang, Q.; Zhao, R.; Lei, S.; Hu, W. Application of organic–graphene hybrids in high performance photodetectors. *Mater. Chem. Front.* **2020,** *4* (2), 354-368.
(306) De Feyter, S.; De Schryver, F. C. Two-dimensional supramolecular self-assembly probed by scanning tunneling microscopy. *Chem. Soc. Rev.* **2003,** *32* (3), 139-150.
(307) Rabe, J. P.; Buchholz, S. Commensurability and Mobility in Two-Dimensional Molecular Patterns on Graphite. *Science* **1991,** *253* (5018), 424-427.
(308) Palma, C.-A.; Cecchini, M.; Samorì, P. Predicting self-assembly: from empirism to determinism. *Chem. Soc. Rev.* **2012,** *41* (10), 3713-3730.
(309) Daukiya, L.; Seibel, J.; De Feyter, S. Chemical modification of 2D materials using molecules and assemblies of molecules. *Adv. Phys.: X* **2019,** *4* (1), 1625723.
(310) Ciesielski, A.; Palma, C.-A.; Bonini, M.; Samorì, P. Towards Supramolecular Engineering of Functional Nanomaterials: Pre-Programming Multi-Component 2D Self-Assembly at Solid-Liquid Interfaces. *Adv. Mater.* **2010,** *22* (32), 3506-3520.
(311) Goronzy, D. P.; Ebrahimi, M.; Rosei, F.; Arramel; Fang, Y.; De Feyter, S.; Tait, S. L.; Wang, C.; Beton, P. H.; Wee, A. T. S.et al. Supramolecular Assemblies on Surfaces: Nanopatterning, Functionality, and Reactivity. *ACS Nano* **2018,** *12* (8), 7445-7481.
(312) Mali, K. S.; Pearce, N.; De Feyter, S.; Champness, N. R. Frontiers of supramolecular chemistry at solid surfaces. *Chem. Soc. Rev.* **2017,** *46* (9), 2520-2542.
(313) Dreher, M.; Günder, D.; Zörb, S.; Witte, G. Van der Waals Bound Organic Semiconductor/2D-Material Hybrid Heterosystems: Intrinsic Epitaxial Alignment of Perfluoropentacene Films on Transition Metal Dichalcogenides. *Chem. Mater.* **2020,** *32* (20), 9034-9043.
(314) Tilmann, R.; Weiß, C.; Cullen, C. P.; Peters, L.; Hartwig, O.; Höltgen, L.; Stimpel-Lindner, T.; Knirsch, K. C.; McEvoy, N.; Hirsch, A.et al. Highly Selective Non-Covalent On-Chip Functionalization of Layered Materials. *Adv. Electron. Mater.* **2021,** *7* (7), 2000564.
(315) Hagara, J.; Mrkyvkova, N.; Nádaždy, P.; Hodas, M.; Bodík, M.; Jergel, M.; Majková, E.; Tokár, K.; Hutár, P.; Sojková, M.et al. Reorientation of π-conjugated molecules on few-layer MoS_2 films. *Phys. Chem. Chem. Phys.* **2020,** *22* (5), 3097-3104.
(316) Amsterdam, S. H.; LaMountain, T.; Stanev, T. K.; Sangwan, V. K.; López-Arteaga, R.; Padgaonkar, S.; Watanabe, K.; Taniguchi, T.; Weiss, E. A.; Marks, T. J.et al. Tailoring the Optical Response of Pentacene Thin Films via Templated Growth on Hexagonal Boron Nitride. *J. Phys. Chem. Lett.* **2021,** *12* (1), 26-31.
(317) Günder, D.; Watanabe, K.; Taniguchi, T.; Witte, G. Van der Waals Bound Organic/2D Insulator Hybrid Structures: Epitaxial Growth of Acene Films on hBN(001) and the Influence of Surface Defects. *ACS Appl. Mater. Interfaces* **2020,** *12* (34), 38757-38767.
(318) MacLeod, J. M.; Rosei, F. Molecular Self-Assembly on Graphene. *Small* **2014,** *10* (6), 1038-1049.
(319) Gobbi, M.; Bonacchi, S.; Lian, J. X.; Vercouter, A.; Bertolazzi, S.; Zyska, B.; Timpel, M.;

Tatti, R.; Olivier, Y.; Hecht, S.et al. Collective Molecular Switching in Hybrid Superlattices for Light-Modulated Two-Dimensional Electronics. *Nat. Commun.* **2018,** *9* (1), 2661.
(320) Gobbi, M.; Galanti, A.; Stoeckel, M.-A.; Zyska, B.; Bonacchi, S.; Hecht, S.; Samorì, P. Graphene transistors for real-time monitoring molecular self-assembly dynamics. *Nat. Commun.* **2020,** *11* (1), 4731.
(321) Phillipson, R.; Lockhart de la Rosa, C. J.; Teyssandier, J.; Walke, P.; Waghray, D.; Fujita, Y.; Adisoejoso, J.; Mali, K. S.; Asselberghs, I.; Huyghebaert, C.et al. Tunable doping of graphene by using physisorbed self-assembled networks. *Nanoscale* **2016,** *8* (48), 20017-20026.
(322) Li, B.; Klekachev, A. V.; Cantoro, M.; Huyghebaert, C.; Stesmans, A.; Asselberghs, I.; De Gendt, S.; De Feyter, S. Toward tunable doping in graphene FETs by molecular self-assembled monolayers. *Nanoscale* **2013,** *5* (20), 9640-9644.
(323) He, D.; Zhang, Y.; Wu, Q.; Xu, R.; Nan, H.; Liu, J.; Yao, J.; Wang, Z.; Yuan, S.; Li, Y.et al. Two-dimensional quasi-freestanding molecular crystals for high-performance organic field-effect transistors. *Nat. Commun.* **2014,** *5* (1), 5162.
(324) Wang, J.; Yu, H.; Zhou, X.; Liu, X.; Zhang, R.; Lu, Z.; Zheng, J.; Gu, L.; Liu, K.; Wang, D.et al. Probing the Crystallographic Orientation of Two-Dimensional Atomic Crystals with Supramolecular Self-Assembly. *Nat. Commun.* **2017,** *8* (1), 377.
(325) Davis, T. C.; Russell, S. R.; Claridge, S. A. Edge-on adsorption of multi-chain functional alkanes stabilizes noncovalent monolayers on MoS_2. *Chem. Commun.* **2018,** *54* (83), 11709-11712.
(326) Koma, A. Van der Waals epitaxy—a new epitaxial growth method for a highly lattice-mismatched system. *Thin Solid Films* **1992,** *216* (1), 72-76.
(327) Jang, A. R.; Jeon, E. K.; Kang, D.; Kim, G.; Kim, B.-S.; Kang, D. J.; Shin, H. S. Reversibly Light-Modulated Dirac Point of Graphene Functionalized with Spiropyran. *ACS Nano* **2012,** *6* (10), 9207-9213.
(328) Kim, M.; Safron, N. S.; Huang, C.; Arnold, M. S.; Gopalan, P. Light-Driven Reversible Modulation of Doping in Graphene. *Nano Lett.* **2012,** *12* (1), 182-187.
(329) Burzurí, E.; García-Fuente, A.; García-Suárez, V.; Senthil Kumar, K.; Ruben, M.; Ferrer, J.; van der Zant, H. S. J. Spin-state dependent conductance switching in single molecule-graphene junctions. *Nanoscale* **2018,** *10* (17), 7905-7911.
(330) Cervetti, C.; Rettori, A.; Pini, M. G.; Cornia, A.; Repollés, A.; Luis, F.; Dressel, M.; Rauschenbach, S.; Kern, K.; Burghard, M.et al. The classical and quantum dynamics of molecular spins on graphene. *Nat. Mater.* **2016,** *15* (2), 164-168.
(331) Yu, Y.-J.; Lee, G.-H.; Choi, J. I.; Shim, Y. S.; Lee, C.-H.; Kang, S. J.; Lee, S.; Rim, K. T.; Flynn, G. W.; Hone, J.et al. Epitaxially Self-Assembled Alkane Layers for Graphene Electronics. *Adv. Mater.* **2017,** *29* (5), 1603925.
(332) Wehling, T. O.; Lichtenstein, A. I.; Katsnelson, M. I. First-principles studies of water adsorption on graphene: The role of the substrate. *Appl. Phys. Lett.* **2008,** *93* (20), 202110.
(333) Stoeckel, M.-A.; Gobbi, M.; Leydecker, T.; Wang, Y.; Eredia, M.; Bonacchi, S.; Verucchi, R.; Timpel, M.; Nardi, M. V.; Orgiu, E.et al. Boosting and Balancing Electron and Hole Mobility in Single- and Bilayer WSe_2 Devices via Tailored Molecular Functionalization. *ACS Nano* **2019,** *13* (10), 11613-11622.
(334) Yu, Y.-J.; Zhao, Y.; Ryu, S.; Brus, L. E.; Kim, K. S.; Kim, P. Tuning the Graphene Work Function by Electric Field Effect. *Nano Lett.* **2009,** *9* (10), 3430-3434.
(335) Sojoudi, H.; Baltazar, J.; Tolbert, L. M.; Henderson, C. L.; Graham, S. Creating Graphene

p–n Junctions Using Self-Assembled Monolayers. *ACS Appl. Mater. Interfaces* **2012,** *4* (9), 4781-4786.
(336) Mahmood, A.; Yang, C.-S.; Jang, S.; Routaboul, L.; Chang, H.; Ghisolfi, A.; Braunstein, P.; Bernard, L.; Verduci, T.; Dayen, J.-F.et al. Tuning graphene transistors through ad hoc electrostatics induced by a nanometer-thick molecular underlayer. *Nanoscale* **2019,** *11* (42), 19705-19712.
(337) Yokota, K.; Takai, K.; Enoki, T. Carrier Control of Graphene Driven by the Proximity Effect of Functionalized Self-assembled Monolayers. *Nano Lett.* **2011,** *11* (9), 3669-3675.
(338) Yan, Z.; Sun, Z.; Lu, W.; Yao, J.; Zhu, Y.; Tour, J. M. Controlled Modulation of Electronic Properties of Graphene by Self-Assembled Monolayers on SiO_2 Substrates. *ACS Nano* **2011,** *5* (2), 1535-1540.
(339) Ulman, A. Formation and Structure of Self-Assembled Monolayers. *Chem. Rev.* **1996,** *96* (4), 1533-1554.
(340) Lee, B.; Chen, Y.; Duerr, F.; Mastrogiovanni, D.; Garfunkel, E.; Andrei, E. Y.; Podzorov, V. Modification of Electronic Properties of Graphene with Self-Assembled Monolayers. *Nano Lett.* **2010,** *10* (7), 2427-2432.
(341) Artel, V.; Guo, Q.; Cohen, H.; Gasper, R.; Ramasubramaniam, A.; Xia, F.; Naveh, D. Protective molecular passivation of black phosphorus. *npj 2D Mater. Appl.* **2017,** *1* (1), 6.
(342) Kang, D.-H.; Kim, M.-S.; Shim, J.; Jeon, J.; Park, H.-Y.; Jung, W.-S.; Yu, H.-Y.; Pang, C.-H.; Lee, S.; Park, J.-H. High-Performance Transition Metal Dichalcogenide Photodetectors Enhanced by Self-Assembled Monolayer Doping. *Adv. Funct. Mater.* **2015,** *25* (27), 4219-4227.
(343) Calavalle, F.; Dreher, P.; Surdendran, A. P.; Wan, W.; Timpel, M.; Verucchi, R.; Rogero, C.; Bauch, T.; Lombardi, F.; Casanova, F.et al. Tailoring Superconductivity in Large-Area Single-Layer $NbSe_2$ via Self-Assembled Molecular Adlayers. *Nano Lett.* **2021,** *21* (1), 136-143.
(344) Chen, W.; Chen, S.; Qi, D. C.; Gao, X. Y.; Wee, A. T. S. Surface Transfer p-Type Doping of Epitaxial Graphene. *J. Am. Chem. Soc.* **2007,** *129* (34), 10418-10422.
(345) Brülls, S. M.; Cantatore, V.; Wang, Z.; Tam, P. L.; Malmberg, P.; Stubbe, J.; Sarkar, B.; Panas, I.; Mårtensson, J.; Eigler, S. Evidence for Electron Transfer between Graphene and Non-Covalently Bound π-Systems. *Chem. Eur. J.* **2020,** *26* (29), 6694-6702.
(346) Yarali, M.; Zhong, Y.; Reed, S. N.; Wang, J.; Ulman, K. A.; Charboneau, D. J.; Curley, J. B.; Hynek, D. J.; Pondick, J. V.; Yazdani, S.et al. Near-Unity Molecular Doping Efficiency in Monolayer MoS_2. *Adv. Electron. Mater.* **2021,** *7* (2), 2000873.
(347) Coletti, C.; Riedl, C.; Lee, D. S.; Krauss, B.; Patthey, L.; von Klitzing, K.; Smet, J. H.; Starke, U. Charge neutrality and band-gap tuning of epitaxial graphene on SiC by molecular doping. *Phys. Rev. B* **2010,** *81* (23), 235401.
(348) He, H.; Kim, K. H.; Danilov, A.; Montemurro, D.; Yu, L.; Park, Y. W.; Lombardi, F.; Bauch, T.; Moth-Poulsen, K.; Iakimov, T.et al. Uniform doping of graphene close to the Dirac point by polymer-assisted assembly of molecular dopants. *Nat. Commun.* **2018,** *9* (1), 3956.
(349) Pinto, H.; Jones, R.; Goss, J. P.; Briddon, P. R. p-type doping of graphene with F4-TCNQ. *J. Phys.: Condens. Matter* **2009,** *21* (40), 402001.
(350) Wang, J.; Ji, Z.; Yang, G.; Chuai, X.; Liu, F.; Zhou, Z.; Lu, C.; Wei, W.; Shi, X.; Niu, J.et al. Charge Transfer within the F_4TCNQ-MoS_2 van der Waals Interface: Toward Electrical Properties Tuning and Gas Sensing Application. *Adv. Funct. Mater.* **2018,** *28* (51), 1806244.
(351) Li, Z.; Bretscher, H.; Zhang, Y.; Delport, G.; Xiao, J.; Lee, A.; Stranks, S. D.; Rao, A.

Mechanistic Insight to the Chemical Treatments of Monolayer Transition Metal Disulfides for Photoluminescence Enhancement. *arXiv* **2020**, 2009.11123.

(352) Yu, W. J.; Liao, L.; Chae, S. H.; Lee, Y. H.; Duan, X. Toward Tunable Band Gap and Tunable Dirac Point in Bilayer Graphene with Molecular Doping. *Nano Lett*. **2011,** *11* (11), 4759-4763.

(353) Greulich, K.; Belser, A.; Bölke, S.; Grüninger, P.; Karstens, R.; Sättele, M. S.; Ovsyannikov, R.; Giangrisostomi, E.; Basova, T. V.; Klyamer, D.et al. Charge Transfer from Organic Molecules to Molybdenum Disulfide: Influence of the Fluorination of Iron Phthalocyanine. *J. Phys. Chem. C* **2020,** *124* (31), 16990-16999.

(354) Wang, Y.; Slassi, A.; Cornil, J.; Beljonne, D.; Samorì, P. Tuning the Optical and Electrical Properties of Few-Layer Black Phosphorus via Physisorption of Small Solvent Molecules. *Small* **2019,** *15* (47), 1903432.

(355) Rijal, K.; Rudayni, F.; Kafle, T. R.; Chan, W.-L. Collective Effects of Band Offset and Wave Function Dimensionality on Impeding Electron Transfer from 2D to Organic Crystals. *J. Phys. Chem. Lett*. **2020,** *11* (18), 7495-7501.

(356) Tebyetekerwa, M.; Cheng, Y.; Zhang, J.; Li, W.; Li, H.; Neupane, G. P.; Wang, B.; Truong, T. N.; Xiao, C.; Al-Jassim, M. M.et al. Emission Control from Transition Metal Dichalcogenide Monolayers by Aggregation-Induced Molecular Rotors. *ACS Nano* **2020,** *14* (6), 7444-7453.

(357) Kappera, R.; Voiry, D.; Yalcin, S. E.; Branch, B.; Gupta, G.; Mohite, A. D.; Chhowalla, M. Phase-engineered low-resistance contacts for ultrathin MoS_2 transistors. *Nat. Mater.* **2014,** *13* (12), 1128-1134.

(358) Kappera, R.; Voiry, D.; Yalcin, S. E.; Jen, W.; Acerce, M.; Torrel, S.; Branch, B.; Lei, S.; Chen, W.; Najmaei, S.et al. Metallic 1T phase source/drain electrodes for field effect transistors from chemical vapor deposited MoS_2. *APL Mater.* **2014,** *2* (9), 092516.

(359) Wan, J.; Lacey, S. D.; Dai, J.; Bao, W.; Fuhrer, M. S.; Hu, L. Tuning two-dimensional nanomaterials by intercalation: materials, properties and applications. *Chem. Soc. Rev.* **2016,** *45* (24), 6742-6765.

(360) Huang, Y.; Liang, J.; Wang, C.; Yin, S.; Fu, W.; Zhu, H.; Wan, C. Hybrid superlattices of two-dimensional materials and organics. *Chem. Soc. Rev.* **2020,** *49* (19), 6866-6883.

(361) Rajapakse, M.; Karki, B.; Abu, U. O.; Pishgar, S.; Musa, M. R. K.; Riyadh, S. M. S.; Yu, M.; Sumanasekera, G.; Jasinski, J. B. Intercalation as a versatile tool for fabrication, property tuning, and phase transitions in 2D materials. *npj 2D Mater. Appl*. **2021,** *5* (1), 30.

(362) Cao, Q.; Grote, F.; Huβmann, M.; Eigler, S. Emerging field of few-layered intercalated 2D materials. *Nanoscale Adv.* **2021,** *3* (4), 963-982.

(363) Wang, C.; He, Q.; Halim, U.; Liu, Y.; Zhu, E.; Lin, Z.; Xiao, H.; Duan, X.; Feng, Z.; Cheng, R.et al. Monolayer atomic crystal molecular superlattices. *Nature* **2018,** *555* (7695), 231-236.

(364) Wang, N.; Tang, H.; Shi, M.; Zhang, H.; Zhuo, W.; Liu, D.; Meng, F.; Ma, L.; Ying, J.; Zou, L.et al. Transition from Ferromagnetic Semiconductor to Ferromagnetic Metal with Enhanced Curie Temperature in $Cr_2Ge_2Te_6$ via Organic Ion Intercalation. *J. Am. Chem. Soc*. **2019,** *141* (43), 17166-17173.

(365) Ma, L. K.; Shi, M. Z.; Kang, B. L.; Peng, K. L.; Meng, F. B.; Zhu, C. S.; Cui, J. H.; Sun, Z. L.; Ma, D. H.; Wang, H. H.et al. Quasi-two-dimensional superconductivity in $SnSe_2$ via organic ion intercalation. *Phys. Rev. Mater.* **2020,** *4* (12), 124803.

(366) He, Q.; Lin, Z.; Ding, M.; Yin, A.; Halim, U.; Wang, C.; Liu, Y.; Cheng, H.-C.; Huang, Y.;

Duan, X. In Situ Probing Molecular Intercalation in Two-Dimensional Layered Semiconductors. *Nano Lett*. **2019,** *19* (10), 6819-6826.
(367) Dresselhaus, M. S. *Intercalation in layered materials*; Plenum published in cooperation with NATO Scientific Affairs Division: New York ; London, 1986.
(368) Lu, J.; Carvalho, A.; Chan, X. K.; Liu, H.; Liu, B.; Tok, E. S.; Loh, K. P.; Castro Neto, A. H.; Sow, C. H. Atomic Healing of Defects in Transition Metal Dichalcogenides. *Nano Lett*. **2015,** *15* (5), 3524-3532.
(369) Barja, S.; Refaely-Abramson, S.; Schuler, B.; Qiu, D. Y.; Pulkin, A.; Wickenburg, S.; Ryu, H.; Ugeda, M. M.; Kastl, C.; Chen, C.et al. Identifying substitutional oxygen as a prolific point defect in monolayer transition metal dichalcogenides. *Nat. Commun*. **2019,** *10* (1), 3382.
(370) Greben, K.; Kovalchuk, S.; Valencia, A. M.; Kirchhof, J. N.; Heeg, S.; Rietsch, P.; Reich, S.; Cocchi, C.; Eigler, S.; Bolotin, K. I. In situ functionalization of graphene. *2D Mater.* **2020,** *8* (1), 015022.
(371) Qiu, H.; Xu, T.; Wang, Z.; Ren, W.; Nan, H.; Ni, Z.; Chen, Q.; Yuan, S.; Miao, F.; Song, F.et al. Hopping transport through defect-induced localized states in molybdenum disulphide. *Nat. Commun*. **2013,** *4*, 2642.
(372) Zhao, Q.; Wang, W.; Carrascoso-Plana, F.; Jie, W.; Wang, T.; Castellanos-Gomez, A.; Frisenda, R. The role of traps in the photocurrent generation mechanism in thin InSe photodetectors. *Mater. Horiz*. **2020,** *7* (1), 252-262.
(373) Cai, Z.; Liu, B.; Zou, X.; Cheng, H.-M. Chemical Vapor Deposition Growth and Applications of Two-Dimensional Materials and Their Heterostructures. *Chem. Rev*. **2018,** *118* (13), 6091-6133.
(374) Bonaccorso, F.; Bartolotta, A.; Coleman, J. N.; Backes, C. 2D-Crystal-Based Functional Inks. *Adv. Mater.* **2016,** *28* (29), 6136-6166.
(375) Han, H.-V.; Lu, A.-Y.; Lu, L.-S.; Huang, J.-K.; Li, H.; Hsu, C.-L.; Lin, Y.-C.; Chiu, M.-H.; Suenaga, K.; Chu, C.-W.et al. Photoluminescence Enhancement and Structure Repairing of Monolayer $MoSe_2$ by Hydrohalic Acid Treatment. *ACS Nano* **2016,** *10* (1), 1454-1461.
(376) Hirsch, A.; Hauke, F. Post-Graphene 2D Chemistry: The Emerging Field of Molybdenum Disulfide and Black Phosphorus Functionalization. *Angew. Chem., Int. Ed*. **2018,** *57* (16), 4338-4354.
(377) Bertolazzi, S.; Gobbi, M.; Zhao, Y.; Backes, C.; Samorì, P. Molecular chemistry approaches for tuning the properties of two-dimensional transition metal dichalcogenides. *Chem. Soc. Rev*. **2018,** *47* (17), 6845-6888.
(378) Greben, K.; Arora, S.; Harats, M. G.; Bolotin, K. I. Intrinsic and Extrinsic Defect-Related Excitons in TMDCs. *Nano Lett*. **2020,** *20* (4), 2544-2550.
(379) Cho, K.; Min, M.; Kim, T.-Y.; Jeong, H.; Pak, J.; Kim, J.-K.; Jang, J.; Yun, S. J.; Lee, Y. H.; Hong, W.-K.et al. Electrical and Optical Characterization of MoS_2 with Sulfur Vacancy Passivation by Treatment with Alkanethiol Molecules. *ACS Nano* **2015,** *9* (8), 8044-8053.
(380) Chou, S. S.; De, M.; Kim, J.; Byun, S.; Dykstra, C.; Yu, J.; Huang, J.; Dravid, V. P. Ligand Conjugation of Chemically Exfoliated MoS_2. *J. Am. Chem. Soc*. **2013,** *135* (12), 4584-4587.
(381) Kim, J.-S.; Yoo, H.-W.; Choi, H. O.; Jung, H.-T. Tunable Volatile Organic Compounds Sensor by Using Thiolated Ligand Conjugation on MoS_2. *Nano Lett*. **2014,** *14* (10), 5941-5947.
(382) Presolski, S.; Wang, L.; Loo, A. H.; Ambrosi, A.; Lazar, P.; Ranc, V.; Otyepka, M.; Zboril, R.; Tomanec, O.; Ugolotti, J.et al. Functional Nanosheet Synthons by Covalent

Modification of Transition-Metal Dichalcogenides. *Chem. Mater.* **2017,** *29* (5), 2066-2073.
(383) Liu, Y.; Stradins, P.; Wei, S.-H. Air Passivation of Chalcogen Vacancies in Two-Dimensional Semiconductors. *Angew. Chem., Int. Ed.* **2016,** *55* (3), 965-968.
(384) Zhao, P.; Kiriya, D.; Azcatl, A.; Zhang, C.; Tosun, M.; Liu, Y.-S.; Hettick, M.; Kang, J. S.; McDonnell, S.; Santosh, K. C.et al. Air Stable p-Doping of WSe_2 by Covalent Functionalization. *ACS Nano* **2014,** *8* (10), 10808-10814.
(385) Yang, L.; Majumdar, K.; Liu, H.; Du, Y.; Wu, H.; Hatzistergos, M.; Hung, P. Y.; Tieckelmann, R.; Tsai, W.; Hobbs, C.et al. Chloride Molecular Doping Technique on 2D Materials: WS_2 and MoS_2. *Nano Lett.* **2014,** *14* (11), 6275-6280.
(386) Paulus, G. L. C.; Wang, Q. H.; Strano, M. S. Covalent Electron Transfer Chemistry of Graphene with Diazonium Salts. *Acc. Chem. Res.* **2013,** *46* (1), 160-170.
(387) Knirsch, K. C.; Berner, N. C.; Nerl, H. C.; Cucinotta, C. S.; Gholamvand, Z.; McEvoy, N.; Wang, Z.; Abramovic, I.; Vecera, P.; Halik, M.et al. Basal-plane functionalization of chemically exfoliated molybdenum disulfide by diazonium salts. *ACS Nano* **2015,** *9* (6), 6018-6030.
(388) Wang, Q. H.; Jin, Z.; Kim, K. K.; Hilmer, A. J.; Paulus, G. L. C.; Shih, C.-J.; Ham, M.-H.; Sanchez-Yamagishi, J. D.; Watanabe, K.; Taniguchi, T.et al. Understanding and controlling the substrate effect on graphene electron-transfer chemistry via reactivity imprint lithography. *Nat. Chem.* **2012,** *4* (9), 724-732.
(389) Shih, C.-J.; Wang, Q. H.; Jin, Z.; Paulus, G. L. C.; Blankschtein, D.; Jarillo-Herrero, P.; Strano, M. S. Disorder Imposed Limits of Mono- and Bilayer Graphene Electronic Modification Using Covalent Chemistry. *Nano Lett.* **2013,** *13* (2), 809-817.
(390) Voiry, D.; Goswami, A.; Kappera, R.; Silva, C. d. C. C. e.; Kaplan, D.; Fujita, T.; Chen, M.; Asefa, T.; Chhowalla, M. Covalent functionalization of monolayered transition metal dichalcogenides by phase engineering. *Nat. Chem.* **2015,** *7* (1), 45-49.
(391) Canton-Vitoria, R.; Scharl, T.; Stergiou, A.; Cadranel, A.; Arenal, R.; Guldi, D. M.; Tagmatarchis, N. Ping-Pong Energy Transfer in Covalently Linked Porphyrin-MoS_2 Architectures. *Angew. Chem., Int. Ed.* **2020,** *59* (10), 3976-3981.
(392) Villalva, J.; Moreno-Da Silva, S.; Villa, P.; Ruiz-González, L.; Navío, C.; Garcia-Orrit, S.; Vega-Mayoral, V.; Cabanillas-González, J.; Castellanos-Gomez, A.; Giovanelli, E.et al. Covalent modification of franckeite with maleimides: connecting molecules and van der Waals heterostructures. *Nanoscale Horiz.* **2021,** *6* (7), 551-558.
(393) Morant-Giner, M.; Sanchis-Gual, R.; Romero, J.; Alberola, A.; García-Cruz, L.; Agouram, S.; Galbiati, M.; Padial, N. M.; Waerenborgh, J. C.; Martí-Gastaldo, C.et al. Prussian Blue@MoS_2 Layer Composites as Highly Efficient Cathodes for Sodium- and Potassium-Ion Batteries. *Adv. Funct. Mater.* **2018,** *28* (27), 1706125.
(394) Gómez-Muñoz, I.; Laghouati, S.; Torres-Cavanillas, R.; Morant-Giner, M.; Vassilyeva, N. V.; Forment-Aliaga, A.; Giménez-Marqués, M. Fast Polymeric Functionalization Approach for the Covalent Coating of MoS_2 Layers. *ACS Appl. Mater. Interfaces* **2021,** *13* (30), 36475-36481.
(395) Lihter, M.; Graf, M.; Iveković, D.; Zhang, M.; Shen, T.-H.; Zhao, Y.; Macha, M.; Tileli, V.; Radenovic, A. Electrochemical Functionalization of Selectively Addressed MoS_2 Nanoribbons for Sensor Device Fabrication. *ACS Appl. Nano Mater.* **2021,** *4* (2), 1076-1084.
(396) Peimyoo, N.; Yang, W.; Shang, J.; Shen, X.; Wang, Y.; Yu, T. Chemically Driven Tunable Light Emission of Charged and Neutral Excitons in Monolayer WS_2. *ACS Nano* **2014,** *8*

(11), 11320-11329.
(397) Island, J. O.; Holovchenko, A.; Koole, M.; Alkemade, P. F.; Menelaou, M.; Aliaga-Alcalde, N.; Burzurí, E.; van der Zant, H. S. Fabrication of hybrid molecular devices using multi-layer graphene break junctions. *J. Phys. Condens. Matter.* **2014,** *26* (47), 474205.
(398) Molina-Mendoza, A. J.; Vaquero-Garzon, L.; Leret, S.; de Juan-Fernández, L.; Pérez, E. M.; Castellanos-Gomez, A. Engineering the optoelectronic properties of MoS_2 photodetectors through reversible noncovalent functionalization. *Chem. Commun.* **2016,** *52* (100), 14365-14368.
(399) Park, H.-Y.; Dugasani, S. R.; Kang, D.-H.; Yoo, G.; Kim, J.; Gnapareddy, B.; Jeon, J.; Kim, M.; Song, Y. J.; Lee, S.et al. M-DNA/Transition Metal Dichalcogenide Hybrid Structure-based Bio-FET sensor with Ultra-high Sensitivity. *Sci. Rep.* **2016,** *6* (1), 35733.
(400) de la Rosa, C. J. L.; Phillipson, R.; Teyssandier, J.; Adisoejoso, J.; Balaji, Y.; Huyghebaert, C.; Radu, I.; Heyns, M.; De Feyter, S.; De Gendt, S. Molecular doping of MoS_2 transistors by self-assembled oleylamine networks. *Appl. Phys. Lett.* **2016,** *109* (25), 253112.
(401) Tarasov, A.; Zhang, S.; Tsai, M.-Y.; Campbell, P. M.; Graham, S.; Barlow, S.; Marder, S. R.; Vogel, E. M. Controlled Doping of Large-Area Trilayer MoS_2 with Molecular Reductants and Oxidants. *Adv. Mater.* **2015,** *27* (7), 1175-1181.
(402) Benjamin, C. J.; Zhang, S.; Chen, Z. Controlled doping of transition metal dichalcogenides by metal work function tuning in phthalocyanine compounds. *Nanoscale* **2018,** *10* (11), 5148-5153.
(403) Huang, Y.; Zhuge, F.; Hou, J.; Lv, L.; Luo, P.; Zhou, N.; Gan, L.; Zhai, T. Van der Waals coupled organic molecules with monolayer MoS_2 for fast response photodetectors with gate-tunable responsivity. *ACS Nano* **2018,** *12* (4), 4062–4073.
(404) Su, W.; Jin, L.; Qu, X.; Huo, D.; Yang, L. Defect passivation induced strong photoluminescence enhancement of rhombic monolayer MoS_2. *Phys. Chem. Chem. Phys.* **2016,** *18* (20), 14001-14006.
(405) Amsterdam, S. H.; Stanev, T. K.; Zhou, Q.; Lou, A. J. T.; Bergeron, H.; Darancet, P.; Hersam, M. C.; Stern, N. P.; Marks, T. J. Electronic Coupling in Metallophthalocyanine–Transition Metal Dichalcogenide Mixed-Dimensional Heterojunctions. *ACS Nano* **2019,** *13* (4), 4183-4190.
(406) Park, J. H.; Sanne, A.; Guo, Y.; Amani, M.; Zhang, K.; Movva, H. C. P.; Robinson, J. A.; Javey, A.; Robertson, J.; Banerjee, S. K.et al. Defect passivation of transition metal dichalcogenides via a charge transfer van der Waals interface. *Sci. Adv.* **2017,** *3* (10), e1701661.
(407) Kafle, T. R.; Kattel, B.; Yao, P.; Zereshki, P.; Zhao, H.; Chan, W.-L. Effect of the Interfacial Energy Landscape on Photoinduced Charge Generation at the ZnPc/MoS_2 Interface. *J. Am. Chem. Soc.* **2019,** *141* (28), 11328-11336.
(408) Ciesielski, A.; Haar, S.; El Gemayel, M.; Yang, H.; Clough, J.; Melinte, G.; Gobbi, M.; Orgiu, E.; Nardi, M. V.; Ligorio, G.et al. Harnessing the Liquid-Phase Exfoliation of Graphene Using Aliphatic Compounds: A Supramolecular Approach. *Angew. Chem., Int. Ed.* **2014,** *53* (39), 10355-10361.
(409) Hu, G.; Kang, J.; Ng, L. W. T.; Zhu, X.; Howe, R. C. T.; Jones, C. G.; Hersam, M. C.; Hasan, T. Functional inks and printing of two-dimensional materials. *Chem. Soc. Rev.* **2018,** *47* (9), 3265-3300.
(410) Kelly, A. G.; Hallam, T.; Backes, C.; Harvey, A.; Esmaeily, A. S.; Godwin, I.; Coelho, J.; Nicolosi, V.; Lauth, J.; Kulkarni, A.et al. All-printed thin-film transistors from networks of

liquid-exfoliated nanosheets. *Science* **2017,** *356* (6333), 69-73.
(411) McManus, D.; Vranic, S.; Withers, F.; Sanchez-Romaguera, V.; Macucci, M.; Yang, H.; Sorrentino, R.; Parvez, K.; Son, S.-K.; Iannaccone, G.et al. Water-based and biocompatible 2D crystal inks for all-inkjet-printed heterostructures. *Nat. Nanotechnol.* **2017,** *12* (4), 343-350.
(412) Frank, D. J.; Taur, Y.; Wong, H. P. Generalized scale length for two-dimensional effects in MOSFETs. *IEEE Electron Device Lett.* **1998,** *19* (10), 385-387.
(413) English, C. D.; Smithe, K. K. H.; Xu, R. L.; Pop, E. 2016 IEEE International Electron Devices Meeting (IEDM), 2016; p 5.6.1-5.6.4.
(414) Schwierz, F.; Pezoldt, J.; Granzner, R. Two-dimensional materials and their prospects in transistor electronics. *Nanoscale* **2015,** *7* (18), 8261-8283.
(415) Komsa, H.-P.; Kurasch, S.; Lehtinen, O.; Kaiser, U.; Krasheninnikov, A. V. From point to extended defects in two-dimensional MoS_2: Evolution of atomic structure under electron irradiation. *Phys. Rev. B* **2013,** *88* (3), 035301.
(416) Kim, E.; Ko, C.; Kim, K.; Chen, Y.; Suh, J.; Ryu, S.-G.; Wu, K.; Meng, X.; Suslu, A.; Tongay, S.et al. Site Selective Doping of Ultrathin Metal Dichalcogenides by Laser-Assisted Reaction. *Adv. Mater.* **2016,** *28* (2), 341-346.
(417) Li, H.-M.; Lee, D.; Qu, D.; Liu, X.; Ryu, J.; Seabaugh, A.; Yoo, W. J. Ultimate thin vertical p–n junction composed of two-dimensional layered molybdenum disulfide. *Nat. Commun.* **2015,** *6*, 6564.
(418) Huo, N.; Konstantatos, G. Ultrasensitive all-2D MoS_2 phototransistors enabled by an out-of-plane MoS_2 PN homojunction. *Nat. Commun.* **2017,** *8* (1), 572.
(419) Ji, H. G.; Solís-Fernández, P.; Yoshimura, D.; Maruyama, M.; Endo, T.; Miyata, Y.; Okada, S.; Ago, H. Chemically Tuned p- and n-Type WSe_2 Monolayers with High Carrier Mobility for Advanced Electronics. *Adv. Mater.* **2019,** *31* (42), 1903613.
(420) Choi, M. S.; Qu, D.; Lee, D.; Liu, X.; Watanabe, K.; Taniguchi, T.; Yoo, W. J. Lateral MoS_2 p–n Junction Formed by Chemical Doping for Use in High-Performance Optoelectronics. *ACS Nano* **2014,** *8* (9), 9332-9340.
(421) Sun, M.; Xie, D.; Sun, Y.; Li, W.; Ren, T. Locally hydrazine doped WSe_2 p-n junction toward high-performance photodetectors. *Nanotechnology* **2018,** *29* (1), 015203.
(422) Sun, J.; Wang, Y.; Guo, S.; Wan, B.; Dong, L.; Gu, Y.; Song, C.; Pan, C.; Zhang, Q.; Gu, L.et al. Lateral 2D WSe_2 p–n Homojunction Formed by Efficient Charge-Carrier-Type Modulation for High-Performance Optoelectronics. *Adv. Mater.* **2020,** *32* (9), 1906499.
(423) Iqbal, M. W.; Iqbal, M. Z.; Khan, M. F.; Shehzad, M. A.; Seo, Y.; Eom, J. Deep-ultraviolet-light-driven reversible doping of WS2 field-effect transistors. *Nanoscale* **2015,** *7* (2), 747-757.
(424) Aftab, S.; Samiya, M.; Raza, A.; Iqbal, M. W.; Haque, H. M. U.; Ramachandraiah, K.; Yousuf, S.; Jun, S. C.; Rehman, A. U.; Iqbal, M. Z. A reversible and stable doping technique to invert the carrier polarity of $MoTe_2$. *Nanotechnology* **2021,** *32* (28), 285701.
(425) Das, S.; Chen, H.-Y.; Penumatcha, A. V.; Appenzeller, J. High Performance Multilayer MoS_2 Transistors with Scandium Contacts. *Nano Lett.* **2013,** *13* (1), 100-105.
(426) Sze, S. M.; Ng, K. K. In *Physics of Semiconductor Devices*; John Wiley & Sons, Inc., 2006.
(427) Ma, Y.; Liu, B.; Zhang, A.; Chen, L.; Fathi, M.; Shen, C.; Abbas, A. N.; Ge, M.; Mecklenburg, M.; Zhou, C. Reversible Semiconducting-to-Metallic Phase Transition in Chemical Vapor Deposition Grown Monolayer WSe_2 and Applications for Devices. *ACS Nano* **2015,** *9* (7), 7383-7391.

(428) Mayorga-Martinez, C. C.; Ambrosi, A.; Eng, A. Y. S.; Sofer, Z.; Pumera, M. Metallic 1T-WS_2 for Selective Impedimetric Vapor Sensing. *Adv. Funct. Mater.* **2015,** *25* (35), 5611-5616.
(429) Wang, J.; Yao, Q.; Huang, C.-W.; Zou, X.; Liao, L.; Chen, S.; Fan, Z.; Zhang, K.; Wu, W.; Xiao, X.et al. High Mobility MoS_2 Transistor with Low Schottky Barrier Contact by Using Atomic Thick h-BN as a Tunneling Layer. *Adv. Mater.* **2016,** *28* (37), 8302-8308.
(430) Chen, J.-R.; Odenthal, P. M.; Swartz, A. G.; Floyd, G. C.; Wen, H.; Luo, K. Y.; Kawakami, R. K. Control of Schottky Barriers in Single Layer MoS_2 Transistors with Ferromagnetic Contacts. *Nano Lett.* **2013,** *13* (7), 3106-3110.
(431) Lee, S.; Tang, A.; Aloni, S.; Wong, H. S. P. Statistical Study on the Schottky Barrier Reduction of Tunneling Contacts to CVD Synthesized MoS_2. *Nano Lett.* **2016,** *16* (1), 276-281.
(432) Cho, K.; Pak, J.; Kim, J.-K.; Kang, K.; Kim, T.-Y.; Shin, J.; Choi, B. Y.; Chung, S.; Lee, T. Contact-Engineered Electrical Properties of MoS_2 Field-Effect Transistors via Selectively Deposited Thiol-Molecules. *Adv. Mater.* **2018,** *30* (18), 1705540.
(433) Liu, Y.; Guo, J.; Zhu, E.; Liao, L.; Lee, S.-J.; Ding, M.; Shakir, I.; Gambin, V.; Huang, Y.; Duan, X. Approaching the Schottky–Mott Limit in van der Waals Metal–Semiconductor Junctions. *Nature* **2018,** *557* (7707), 696-700.
(434) Wang, Y.; Kim, J. C.; Wu, R. J.; Martinez, J.; Song, X.; Yang, J.; Zhao, F.; Mkhoyan, A.; Jeong, H. Y.; Chhowalla, M. Van der Waals contacts between three-dimensional metals and two-dimensional semiconductors. *Nature* **2019,** *568* (7750), 70-74.
(435) Li, X.; Mullen, J. T.; Jin, Z.; Borysenko, K. M.; Nardelli, M. B.; Kim, K. W. Intrinsic electrical transport properties of monolayer silicene and MoS_2 from first principles. *Phys. Rev. B* **2013,** *87* (11), 115418.
(436) Kaasbjerg, K.; Thygesen, K. S.; Jacobsen, K. W. Phonon-limited mobility in n-type single-layer MoS_2 from first principles. *Phys. Rev. B* **2012,** *85* (11), 115317.
(437) Radisavljevic, B.; Kis, A. Mobility engineering and a metal-insulator transition in monolayer MoS_2. *Nat. Mater.* **2013,** *12* (9), 815-820.
(438) Schmidt, H.; Wang, S.; Chu, L.; Toh, M.; Kumar, R.; Zhao, W.; Neto, A. H. C.; Martin, J.; Adam, S.; Oezyilmaz, B.et al. Transport Properties of Monolayer MoS_2 Grown by Chemical Vapor Deposition. *Nano Lett.* **2014,** *14* (4), 1909-1913.
(439) Liu, H.; Si, M.; Najmaei, S.; Neal, A. T.; Du, Y.; Ajayan, P. M.; Lou, J.; Ye, P. D. Statistical Study of Deep Submicron Dual-Gated Field-Effect Transistors on Monolayer Chemical Vapor Deposition Molybdenum Disulfide Films. *Nano Lett.* **2013,** *13* (6), 2640-2646.
(440) Dean, C. R.; Young, A. F.; Meric, I.; Lee, C.; Wang, L.; Sorgenfrei, S.; Watanabe, K.; Taniguchi, T.; Kim, P.; Shepard, K. L.et al. Boron nitride substrates for high-quality graphene electronics. *Nat. Nanotechnol.* **2010,** *5* (10), 722-726.
(441) Radisavljevic, B.; Kis, A. Mobility engineering and a metal–insulator transition in monolayer MoS2. *Nat. Mater.* **2013,** *12* (9), 815-820.
(442) Chen, J. H.; Jang, C.; Adam, S.; Fuhrer, M. S.; Williams, E. D.; Ishigami, M. Charged-impurity scattering in graphene. *Nat. Phys.* **2008,** *4* (5), 377-381.
(443) Fenglin, W.; Petr, S.; Mason, G.; Chun Ning, L. Annealing and transport studies of suspended molybdenum disulfide devices. *Nanotechnology* **2015,** *26* (10), 105709.
(444) Konar, A.; Fang, T.; Jena, D. Effect of high-kappa gate dielectrics on charge transport in graphene-based field effect transistors. *Phys. Rev. B* **2010,** *82* (11), 115452.
(445) Jena, D.; Konar, A. Enhancement of carrier mobility in semiconductor nanostructures by

dielectric engineering. *Phys. Rev. Lett.* **2007,** *98* (13), 136805.
(446) Kim, S.; Konar, A.; Hwang, W.-S.; Lee, J. H.; Lee, J.; Yang, J.; Jung, C.; Kim, H.; Yoo, J.-B.; Choi, J.-Y.et al. High-mobility and low-power thin-film transistors based on multilayer MoS2 crystals. *Nat. Commun.* **2012,** *3*, 1011.
(447) Najmaei, S.; Zou, X.; Er, D.; Li, J.; Jin, Z.; Gao, W.; Zhang, Q.; Park, S.; Ge, L.; Lei, S.et al. Tailoring the Physical Properties of Molybdenum Disulfide Monolayers by Control of Interfacial Chemistry. *Nano Lett.* **2014,** *14* (3), 1354-1361.
(448) Feng, W.; Zheng, W.; Cao, W.; Hu, P. Back Gated Multilayer InSe Transistors with Enhanced Carrier Mobilities via the Suppression of Carrier Scattering from a Dielectric Interface. *Adv. Mater.* **2014,** *26* (38), 6587-6593.
(449) Wang, Y.; Wang, H.; Gali, S. M.; Turetta, N.; Yao, Y.; Wang, C.; Chen, Y.; Beljonne, D.; Samorì, P. Molecular Doping of 2D Indium Selenide for Ultrahigh Performance and Low-Power Consumption Broadband Photodetectors. *Adv. Funct. Mater.* **2021,** *31* (30), 2103353.
(450) Shokouh, S. H. H.; Jeon, P. J.; Pezeshki, A.; Choi, K.; Lee, H. S.; Kim, J. S.; Park, E. Y.; Im, S. High-Performance, Air-Stable, Top-Gate, p-Channel WSe_2 Field-Effect Transistor with Fluoropolymer Buffer Layer. *Adv. Funct. Mater.* **2015,** *25* (46), 7208-7214.
(451) Li, W.; Zhou, J.; Cai, S.; Yu, Z.; Zhang, J.; Fang, N.; Li, T.; Wu, Y.; Chen, T.; Xie, X.et al. Uniform and ultrathin high-κ gate dielectrics for two-dimensional electronic devices. *Nat. Electron.* **2019,** *2* (12), 563-571.
(452) Zheng, Y.; Ni, G.-X.; Toh, C.-T.; Zeng, M.-G.; Chen, S.-T.; Yao, K.; Özyilmaz, B. Gate-controlled nonvolatile graphene-ferroelectric memory. *Appl. Phys. Lett.* **2009,** *94* (16), 163505.
(453) Ni, G.-X.; Zheng, Y.; Bae, S.; Tan, C. Y.; Kahya, O.; Wu, J.; Hong, B. H.; Yao, K.; Özyilmaz, B. Graphene–Ferroelectric Hybrid Structure for Flexible Transparent Electrodes. *ACS Nano* **2012,** *6* (5), 3935-3942.
(454) Bae, S.-H.; Kahya, O.; Sharma, B. K.; Kwon, J.; Cho, H. J.; Özyilmaz, B.; Ahn, J.-H. Graphene-P(VDF-TrFE) Multilayer Film for Flexible Applications. *ACS Nano* **2013,** *7* (4), 3130-3138.
(455) Wang, X.; Tang, M.; Chen, Y.; Wu, G.; Huang, H.; Zhao, X.; Tian, B.; Wang, J.; Sun, S.; Shen, H.et al. Flexible graphene field effect transistor with ferroelectric polymer gate. *Opt. Quantum Electron.* **2016,** *48* (7), 345.
(456) Lee, H. S.; Min, S.-W.; Park, M. K.; Lee, Y. T.; Jeon, P. J.; Kim, J. H.; Ryu, S.; Im, S. MoS_2 Nanosheets for Top-Gate Nonvolatile Memory Transistor Channel. *Small* **2012,** *8* (20), 3111-3115.
(457) Wang, X.; Wang, P.; Wang, J.; Hu, W.; Zhou, X.; Guo, N.; Huang, H.; Sun, S.; Shen, H.; Lin, T.et al. Ultrasensitive and Broadband MoS_2 Photodetector Driven by Ferroelectrics. *Adv. Mater.* **2015,** *27* (42), 6575-6581.
(458) Xiao, Z.; Song, J.; Ferry, D. K.; Ducharme, S.; Hong, X. Ferroelectric-Domain-Patterning-Controlled Schottky Junction State in Monolayer MoS_2. *Phys. Rev. Lett.* **2017,** *118* (23), 236801.
(459) Lv, L.; Zhuge, F.; Xie, F.; Xiong, X.; Zhang, Q.; Zhang, N.; Huang, Y.; Zhai, T. Reconfigurable two-dimensional optoelectronic devices enabled by local ferroelectric polarization. *Nat. Commun.* **2019,** *10* (1), 3331.
(460) Li, D.; Xiao, Z.; Mu, S.; Wang, F.; Liu, Y.; Song, J.; Huang, X.; Jiang, L.; Xiao, J.; Liu, L.et al. A Facile Space-Confined Solid-Phase Sulfurization Strategy for Growth of High-Quality Ultrathin Molybdenum Disulfide Single Crystals. *Nano Lett.* **2018,** *18* (3), 2021-

2032.
(461) Park, W.; Yang, J. H.; Kang, C. G.; Lee, Y. G.; Hwang, H. J.; Cho, C.; Lim, S. K.; Kang, S. C.; Hong, W.-K.; Lee, S. K.et al. Characteristics of a pressure sensitive touch sensor using a piezoelectric PVDF-TrFE/MoS_2 stack. *Nanotechnology* **2013,** *24* (47), 475501.
(462) McGuire, F. A.; Cheng, Z.; Price, K.; Franklin, A. D. Sub-60 mV/decade switching in 2D negative capacitance field-effect transistors with integrated ferroelectric polymer. *Appl. Phys. Lett.* **2016,** *109* (9), 093101.
(463) Wang, X.; Chen, Y.; Wu, G.; Li, D.; Tu, L.; Sun, S.; Shen, H.; Lin, T.; Xiao, Y.; Tang, M.et al. Two-dimensional negative capacitance transistor with polyvinylidene fluoride-based ferroelectric polymer gating. *npj 2D Mater. Appl.* **2017,** *1* (1), 38.
(464) Liu, X.; Liang, R.; Gao, G.; Pan, C.; Jiang, C.; Xu, Q.; Luo, J.; Zou, X.; Yang, Z.; Liao, L.et al. MoS_2 Negative-Capacitance Field-Effect Transistors with Subthreshold Swing below the Physics Limit. *Adv. Mater.* **2018,** *30* (28), 1800932.
(465) Huang, H.; Wang, X.; Wang, P.; Wu, G.; Chen, Y.; Meng, C.; Liao, L.; Wang, J.; Hu, W.; Shen, H.et al. Ferroelectric polymer tuned two dimensional layered $MoTe_2$ photodetector. *RSC Adv.* **2016,** *6* (90), 87416-87421.
(466) Wu, G.; Wang, X.; Chen, Y.; Wu, S.; Wu, B.; Jiang, Y.; Shen, H.; Lin, T.; Liu, Q.; Wang, X.et al. $MoTe_2$ p–n Homojunctions Defined by Ferroelectric Polarization. *Adv. Mater.* **2020,** *32* (16), 1907937.
(467) Wu, G.; Wang, X.; Chen, Y.; Wu, S.; Shen, H.; Lin, T.; Ge, J.; Hu, W.; Zhang, S.-T.; Meng, X. J.et al. Two-dimensional series connected photovoltaic cells defined by ferroelectric domains. *Appl. Phys. Lett.* **2020,** *116* (7), 073101.
(468) Wu, G.; Tian, B.; Liu, L.; Lv, W.; Wu, S.; Wang, X.; Chen, Y.; Li, J.; Wang, Z.; Wu, S.et al. Programmable transition metal dichalcogenide homojunctions controlled by nonvolatile ferroelectric domains. *Nat. Electron.* **2020,** *3* (1), 43-50.
(469) Wu, G.; Wang, X.; Wang, P.; Huang, H.; Chen, Y.; Sun, S.; Shen, H.; Lin, T.; Wang, J.; Zhang, S.et al. Visible to short wavelength infrared In_2Se_3-nanoflake photodetector gated by a ferroelectric polymer. *Nanotechnology* **2016,** *27* (36), 364002.
(470) Li, D.; Wang, X.; Chen, Y.; Zhu, S.; Gong, F.; Wu, G.; Meng, C.; Liu, L.; Wang, L.; Lin, T.et al. The ambipolar evolution of a high-performance WSe_2 transistor assisted by a ferroelectric polymer. *Nanotechnology* **2018,** *29* (10), 105202.
(471) Qiu, H.; Herder, M.; Hecht, S.; Samorì, P. Ternary-Responsive Field-Effect Transistors and Multilevel Memories Based on Asymmetrically Functionalized Janus Few-Layer WSe_2. *Adv. Funct. Mater.* **2021**, 2102721.
(472) Qiu, H.; Ippolito, S.; Galanti, A.; Liu, Z.; Samorì, P. Asymmetric Dressing of WSe_2 with (Macro)molecular Switches: Fabrication of Quaternary-Responsive Transistors. *ACS Nano* **2021,** *15* (6), 10668-10677.
(473) Yang, J. H.; Hwang, H. J.; Kang, S. C.; Lee, B. H. Sensitivity improvement of graphene/Al_2O_3/PVDF–TrFE stacked touch device through Al seed assisted dielectric scaling. *Microelectron. Eng.* **2015,** *147*, 79-84.
(474) Alam, M. A.; Si, M.; Ye, P. D. A critical review of recent progress on negative capacitance field-effect transistors. *Appl. Phys. Lett.* **2019,** *114* (9), 090401.
(475) Salahuddin, S.; Datta, S. Use of Negative Capacitance to Provide Voltage Amplification for Low Power Nanoscale Devices. *Nano Lett.* **2008,** *8* (2), 405-410.
(476) McGuire, F. A.; Lin, Y.-C.; Price, K.; Rayner, G. B.; Khandelwal, S.; Salahuddin, S.; Franklin, A. D. Sustained Sub-60 mV/decade Switching via the Negative Capacitance

Effect in MoS_2 Transistors. *Nano Lett*. **2017,** *17* (8), 4801-4806.
(477) Yu, Z.; Wang, H.; Li, W.; Xu, S.; Song, X.; Wang, S.; Wang, P.; Zhou, P.; Shi, Y.; Chai, Y.et al. 2017 IEEE International Electron Devices Meeting (IEDM), 2017; p 23.26.21-23.26.24.
(478) Si, M.; Su, C.-J.; Jiang, C.; Conrad, N. J.; Zhou, H.; Maize, K. D.; Qiu, G.; Wu, C.-T.; Shakouri, A.; Alam, M. A.et al. Steep-slope hysteresis-free negative capacitance MoS_2 transistors. *Nat. Nanotechnol*. **2018,** *13* (1), 24-28.
(479) Yu, X.; Zhang, S.; Zeng, H.; Wang, Q. J. Lateral black phosphorene P–N junctions formed via chemical doping for high performance near-infrared photodetector. *Nano Energy* **2016,** *25*, 34-41.
(480) Liu, X.; Qu, D.; Ryu, J.; Ahmed, F.; Yang, Z.; Lee, D.; Yoo, W. J. P-Type Polar Transition of Chemically Doped Multilayer MoS_2 Transistor. *Adv. Mater.* **2016,** *28* (12), 2345-2351.
(481) Jo, S.-H.; Park, H.-Y.; Kang, D.-H.; Shim, J.; Jeon, J.; Choi, S.; Kim, M.; Park, Y.; Lee, J.; Song, Y. J.et al. Broad Detection Range Rhenium Diselenide Photodetector Enhanced by (3-Aminopropyl)Triethoxysilane and Triphenylphosphine Treatment. *Adv. Mater.* **2016,** *28* (31), 6711-6718.
(482) Lockhart de la Rosa, C. J.; Nourbakhsh, A.; Heyne, M.; Asselberghs, I.; Huyghebaert, C.; Radu, I.; Heyns, M.; De Gendt, S. Highly efficient and stable MoS_2 FETs with reversible n-doping using a dehydrated poly(vinyl-alcohol) coating. *Nanoscale* **2017,** *9* (1), 258-265.
(483) Jo, S.-H.; Kang, D.-H.; Shim, J.; Jeon, J.; Jeon, M. H.; Yoo, G.; Kim, J.; Lee, J.; Yeom, G. Y.; Lee, S.et al. A High-Performance WSe_2/h-BN Photodetector using a Triphenylphosphine (PPh_3)-Based n-Doping Technique. *Adv. Mater.* **2016,** *28* (24), 4824-4831.
(484) Du, Y.; Yang, L.; Zhou, H.; Ye, P. D. Performance Enhancement of Black Phosphorus Field-Effect Transistors by Chemical Doping. *IEEE Electron Device Lett*. **2016,** *37* (4), 429-432.
(485) Qu, D.; Liu, X.; Huang, M.; Lee, C.; Ahmed, F.; Kim, H.; Ruoff, R. S.; Hone, J.; Yoo, W. J. Carrier-Type Modulation and Mobility Improvement of Thin $MoTe_2$. *Adv. Mater.* **2017,** *29* (39), 1606433.
(486) Ichimiya, H.; Takinoue, M.; Fukui, A.; Miura, K.; Yoshimura, T.; Ashida, A.; Fujimura, N.; Kiriya, D. Tuning Transition-Metal Dichalcogenide Field-Effect Transistors by Spontaneous Pattern Formation of an Ultrathin Molecular Dopant Film. *ACS Nano* **2018,** *12* (10), 10123-10129.
(487) Lee, D. S.; Kim, J. Y.; Shin, D. Y.; Lee, Y.; Kim, J.; Lee, S. J.; Joo, J. Significantly Increased Photoresponsivity of WSe_2-Based Transistors through Hybridization with Gold-Tetraphenylporphyrin as Efficient n-Type Dopant. *Adv. Electron. Mater.* **2019,** *5* (4), 1800802.
(488) Nie, C.; Zhang, B.; Gao, Y.; Yin, M.; Yi, X.; Zhao, C.; Zhang, Y.; Luo, L.; Wang, S. Thickness-Dependent Enhancement of Electronic Mobility of MoS_2 Transistors via Surface Functionalization. *J. Phys. Chem. C* **2020,** *124* (31), 16943-16950.
(489) Li, X.-K.; Sun, R.-X.; Guo, H.-W.; Su, B.-W.; Li, D.-K.; Yan, X.-Q.; Liu, Z.-B.; Tian, J.-G. Controllable Doping of Transition-Metal Dichalcogenides by Organic Solvents. *Adv. Electron. Mater.* **2020,** *6* (3), 1901230.
(490) Tang, J.; Wei, Z.; Wang, Q.; Wang, Y.; Han, B.; Li, X.; Huang, B.; Liao, M.; Liu, J.; Li, N.et al. In Situ Oxygen Doping of Monolayer MoS_2 for Novel Electronics. *Small* **2020,** *16* (42), 2004276.
(491) Ogura, H.; Kaneda, M.; Nakanishi, Y.; Nonoguchi, Y.; Pu, J.; Ohfuchi, M.; Irisawa, T.; Lim,

H. E.; Endo, T.; Yanagi, K.et al. Air-stable and efficient electron doping of monolayer MoS_2 by salt–crown ether treatment. *Nanoscale* **2021,** *13* (19), 8784-8789.
(492) Trung, N. T.; Hossain, M. I.; Alam, M. I.; Ando, A.; Kitakami, O.; Kikuchi, N.; Takaoka, T.; Sainoo, Y.; Arafune, R.; Komeda, T. In Situ Study of Molecular Doping of Chlorine on MoS_2 Field Effect Transistor Device in Ultrahigh Vacuum Conditions. *ACS Omega* **2020,** *5* (43), 28108-28115.
(493) Yue, D.; Kim, C.; Lee, K. Y.; Yoo, W. J. Ohmic Contact in 2D Semiconductors via the Formation of a Benzyl Viologen Interlayer. *Adv. Funct. Mater.* **2019,** *29* (7), 1807338.
(494) Yoo, H.; Hong, S.; Moon, H.; On, S.; Ahn, H.; Lee, H.-K.; Kim, S.; Hong, Y. K.; Kim, J.-J. Chemical Doping Effects on CVD-Grown Multilayer $MoSe_2$ Transistor. *Adv. Electron. Mater.* **2018,** *4* (6), 1700639.
(495) Park, J. H.; Rai, A.; Hwang, J.; Zhang, C.; Kwak, I.; Wolf, S. F.; Vishwanath, S.; Liu, X.; Dobrowolska, M.; Furdyna, J.et al. Band Structure Engineering of Layered WSe_2 via One-Step Chemical Functionalization. *ACS Nano* **2019,** *13* (7), 7545-7555.
(496) Wei, S.; Ge, C.; Zhou, L.; Zhang, S.; Dai, M.; Gao, F.; Sun, Y.; Qiu, Y.; Wang, Z.; Zhang, J.et al. Performance Improvement of Multilayered SnS_2 Field Effect Transistors through Synergistic Effect of Vacancy Repairing and Electron Doping Introduced by EDTA. *ACS Appl. Electron. Mater.* **2019,** *1* (11), 2380-2388.
(497) Guo, R.; Li, Q.; Zheng, Y.; Lei, B.; Sun, H.; Hu, Z.; Zhang, J.; Wang, L.; Longhi, E.; Barlow, S.et al. Degenerate electron-doping in two-dimensional tungsten diselenide with a dimeric organometallic reductant. *Mater. Today* **2019,** *30*, 26-33.
(498) Cho, Y.; Park, J. H.; Kim, M.; Jeong, Y.; Yu, S.; Lim, J. Y.; Yi, Y.; Im, S. Impact of Organic Molecule-Induced Charge Transfer on Operating Voltage Control of Both n-MoS_2 and p-$MoTe_2$ Transistors. *Nano Lett.* **2019,** *19* (4), 2456-2463.
(499) Liu, X.; Qu, D.; Choi, M. S.; Lee, C.; Kim, H.; Yoo, W. J. Homogeneous molybdenum disulfide tunnel diode formed via chemical doping. *Appl. Phys. Lett.* **2018,** *112* (18), 183103.
(500) Yang, S.; Lee, G.; Kim, J. Selective p-Doping of 2D WSe_2 via UV/Ozone Treatments and Its Application in Field-Effect Transistors. *ACS Appl. Mater. Interfaces* **2021,** *13* (1), 955-961.
(501) Arnold, A. J.; Schulman, D. S.; Das, S. Thickness Trends of Electron and Hole Conduction and Contact Carrier Injection in Surface Charge Transfer Doped 2D Field Effect Transistors. *ACS Nano* **2020,** *14* (10), 13557-13568.
(502) Luo, W.; Zhu, M.; Peng, G.; Zheng, X.; Miao, F.; Bai, S.; Zhang, X.-A.; Qin, S. Carrier Modulation of Ambipolar Few-Layer $MoTe_2$ Transistors by MgO Surface Charge Transfer Doping. *Adv. Funct. Mater.* **2018,** *28* (15), 1704539.
(503) Wang, G.; Bao, L.; Pei, T.; Ma, R.; Zhang, Y.-Y.; Sun, L.; Zhang, G.; Yang, H.; Li, J.; Gu, C.et al. Introduction of Interfacial Charges to Black Phosphorus for a Family of Planar Devices. *Nano Lett.* **2016,** *16* (11), 6870-6878.
(504) Wang, C.; He, Q.; Halim, U.; Liu, Y.; Zhu, E.; Lin, Z.; Xiao, H.; Duan, X.; Feng, Z.; Cheng, R.et al. Monolayer atomic crystal molecular superlattices. *Nature* **2018,** *555*, 231.
(505) Kang, D.-H.; Jeon, M. H.; Jang, S. K.; Choi, W.-Y.; Kim, K. N.; Kim, J.; Lee, S.; Yeom, G. Y.; Park, J.-H. Self-Assembled Layer (SAL)-Based Doping on Black Phosphorus (BP) Transistor and Photodetector. *ACS Photonics* **2017,** *4* (7), 1822-1830.
(506) Goossens, S.; Navickaite, G.; Monasterio, C.; Gupta, S.; Piqueras, J. J.; Pérez, R.; Burwell, G.; Nikitskiy, I.; Lasanta, T.; Galán, T.et al. Broadband image sensor array based on

graphene–CMOS integration. *Nat. Photonics* **2017,** *11* (6), 366-371.
(507) Joo, P.; Kim, B. J.; Jeon, E. K.; Cho, J. H.; Kim, B.-S. Optical switching of the Dirac point in graphene multilayer field-effect transistors functionalized with spiropyran. *Chem. Commun*. **2012,** *48* (89), 10978-10980.
(508) Liu, Z.; Qiu, H.; Wang, C.; Chen, Z.; Zyska, B.; Narita, A.; Ciesielski, A.; Hecht, S.; Chi, L.; Müllen, K.et al. Photomodulation of Charge Transport in All-Semiconducting 2D–1D van der Waals Heterostructures with Suppressed Persistent Photoconductivity Effect. *Adv. Mater.* **2020,** *32* (26), 2001268.
(509) Qiu, H.; Zhao, Y.; Liu, Z.; Herder, M.; Hecht, S.; Samorì, P. Modulating the Charge Transport in 2D Semiconductors via Energy-Level Phototuning. *Adv. Mater.* **2019,** *31* (39), 1903402.
(510) Jin, Y.; Keum, D. H.; An, S.-J.; Kim, J.; Lee, H. S.; Lee, Y. H. A Van Der Waals Homojunction: Ideal p–n Diode Behavior in $MoSe_2$. *Adv. Mater.* **2015,** *27* (37), 5534-5540.
(511) Pospischil, A.; Furchi, M. M.; Mueller, T. Solar-energy conversion and light emission in an atomic monolayer p–n diode. *Nat. Nanotechnol*. **2014,** *9*, 257.
(512) Katagiri, Y.; Nakamura, T.; Ishii, A.; Ohata, C.; Hasegawa, M.; Katsumoto, S.; Cusati, T.; Fortunelli, A.; Iannaccone, G.; Fiori, G.et al. Gate-Tunable Atomically Thin Lateral MoS_2 Schottky Junction Patterned by Electron Beam. *Nano Lett*. **2016,** *16* (6), 3788-3794.
(513) Huang, H.; Xu, W.; Chen, T.; Chang, R.-J.; Sheng, Y.; Zhang, Q.; Hou, L.; Warner, J. H. High-Performance Two-Dimensional Schottky Diodes Utilizing Chemical Vapour Deposition-Grown Graphene–MoS_2 Heterojunctions. *ACS Appl. Mater. Interfaces* **2018,** *10* (43), 37258-37266.
(514) Margapoti, E.; Li, J.; Ceylan, Ö.; Seifert, M.; Nisic, F.; Anh, T. L.; Meggendorfer, F.; Dragonetti, C.; Palma, C.-A.; Barth, J. V.et al. A 2D Semiconductor–Self-Assembled Monolayer Photoswitchable Diode. *Adv. Mater.* **2015,** *27* (8), 1426-1431.
(515) Baugher, B. W. H.; Churchill, H. O. H.; Yang, Y.; Jarillo-Herrero, P. Optoelectronic devices based on electrically tunable p-n diodes in a monolayer dichalcogenide. *Nat. Nanotechnol*. **2014,** *9* (4), 262-267.
(516) Li, D.; Chen, M.; Sun, Z.; Yu, P.; Liu, Z.; Ajayan, P. M.; Zhang, Z. Two-dimensional non-volatile programmable p–n junctions. *Nat. Nanotechnol*. **2017,** *12*, 901.
(517) Bertolazzi, S.; Bondavalli, P.; Roche, S.; San, T.; Choi, S.-Y.; Colombo, L.; Bonaccorso, F.; Samorì, P. Nonvolatile Memories Based on Graphene and Related 2D Materials. *Adv. Mater.* **2019,** *31* (10), 1806663.
(518) Akkerman, H. B.; Blom, P. W. M.; de Leeuw, D. M.; de Boer, B. Towards molecular electronics with large-area molecular junctions. *Nature* **2006,** *441*, 69.
(519) Jia, C.; Ma, B.; Xin, N.; Guo, X. Carbon Electrode–Molecule Junctions: A Reliable Platform for Molecular Electronics. *Acc. Chem. Res*. **2015,** *48* (9), 2565-2575.
(520) Morant-Giner, M.; Carbonell-Vilar, J. M.; Viciano-Chumillas, M.; Forment-Aliaga, A.; Cano, J.; Coronado, E. Functionalisation of MoS_2 2D layers with diarylethene molecules. *J. Mater. Chem. C* **2021,** *9* (33), 10975-10984.
(521) Qiu, H.; Liu, Z.; Yao, Y.; Herder, M.; Hecht, S.; Samorì, P. Simultaneous Optical Tuning of Hole and Electron Transport in Ambipolar WSe_2 Interfaced with a Bicomponent Photochromic Layer: From High-Mobility Transistors to Flexible Multilevel Memories. *Adv. Mater.* **2020,** *32* (11), 1907903.
(522) Seo, S.; Min, M.; Lee, S. M.; Lee, H. Photo-switchable molecular monolayer anchored between highly transparent and flexible graphene electrodes. *Nat. Commun*. **2013,** *4*, 1920.

(523) Lu, J.; Lipatov, A.; Vorobeva, N. S.; Muratov, D. S.; Sinitskii, A. Photoswitchable Monolayer and Bilayer Graphene Devices Enabled by In Situ Covalent Functionalization. *Adv. Electron. Mater.* **2018,** *4* (8), 1800021.
(524) Nguyen, P.; Li, J.; Sreeprasad, T. S.; Jasuja, K.; Mohanty, N.; Ikenberry, M.; Hohn, K.; Shenoy, V. B.; Berry, V. Covalent Functionalization of Dipole-Modulating Molecules on Trilayer Graphene: An Avenue for Graphene-Interfaced Molecular Machines. *Small* **2013,** *9* (22), 3823-3828.
(525) Jia, C.; Grace, I. M.; Wang, P.; Almeshal, A.; Huang, Z.; Wang, Y.; Chen, P.; Wang, L.; Zhou, J.; Feng, Z.et al. Redox Control of Charge Transport in Vertical Ferrocene Molecular Tunnel Junctions. *Chem* **2020,** *6* (5), 1172-1182.
(526) Wang, Z.; Dong, H.; Li, T.; Hviid, R.; Zou, Y.; Wei, Z.; Fu, X.; Wang, E.; Zhen, Y.; Nørgaard, K.et al. Role of redox centre in charge transport investigated by novel self-assembled conjugated polymer molecular junctions. *Nat. Commun.* **2015,** *6* (1), 7478.
(527) Wang, Y.; Kim, C.-H.; Yoo, Y.; Johns, J. E.; Frisbie, C. D. Field Effect Modulation of Heterogeneous Charge Transfer Kinetics at Back-Gated Two-Dimensional MoS_2 Electrodes. *Nano Lett.* **2017,** *17* (12), 7586-7592.
(528) Zhao, Y.; Bertolazzi, S.; Maglione, M. S.; Rovira, C.; Mas-Torrent, M.; Samorì, P. Molecular Approach to Electrochemically Switchable Monolayer MoS_2 Transistors. *Adv. Mater.* **2020,** *32* (19), 2000740.
(529) Reynolds, M. F.; Guimarães, M. H. D.; Gao, H.; Kang, K.; Cortese, A. J.; Ralph, D. C.; Park, J.; McEuen, P. L. MoS_2 pixel arrays for real-time photoluminescence imaging of redox molecules. *Sci. Adv.* **2019,** *5* (11), eaat9476.
(530) Žutić, I.; Matos-Abiague, A.; Scharf, B.; Dery, H.; Belashchenko, K. Proximitized materials. *Mater. Today* **2019,** *22*, 85-107.
(531) Dayen, J.-F.; Konstantinov, N.; Palluel, M.; Daro, N.; Kundys, B.; Soliman, M.; Chastanet, G.; Doudin, B. Room temperature optoelectronic devices operating with spin crossover nanoparticles. *Mater. Horiz.* **2021,** *8* (8), 2310-2315.
(532) Burzurí, E.; Island, J. O.; Díaz-Torres, R.; Fursina, A.; González-Campo, A.; Roubeau, O.; Teat, S. J.; Aliaga-Alcalde, N.; Ruiz, E.; van der Zant, H. S. Sequential Electron Transport and Vibrational Excitations in an Organic Molecule Coupled to Few-Layer Graphene Electrodes. *ACS Nano* **2016,** *10* (2), 2521-2527.
(533) Cao, Y.; Dong, S.; Liu, S.; He, L.; Gan, L.; Yu, X.; Steigerwald, M. L.; Wu, X.; Liu, Z.; Guo, X. Building high-throughput molecular junctions using indented graphene point contacts. *Angew. Chem. Int. Ed.* **2012,** *51* (49), 12228-12232.
(534) Gehring, P.; Sowa, J. K.; Cremers, J.; Wu, Q.; Sadeghi, H.; Sheng, Y.; Warner, J. H.; Lambert, C. J.; Briggs, G. A. D.; Mol, J. A. Distinguishing Lead and Molecule States in Graphene-Based Single-Electron Transistors. *ACS Nano* **2017,** *11* (6), 5325-5331.
(535) Gehring, P.; Harzheim, A.; Spièce, J.; Sheng, Y.; Rogers, G.; Evangeli, C.; Mishra, A.; Robinson, B. J.; Porfyrakis, K.; Warner, J. H.et al. Field-Effect Control of Graphene-Fullerene Thermoelectric Nanodevices. *Nano Lett.* **2017,** *17* (11), 7055-7061.
(536) Lumetti, S.; Candini, A.; Godfrin, C.; Balestro, F.; Wernsdorfer, W.; Klyatskaya, S.; Ruben, M.; Affronte, M. Single-molecule devices with graphene electrodes. *Dalton Trans.* **2016,** *45* (42), 16570-16574.
(537) Mol, J. A.; Lau, C. S.; Lewis, W. J.; Sadeghi, H.; Roche, C.; Cnossen, A.; Warner, J. H.; Lambert, C. J.; Anderson, H. L.; Briggs, G. A. Graphene-porphyrin single-molecule transistors. *Nanoscale* **2015,** *7* (31), 13181-13185.

(538) Sadeghi, H.; Sangtarash, S.; Lambert, C. Robust Molecular Anchoring to Graphene Electrodes. *Nano Lett*. **2017,** *17* (8), 4611-4618.
(539) Wen, H.; Li, W.; Chen, J.; He, G.; Li, L.; Olson, M. A.; Sue, A. C.; Stoddart, J. F.; Guo, X. Complex formation dynamics in a single-molecule electronic device. *Sci*. *Adv*. **2016,** *2* (11), e1601113.
(540) Xin, N.; Li, X.; Jia, C.; Gong, Y.; Li, M.; Wang, S.; Zhang, G.; Yang, J.; Guo, X. Tuning Charge Transport in Aromatic-Ring Single-Molecule Junctions via Ionic-Liquid Gating. *Angew*. *Chem*. *Int*. *Ed*. **2018,** *57* (43), 14026-14031.
(541) Xin, N.; Wang, J.; Jia, C.; Liu, Z.; Zhang, X.; Yu, C.; Li, M.; Wang, S.; Gong, Y.; Sun, H.et al. Stereoelectronic Effect-Induced Conductance Switching in Aromatic Chain Single-Molecule Junctions. *Nano Lett*. **2017,** *17* (2), 856-861.
(542) Xu, Q.; Scuri, G.; Mathewson, C.; Kim, P.; Nuckolls, C.; Bouilly, D. Single Electron Transistor with Single Aromatic Ring Molecule Covalently Connected to Graphene Nanogaps. *Nano Lett*. **2017,** *17* (9), 5335-5341.
(543) Yang, C.; Qin, A.; Tang, B. Z.; Guo, X. Fabrication and functions of graphene-molecule-graphene single-molecule junctions. *J*. *Chem*. *Phys*. **2020,** *152* (12), 120902.
(544) Holovchenko, A.; Dugay, J.; Giménez-Marqués, M.; Torres-Cavanillas, R.; Coronado, E.; van der Zant, H. S. Near Room-Temperature Memory Devices Based on Hybrid Spin-Crossover@SiO_2 Nanoparticles Coupled to Single-Layer Graphene Nanoelectrodes. *Adv*. *Mater*. **2016,** *28* (33), 7228-7233.
(545) van Geest, E. P.; Shakouri, K.; Fu, W.; Robert, V.; Tudor, V.; Bonnet, S.; Schneider, G. F. Contactless Spin Switch Sensing by Chemo-Electric Gating of Graphene. *Adv*. *Mater*. **2020,** *32* (10), e1903575.
(546) Konstantinov, N.; Tauzin, A.; Noumbé, U. N.; Dragoe, D.; Kundys, B.; Majjad, H.; Brosseau, A.; Lenertz, M.; Singh, A.; Berciaud, S.et al. Electrical read-out of light-induced spin transition in thin film spin crossover/graphene heterostructures. *J*. *Mater*. *Chem*. *C* **2021,** *9* (8), 2712-2720.
(547) Ramón, T.-C.; Marc, M.-G.; Garin, E.-A.; Julien, D.; J., C.-F.; Sergio, T.; Salvador, C.-S.; Dr. Mónica, G. M.; Marta, G.; Alicia, F.-A.et al. Smart molecular/MoS_2 Heterostructures Featuring Light and Thermally-Induced Strain Driven by Spin Switching. *ChemRxiv* **2020**, https://doi.org/10.26434/chemrxiv.12664799.v12664791.
(548) Datta, S.; Cai, Y.; Yudhistira, I.; Zeng, Z.; Zhang, Y.-W.; Zhang, H.; Adam, S.; Wu, J.; Loh, K. P. Tuning magnetoresistance in molybdenum disulphide and graphene using a molecular spin transition. *Nat*. *Commun*. **2017,** *8* (1), 677.
(549) Leuenberger, M. N.; Loss, D. Quantum computing in molecular magnets. *Nature* **2001,** *410* (6830), 789-793.
(550) Ding, Y.-S.; Deng, Y.-F.; Zheng, Y.-Z. The Rise of Single-Ion Magnets as Spin Qubits. *Magnetochemistry* **2016,** *2* (4), 40.
(551) Lombardi, F.; Lodi, A.; Ma, J.; Liu, J.; Slota, M.; Narita, A.; Myers, W. K.; Müllen, K.; Feng, X.; Bogani, L. Quantum units from the topological engineering of molecular graphenoids. *Science* **2019,** *366* (6469), 1107.
(552) Slota, M.; Keerthi, A.; Myers, W. K.; Tretyakov, E.; Baumgarten, M.; Ardavan, A.; Sadeghi, H.; Lambert, C. J.; Narita, A.; Müllen, K.et al. Magnetic edge states and coherent manipulation of graphene nanoribbons. *Nature* **2018,** *557* (7707), 691-695.
(553) Vincent, R.; Klyatskaya, S.; Ruben, M.; Wernsdorfer, W.; Balestro, F. Electronic read-out of a single nuclear spin using a molecular spin transistor. *Nature* **2012,** *488* (7411), 357-

360.
(554) Thiele, S.; Balestro, F.; Ballou, R.; Klyatskaya, S.; Ruben, M.; Wernsdorfer, W. Electrically driven nuclear spin resonance in single-molecule magnets. *Science* **2014,** *344* (6188), 1135.
(555) Candini, A.; Klyatskaya, S.; Ruben, M.; Wernsdorfer, W.; Affronte, M. Graphene spintronic devices with molecular nanomagnets. *Nano Lett*. **2011,** *11* (7), 2634-2639.
(556) Urdampilleta, M.; Klyatskaya, S.; Cleuziou, J. P.; Ruben, M.; Wernsdorfer, W. Supramolecular spin valves. *Nat. Mater.* **2011,** *10* (7), 502-506.
(557) Tang, C.; Zhang, Z.; Lai, S.; Tan, Q.; Gao, W. B. Magnetic Proximity Effect in Graphene/$CrBr_3$ van der Waals Heterostructures. *Adv. Mater.* **2020,** *32* (16), 1908498.
(558) Wang, Z.; Tang, C.; Sachs, R.; Barlas, Y.; Shi, J. Proximity-induced ferromagnetism in graphene revealed by the anomalous Hall effect. *Phys. Rev. Lett*. **2015,** *114* (1), 016603.
(559) Wei, P.; Lee, S.; Lemaitre, F.; Pinel, L.; Cutaia, D.; Cha, W.; Katmis, F.; Zhu, Y.; Heiman, D.; Hone, J.et al. Strong interfacial exchange field in the graphene/EuS heterostructure. *Nat. Mater.* **2016,** *15* (7), 711-716.
(560) Hirohata, A.; Yamada, K.; Nakatani, Y.; Prejbeanu, I.-L.; Diény, B.; Pirro, P.; Hillebrands, B. Review on spintronics: Principles and device applications. *J. Magn. Magn. Mater.* **2020,** *509*, 166711.
(561) Kim, M.; Park, G. H.; Lee, J.; Lee, J. H.; Park, J.; Lee, H.; Lee, G. H.; Lee, H. J. Strong Proximity Josephson Coupling in Vertically Stacked $NbSe_2$–Graphene–$NbSe_2$ van der Waals Junctions. *Nano Lett*. **2017,** *17* (10), 6125-6130.
(562) Wang, J. I.; Rodan-Legrain, D.; Bretheau, L.; Campbell, D. L.; Kannan, B.; Kim, D.; Kjaergaard, M.; Krantz, P.; Samach, G. O.; Yan, F.et al. Coherent control of a hybrid superconducting circuit made with graphene-based van der Waals heterostructures. *Nat. Nanotechnol*. **2019,** *14* (2), 120-125.
(563) Yabuki, N.; Moriya, R.; Arai, M.; Sata, Y.; Morikawa, S.; Masubuchi, S.; Machida, T. Supercurrent in van der Waals Josephson junction. *Nat. Commun*. **2016,** *7*, 10616.
(564) Wang, Z.; Sapkota, D.; Taniguchi, T.; Watanabe, K.; Mandrus, D.; Morpurgo, A. F. Tunneling spin valves based on Fe_3GeTe_2/hBN/Fe_3GeTe_2 van der Waals heterostructures. *Nano Lett*. **2018,** *18* (7), 4303-4308.
(565) Song, T.; Cai, X.; Tu, M. W.; Zhang, X.; Huang, B.; Wilson, N. P.; Seyler, K. L.; Zhu, L.; Taniguchi, T.; Watanabe, K.et al. Giant tunneling magnetoresistance in spin-filter van der Waals heterostructures. *Science* **2018,** *360* (6394), 1214-1218.
(566) Wang, Z.; Gutiérrez-Lezama, I.; Ubrig, N.; Kroner, M.; Gibertini, M.; Taniguchi, T.; Watanabe, K.; Imamoğlu, A.; Giannini, E.; Morpurgo, A. F. Very large tunneling magnetoresistance in layered magnetic semiconductor CrI_3. *Nat. Commun*. **2018,** *9* (1), 2516.
(567) Albarakati, S.; Tan, C.; Chen, Z.-J.; Partridge, J. G.; Zheng, G.; Farrar, L.; Mayes, E. L. H.; Field, M. R.; Lee, C.; Wang, Y.et al. Antisymmetric magnetoresistance in van der Waals Fe_3GeTe_2/graphite/Fe_3GeTe_2 trilayer heterostructures. *Sci. Adv.* **2019,** *5* (7), eaaw0409.
(568) Cao, Y.; Mishchenko, A.; Yu, G. L.; Khestanova, E.; Rooney, A. P.; Prestat, E.; Kretinin, A. V.; Blake, P.; Shalom, M. B.; Woods, C.et al. Quality Heterostructures from Two-Dimensional Crystals Unstable in Air by Their Assembly in Inert Atmosphere. *Nano Lett*. **2015,** *15* (8), 4914-4921.
(569) Staley, N. E.; Wu, J.; Eklund, P.; Liu, Y.; Li, L.; Xu, Z. Electric field effect on superconductivity in atomically thin flakes of $NbSe_2$. *Phys. Rev. B* **2009,** *80* (18), 184505.
(570) Xi, X.; Berger, H.; Forró, L.; Shan, J.; Mak, K. F. Gate Tuning of Electronic Phase

Transitions in Two-Dimensional $NbSe_2$. *Phys. Rev. Lett.* **2016,** *117* (10), 106801.
(571) Verzhbitskiy, I. A.; Kurebayashi, H.; Cheng, H.; Zhou, J.; Khan, S.; Feng, Y. P.; Eda, G. Controlling the magnetic anisotropy in $Cr_2Ge_2Te_6$ by electrostatic gating. *Nat. Electron.* **2020,** *3* (8), 460-465.
(572) Jiang, S.; Li, L.; Wang, Z.; Mak, K. F.; Shan, J. Controlling magnetism in 2D CrI_3 by electrostatic doping. *Nat. Nanotechnol.* **2018,** *13* (7), 549-553.
(573) Xi, X.; Zhao, L.; Wang, Z.; Berger, H.; Forró, L.; Shan, J.; Mak, K. F. Strongly enhanced charge-density-wave order in monolayer $NbSe_2$. *Nat. Nanotechnol.* **2015,** *10* (9), 765-769.
(574) Ugeda, M. M.; Bradley, A. J.; Zhang, Y.; Onishi, S.; Chen, Y.; Ruan, W.; Ojeda-Aristizabal, C.; Ryu, H.; Edmonds, M. T.; Tsai, H.-Z.et al. Characterization of collective ground states in single-layer $NbSe_2$. *Nat. Phys.* **2016,** *12* (1), 92-97.
(575) Tsen, A. W.; Hunt, B.; Kim, Y. D.; Yuan, Z. J.; Jia, S.; Cava, R. J.; Hone, J.; Kim, P.; Dean, C. R.; Pasupathy, A. N. Nature of the quantum metal in a two-dimensional crystalline superconductor. *Nat. Phys.* **2016,** *12* (3), 208-212.
(576) Xi, X.; Wang, Z.; Zhao, W.; Park, J.-H.; Law, K. T.; Berger, H.; Forró, L.; Shan, J.; Mak, K. F. Ising pairing in superconducting $NbSe_2$ atomic layers. *Nat. Phys.* **2016,** *12* (2), 139-143.
(577) Xing, Y.; Zhao, K.; Shan, P.; Zheng, F.; Zhang, Y.; Fu, H.; Liu, Y.; Tian, M.; Xi, C.; Liu, H.et al. Ising Superconductivity and Quantum Phase Transition in Macro-Size Monolayer $NbSe_2$. *Nano Lett.* **2017,** *17* (11), 6802-6807.
(578) Sohn, E.; Xi, X.; He, W.-Y.; Jiang, S.; Wang, Z.; Kang, K.; Park, J.-H.; Berger, H.; Forró, L.; Law, K. T.et al. An unusual continuous paramagnetic-limited superconducting phase transition in 2D $NbSe_2$. *Nat. Mater.* **2018,** *17* (6), 504-508.
(579) Zhao, K.; Lin, H.; Xiao, X.; Huang, W.; Yao, W.; Yan, M.; Xing, Y.; Zhang, Q.; Li, Z.-X.; Hoshino, S.et al. Disorder-induced multifractal superconductivity in monolayer niobium dichalcogenides. *Nat. Phys.* **2019,** *15* (9), 904-910.
(580) Rubio-Verdú, C.; Garcı´a-Garcı´a, A. M.; Ryu, H.; Choi, D.-J.; Zaldı´var, J.; Tang, S.; Fan, B.; Shen, Z.-X.; Mo, S.-K.; Pascual, J. I.et al. Visualization of Multifractal Superconductivity in a Two-Dimensional Transition Metal Dichalcogenide in the Weak-Disorder Regime. *Nano Lett.* **2020,** *20* (7), 5111-5118.
(581) Kezilebieke, S.; Dvorak, M.; Ojanen, T.; Liljeroth, P. Coupled Yu–Shiba–Rusinov States in Molecular Dimers on $NbSe_2$. *Nano Lett.* **2018,** *18* (4), 2311-2315.
(582) Balatsky, A. V.; Vekhter, I.; Zhu, J.-X. Impurity-induced states in conventional and unconventional superconductors. *Rev. Mod. Phys.* **2006,** *78* (2), 373-433.
(583) Röntynen, J.; Ojanen, T. Topological Superconductivity and High Chern Numbers in 2D Ferromagnetic Shiba Lattices. *Phys. Rev. Lett.* **2015,** *114* (23), 236803.
(584) Choy, T. P.; Edge, J. M.; Akhmerov, A. R.; Beenakker, C. W. J. Majorana fermions emerging from magnetic nanoparticles on a superconductor without spin-orbit coupling. *Phys. Rev. B* **2011,** *84* (19), 195442.
(585) Nadj-Perge, S.; Drozdov, I. K.; Bernevig, B. A.; Yazdani, A. Proposal for realizing Majorana fermions in chains of magnetic atoms on a superconductor. *Phys. Rev. B* **2013,** *88* (2), 020407.
(586) Kezilebieke, S.; Žitko, R.; Dvorak, M.; Ojanen, T.; Liljeroth, P. Observation of Coexistence of Yu-Shiba-Rusinov States and Spin-Flip Excitations. *Nano Lett.* **2019,** *19* (7), 4614-4619.
(587) Alpern, H.; Yavilberg, K.; Dvir, T.; Sukenik, N.; Klang, M.; Yochelis, S.; Cohen, H.; Grosfeld, E.; Steinberg, H.; Paltiel, Y.et al. Magnetic-related States and Order Parameter

Induced in a Conventional Superconductor by Nonmagnetic Chiral Molecules. *Nano Lett*. **2019,** *19* (8), 5167-5175.
(588) Naaman, R.; Paltiel, Y.; Waldeck, D. H. Chiral molecules and the electron spin. *Nat. Rev. Chem*. **2019,** *3* (4), 250-260.
(589) Naaman, R.; Waldeck, D. H. Spintronics and Chirality: Spin Selectivity in Electron Transport Through Chiral Molecules. *Annu. Rev. Phys. Chem*. **2015,** *66* (1), 263-281.
(590) Ben Dor, O.; Yochelis, S.; Radko, A.; Vankayala, K.; Capua, E.; Capua, A.; Yang, S.-H.; Baczewski, L. T.; Parkin, S. S. P.; Naaman, R.et al. Magnetization switching in ferromagnets by adsorbed chiral molecules without current or external magnetic field. *Nat. Commun*. **2017,** *8* (1), 14567.
(591) Shen, S.; Shao, B.; Wen, C.; Yuan, X.; Gao, J.; Nie, Z.; Luo, X.; Huang, B.; Sun, Y.; Meng, S.et al. Single-water-dipole-layer-driven Reversible Charge Order Transition in 1T-TaS_2. *Nano Lett*. **2020,** *20* (12), 8854-8860.
(592) Huang, B.; Clark, G.; Navarro-Moratalla, E.; Klein, D. R.; Cheng, R.; Seyler, K. L.; Zhong, D.; Schmidgall, E.; McGuire, M. A.; Cobden, D. H.et al. Layer-dependent ferromagnetism in a van der Waals crystal down to the monolayer limit. *Nature* **2017,** *546* (7657), 270-273.
(593) Gong, C.; Li, L.; Li, Z.; Ji, H.; Stern, A.; Xia, Y.; Cao, T.; Bao, W.; Wang, C.; Wang, Y.et al. Discovery of intrinsic ferromagnetism in two-dimensional van der Waals crystals. *Nature* **2017,** *546* (7657), 265-269.
(594) Bairagi, K.; Bellec, A.; Repain, V.; Chacon, C.; Girard, Y.; Garreau, Y.; Lagoute, J.; Rousset, S.; Breitwieser, R.; Hu, Y.-C.et al. Tuning the Magnetic Anisotropy at a Molecule-Metal Interface. *Phys. Rev. Lett*. **2015,** *114* (24), 247203.
(595) Tang, C.; Zhang, L.; Du, A. Tunable magnetic anisotropy in 2D magnets via molecular adsorption. *J. Mater. Chem. C* **2020,** *8* (42), 14948-14953.
(596) Zeng, J.; Liu, E.; Fu, Y.; Chen, Z.; Pan, C.; Wang, C.; Wang, M.; Wang, Y.; Xu, K.; Cai, S.et al. Gate-Induced Interfacial Superconductivity in 1T-$SnSe_2$. *Nano Lett*. **2018,** *18* (2), 1410-1415.
(597) Li, Z.; Zhao, Y.; Mu, K.; Shan, H.; Guo, Y.; Wu, J.; Su, Y.; Wu, Q.; Sun, Z.; Zhao, A.et al. Molecule-Confined Engineering toward Superconductivity and Ferromagnetism in Two-Dimensional Superlattice. *J. Am. Chem. Soc*. **2017,** *139* (45), 16398-16404.
(598) Wu, H.; Li, S.; Susner, M.; Kwon, S.; Kim, M.; Haugan, T.; Lv, B. Spacing dependent and cation doping independent superconductivity in intercalated 1T 2D $SnSe_2$. *2D Mater.* **2019,** *6* (4), 045048.
(599) Formstone, C. A.; FitzGerald, E. T.; O'Hare, D.; Cox, P. A.; Kurmoo, M.; Hodby, J. W.; Lillicrap, D.; Goss-Custard, M. Observation of superconductivity in the organometallic intercalation compound $SnSe_2\{Co(\eta\text{-}C_5H_5)_2\}_{0.33}$. *J. Chem. Soc., Chem. Commun*. **1990,** (6), 501-503.
(600) Aoki, D.; Huxley, A.; Ressouche, E.; Braithwaite, D.; Flouquet, J.; Brison, J.-P.; Lhotel, E.; Paulsen, C. Coexistence of superconductivity and ferromagnetism in URhGe. *Nature* **2001,** *413* (6856), 613-616.
(601) Mathur, N. D.; Grosche, F. M.; Julian, S. R.; Walker, I. R.; Freye, D. M.; Haselwimmer, R. K. W.; Lonzarich, G. G. Magnetically mediated superconductivity in heavy fermion compounds. *Nature* **1998,** *394* (6688), 39-43.
(602) Fumega, A. O.; Gobbi, M.; Dreher, P.; Wan, W.; González-Orellana, C.; Peña-Díaz, M.; Rogero, C.; Herrero-Martín, J.; Gargiani, P.; Ilyn, M.et al. Absence of Ferromagnetism in VSe_2 Caused by Its Charge Density Wave Phase. *J. Phys. Chem. C* **2019,** *123* (45), 27802-

27810.
(603) Dietl, T. A ten-year perspective on dilute magnetic semiconductors and oxides. *Nat. Mater.* **2010,** *9* (12), 965-974.
(604) Feng, J.; Biswas, D.; Rajan, A.; Watson, M. D.; Mazzola, F.; Clark, O. J.; Underwood, K.; Marković, I.; McLaren, M.; Hunter, A.et al. Electronic Structure and Enhanced Charge-Density Wave Order of Monolayer VSe_2. *Nano Lett.* **2018,** *18* (7), 4493-4499.
(605) Zhu, X.; Guo, Y.; Cheng, H.; Dai, J.; An, X.; Zhao, J.; Tian, K.; Wei, S.; Cheng Zeng, X.; Wu, C.et al. Signature of coexistence of superconductivity and ferromagnetism in two-dimensional $NbSe_2$ triggered by surface molecular adsorption. *Nat. Commun.* **2016,** *7* (1), 11210.
(606) Li, Z.; Zhang, X.; Zhao, X.; Li, J.; Herng, T. S.; Xu, H.; Lin, F.; Lyu, P.; Peng, X.; Yu, W.et al. Imprinting Ferromagnetism and Superconductivity in Single Atomic Layers of Molecular Superlattices. *Adv. Mater.* **2020,** *32* (25), 1907645.
(607) Ma'Mari, F. A.; Moorsom, T.; Teobaldi, G.; Deacon, W.; Prokscha, T.; Luetkens, H.; Lee, S.; Sterbinsky, G. E.; Arena, D. A.; MacLaren, D. A.et al. Beating the Stoner criterion using molecular interfaces. *Nature* **2015,** *524* (7563), 69-73.
(608) Raman, K. V.; Kamerbeek, A. M.; Mukherjee, A.; Atodiresei, N.; Sen, T. K.; Lazić, P.; Caciuc, V.; Michel, R.; Stalke, D.; Mandal, S. K.et al. Interface-engineered templates for molecular spin memory devices. *Nature* **2013,** *493* (7433), 509-513.
(609) Avsar, A.; Ciarrocchi, A.; Pizzochero, M.; Unuchek, D.; Yazyev, O. V.; Kis, A. Defect induced, layer-modulated magnetism in ultrathin metallic $PtSe_2$. *Nat. Nanotechnol.* **2019,** *14* (7), 674-678.
(610) González-Herrero, H.; Gómez-Rodríguez, J. M.; Mallet, P.; Moaied, M.; Palacios, J. J.; Salgado, C.; Ugeda, M. M.; Veuillen, J.-Y.; Yndurain, F.; Brihuega, I. Atomic-scale control of graphene magnetism by using hydrogen atoms. *Science* **2016,** *352* (6284), 437.
(611) Tayi, A. S.; Kaeser, A.; Matsumoto, M.; Aida, T.; Stupp, S. I. Supramolecular ferroelectrics. *Nat. Chem.* **2015,** *7* (4), 281-294.
(612) Horiuchi, S.; Tokura, Y. Organic ferroelectrics. *Nat. Mater.* **2008,** *7* (5), 357-366.
(613) Chen, Y.; Zhou, Y.; Zhuge, F.; Tian, B.; Yan, M.; Li, Y.; He, Y.; Miao, X. S. Graphene–ferroelectric transistors as complementary synapses for supervised learning in spiking neural network. *npj 2D Mater. Appl.* **2019,** *3* (1), 31.
(614) Zhou, F.; Chai, Y. Near-sensor and in-sensor computing. *Nat. Electron.* **2020,** *3* (11), 664-671.
(615) Lee, J.; Pak, S.; Lee, Y.-W.; Cho, Y.; Hong, J.; Giraud, P.; Shin, H. S.; Morris, S. M.; Sohn, J. I.; Cha, S.et al. Monolayer optical memory cells based on artificial trap-mediated charge storage and release. *Nat. Commun.* **2017,** *8* (1), 14734.
(616) Lee, D.; Hwang, E.; Lee, Y.; Choi, Y.; Kim, J. S.; Lee, S.; Cho, J. H. Multibit MoS_2 Photoelectronic Memory with Ultrahigh Sensitivity. *Adv. Mater.* **2016,** *28* (41), 9196-9202.
(617) Kang, K.; Xie, S.; Huang, L.; Han, Y.; Huang, P. Y.; Mak, K. F.; Kim, C.-J.; Muller, D.; Park, J. High-mobility three-atom-thick semiconducting films with wafer-scale homogeneity. *Nature* **2015,** *520* (7549), 656-660.
(618) Mennel, L.; Symonowicz, J.; Wachter, S.; Polyushkin, D. K.; Molina-Mendoza, A. J.; Mueller, T. Ultrafast machine vision with 2D material neural network image sensors. *Nature* **2020,** *579* (7797), 62-66.
(619) Li, J.; Ye, F.; Vaziri, S.; Muhammed, M.; Lemme, M. C.; Östling, M. Efficient Inkjet Printing of Graphene. *Adv. Mater.* **2013,** *25* (29), 3985-3992.

(620) Carey, T.; Jones, C.; Le Moal, F.; Deganello, D.; Torrisi, F. Spray-Coating Thin Films on Three-Dimensional Surfaces for a Semitransparent Capacitive-Touch Device. *ACS Appl. Mater. Interfaces* **2018,** *10* (23), 19948-19956.
(621) Cinti, S.; Arduini, F. Graphene-based screen-printed electrochemical (bio)sensors and their applications: efforts and criticisms. *Biosens. Bioelectron.* **2017,** *89*, 107-122.
(622) Lin, Z.; Liu, Y.; Halim, U.; Ding, M.; Liu, Y.; Wang, Y.; Jia, C.; Chen, P.; Duan, X.; Wang, C.et al. Solution-processable 2D semiconductors for high-performance large-area electronics. *Nature* **2018,** *562* (7726), 254-258.
(623) Fan, S.; Vu, Q. A.; Tran, M. D.; Adhikari, S.; Lee, Y. H. Transfer assembly for two-dimensional van der Waals heterostructures. *2D Mater.* **2020,** *7* (2), 022005.